The prediction and back analysis of excavation behaviour in Oxford Clay

by

Nicholas David Pierpoint
MEng (Sheffield)

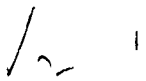

A thesis submitted to
The University of Sheffield
Department of Civil and Structural Engineering
for the degree of Doctor of Philosophy

June 1996

THE UNIVERSITY OF SHEFFIELD

ACCESS TO THESIS

THIS SHEET MUST BE BOUND IN THE FRONT OF THE THESIS BEFORE IT IS SUBMITTED

One copy of every thesis submitted to the Registrar and Secretary and which is accepted as worthy for a higher degree, will be deposited in the Library, where it will be made available for borrowing or consultation in accordance with the regulations. In certain cases where confidentiality of information is concerned the Library will withhold the thesis from loan or consultation for a period of five years from the date of its submission, if either the author or the supervisor so requests. Section A must be completed by both the author and the supervisor.

The copyright of the thesis is vested in the author unless he or she has assigned it in whole or in part to another person or institution. Request for the loan of theses are frequently received from other libraries in the UK and overseas. The conservation of the original thesis is better assured if the Library can fulfil such requests by sending a copy. Such copies may be made by the Library itself, but together with the libraries of many other UK universities the Library has entered into an arrangement with the British Library whereby theses are copied in anticipation of demand, the negative film of each thesis being held by the Lending Division at Boston Spa to which all requests are transmitted. If you are willing to give permission for the University of Sheffield and to the British Library to produce your thesis in whole or in part for the purpose of making it available to other libraries will you please complete Section B below.

SECTION A Delete (a) or (b)

(a) I, the author, agree to this thesis being made immediately available through the library for loan or consultation.

(b) ~~I, the author, request that this thesis be withheld from loan, consultation or reproduction for a period of five years from the date of its submission.~~

NAME Nick Pierpoint

ADDRESS Foundations & Geotechnics Division
Mott MacDonald
St. Anne House, 20-26 Wellesley Road, Croydon, CR9 2UL, UK.

SIGNED _____ DATE _____

(a) I, the supervisor, agree to this thesis being made immediately available through the library for loan or consultation.

(b) ~~I, the supervisor, request that this thesis be withheld from loan, consultation or reproduction for a period of five years from the date of its submission.~~

NAME Dr. Charles Hird

ADDRESS Department of Civil & Structural Engineering
University of Sheffield
Sir Frederick Mappin Building, Mappin Street, Sheffield, S1 3JD, UK.

SIGNED _____ DATE _____

SECTION B

I, the author, give permission to the University of Sheffield and to the British Library to reproduce this thesis in whole or in part in order to supply single copies for the purpose of research or private study (except during a period of five years from the date of its submission if so requested in Section A above).

NAME Nick Pierpoint

ADDRESS Foundations & Geotechnics Division
Mott MacDonald
St. Anne House, 20-26 Wellesley Road, Croydon, CR9 2UL, UK.

SIGNED _____ DATE _____

Acknowledgements

The work described here was carried out at in the Department of Civil and Structural Engineering at the University of Sheffield and was funded by a CASE award from the former Science and Engineering Research Council in conjunction with Mott MacDonald Consulting Engineers.

This has taken me longer than I thought it would, and now that it is finished there are many others I would like to thank for helping me complete this work.

Charles Hird, my supervisor, helped me enormously, and always made time to discuss and comment on my work. I was also helped extensively by many at Mott MacDonald who guided me through the numerous volumes of site investigation data. In particular, thank you to Dave Young, Jim Beveridge, Bill Rankin, Peter Rutty and Tim Spink.

A large part of this work derived from experiments carried out in the Geotechnics Research Laboratory at Sheffield University. This laboratory is kept running smoothly by Paul Osborne and Mark Foster who push an endless stream of researchers through the process of flooding the lab and shorting out their equipment. I would like to sincerely thank Paul and Mark for always kindly considering my ideas before we continued with their better ones.

I would like to thank my fellow researchers, the lecturers, and other friends in the Department who helped me keep my sanity thoughout my research. I made some great and continuing friendships while in Sheffield, and thank you to Jan, Liz and Esther for being there when work was going less than brilliantly. My greatest thanks, however, must go to Carole for her unending patience.

I would like to dedicate this to my Mum, and to my Dad, who both continue to inspire me.

Nick Pierpoint, 1996.

Summary

The work described in this thesis involved the prediction and back-analysis of ground movements and pore water pressures around a temporary excavation, 10m deep, 105m long and 35m wide (50m long and 10m wide at its base) in the heavily overconsolidated Oxford Clay.

An experimental programme was carried out which was designed to investigate the non-linearity and the anisotropy in the soil's response. A series of computer controlled triaxial stress path tests were carried out on specimens of Oxford Clay trimmed from block samples. The initial anisotropic stress state resulted in a highly stress path dependent stiffness, and the stress-strain behaviour was closely linked to the time at which the specimen had been held at constant stress prior to a change in loading.

In the triaxial apparatus, shear wave propagation tests using square wave input functions into bender element apparatus were significantly affected by near-field effects and by additional wave components. Tests carried out using sine wave inputs provided a far more consistent output allowing correlation analyses and easier visual identification of the travelling shear wave. The shear modulus of the soil at very small strains could then be determined.

A stress path dependent, non-linear, cross-anisotropic elastic model was developed and implemented into the finite element program CRISP. A genuine prediction of the Elstow excavation was carried out while the instrumentation data from the site investigation were temporarily withheld. It was found that the horizontal displacements were modelled satisfactorily but that the vertical displacements were in error by as much as 2 or 3 times. This discrepancy was attributed to volumetric changes suggested by the instrumentation data. A parametric analysis was carried out in which the effects of the initial stress state, the degree of anisotropy, and the degree of non-linearity were investigated. This showed that although it was possible to improve the accuracy of the prediction locally, it was not possible to improve on the overall pattern of behaviour predicted by the first non-linear cross-anisotropic analysis.

Contents

List of symbols and abbreviations

α	anisotropic factor for a cross-anisotropic material, $\alpha^2 = E_h/E_v$
β	ratio of coupling stiffnesses such that $J' = J'_{ps} + \beta\left(J'_{qv} - J'_{ps}\right)$
$\varepsilon_x, \varepsilon_y, \varepsilon_z$	normal strains in the direction of the indices
$\varepsilon_a, \varepsilon_r$	axial and radial strains respectively
ε_v	volumetric strain
ε_s	deviatoric strain or triaxial shear strain
$\delta\varepsilon$	strain increment vector
$\gamma_{xy}, \gamma_{yz}, \gamma_{xz}$	shear strains in the direction of the indices
$\sigma'_x, \sigma'_y, \sigma'_z$	effective normal stresses in the direction of the indices
σ'_a, σ'_r	axial and radial effective normal stress respectively
$\delta\sigma'$	effective stress increment vector
σ_e, ε_e	stress and strain at the linear (elastic) limit
$\tau_{xy}, \tau_{xy}, \tau_{xy}$	shear stresses within the plane defined by the indices
λ	wavelength of the transmitted signal in wave propagation tests
η	stress ratio, q/p'
κ	slope of a swelling line
ϕ'	angle of friction at failure
ϕ'_{mob}	mobilised angle of friction
ν	Poisson's ratio
ν_{hv}	Poisson' ratio of strain in vertical direction to applied strain in horizontal direction
ν_{vh}	Poisson' ratio of strain in horizontal direction to applied strain in vertical direction
ν_{hh}	Poisson' ratio of strain in horizontal direction to applied strain in horizontal direction
ν^*	Poisson's ratio for a cross-anisotropic material
θ	direction of stress path probe in q-p' space

c_u	undrained shear strength
c'	undrained shear strength
c_s	shear wave velocity
d	separation of source and receiver in wave propagation tests
p'	effective mean normal stress
p	total mean normal stress
p'_o	initial effective mean normal stress
p_r	reference pressure (1kPa say)
q	deviator stress or shear stress
v	specific volume,
v_p	dilational or compressive wave velocity, subscript p denotes primary
v_s	distortional or shear wave velocity, subscript s denotes secondary
$Corr(g,h)$	cross-correlation between functions g and h
C_{io}	normalised cross correlation coefficient, $[Corr(g,h)]_{max}$ / $Corr(g,h)$
$\boldsymbol{C}$	compliance matrix
$\boldsymbol{D}$, $\boldsymbol{S}$	stiffness matrix
$\boldsymbol{D}_{ep}$	elastoplastic stiffness matrix
$\boldsymbol{D}_e$	elastic stiffness matrix
$\boldsymbol{D}_p$	plastic stiffness matrix
E^*	Young's modulus for a cross-anisotropic material
E_u	undrained Young's modulus
$E_{u_{0.1}}$	undrained Young's modulus at 0.1% axial strain
E_v	Young's modulus in vertical direction
E_h	Young's modulus in horizontal direction
F	plastic yield function
FFT	fast Fourier transform
G_{hv}	shear modulus in any vertical plane
G_{hh}	shear modulus in any horizontal plane
G'	deviatoric stiffness defined for effective stresses
G_{dyn}	dynamic isotropic shear stiffness
G_o	shear stiffness at very small strains
$G_{o_{vh}}$	very small strain shear modulus in vertical plane
$G_{o_{hh}}$	very small strain shear modulus in horizontal plane
H	plastic hardening function
J'_{qv}	coupling stiffness linking changes in deviatoric stress and changes in volumetric strain
J'_{ps}	coupling stiffness linking changes in effective mean normal stress and changes in deviatoric strain

J'	coupling stiffness
K_o'	coefficient of earth pressure at rest, $K_o' = \sigma_h'/\sigma_v'$
K'	volumetric stiffness defined for effective stresses
K_{o_v}	volumetric stiffness in vertical direction
K_{o_h}	volumetric stiffness in horizontal direction
OCR	overconsolidation ratio, σ_{vm}'/σ_v' (σ_{vm}' = maximum past vertical effective stress)
Q	plastic potential
R_o	overconsolidation ratio, p_c'/p'
U	total strain energy
ΔU	incremental strain energy

MM	Mott MacDonald Consulting Engineers
NWSEL	Norwest Holst Soil Engineering Limited
CEGB	Central Electricity Generating Board
AOD	Above Ordnance Datum
LBC	London Brick Company

List of figures

List of tables

1. Introduction

1.1 Project background and objectives

The ability to accurately predict ground movements is essential if geotechnical structures are to be designed effectively. An inability to describe the expected ground response may lead to expensive overdesign to ensure the serviceability of a structure. The prediction of ground movements requires a knowledge of the stress-strain properties of the soil. This will be dependent on the deposit's material properties and its geological stress history, and will be modified by its recent stress history, e.g. due to construction activities.

It has long been realised that non-linearity and anisotropy play an important role in the prediction or explanation of ground movements (Simpson *et al.*, 1979). Early attempts to model the ground using simple linear isotropic elastic ground models coupled with parameters derived from conventional laboratory testing greatly overestimated the magnitude of ground movements and failed to reproduce the overall form of the ground deformation response (St. John, 1975).

In laboratory testing, the development of local instrumentation for measuring strains directly on a soil specimen was a major step forward. This allowed the non-linear stress-strain relations to be determined and showed that the initial stiffness reflected the magnitudes that had been recorded for several years during *in situ* tests. The importance of the small strains in predicting ground deformation was then clear (Burland, 1989).

Further refinements to laboratory testing techniques (Tatsuoka and Shibuya, 1992) allowed static measurements to be directly linked with dynamic testing, in which very small strain levels are imposed. The importance of the very small strain elastic shear stiffness, G_o, was realised in providing an upper bound for the corresponding static measurement.

Small strain stiffness equations derived from experimental investigations have been incorporated into finite element codes for parametric studies (e.g. Jardine *et al.*, 1986), case studies (e.g. Jardine *et al.*, 1991) and predictions for full scale projects (e.g. St. John *et al.*, 1992). This has provided valuable insight into soil behaviour at both a fundamental and a practical level.

The work described in this thesis involved the prediction (Class C, Lambe, 1973) and back-analysis of ground movements and pore water pressures around a temporary excavation, 10m deep, 105m long and 35m wide (50m long and 10m wide at its base) in the Oxford Clay at Elstow, Hertfordshire. The excavation, which was heavily instrumented, took place as part of the initial site investigations for a series of low level nuclear waste disposal sites carried out by

Mott MacDonald on behalf of Nirex (UK) Ltd. Excavation work was carried out in March and April 1987. Instrument monitoring continued for a further three months until the trial excavation was back-filled in August 1987.

The work took advantage of an opportunity to test relatively undisturbed soil and extend existing knowledge concerning the stiffness of overconsolidated clays at small strain levels, including the effects of anisotropy. Furthermore, the Elstow excavation represented an extremely well controlled full-scale experiment providing an invaluable benchmark for the calibration of numerical analysis. This study permitted the data from the excavation to be properly organised and presented for future use. It was also possible to assess the capability of current methods of site investigation and laboratory testing, allied to numerical modelling techniques, in predicting the deformations of clay strata affected by excavation for civil engineering works.

1.2 Experimental programme

An experimental programme was carried out which focused on the non-linearity and the anisotropy in the soil's response to loading from very small to intermediate strain levels (0.0001%-0.1%). The stress-strain properties of the Oxford Clay were determined by conducting triaxial stress path tests on specimens trimmed from block samples, either retrieved during the site investigation and carefully preserved, or freshly taken from an adjacent brick pit. The imposed stress paths were designed to account for the recent stress history of the soil and to investigate the anticipated stress path dependent response. From an estimated *in situ* stress a series of stress path probes was carried out in which either the effective mean normal stress or the deviatoric stress was held constant. This allowed the degree and type of anisotropy to be assessed, and a suitable stress-strain response for soil elements at different points around the excavation to be determined.

The experimental apparatus, developed previously, incorporated computer control and the use of local instrumentation to record small strains. The equipment was modified to include bender element apparatus capable of recording the shear wave travel velocity within a specimen and consequently of quantifying the soil stiffness at very small strain levels.

1.3 Interpretation of site investigation data

The site investigation reports were scrutinised before predictions were made of the ground response due to excavation. However, the instrumentation data were withheld until the experimental programme and initial predictions were complete.

The Elstow excavation was instrumented with a suite of extensometers, inclinometers, and piezometers whose data were analysed to determine the short term time-dependent response of the excavation. It was found that the displacement data were often erratic but that, since there was a degree of redundancy in the instrumentation layout, an averaging process produced valuable data. An attempt was also made to interpret the volumetric response using a strain field calculated from the inclinometer and extensometer data.

1.4 Numerical analysis

It was decided to make a prediction of the excavation behaviour using a constitutive model basically adequate for this purpose rather than to attempt to develop a more generalised or sophisticated model. Consequently, a non-linear cross-anisotropic elastic model, based on the theories proposed by Graham and Houlsby (1983), was implemented in the finite element

program CRISP (Britto and Gunn, 1987). This particular program was chosen since it had been used extensively for modelling geotechnical problems and has an open source code that could be readily modified to incorporate additional features. The model behaviour was developed specifically from the behaviour anticipated on the basis of previous research, or recorded from the experimental programme. The soil element response incorporated the stiffness non-linearity and the cross-anisotropic material response. The influence of stress history effects was also accounted for with a stress path dependent stiffness response and a high stiffness response following a reversal in the stress path direction.

The model implementation was verified, partially validated using data from the experimental work (Hird and Pierpoint, 1994), and then applied to the prediction of the excavation behaviour. Genuine predictions were made since the analysis was performed, initially, in the absence of any knowledge on the part of the Author concerning the actual behaviour. Parametric studies were carried out to assess various aspects of the prediction. A back analysis was then attempted to optimise the input parameters.

1.5 Thesis structure

A review of the literature in the fields connected with the work is presented in Chapter 2. The realisation of the importance of the small strain non-linearity in stress-strain relations is discussed together with the development of accurate strain measurement and appropriate testing techniques. A general picture of the deformation of soil from very small strains to intermediate strains is presented, concentrating of the influence of stress state, stress history, and rate effects. The development of dynamic measurement techniques (particularly involving bender elements) is described and a number of issues concerning wave propagation are introduced. A brief review is made of the development of numerical modelling techniques, discussing relatively commonly used empirical models and the state-of-the-art. The general theoretical framework and the adopted notation are also presented.

Chapters 3 and 4 present and discuss the Elstow site investigation. Chapter 3 describes the context and scope of the site investigation. The site geology is described, and the results of the laboratory and *in situ* testing programme are presented. The location of the instrumentation is presented in Chapter 3, although the data interpretation is described in Chapter 4.

The experimental programme is presented in Chapters 5 and 6. The basis of the experimental programme, a description of the apparatus used, and the methodology of the testing programme are presented in Chapter 5. The results of the experimental work are presented and discussed in Chapter 6, mainly involving the analysis and interpretation of the triaxial stress path tests and the bender element wave propagation tests.

The numerical modelling aspect of the work is presented in Chapters 7 and 8. The theoretical basis of the chosen numerical model and its implementation are presented in Chapter 7. This includes a description of elasticity and a framework of elastic anisotropy compatible with parameters that may be derived from triaxial tests (Graham and Houlsby, 1983). A validation of the model is presented, limited to predictions of triaxial data at small strains. The application of the model, namely for the prediction and back analysis of the Elstow excavation, is described in Chapter 8. The effect of modelling the excavation sequence, non-linear and stress path dependent stiffness, the *in situ* stress state, and the role of anisotropy are highlighted. The model prediction is assessed parametrically.

The entire work is summarised and its findings discussed in Chapter 9. This chapter also suggests a number of further routes for research that may be of value or interest.

2. Theoretical background and Literature review

2.1 Introduction

The theoretical background, and commonly used notation, regarding the non-linear stress-strain response of soil is presented in the form used throughout the rest of the thesis.

A review of the current awareness regarding soil stiffness characteristics is presented, primarily focusing on the small strain response of overconsolidated, stiff clay. The influence of the geological and recent stress history on the stiffness non-linearity of soil is discussed using recent laboratory test data, highlighting those areas where more research is thought necessary.

Recent developments in the triaxial testing apparatus, particularly the use of local instrumentation capable of resolving small strains, are discussed. The incorporation of piezoceramic bender elements in a triaxial apparatus permits the propagation of shear waves through a soil specimen in order to measure its shear stiffness. Such equipment is described here.

Some factors affecting wave propagation in triaxial specimens are described, and a number of methods to interpret bender element test results are presented.

A review of general developments in the constitutive and numerical modelling of soil behaviour is given, from the early use of isotropic elasticity to the incorporation of a non-linear stress-strain response that is both stress level and stress path dependent. Two contrasting modelling styles are evident, an empirical approach (e.g. the inclusion of non-linearity through curve-fitting of experimental data), and the development of more generalised frameworks (e.g. plasticity formulations). Recently proposed models of each type are described.

2.2 Definitions of stress, strain, and stiffness

A constitutive relation governing the non-linear behaviour of a saturated soil must relate increments of effective stress to increments of strain. This may be realised in a compliance, or a stiffness form, as in equation 2.1 or 2.2 respectively.

$$\delta\varepsilon = C.\delta\sigma' \quad \text{..... (2.1)}$$

$$\delta\sigma' = S.\delta\varepsilon \quad \text{..... (2.2)}$$

where, $\delta\varepsilon$ = strain increment vector
$\delta\sigma'$ = effective stress increment vector
C = compliance matrix
S = stiffness matrix

The compliance and stiffness matrices are dependent not only on the current state of the soil, but also on the conditions which brought it to that state. In general stress (or strain) space, the increment vectors may be represented by the three normal stresses (or strains), and three shear stresses (or strains) respectively, associated with the Cartesian co-ordinate axes. Considering the compliance form, we obtain equation 2.3.

$$\begin{bmatrix} \varepsilon_x \\ \varepsilon_y \\ \varepsilon_z \\ \gamma_{xy} \\ \gamma_{yz} \\ \gamma_{xz} \end{bmatrix} = C \cdot \begin{bmatrix} \sigma'_x \\ \sigma'_y \\ \sigma'_z \\ \tau_{xy} \\ \tau_{yz} \\ \tau_{xz} \end{bmatrix} \quad \text{..... (2.3)}$$

where, $\varepsilon_x, \varepsilon_y, \varepsilon_z$ = normal strains in the direction of the indices
$\gamma_{xy}, \gamma_{yz}, \gamma_{xz}$ = shear strains within the plane defined by the indices
$\sigma'_x, \sigma'_y, \sigma'_z$ = effective normal stresses in the direction of the indices
$\tau_{xy}, \tau_{xy}, \tau_{xy}$ = shear stresses within the plane defined by the indices

The present work makes use of the advantages gained by interpreting soil behaviour in terms of its *volumetric* and *distortional* responses, describing changes in size and changes in shape respectively. Suitable invariant stress parameters considered are consequently those of *effective mean normal stress* and *distortional stress*; the invariant strain parameters are those of *volumetric strain* and *distortional strain*. The experimental work described here is generally associated with the triaxial testing apparatus, and therefore the limited triaxial stress space in which shearing stresses may not be applied directly. Under these conditions, stresses and strains that lead to changes in shape are termed *deviatoric*. The effective mean normal stress, p', in equation 2.4 below, and deviatoric stress, q, in equation 2.5, are defined for triaxial conditions, in which the subscripts a and r refer to the axial and radial directions respectively.

$$p' = \frac{\sigma'_a + 2\sigma'_r}{3} \quad \text{..... (2.4)}$$

$$q = \sigma'_a - \sigma'_r \quad \text{..... (2.5)}$$

For general stress space equations 2.6 and 2.7 apply,

$$p' = \frac{\sigma'_x + \sigma'_y + \sigma'_z}{3} \quad \text{..... (2.6)}$$

$$q = \sqrt{\frac{\left(\sigma'_x - \sigma'_y\right)^2 + \left(\sigma'_y - \sigma'_z\right)^2 + \left(\sigma'_z - \sigma'_x\right)^2}{2} + 3\left(\tau_{xy}^2 + \tau_{yz}^2 + \tau_{zx}^2\right)} \quad \text{..... (2.7)}$$

The corresponding relations for strain (volumetric strain, ε_v, and deviatoric strain/triaxial shear strain, ε_s) follow from the definition of a compatible incremental strain energy or work input per unit volume relation. Equations 2.8 and 2.9 apply for triaxial conditions,

$$\varepsilon_v = \varepsilon_a + 2\varepsilon_r \quad \text{..... (2.8)}$$

$$\varepsilon_s = \frac{2}{3}\left(\varepsilon_a - \varepsilon_r\right) \quad \text{..... (2.9)}$$

and equations 2.10 and 2.11 apply for general stress states,

$$\varepsilon_v = \varepsilon_x + \varepsilon_y + \varepsilon_z \quad \text{..... (2.10)}$$

$$\varepsilon_s = \frac{1}{3}\sqrt{2\left[\left(\varepsilon_x - \varepsilon_y\right)^2 + \left(\varepsilon_y - \varepsilon_z\right)^2 + \left(\varepsilon_z - \varepsilon_x\right)^2\right] + 3\left(\gamma_{xy}^2 + \gamma_{yz}^2 + \gamma_{zx}^2\right)} \quad \text{..... (2.11)}$$

These compatible definitions of stress and strain allow an incremental constitutive equation for soil to be defined in terms of volumetric and distortional components as in equation 2.12.

$$\begin{bmatrix} \delta\varepsilon_v \\ \delta\varepsilon_s \end{bmatrix} = \begin{bmatrix} \frac{1}{K'} & \frac{1}{J'_{qv}} \\ \frac{1}{J'_{ps}} & \frac{1}{3G'} \end{bmatrix} \cdot \begin{bmatrix} \delta p' \\ \delta q \end{bmatrix} \quad \text{..... (2.12)}$$

where, $\delta\varepsilon_v$ = incremental volumetric strain
$\delta\varepsilon_s$ = incremental deviatoric strain
$\delta p'$ = incremental effective mean normal stress
δq = incremental deviatoric stress
K' = volumetric stiffness defined for effective stresses
G' = deviatoric stiffness defined for effective stresses
J'_{qv} = coupling stiffness linking changes in deviatoric stress and changes in volumetric strain
J'_{ps} = coupling stiffness linking changes in effective mean normal stress and changes in deviatoric strain

The stiffness parameters J'_{ps} and J'_{qv}, which couple the volumetric and deviatoric responses, are analogous to the parameters J'_1 and J'_2 respectively as defined by Atkinson and Sällfors (1991). The indices used in the present work are considered preferable, however, since they indicate the stress and strain parameters that they couple, and because J'_1 and J'_2 are traditionally defined in mechanics as the first and second deviatoric stress tensor respectively.

The response to loading of a given soil may therefore be predicted if the parameters K', G', J'_{qv}, and J'_{ps} are known for any proposed small stress increment.

2.3 The realisation of the importance of the small strain behaviour of soil

Burland (1989) indicated the importance of the small strain behaviour of soil by showing that, for a range of construction projects (Kriegel and Weisner, 1973; Burland *et al.*, 1973; Attewell and Farmer, 1974; Bauer *et al.*, 1976), the level of direct straining in the ground was generally

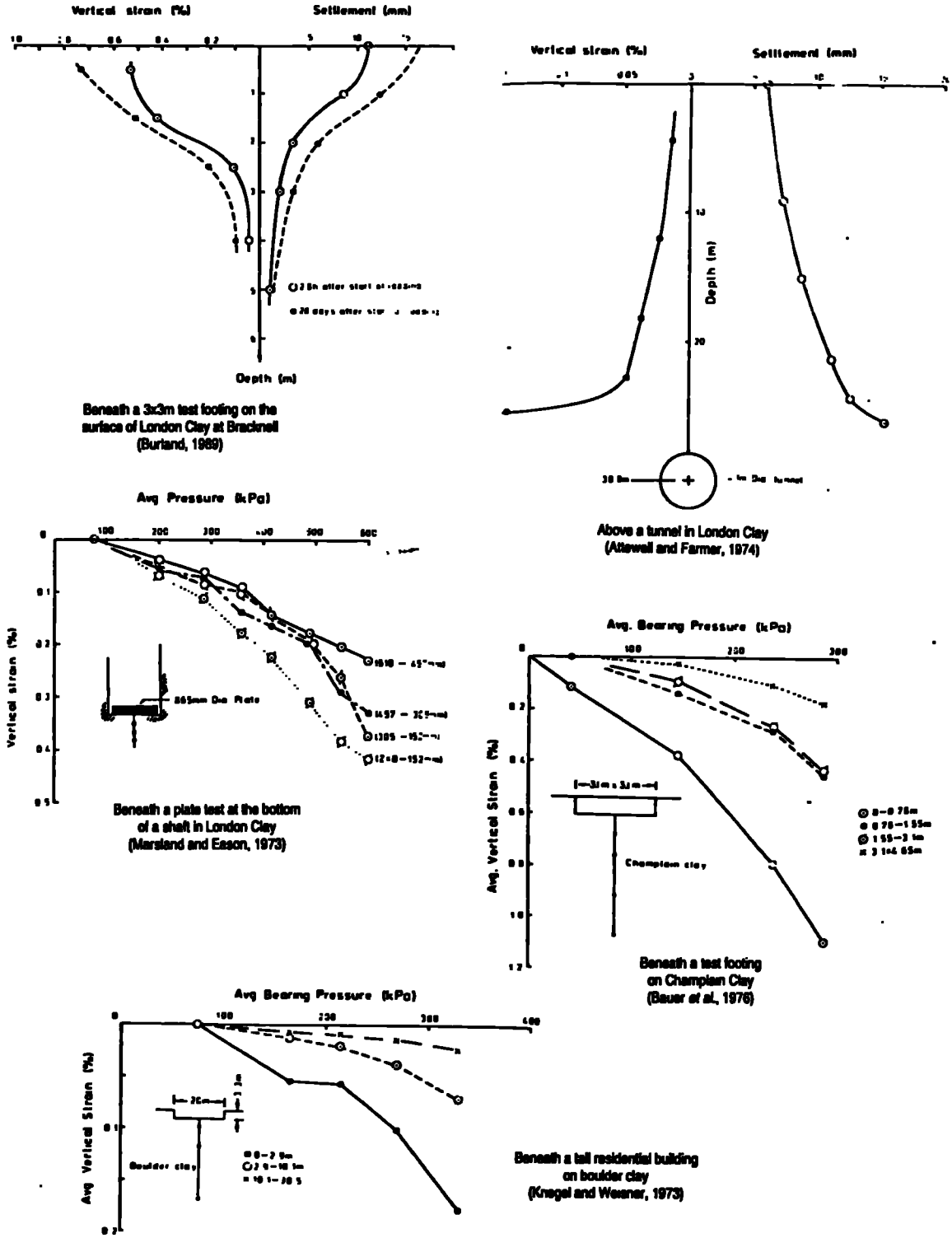

Figure 2.1 - Settlements and strains at a number of construction projects

less then 0.1%. Only locally, near to loaded boundaries, did the ground strain exceed 0.1% (see Figure 2.1)

The development of the finite element technique led to the back analysis of the deformation response of both full scale geotechnical structures and *in situ* field test data. In one of the first geotechnical applications of the finite element method, Cole and Burland (1972) back analysed the movements recorded of a retaining wall adjacent to a large excavation in London Clay at the Britannic House development. By carrying out a series of linear isotropic elastic analyses then deemed appropriate for a heavily overconsolidated clay, a depth profile of the undrained Young's modulus was determined which adequately reproduced the observed ground movements. Similar analyses were carried out for six other field studies by St. John (1975) and from the collection of results, shown in Figure 2.2, two important conclusions were made:

1. The magnitude of the equivalent undrained isotropic elastic Young's modulus increased with depth or effective mean normal stress.
2. The values of the Young's modulus back analysed from the ground movements far exceeded those measured in a series of conventional triaxial tests carried out by Bishop *et al.* (1965).

It was discovered that the stiffness values estimated from the back analysis of engineering structures invariably agreed far more closely with values derived from *in situ* field tests than those from conventional triaxial tests. A direct comparison of triaxial tests and plate loading tests was carried out in a comprehensive study by Marsland (1971), related to the degree of fissuring of London Clay. Typical results from this study are shown in Figure 2.3. Marsland found that the stiffnesses derived from the plate loading tests were between 1.8 and 4.8 times those determined from standard undrained triaxial tests on 38mm and 75mm diameter specimens trimmed from 98mm diameter tube samples. At the time of this study, the

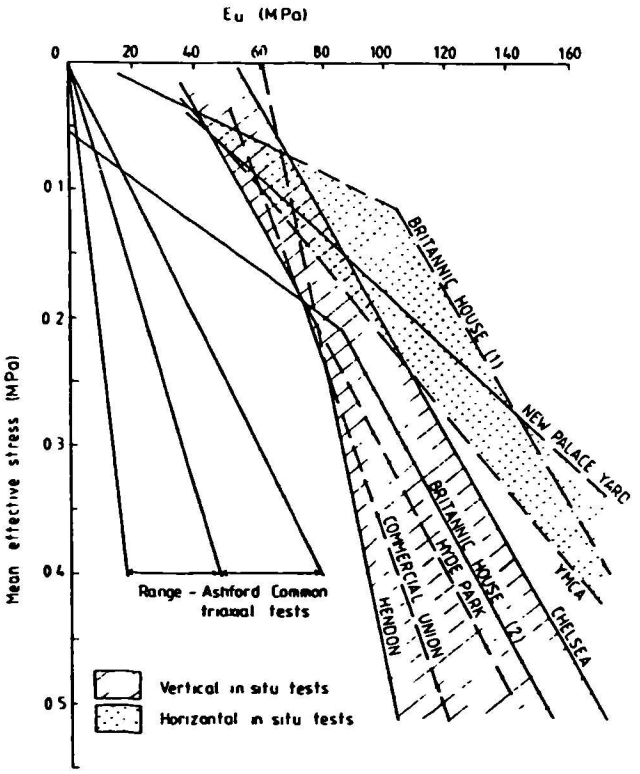

Figure 2.2 - Variation of the equivalent undrained isotropic elastic Young's modulus, E_u, with effective mean normal stress, p', for a number of sites on London Clay (St. John, 1975)

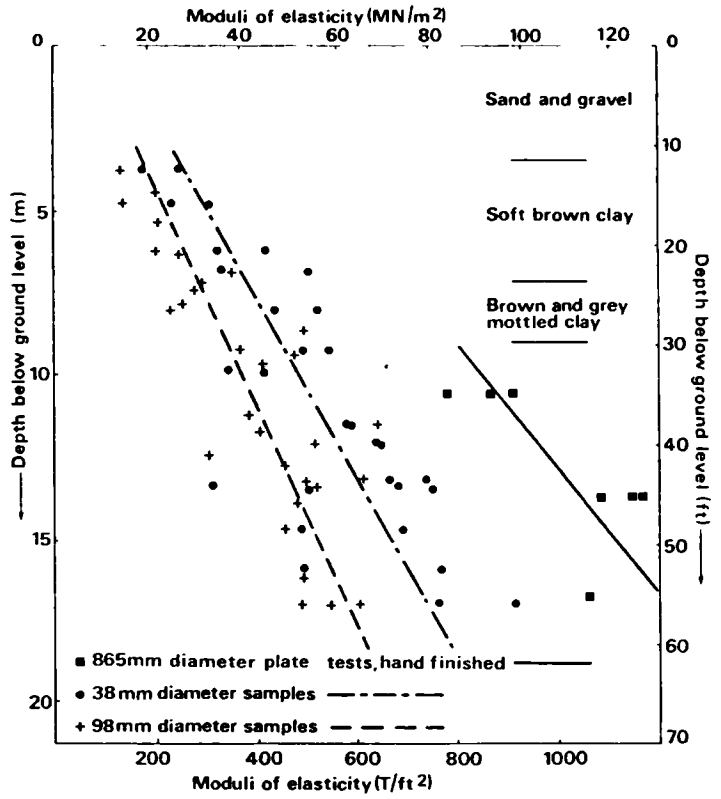

Figure 2.3 - Comparison of moduli derived from the first loading cycle of triaxial tests and plate loading tests on London Clay from Chelsea (Marsland, 1971)

discrepancy between the field data and the laboratory data was attributed to disturbance of the soil during and subsequent to sampling.

The realisation that there was a large discrepancy between field and laboratory measurements of soil stiffness, and that the use of the higher field values in finite element analyses led to much closer predictions in ground deformation analyses, led Simpson *et al.* (1979) to postulate the existence of a kinematic region of high stiffness at small values of strain for London Clay. This model developed had a far reaching influence on the modelling of soil behaviour and is discussed in greater detail in section 2.7. Influenced by Atkinson's (1973a) conclusions on threshold effects, Simpson *et al.* suggested that "when London Clay is subjected to very small strain increments following a period of rest or a change of the direction of straining, its stiffness is much greater than that at the larger strains normally measured in the laboratory." This model, one of the first to incorporate the non-linearity of the small-strain stiffness response, was used to predict the behaviour at the site of the underground car park at the House of Commons (Burland and Hancock, 1977), shown in Figure 2.4. Prior to construction, the ground response due to excavation had been predicted with a linear elastic model (Ward and Burland, 1973), using stiffness parameters derived from the Britannic House development discussed above. The comparison of the two analyses, shown in Figure 2.4(a) and (b), quantified the influence of non-linearity, since the linear model incorporated the small strain stiffnesses back analysed

from a previous excavation. Although the magnitude of the maximum heave and settlement was similar in both the linear and non-linear analyses, the pattern of displacements was predicted far more effectively when non-linearity was assumed. The incorporation of non-linearity in the soil model allowed a concentration of the deformations near the loaded boundaries, whereas, in the linear elastic model, the ground displacement spread to a much greater extent. A practical example of the importance of determining not only the magnitude, but the overall form of the ground movement was given in the predicted and observed behaviour of the tilting of Big Ben caused by the excavation. The location of the settlement trough for the linear analysis suggested that Big Ben would tilt away from the excavation by 1 in 6000; the concentration of displacements due to the non-linearity actually caused a tilting of 1 in 7000 towards the excavation.

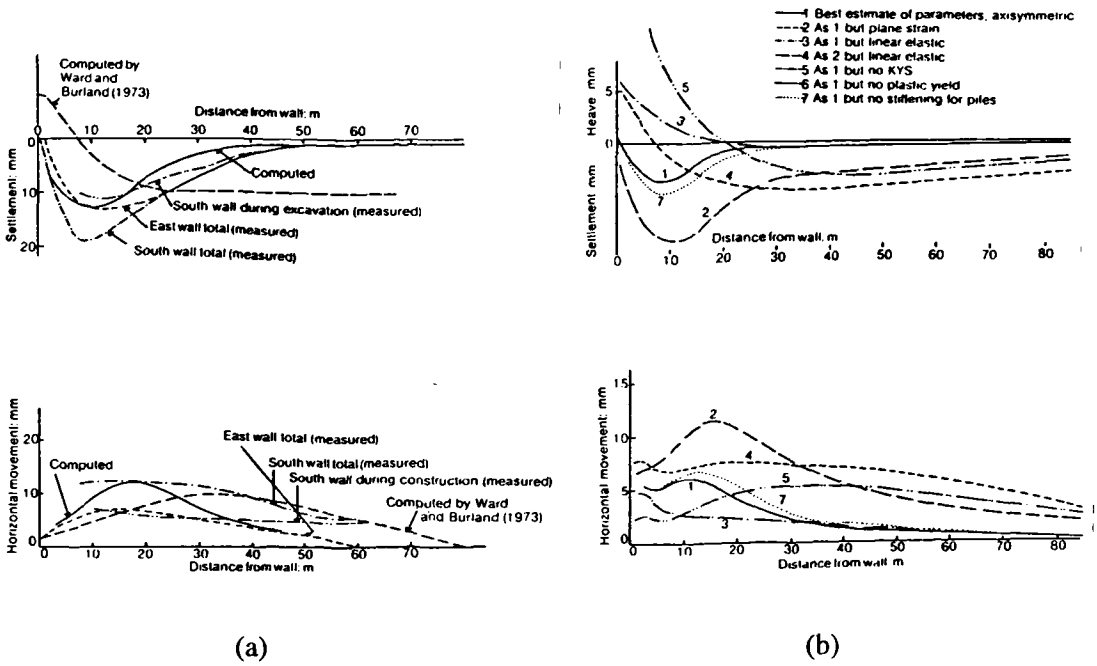

(a) (b)

Figure 2.4 - (a) Observed and predicted horizontal and vertical displacements at the ground surface measured from the edge of the excavation at New Palace Yard (b) Parametric study of the model parameters (Simpson *et al.*, 1979)

The discrepancy between the field and laboratory measured values of stiffness was being investigated simultaneously by carrying out triaxial tests in which strains were measured locally, directly on the soil specimen, in order to eliminate any errors associated with bedding at the specimen ends (see section 2.5.2). Costa-Filho and Vaughan (1980) showed that the stress-strain response of soil in triaxial tests was non-linear and exhibited a relatively high stiffness compared to those recorded for the higher strain levels measured in conventional triaxial tests.

This early work, outlined above, led to the extensive development of small strain measurement and non-linear modelling techniques for investigating and predicting the response of soil to changes in effective stress.

It is now generally recognised that the small strain non-linearity of stiffness is an essential aspect governing the overall deformation response of the ground to engineering structures.

2.4 Deformation of soil

The response of a soil to loading represents an extremely complicated problem in contact mechanics. Soil is a particulate, multi-phase material whose deformation response is dependent on frictional and cohesive interaction between the particles. As the material deforms, the nature of the interaction between the particles changes and the overall material response consequently changes also. It is convenient to review the soil response dependent on the general degree of deformation it has experienced.

2.4.1 Very small strains

Jardine (1992) suggested the existence of three general zones of material behaviour upon monotonic loading of a soil element initially in equilibrium. The first of these zones is a perfectly linear elastic region in which strains are fully recoverable. To truly prove the existence of such a region, the behaviour must be shown to be totally recoverable and, consequently, unload-reload loops should show no hysteresis in either volumetric or distortional responses. Such an elastic region could be attributed to a form of soil response in which there was no slippage or relative movement between particle contacts. The extent of such a strictly defined zone must indeed be small since contact mechanics theory can show that, for a purely frictional material, yielding at particle contacts can occur for an assemblage of particles under normal stress on the application of infinitesimally small shear strains (Johnson, 1985). Since this yielding is unlikely to be reversible, it could be argued that an elastic region would not exist for such a material. Similarly, the effect of continual creep strains would imply irreversible behaviour regardless of their magnitude. However, at the scale of laboratory test specimens, the presence of such local yielding may be negligible in regard to overall specimen deformation and the irreversibility of behaviour may be shown to exist at a scale much larger than the particle size.

Tatsuoka and Shibuya (1992) presented a series of results investigating the very small strain response for a range of rock and soil types. The initial portion of the stress-strain curve for triaxial compression tests on a cement-treated sandy soil suggested that at axial strains less than about 0.01% the behaviour was both virtually linear and fully recoverable. The results of torsional simple shear tests carried out on Toyoura Sand are shown in Figure 2.5. The region of

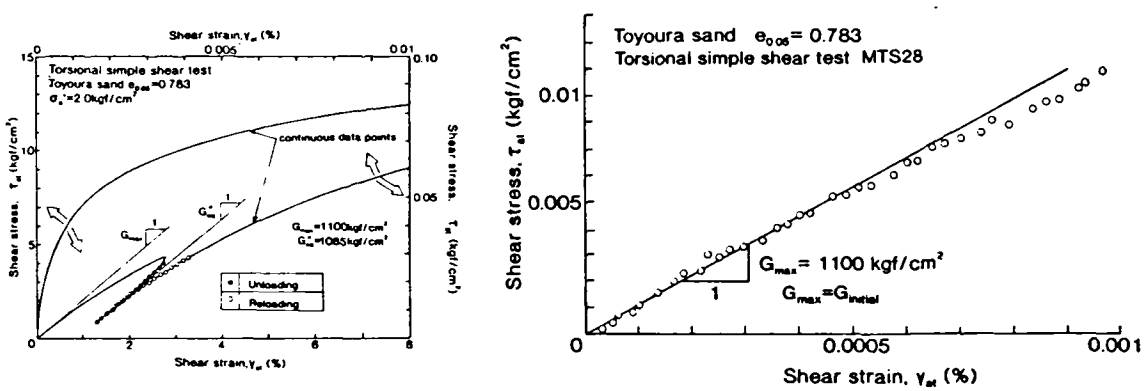

Figure 2.5 - Stress-strain response of Toyoura Sand in a torsional simple shear test (Tatsuoka and Shibuya, 1992)

linear behaviour extends only to 0.0005% shear strain. In plain strain compression tests on the same material shown in Figure 2.6, the first unload-reload cycle at 0.002% axial strain does not demonstrate fully recoverable behaviour and therefore indicates a degree of inelasticity. Similar plain strain compression tests on Silver Leighton Buzzard Sand and wet Onhama Sand suggest a linear region extending to between 0.001% and 0.002% axial strain.

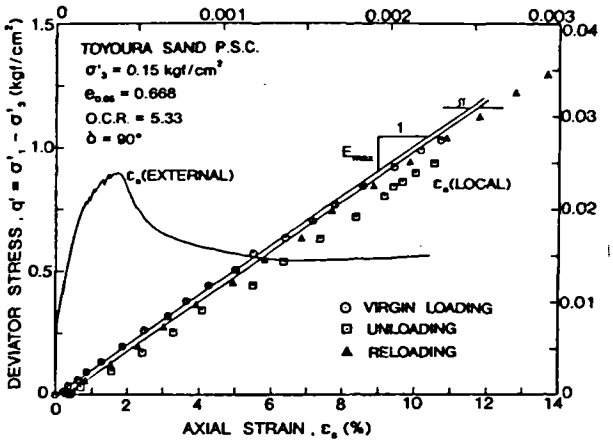

Figure 2.6 - Stress-strain response of Toyoura Sand under plain strain (Tatsuoka and Shibuya, 1992)

A series of triaxial compression tests for the stress paths shown in Figure 2.7 was carried out on undisturbed samples of Tokyo Bay Clay and on reconstituted kaolin. The Tokyo Bay clay was anisotropically consolidated to the estimated *in situ* stress levels and the kaolin was normally consolidated either isotropically or anisotropically. The stress-strain responses for these specimens are also shown in Figure 2.7. For the kaolin specimens, linear behaviour extended to 0.001% axial strain, and the first unloading-reloading cycle at 0.002% was not fully recoverable. The undisturbed specimen of Tokyo Bay clay showed a linear response up to 0.002% axial strain. It is noticeable in each of these figures that

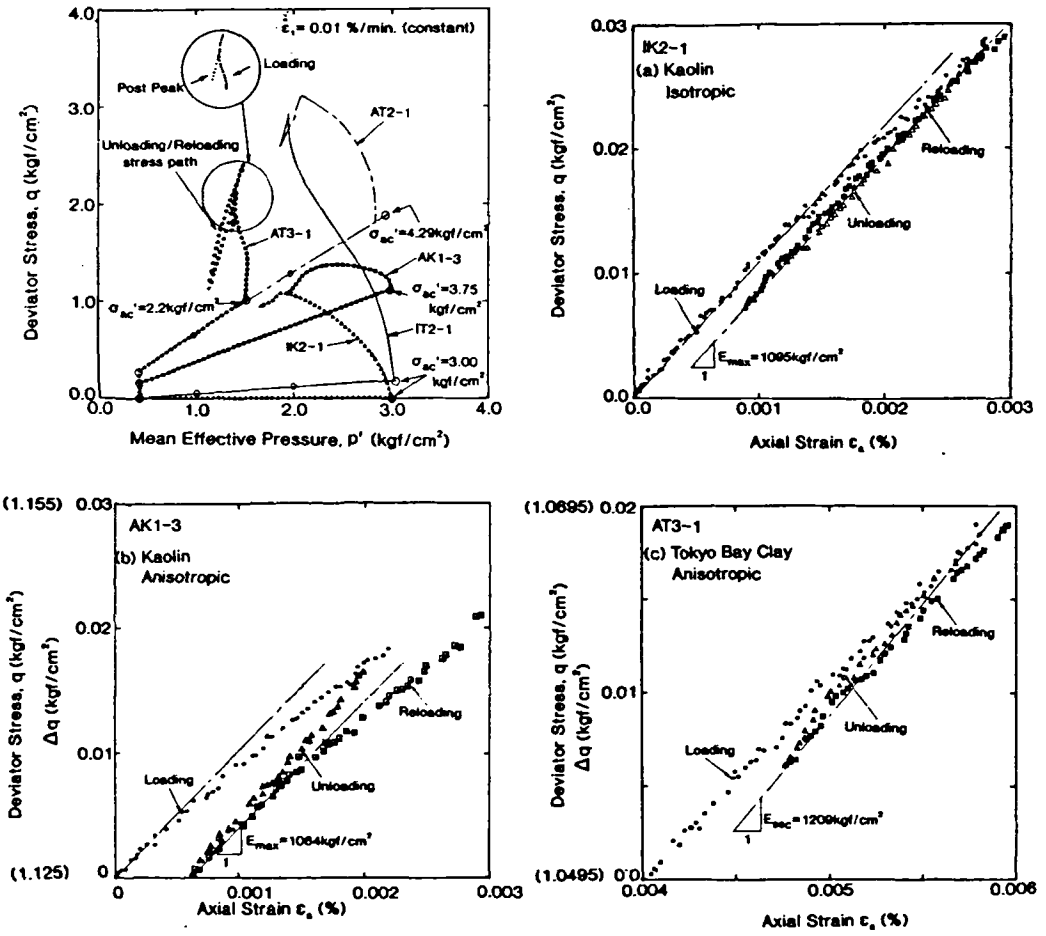

Figure 2.7 - Reconstituted kaolin and undisturbed Tokyo Bay clay stress-strain response after various imposed triaxial stress histories (Mukabi *et al.*, 1991)

at small values of deviatoric stress and axial strain level, the secant stiffness measured from tip to tip of the unloading-reloading cycles is the same as the initial loading stiffness. This is strong evidence for a kinematic zone surrounding the current stress point within which the behaviour is truly elastic (e.g. Jardine *et al.*, 1991; Jardine, 1992).

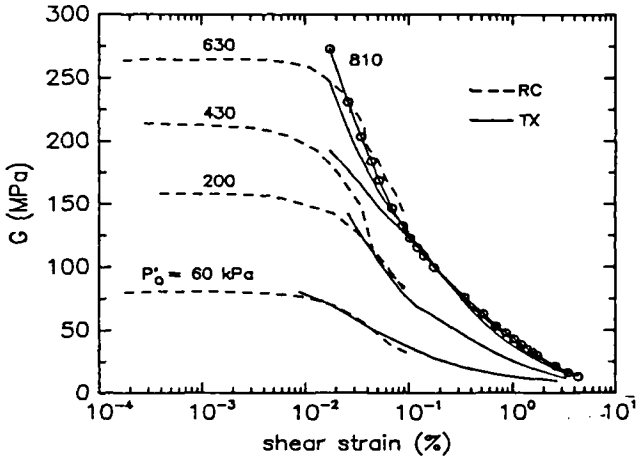

Figure 2.8 - Very small and small strain shear stiffness of Vallericca Clay measured in dynamic and static tests (Burghinoli *et al.*, 1991)

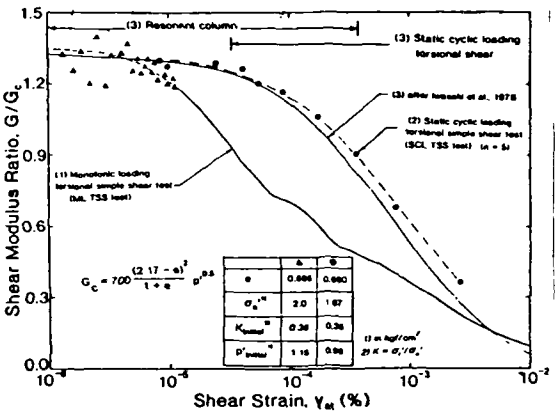

Figure 2.9 - Very small and small strain shear stiffness of Toyoura sand measured in dynamic and static tests (Tatsuoka and Shibuya, 1992)

An aspect of elastic behaviour connected with fully recoverable behaviour is that the soil should not exhibit any memory of the experienced deformation, implying a rate independent response (Shibuya *et al.*, 1991a; Burghinoli *et al.*, 1991). A stiffness independent of loading rate suggests that the response recorded in dynamic tests should be the same as in monotonic tests at equivalent stress and strain states. Figure 2.8 compares triaxial test and resonant column test data. Although the triaxial data is limited to a minimum strain of 0.01%, the stiffness curves coincide at the maximum level recorded in the resonant column test; at higher strains the stiffness in both tests falls but the cyclic stiffness is greater. In Figure 2.9 a comparison of secant stiffnesses is made between dynamic resonant column data and low strain rate cyclic torsional simple shear and monotonic torsional simple shear tests for Toyoura Sand. At strains of less than 0.001%, the dynamic and static test results coincide suggesting that, at this strain level, the rate of deformation is unimportant. The point where the monotonic torsional simple shear and the resonant column data separate could be taken as the limit of elastic behaviour. The applicability of the resonant column derived stiffness ratio is not assured beyond the very small elastic limiting strain, however, since the interpretation assumes a linear elastic soil response (Isenhower, 1979). Nevertheless, the results suggest that stiffness is greater at faster rates of strain beyond the limit of elastic behaviour. The effect of strain rate at very small strain levels for a clay is shown in Figure 2.10 in which triaxial compression tests on kaolin were carried out for axial strain rates varying over 2 orders of magnitude between 0.002%/min and 0.5%/min. Again these are monotonic tests with additional small unload-reload loops. For all strain rates the elastic threshold is passed at the first unload-reload cycle but the proportion of recoverable strain was greater for the higher strain rates. The 0.002% axial strain/min result particularly shows a large amount of irrecoverable plastic straining. The interpreted deviatoric stiffness is shown in Figure 2.12 against axial strain rate for both isotropically and

anisotropically consolidated specimens. The very small strain stiffness is unaffected by strain rate. However, at the small and intermediate strain level (0.001-0.1%) the stiffness is apparently affected by the strain rate. The effect is greater at small strains than at intermediate strains, and more pronounced for isotropic than for anisotropic consolidation.

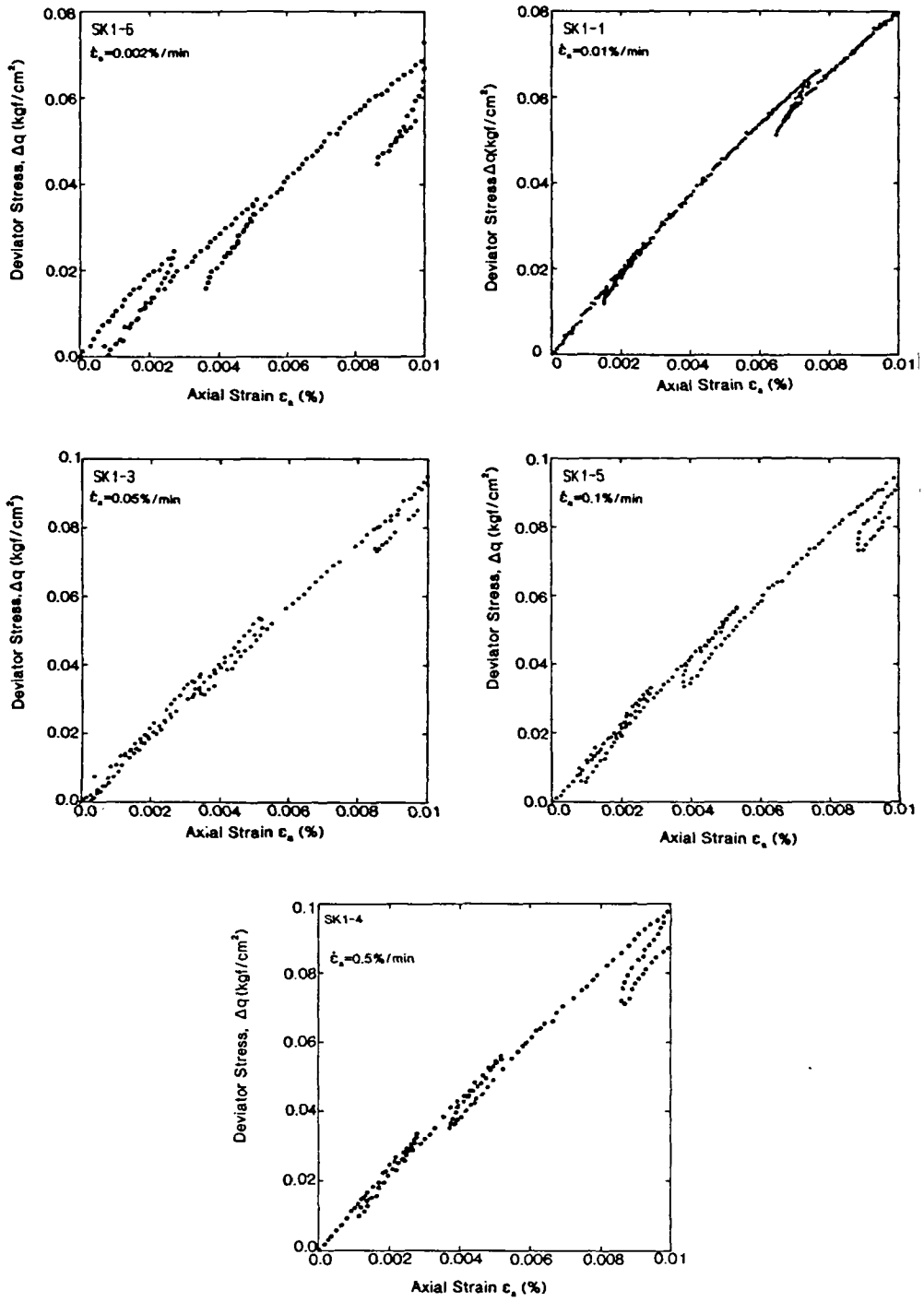

Figure 2.10 - Influence of strain rate on the stress-strain response of anisotropically normally consolidated kaolin (Tatsuoka and Shibuya, 1992)

Tatsuoka and Shibuya (1992) introduced the concept of the elastic limiting line to show the influence of strain rate on elastic deformation properties. Shown schematically in Figure 2.13, it requires that the limit of recoverable behaviour increases with increasing strain rate, although the concept of an elastic region breaks down for very small rates of straining where creep strains are significant (Figure 2.10(a)). The influence of strain rate on an undrained torsional simple shear test on anisotropically consolidated kaolin is shown in Figure 2.11. Following a constant small rate of strain (0.004%/min), the loading was halted and the specimen continued to strain at constant shear stress. For very slow rates of loading, the residual strain rate reduces to a value similar to the residual irrecoverable creep strain, and consequently the concept of a recoverable strain is not tenable.

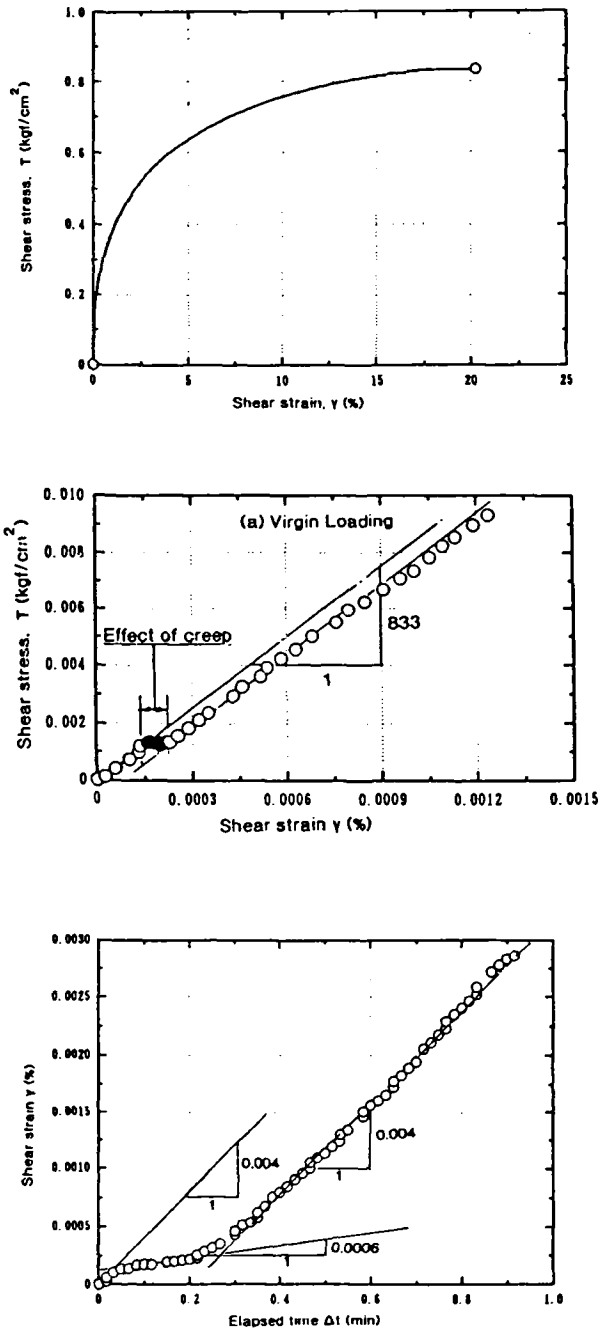

Figure 2.11 - Stress-strain and strain-time relationships showing the effect of creep in an undrained torsional simple shear test on kaolin (Ampadu, 1991)

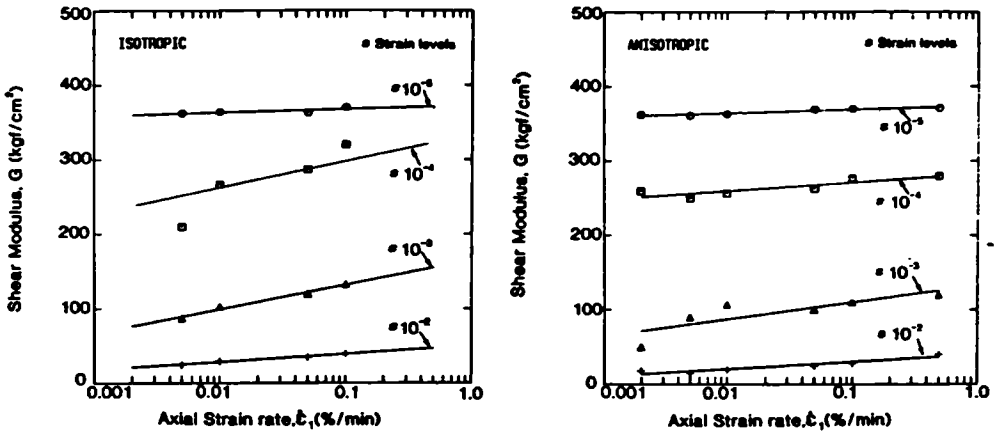

Figure 2.12 - Influence of strain rate on the secant Young's modulus of anisotropically and isotropically normally consolidated kaolin (Mukabi *et al.*, 1991b)

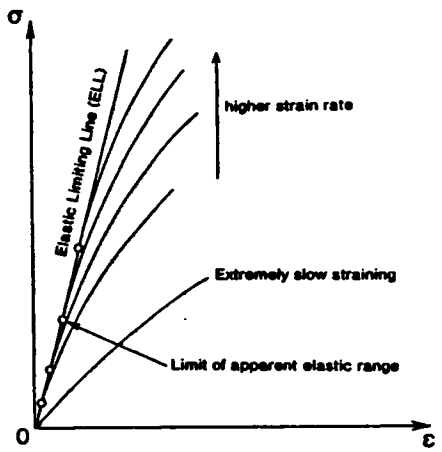

Figure 2.13 - Concept of the elastic limit line (Tatsuoka and Shibuya, 1992)

To date, the investigation of the very small strain region under static loading conditions has only been carried out by a few researchers outside Japan. Recently, however, modifications and developments in equipment have allowed the required order of magnitude improvement in stress and strain measurements at a number of laboratories and further research into this area is anticipated (Lo Presti *et al.*, 1993; Jamiolkowski *et al.*, 1994; Stallebrass, 1994; Lo Presti *et al.*, 1995). The minimum requirement for small strain testing must therefore be considered to be the accurate resolution of strains to 0.0001%, and stresses to 0.1kPa (see, for example, Figure 2.14).

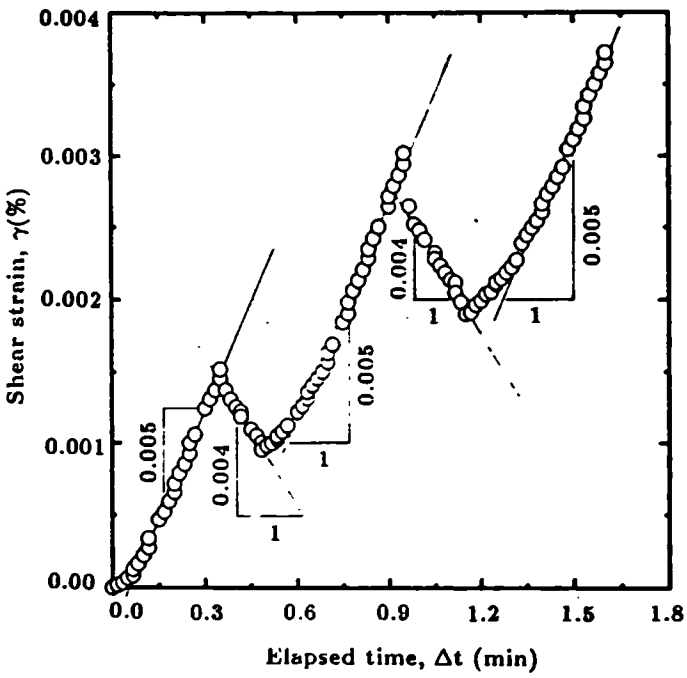

Figure 2.14 - Degree of control attained for very small unload-reload loops (Ampadu and Tatsuoka, 1993)

2.4.2 Small strains

Beyond the very small strain region, from small to intermediate to large strains, the stiffness falls dramatically, possibly by over an order of magnitude. The non-linearity of stiffness in the small-intermediate strain range has been shown for many soil types and by many authors and its importance in soil deformation response in undisputed (see section 2.3). It was recognised under dynamic loading as the reduction in shear modulus with dynamically applied shear strain (e.g. Iwasaki *et al.*, 1978) before the improvement of strain measurement techniques revealed a similar pattern under static loading conditions (see section 2.5.2). Much of the early work concerning the non-linearity of stress-strain relations was carried out in connection with London Clay and was pioneered at Imperial College (Webb, 1966; Som, 1968; Atkinson, 1973a). Interest increased significantly with the advent of local strain measurements (see section 2.5.2) and the accurate measurement of small strains allowed the production of the S-shaped stiffness curves on a logarithmic strain scale typical of dynamic measurements. The development of measurement techniques also led to the comparison of field and laboratory stiffnesses (Jardine *et al.*, 1985a). This showed that the stiffness parameters were similar in each case, allowing the laboratory derived measurements to be applied in a predictive way (Jardine *et al.*, 1986).

Strain is typically plotted on a logarithmic scale to show the important small strain behaviour region in greater detail. To compare stiffness parameters obtained under various test conditions, a normalising parameter is used. The common parameter is the peak undrained shear strength, c_u. Although the peak undrained shear strength is an easily determined parameter, its use adds a degree of ambiguity to the interpretation, since its value is dependent on such factors as the specimen size and testing rate (Jardine *et al.*, 1984). For stiff soils, the factors that influence the undrained shear strength, such as dilatancy and the presence of fissures, are likely to have less effect on the soil stiffness at small strains (Simpson *et al.*, 1981; Costa-Filho, 1984). Alternative, more fundamental normalising parameters are the initial effective mean normal stress, p'_o, (Wroth, 1971; Atkinson, 1973a) or the product of specific volume and the initial effective mean normal stress, vp'_o, (Atkinson, 1975; Richardson, 1988). O'Brien *et al.* (1992) compared the choice of normalising parameters for a number of stiff clays and weak rocks and concluded, as shown in Figure 2.15, that vp'_o was the most fundamental normalisation parameters since it reduced the scatter between tests on the same specimen by the greatest amount.

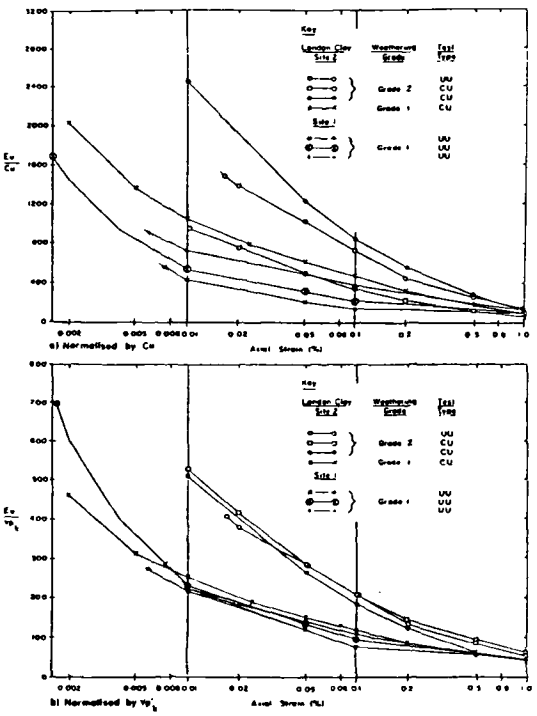

Figure 2.15 - Comparison of normalisation procedures for London Clay (O'Brien *et al.*, 1992)

One of the most significant influences on the non-linear stress-strain characteristics has been found to be the previous stress history imposed on the soil. Jardine *et al.* (1984) carried out a series of small strain tests on a low plasticity clay from the North Sea with comparative tests on

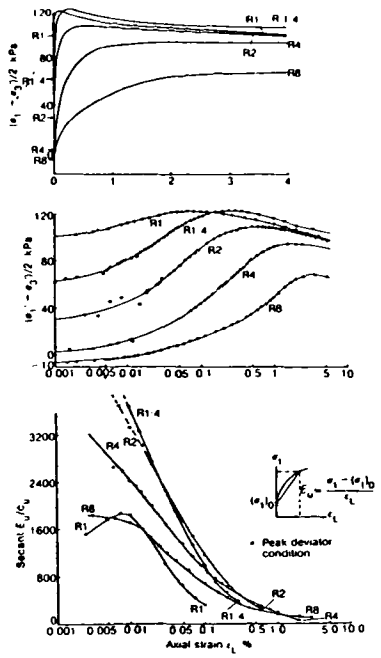

Figure 2.16 - Stress-strain and stiffness response of lightly overconsolidated North Sea Clay (Jardine *et al.*, 1986)

Stress path	p'_o (kPa)	c_u (Pa)	$\frac{E_{u0.1}}{p'_o}$	$\frac{E_{u0.25}}{p'_o}$	$\frac{E_{u0.5}}{p'_o}$	$\frac{E_{u0.25}}{c_u}$
1	214-351	280-397	362	247	178	204
2	325	317-390	503	321	204	301
3-4	325	322-355	297	215	195	206
5	325	340-355	683	444	395	509

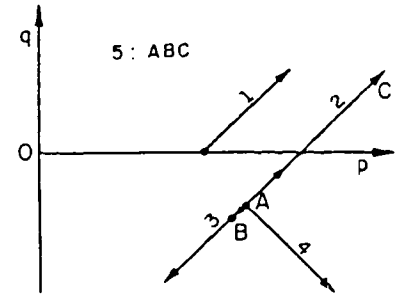

Figure 2.17 - Influence of stress history on the non-linear stress-strain characteristics of London Clay (Costa-Filho, 1986)

Ham River Sand, London Clay and Intact Chalk. The stress-strain and stiffness characteristics of the North Sea Clay specimens is shown in Figure 2.16. They found that the small strain region extended to approximately 0.1% axial strain, at which point a marked drop in stiffness occurred. All samples tested showed a non-linear response but the degree of non-linearity was greatest for normally consolidated specimens. For the clays, the degree of linearity increased with overconsolidation ratio, with the most linear behaviour recorded for intact specimens of heavily overconsolidated London Clay reconsolidated to estimated *in situ* stresses. The most linear behaviour of all the samples was recorded in the tests on the intact cemented chalk specimens. In such specimens the fall in stiffness at small strains is reduced due to the stronger interparticle bonding.

A significant early contribution to understanding the undisturbed behaviour of London Clay was made by Costa Filho (1986) who reviewed a number of aspects of the undisturbed material behaviour that could possibly influence the deformation characteristics. A bonded structure could have resulted from the previous high magnitude of sustained loading leading to diagenetic bonding (Bjerrum, 1967), evidence of which was provided by tensile tests on intact material (Bishop and Garga, 1969). It was also suggested that the presence of fissures would have relatively little influence on the consequent small strain behaviour as long as they remained closed (Costa-Filho, 1984). Costa-Filho (1986) carried out a series of laboratory tests on specimens of London Clay which had been trimmed from block samples. Local strain measurements were made although the measurement accuracy was only ±0.005% up to 0.05% axial strain. The tests investigated the influence of stress path direction on the stiffness response after reconsolidation to *in situ* stresses. The imposed total stress paths and the resulting stiffness response at specific axial strain values are shown in Figure 2.17. These results show both the influence of reinstatement of *in situ* stresses and the influence of stress path direction. After being anisotropically reconsolidated to the estimated field stress level the stiffness upon compression loading was higher than for the specimens sheared from an initially isotropic state of stress. Costa-Filho compared this situation to that occurring for a soil element

that had not suffered significant reloading after geological unloading and was subsequently situated under a footing or raft foundation or in the sides of an excavation. In contrast, an element of soil at the base of an excavation, although showing a non-linear response was not as stiff as the equivalent compression loading. The effect of a sharp change in stress path direction (stress path 5 in Figure 2.17) simulating a plate loading test at depth produced the stiffest initial behaviour and extended the high stiffness region to greater stresses. Costa-Filho concluded that whenever there was a change in the stress path direction, an increase in stiffness of the material was to be expected.

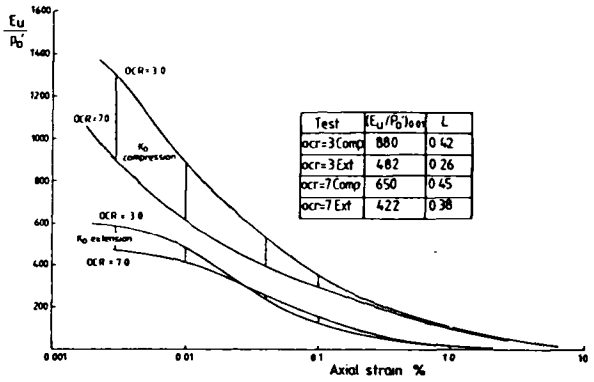

Figure 2.18 - Stress-history influencing the small strain stiffness of London Clay in compression and extension (Jardine *et al.*, 1985b)

Jardine *et al.* (1985b) also reported a stress history effect for specimens of reconstituted London Clay that were one-dimensionally consolidated and swelled to various overconsolidation ratios. Subsequent undrained compression and extension tests showed the stiffness in compression (following a change in loading direction) to be approximately 50% higher than that in extension (following a continuation in the loading path) as shown in Figure 2.18.

Jardine *et al.* (1991) described a series of constant p' stress paths for increasing and decreasing q for a series of consolidation paths, and on a variety of intact and reconstituted London Clay specimens (see Figure 2.19). The influence of stress history was quantified as the ratio of undrained tangent stiffness at 0.01% in both compression and extension $[(E_{u_{0.01}})_c / (E_{u_{0.01}})_e]$. They found that the undrained Young's Modulus ratio (and, similarly, the bulk modulus ratio)

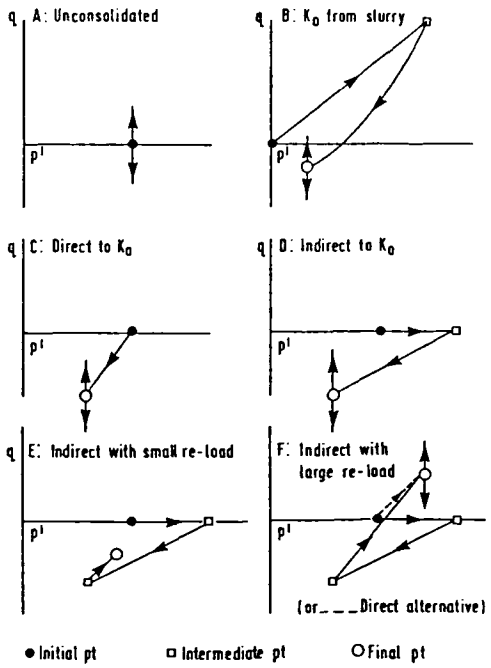

Test Series	Consolidation Path	$\frac{Eu_{0.01}c}{Eu_{0.01}e}$	$\frac{Eu_{0.01}(c+e)}{p'}$
(1) Means, 3 sites, thin-wall samples	A	1.67	1000
(2) Reconstituted, K_0 consolidated $OCR=7$	B	2.52	1480
(3) Bell Common (means), Hellings (1988)	C	1.40	1545
(4) Whitefrairs (means)	E	1.59	1435
(5) Lambeth (means)	F	0.79	1565
(6) City of London (means)	E/F	0.75	1330

Figure 2.19 - Ratio of Young's modulus in compression and extension for London Clay with various consolidation histories (Jardine *et al.*, 1991)

depended heavily on the final consolidation path. It may be noted that for cases A-D shown in Figure 2.19, the soil is stiffer in compression than in extension. This is also true in case E where the final reloading path is relatively short. For case F, however, the response is stiffer for extension loading. Hight *et al.* (1985) noticed that the specimen stiffness response depended not only on the consolidation history, but also on the holding period at constant stress before the new stress path was applied, and on the rate of loading along this path.

Jardine (1985) identified (in stress space) three regions of specimen response to stress change from a comprehensive series of cyclic tests on a low plasticity clay. Beyond the very small strain elastic region (zone I) discussed in section 2.4.1, lies zone II, representing the region in which the behaviour is non-linear and hysteretic although complete unload-reload cycles form closed loops. The hysteresis implies that there is energy dissipation but the plastic straining is said to be the result of small-scale yielding at inter particle contacts. Such straining may be termed 'resilient' after O'Reilly and Brown (1992). The limit to this zone is the point at which

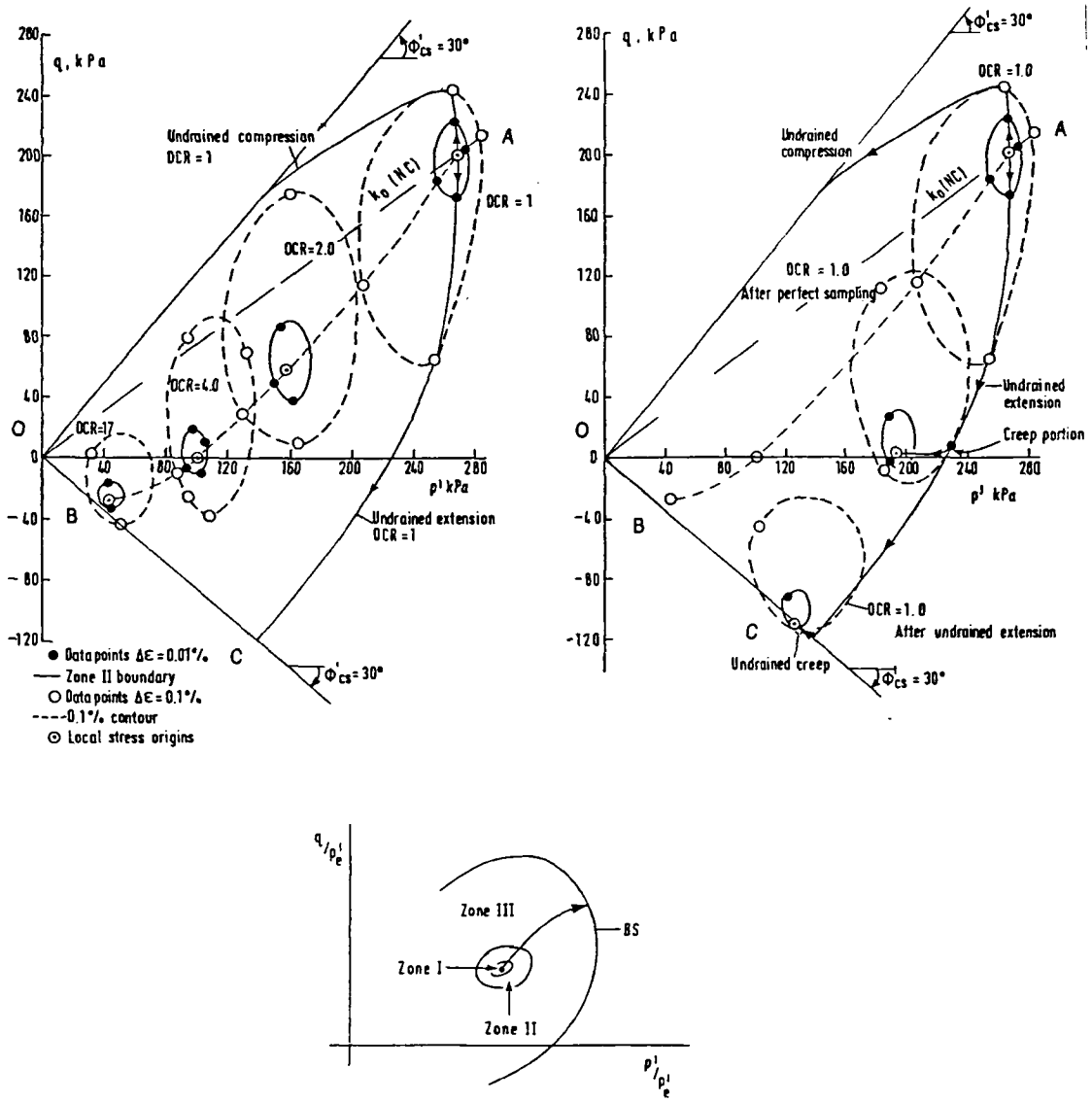

Figure 2.20 - Contours of strain describing qualitative changes in fundamental material stress-strain behaviour (Jardine, 1985; 1992)

irrecoverable strain develops and unload-reload loops are no longer closed. The physical explanation for this behaviour is that the small scale interparticle yielding has developed sufficiently to allow the particles to freely move past each other. As straining continues, large scale changes in particle orientation take place and the response may be dilative or contractive as the boundary surface is intercepted. Jardine carried out a series of stress probing tests on specimens of Magnus Till subjected to a common stress history to determine the limiting strain for each of the zones of behaviour defined above and strain contours associated with each of these tests are shown in Figure 2.20. In this figure, path OA represents the one-dimensional sedimentation, normal consolidation, and equilibration at point A. From point A, the specimen was either unloaded one-dimensionally to point B, or unloaded by undrained removal of deviator stress followed by equalisation to point C. Strain contours are shown, derived from stress probes carried out from points after either one-dimensional swelling or undrained extension. A holding period after undrained extension allowed undrained creep strains to reduce to insignificant levels. To rigorously define these zones, extended series of cyclic probing paths are required, and the zone boundaries in these figures represent nominal values and not necessarily strict boundaries. It is clear from these figures that the deformation response is dependent on the stress increment direction relative to the previous applied stress path, and that the zones of material behaviour translate with the current stress path. This kinematic nature of soil stiffness was suggested by Skinner (1975) and has proved to be a powerful concept for both the experimentalist and the numerical modeller (see section 2.7).

Burland and Georgiannou (1991) investigated the small strain behaviour of clayey sands by plotting contours of incremental strain energy as shown in Figure 2.21 (for a definition of strain energy, see section 2.7). The stress state and history dependent behaviour of the soil is apparent in this case also since the contours are not symmetrical about the initial stress point, but rather

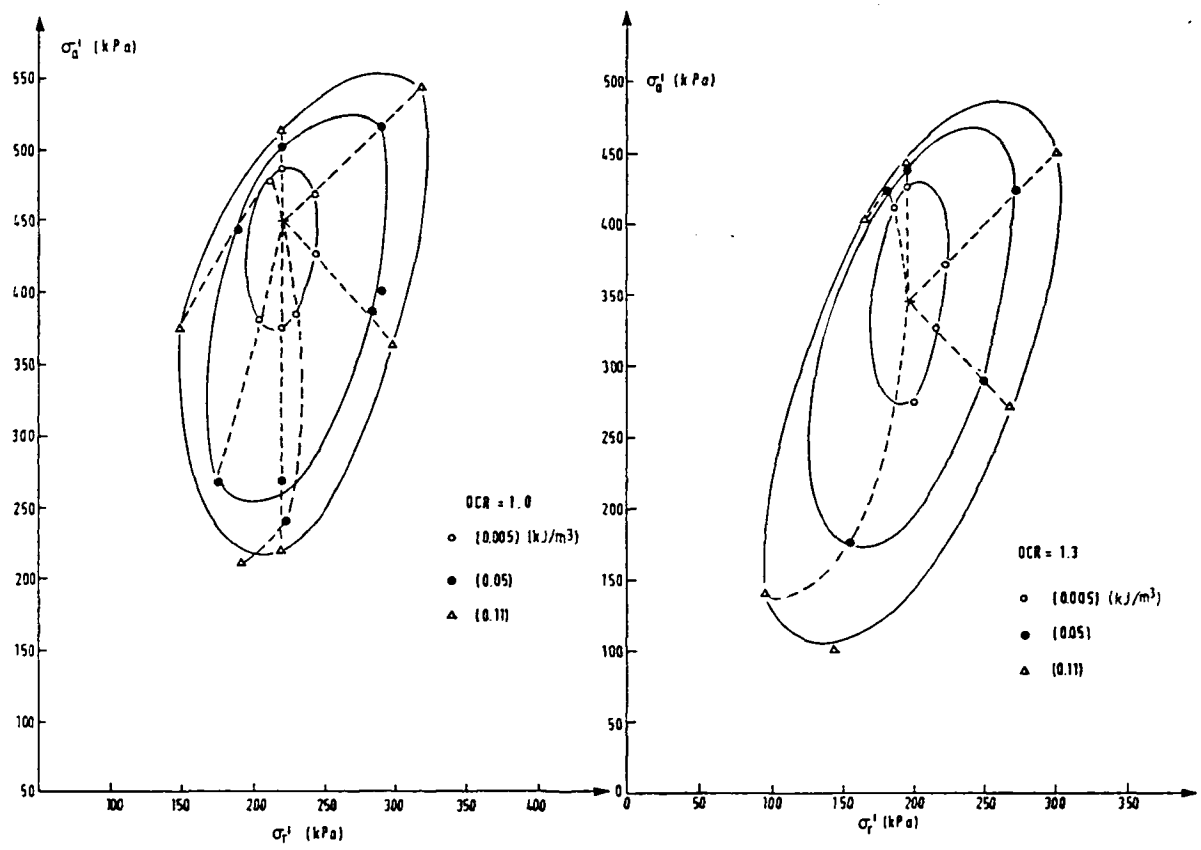

Figure 2.21 - Contours of strain energy describing small strain anisotropy (Burland and Georgiannou, 1991)

bunched in the direction of the closest yield surface. It can be noted, however, that the inner contour (0.005kJ/m^3) is more symmetrical about the stress origin than the contours of higher strain energy. This would suggest that the very small strain response is less affected by the recent stress history than the small to intermediate strain response. This is indicative of the behaviour at this strain level being generally more recoverable (elastic) than irrecoverable (plastic). The size and orientation of the strain energy contours are discussed in section 6.4.10, but it is clear that elliptical contours in principal stress space indicate anisotropy in the response. When the ellipse is elongated with the major axis vertical the material is stiffer in the vertical direction than in the horizontal direction. For a heavily overconsolidated deposit, it would be expected that the soil would be stiffer horizontally and in such cases the major axis of the ellipse would be horizontal. The relatively symmetrical shape of the inner elliptical contour is consistent with a cross-anisotropic elastic nature (see sections 2.2 and 6.4.10).

In plotting strain contours of the type discussed above, both Jardine (1985) and Georgiannou (1988) appreciated that the size and shape of the contours were dependent on the transient aspects of the testing procedure e.g. the rate of loading and the duration of the initial holding period at constant stress before imparting a subsequent change. Georgiannou noticed an increase in size of the inner yield locus with duration of holding period, and attributed this to the development of interparticle bonds in an ageing process. Such an ageing process may be chemical or mechanical (Schmertmann, 1991) to produce a similar effect. Hight *et al.* (1987) commented on the same effect and noted that slowing down the rate of strain produced the opposite effect i.e. reduced size of the yield loci. This highlights the need for a standardised testing procedure to eliminate the effect of these factors in relative terms (Jardine, 1992).

A considerable contribution to understanding the effect of recent stress history on soil response was carried out by Atkinson and his co-workers (Atkinson, 1973a; Richardson, 1988; Stallebrass, 1990a; Böese, 1992). Simpson *et al.* (1979) thought it useful to quote Atkinson:

> "... where a delay at constant stress state is involved or where the direction of the stress probe differs from the previous stress path the strain produced by a small stress increment may be very much smaller than the strain produced by a large increment or those where there was no rest period or where the direction of the stress probe did not deviate much from the previous loading path. This apparent stiffening of a soil may be likened to a threshold effect; that is to say that there exists a threshold of the probing stress increment below which the soil is apparently very much stiffer than for a larger probe." Atkinson (1973a)

Atkinson was commenting on early work by Som (1968) and Lewin (1970), although perhaps the most significant experimental investigation was carried out by Richardson (1988), whose work was continued by Stallebrass (1990a). Again, realising the rate dependence of the threshold effects, the majority of these tests were carried out with these factors held constant. To investigate the effect of recent stress history, stress paths of the sort shown in Figure 2.22 were carried out. From a common starting point, O, a variety of approach paths were employed to investigate the effect of the rotation in the stress path upon the subsequent stress-strain

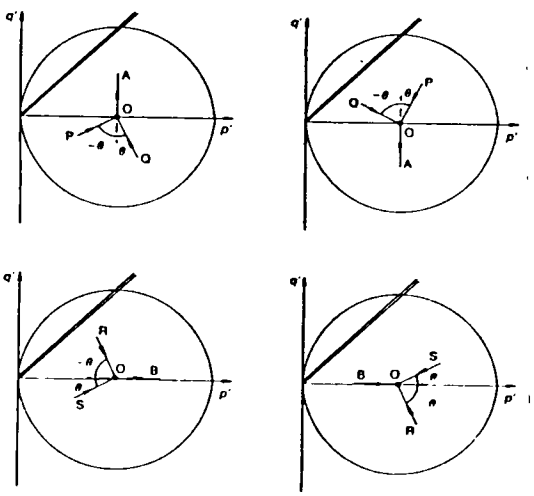

Figure 2.22 - Constant p' and constant q stress paths used to investigate recent stress history effects (Atkinson *et al.*, 1990)

strain level. At large strain the deviatoric stiffness tends to zero as failure is approached, and the volumetric stiffness tends to finite values corresponding to isotropic normal compression or isotropic normal swelling. However, in the small strain region, the stiffness is directly associated with the degree of rotation of the stress path. Relative to the approach path, a direct reversal produces the stiffest response, a continuation path produces little change in stiffness, and a ±90° turn produces an intermediate change in stiffness. The small strain deviatoric stiffness is shown in Figure 2.24 to vary almost linearly with the angle of stress path rotation, whereas the large strain stiffness is unaffected. Figure 2.25 shows that the increase in stiffness for the 180° reversal compared to that for a continuation path also increases with the plasticity index. The strain paths also reveal fundamental differences in the type of behaviour following different path rotations. For constant p' type stress paths, the volumetric response of the specimens is the same as for the previous stress path, such that if the specimen was swelled isotropically, the specimen would continue to dilate during a constant p' stress path with increasing q. Conversely, if the specimen was compressed isotropically, the specimen would continue to compress during a constant p' stress path with increasing q. For constant p' stress paths with decreasing q, the effect is not as marked although there is relatively more dilation with a swelling constant q path preceding it. Stallebrass (1992a) found that the strain paths on undisturbed material were different with different stress path rotations. However, the pattern of behaviour was not clear, and was not consistent with that observed for the reconstituted material with a much lower overconsolidation ratio.

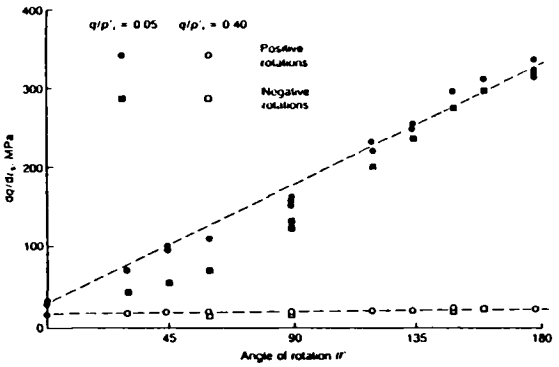

Figure 2.24 - Influence of degree of rotation on the deviatoric stiffness (Atkinson *et al.*, 1990)

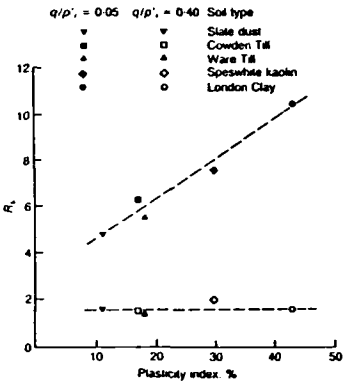

Figure 2.25 - Influence of plasticity on the deviatoric stiffness following a change in stress path direction (Atkinson *et al.*, 1990)

A similar stress history effect to that described above for clays has also been observed for sand as shown in Figure 2.26. This shows the imposed stress paths and the resulting deformation behaviour of specimens of Toyoura sand following anisotropic compression at various stress ratios followed by an increase in the axial stress at constant radial stress. The stress-strain curves show that the lower the anisotropic consolidation stress ratio (and hence the degree of stress path rotation) the greater the subsequent stiffness of the initial stress increment. It should be noted that the vast majority of work carried out investigating the recent stress history of soil has been performed on reconstituted or remoulded material and at constant holding periods. Stallebrass (1992) noted that further work was required to investigate the effect of recent stress history on soil samples that have been compressed to very high preconsolidation pressures. The present work provided an opportunity to investigate stress history effects on just such a material.

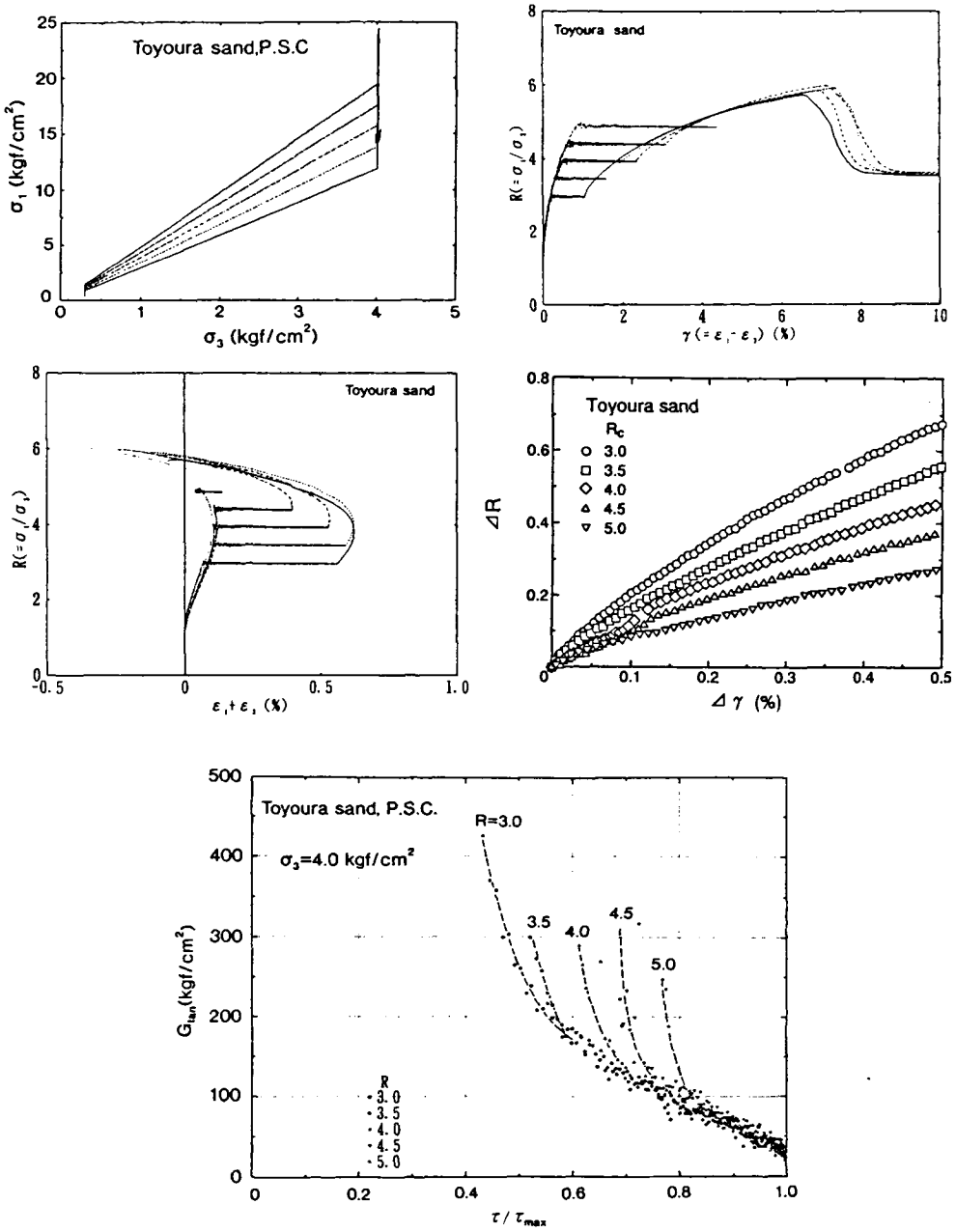

Figure 2.26 - Observation of the recent stress history effect in Toyoura Sand (Tatsuoka and Kohata, 1995)

2.5 Triaxial testing apparatus

2.5.1 Development of the stress path cell

The triaxial cell is perhaps the most used apparatus for deriving stress-strain relationships for soil. The development of the hydraulic triaxial stress path cell (Bishop and Wesley, 1975) represented a significant advance in testing capabilities. This cell allowed a far wider range of stress paths to be followed than in the conventional testing apparatus, in which the cell pressure usually remained constant.

The extensive use of the stress path apparatus has led to numerous improvements to the original design allowing a greater degree and ease of control. Of particular relevance was the addition of computer control, responding to feedback from the cell and the specimen. This, for example, facilitated K_o compression and swelling tests.

2.5.2 The development of local instrumentation

The development of local instrumentation for soil specimens (recording axial deformation directly from the soil specimen as opposed to between the endcaps or from the loading ram) was initiated more than twenty years before the importance of the small strain behaviour of soil was realised. The first local measurements involved the use of a vernier telescope or cathetometer (Bishop and Henkel, 1962) in which the vertical movement of marks on the specimen top cap or on the specimen itself could be recorded from outside the cell. This technique was developed for recording the strains in a conventional triaxial cell during isotropic consolidation. Another early method involved the use of the Demec type strain gauge (Head, 1985) which consisted of an invar bar located at its pinned gauge points into supporting discs that were attached directly to a triaxial specimen. The relative movements of the two points were recorded with a standard dial gauge requiring the cell to be filled with oil rather than water. The weight of the device limited its use to rocks, concrete and very stiff soils.

At a similar time, the need to measure strain in dynamic soil tests led to the development of a soil strain gauge (Truesdale, 1963; Keller and Anderson, 1964; Truesdale and Anderson, 1964) which was also applied to static loading tests, and specifically to the triaxial test (Truesdale, 1964; Truesdale and Schwab, 1966, 1967). The principle of the soil strain gauge is shown schematically in Figure 2.27. The strain sensor consists of

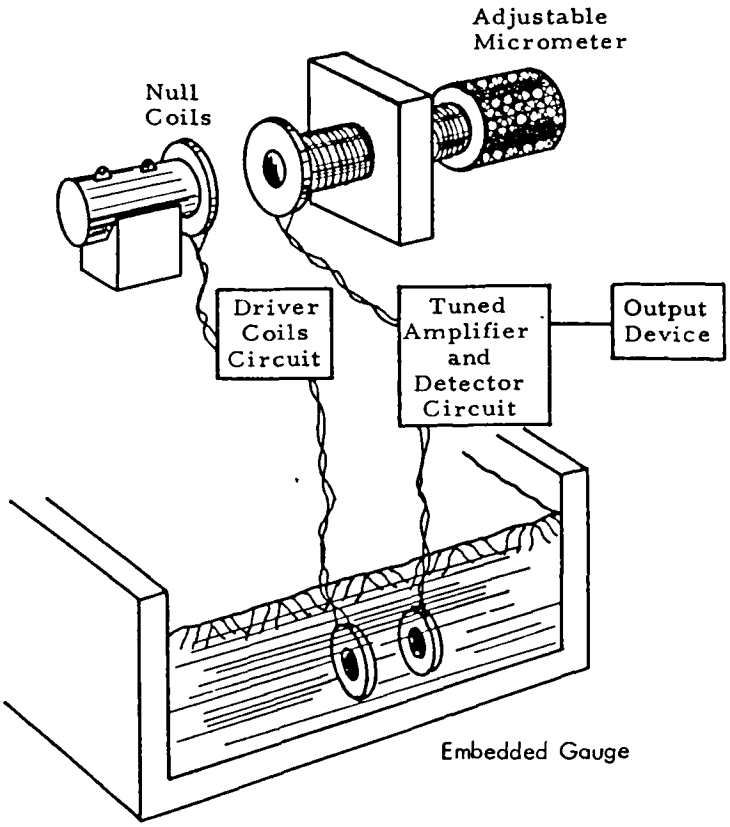

Figure 2.27 - The soil strain gauge (Truesdale, 1964)

two, mechanically uncoupled, flat disc coils of copper wire that are positioned opposite one another and embedded within a soil specimen. Each of these coils is separately connected via an electrical circuit to similar discs remote from the specimen in an adjustable micrometer apparatus. One set of coils is powered by an AC voltage which causes an induced voltage in the second set of coils. The resultant induced voltage is zero when the spacing of the external coils is equal to that of the embedded coils. Static movements may therefore be detected by continually balancing the induced coil voltage and reading the micrometer.

The development of small strain measurement instrumentation specifically for the triaxial test has recently been reviewed by Scholey *et al.* (1995) and consequently will only be summarised here with additional comments where thought appropriate.

The application of the soil strain gauge to the triaxial test was motivated by the realisation that non-uniformities develop during a test due to the restraint imposed at the end caps (Balla, 1960; Rowe and Barden, 1964; Barden and McDermott, 1965; Kirkpatrick and Belshaw, 1968; Kirkpatrick and Younger, 1970). The investigation of these non-uniform strains led to the development of x-ray radiographic imaging techniques for soil testing. The technique involves placing a number of lead shot markers throughout a soil specimen during its preparation, whose movements are subsequently monitored on x-ray images of the specimen taken at intervals during the test. The radiographic technique was initially applied to plain strain testing of sands (Roscoe *et al.*, 1963; Arthur *et al.*, 1964) and subsequently to clays in one-dimensional consolidation tests (Burland and Roscoe, 1969) and later in triaxial tests (Balasubramaniam, 1976). A historical review of the radiographic technique was given by Bordeau (1993). The method is appealing in that it provides a visual impression of the soil deformation throughout the soil specimen giving a detailed impression of the response to loading. The obvious disadvantage, as with the soil strain gauge, is that the intrusive technique could not be applied to determine an undisturbed specimen response. The technique is also limited to the resolution at which lead show movement can be detected on an x-ray film; this is at best 0.1mm and results in axial strains of 0.05-0.1% being resolved for a 200mm long triaxial test specimen. It seems unlikely that, even if the system resolution could be improved, the technique will be developed further since the marker displacement record will always be discontinuous and suffers from several practical restrictions (Scholey *et al.*, 1995). The radiographic technique has, however, recently been used to complement more precise instrumentation (Tatsuoka and Kohata, 1995).

The local strain measurement devices listed above were basic and non-automated devices. The development of automated electronic instrumentation resulted in a significant expansion in the number of strain measurement devices. Initially, this involved the use of linear variable differential transformers (LVDTs). Local strain measurements progressed with the modification of the original K_o ring (Bishop and Henkel, 1962) by replacing the mercury null indicator with a displacement transducer (Nair and Chang, 1973; Brown and Snaith, 1974; Menzies, 1976). The principle of attaching circular collars to the specimen was subsequently adapted to also record axial strains in triaxial tests. Two circular collars (separate to that used to record radial strains) were fixed to gauge points which were targets embedded in the specimen. The body and armature of an LVDT were attached to the upper and lower collar respectively. Two LVDTs, similarly attached either side of a test specimen, have been used by numerous authors to record the average axial strain in the presence of tilting (Nair and Chang, 1973; Brown and Snaith, 1974; Boyce and Brown, 1976; Cole, 1978; Nataatmadja and Parkin, 1990, Salman, 1994). A later development in the use of LVDTs involved a support system which was attached to the triaxial cell body rather than to the specimen to reduce the weight acting on the specimen and to

minimise the effect of loss of verticality of the transducer during shearing (Daramola, 1978; Yuen *et al.*, 1978; Brown *et al.*, 1980; Costa-Filho, 1985). Costa-Filho achieved an accuracy of ±0.005% in the axial strain measurement at small strains. The errors incurred in these measurements were not only attributable to the system resolution but also to the barrelling and tilting of the specimens leading to non-coaxiality and, ultimately, jamming of the LVDT armature. Jamming of the armature can be prevented to some extent with the use of spring loaded armatures (e.g. Salman, 1994). The effect on the LVDTs of non-uniform specimen deformation is a recurring problem for such systems but their calibration is uncomplicated, producing a linear output, and for investigating the small strain behaviour of relatively uniform specimens, their use can still be recommended. Their resolution depends entirely on the electronic system in which they are incorporated (as described later in section 5.4.7) and given a suitable system they are capable of accurately resolving strains to 0.0001% (Stallebrass, 1994). Typical configurations for the use of LVDTs are shown in Figure 2.28.

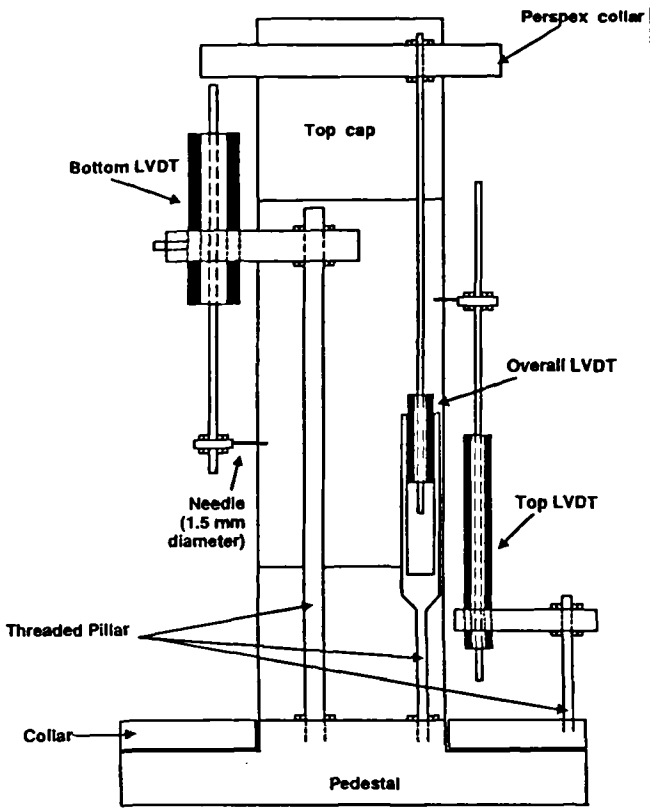

Figure 2.28 - Measurement of small strains using LVDTs (Costa-Filho, 1985)

Alternative early systems for measuring lateral strain included the use of strain gauged strips of stainless steel (El-Ruwayih, 1976), cast resin (Boyce and Brown, 1976), or foil wrapped around the specimen (Houlbec and Finn, 1969).

The awkwardness of the supporting rings and clamps necessary for measuring radial strain with LVDTs prompted an expansion in the use of proximity transducers for lateral deformation (Cole, 1978; Chamberlain, Cole and Johnson, 1979; Khan and Hoag, 1979; Brown *et al.* 1980; Dupas *et al.*, 1988; Hird and Yung, 1989). Proximity transducers have the advantage of being non-contacting and, therefore, do not impede the deformation of the soil. They are inductive devices relying on the interaction between a magnetic field generated by an AC voltage in a coil within the transducer, and a suitable target. A change in the target distance results in a measurable change in inductance caused by the circulation of eddy currents within the target. The choice of target material influences the resolution of the system, and the transducer design is generally optimised for a particular target material. Hird and Yung (1989) used magnetic stainless steel targets lightly glued to the membrane surface, although another type of target, consisting of a thin film of aluminium foil, is more generally used (Cole, 1978). Using a foil target allows any potential membrane penetration effects to be eliminated by placing the target directly onto the soil specimen. The rubber membrane is non-conductive and consequently does not interact with the magnetic field generated by the transducer. The use of a solid target,

however, ensures a plane surface. The influence of non-uniform deformation of a radial proximity target has recently been discussed by Shibuya *et al.* (1994).

Proximity transducer systems have also been developed to record axial deformation (Noma and Ishii, 1986; Hird and Yung, 1987, 1989; Dupas *et al.*, 1988). Examples of proximity transducer systems are shown in Figure 2.29(a)-(d).

A major limitation of the proximity transducer is its limited practical range of 2-5mm (larger range proximity transducers exist but their size prohibits their use in most soil testing apparatus). The response from the proximity transducer is non-linear, the resolution being greatest for shorter target distances. To achieve a sufficiently accurate record of the small strain displacement of the soil specimen, a further reduction in the range of the transducer must be expected. A significant development, therefore, involved mounting the axial and radial proximity transducers such that they were adjustable from outside the triaxial cell (Hajj, 1990; Hird and Hajj, 1995) as shown later in Figure 5.8. This allowed for the target distance to be easily adjusted during a test ensuring the maximum system resolution was always attainable. This system was inherited for the current research and is described in greater detail in Chapter 5.

Following the monitoring of vertical displacement adjacent to piles (Cooke and Price, 1973), axial strain measurement devices were developed at Imperial College based on electrolevel technology (Burland and Symes, 1982). These devices were refined for use with 38mm diameter specimens by Jardine *et al.* (1984) and have been used extensively since (Jardine *et al.*, 1985a, 1985b, 1986, Hight *et al.*, 1992). The device, shown in Figure 2.30(a), consists of two pivoting arms, hinged to support an electrolevel contained in a stainless steel capsule. As the specimen deforms, the electrolevel capsule tilts. The device produces a non-linear calibration relating vertical displacement to tilt. The electrolevel is also affected by overall tilting of the specimen but this is accounted for by mounting two devices on either side of the specimen. The device is attached to the soil specimen by gluing the pads to the specimen membrane and, although susceptible to membrane slippage, it was shown by Burland and Symes (1982) that significant slippage only occurs at large strains. Following experience gained through use, the system was substantially modified by Ackerly *et al.* (1987). This involved replacing the electrolevel capsule with a pendulum inclinometer, and redesigning the pivot mechanism as shown in Figure 2.30(b). These developments produced a more compact device less susceptible to non-uniform specimen deformation, while improving the resolution from ±0.001% to ±0.0005% for a conventional 38mm diameter triaxial specimen.

These inclinometer-type devices were the first to be able to accurately resolve to the small strain level continuously over a wide range of strain. Their use has been proved in numerous research and commercial projects which has resulted in their continued extensive use (for example Zakaria, 1994; Pennington, 1995).

A further development in local strain instrumentation was the Hall effect gauge developed at the University of Surrey (Clayton and Khatrush, 1986; Clayton *et al.*, 1989) and shown in Figure 2.31. The device relies on the output voltage produced when a semi-conductor moves within a fixed magnetic field. As the specimen strains relative movement of the semi-conductor and the magnet takes place and a change in voltage is recorded. To record radial strains, the same configuration is used but mounted horizontally, replacing the LVDT in the circular collar type devices described above. The range of the device is limited to either 2.5mm or 7mm for axial strain, and 1.5mm for radial strain, and is consequently unsuitable for large strains. The

system has been shown to be capable of resolving to 0.0014% for axial strains and 0.0028% for radial strains in a 100mm triaxial apparatus (Clayton *et al.*, 1992).

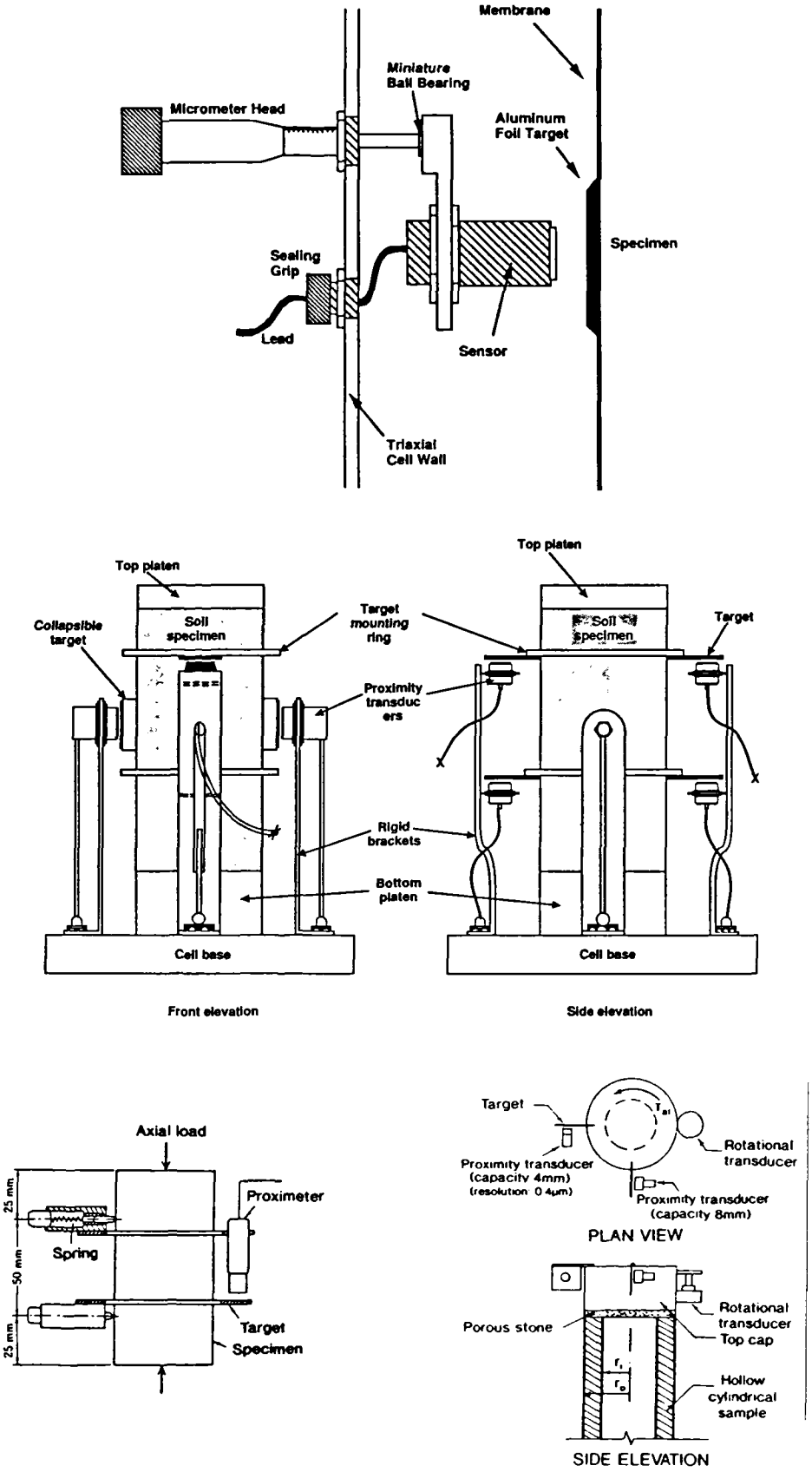

Figure 2.29 - Measurement of small strains using Proximity transducers (Cole, 1978; Noma and Ishii, 1986; Hird and Yung, 1989; Tatsuoka and Shibuya, 1992)

For the devices described above, the maximum attained working accuracy for strain measurements on 100mm triaxial specimens was at best 0.001% axial strain. It has been shown in section 2.4.1 that to record the full non-linearity of the soil response, a greater accuracy, to 0.0001%, is required. The local deformation transducer, developed at the Institute of Industrial Science, University of Tokyo, was the first employed in a triaxial testing system capable of

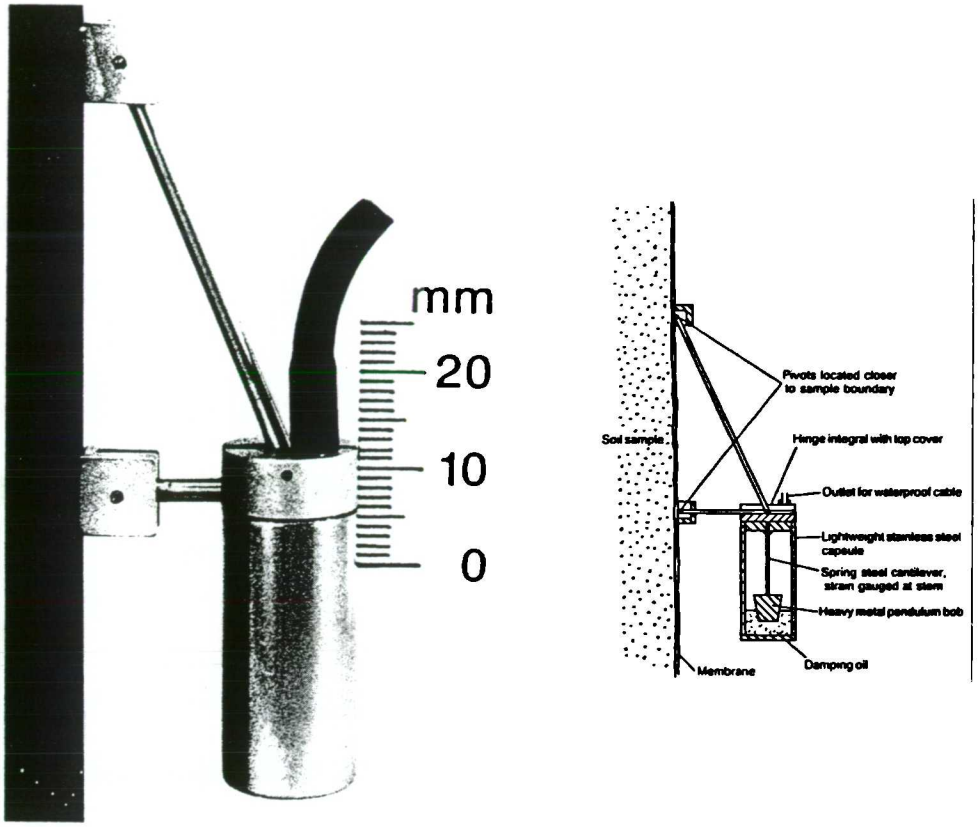

(a) (b)

Figure 2.30 - Measurement of small strains using electrolevel devices (Burland and Symes, 1984; Ackerly *et. al*, 1987)

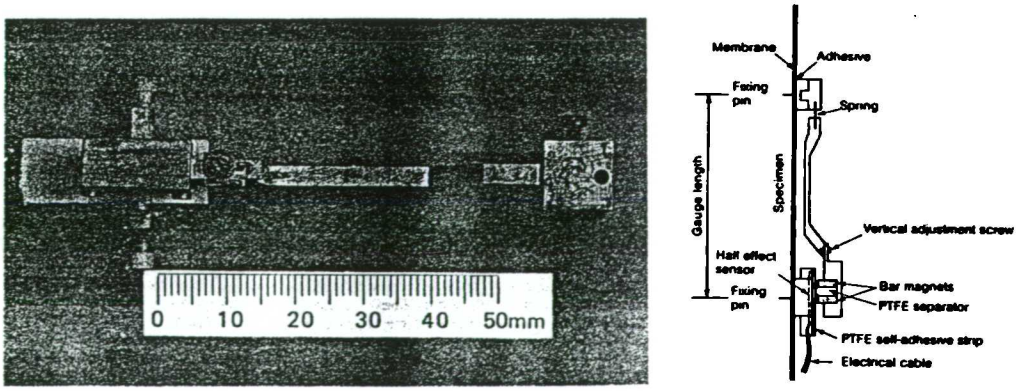

(a) (b)

Figure 2.31 - Measurement of small strains using hall effect devices (Clayton and Khatrush, 1986)

achieving this level of accuracy (Tatsuoka, 1988; Goto *et al.*, 1991). The device, shown in Figure 2.32, consists of thin, initially slightly bent, phosphor bronze strain gauged strips balanced between two pseudo-hinges attached to the specimen over the required gauge length. As the specimen undergoes axial deformation, bending strains develop in the strip and are recorded by the strain gauges. There is a direct, although non-linear, relationship between the output voltage due to bending and the relative movement of the two hinges. Although, in practice, the device has proved to be more difficult to use than first described (Scholey *et al.*, 1995), the results produced (see section 2.4.1 and Kim *et al.* (1994), for example) represent an order of magnitude improvement on any of the other devices described above. Its use is now spreading outside Japan (Jamiolkowski *et. al* , 1994; Dasari *et al.*, 1995).

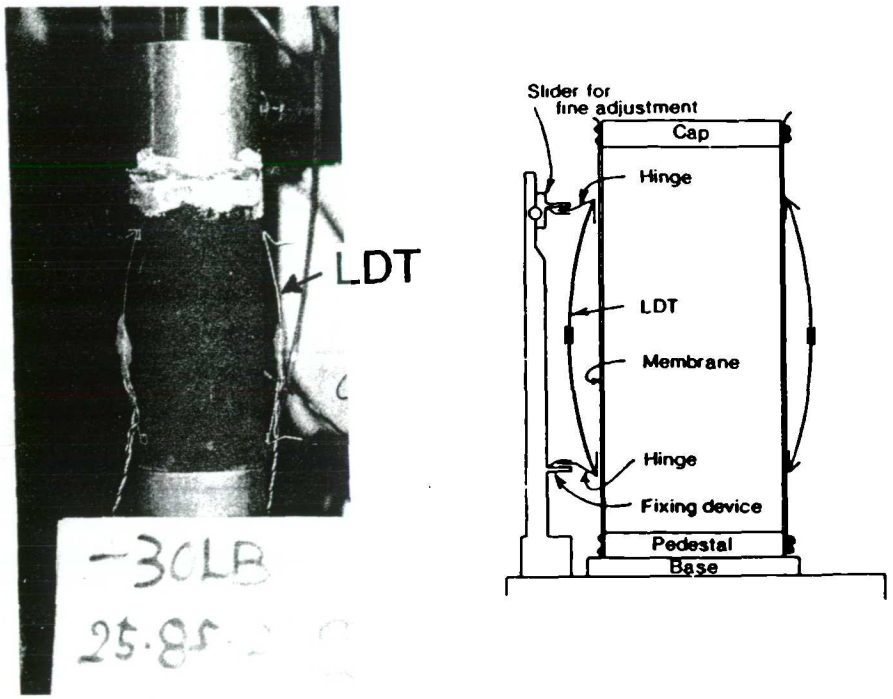

Figure 2.32 - Measurement of small strains using local deformation transducers (Goto *et al.*, 1991)

2.5.3 Improvements in stress path testing and control

It must be remembered that the strain measurement device is only one contributor to the final accuracy of the measured stress-strain characteristic. The level of stress control must be appropriate to the level of strain measurement. If the pressure controller in a particular system is capable of controlling stress paths to within, say, ±1kPa, a soil deposit with an initial Young's modulus of 100MPa, will produce variations of 0.002% axial strain in the initial loading region. Consequently, it is improvement in the stress control rather than strain measurement that is the limiting factor in such a situation. Tatsuoka (1988, 1993) maintained the desired stress path in an otherwise strain controlled test by monotonically increasing or reducing the cell pressure. This testing method provided an accuracy less than that of purely strain controlled tests but greater than conventional stress path testing techniques.

The specification of the boundary of an elastic region for uncemented soils requires extremely accurate measurements for both stress and strain. To date, such quality of measurements has only been obtained by a few researchers. A comprehensive series of results was given by Tatsuoka and Shibuya (1992) who presented the results of several Japanese researchers at the University of Tokyo for a wide range of geomaterials. In these strain controlled tests a series of small unloading-reloading cycles was built into an otherwise monotonic loading path. To be

able to carry out such reversals, a novel system of gears and electromagnetic clutches was developed (Ampadu and Tatsuoka, 1989, 1993; Tatsuoka *et al.*, 1994) so that the direction of gear wheel rotation was constant even when the loading direction reversed. This reduced any backlash effect such that the smallest controllable shear strain was of the order of 0.0001%. In equivalent stress controlled tests, stress control is required to the order of 0.1kPa. The resolution of typical stress path triaxial instrumentation is within this range (see section 5.4.3). However, the control of pressures to such accuracy is not possible with conventional stepper motor technology which only allow pressures to be controlled to within approximately 1kPa (see section 5.4.8). For the small reversals in strain in a stress controlled tests, it is necessary to substantially increase the stress path control. Recently, attempts have been made to modify existing stepper motors to achieve a pressure change of 0.1kPa for a single step on a stepper motor (Pennington, 1995).

2.6 Dynamic soils testing

2.6.1 Introduction

In a dynamic soil test the rate of loading is typically several orders of magnitude greater than in a static test. The development of suitably accurate strain measurement in static tests, established that the stiffness non-linearity encountered at small strain levels was limited by a lower strain limit coinciding with the very small strains imposed in the dynamic tests ($\varepsilon_s < 0.001\%$). This led to a consistent representation of soil stiffness non-linearity from very small strains to large strains (see section 2.4.1).

Dynamic testing of soils in the field or in the laboratory provides fundamental information regarding the very small strain stiffness moduli. Evidence presented in section 2.4 strongly indicates that at these strain levels soil deformation is fully recoverable and, by definition, elastic. The *dynamic stiffness* may consequently also be referred to as the *initial elastic stiffness*. For example, the dynamic isotropic shear stiffness, G_{dyn}, represents the initial elastic shear stiffness at effectively zero strain, G_o.

2.6.2 Measurement techniques

Field measurement techniques have been reviewed by Yoshimi *et al.* (1977), Woods (1978), Atkinson and Sällfors (1991). They commonly involve down-hole and cross-hole wave propagation (Stokoe and Woods, 1972; Stokoe and Hoar, 1978; Woods, 1978; Robertson *et al.*, 1984; Sully and Campanella, 1995) and the analysis of surface waves by refraction surveys (Abbiss, 1981) or spectral analysis (Nazarian and Stokoe, 1984; Stokoe, 1989).

During the Elstow site investigation, field measurements were made using the cross-hole, down-hole, and seismic refraction survey techniques (see section 3.4.4). However, in the present work, the use of dynamic testing techniques is primarily connected with the experimental programme described in Chapter 5.

In the laboratory, probably the most common method of dynamic testing uses the resonant column apparatus (Richart *et al.*, 1970; Drnevich, 1977). In this test, torsional vibrations are applied to a cylindrical soil specimen whose shear modulus may be evaluated from the resonant harmonic frequency. Alternatively, the shear modulus may be determined from the record of free vibrations once excitation ends. In either case, the evaluation of G_o from the frequency response is not trivial (requiring system dependent calibration coefficients) and follows a linear elastic framework. The level of shear strain applied to the soil, inferred from the degree of

torque applied, may be varied precisely between 0.00001% and 1%. The accurate determination of shear modulus, however, is limited by the maximum shear strain at which linear elastic behaviour suitably approximates the true response (Isenhower, 1979), which is perhaps 0.001%.

A more recent development, which has received much attention due to its apparent simplicity, is the use of piezoelectric ceramics as a means of generating and receiving body waves. Piezoelectric materials deform when excited with an electric potential, and generate a voltage output when deformed. A detailed review of the physics of piezoelectric materials, their manufacture and their applications to geotechnical testing is given by Santamarina *et al.* (1991).

The operating principle of the bender element, or piezoceramic biomorph, is that when two piezoceramic films are rigidly attached to each other, the relatively small direct strain due to an applied voltage is converted into a significant flexural motion. The polarized films are aligned and their electrodes are attached such that, when a driving voltage is applied, one plate expands and the other contracts. Conversely, if the bender element deforms, an electrical signal is generated. A bender element test requires two bender elements aligned in a soil specimen, one acting as the transmitter and the other as the receiver. A driving voltage is applied to the transmitter element causing it to bend and apply a dynamic deformation to the soil. The resultant propagating wave is detected at the receiving element due to the electrical signal generated by the forced deformation.

The design may be optimised to provide the maximum efficiency in transmitting, or in receiving. The piezoceramics may be connected in series, as shown in Figure 2.33(a), or in parallel, as shown in Figure 2.33(b). A series connected bender element produces twice the deformation of a parallel connected element for the same input voltage and is therefore favoured as the transmitter. Conversely, a parallel connected bender element produces twice the electrical signal of a series connected element for the same mechanical disturbance and is therefore used as the receiver. The bender element, being a high impedance device, must be encased in a waterproof coating to prevent shorting if inserted into a saturated or partially saturated soil specimen. A typical preparation and mounting of a bender element is shown in Figure 2.34.

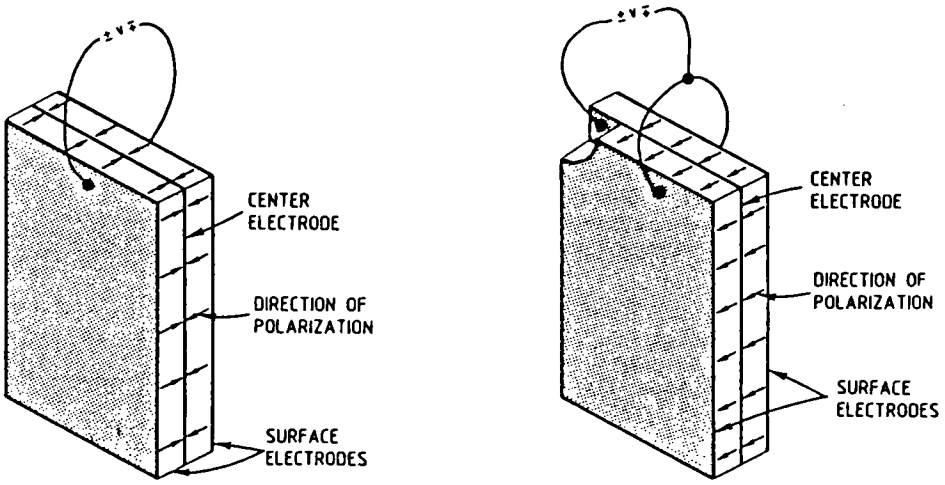

(a) (b)

Figure 2.33 - Connection of piezoceramic plates (a) in series, and (b) in parallel, to produce bender elements (Dyvik and Madshus, 1985)

Although the value of the shear strain applied to the soil by a bender element cannot be determined precisely, a first-order approximation may be calculated by analysing the bender element system as a supported cantilever. A level of shear strain has been quoted by a number of researchers: 10^{-4}-10^{-5} % (Bates, 1989); 10^{-3} % (Dyvik and Madshus, 1985); 10^{-5} % (Thomann and Hryciw, 1990)

If the bender element tip is fixed at one end and inserted into a soil specimen then an applied voltage will cause a shear deformation to the soil, as the tip moves from side to side. If the bender element is fixed at both ends and placed with its side in contact with the soil specimen, an applied voltage will cause a longitudinal deformation to the soil, and propagate a compression wave. The wave propagation velocity is determined by recording the wave travel time over the known distance between receiver and transmitter. The interpretation of the wave

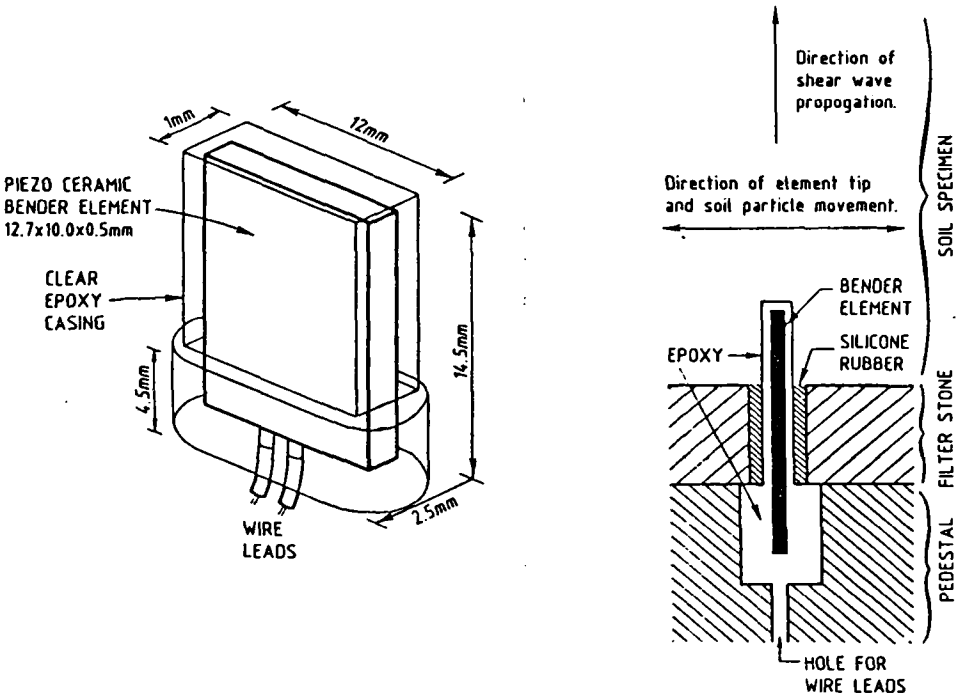

Figure 2.34 - Typical mounting of bender element piezoceramic elements into laboratory testing devices (Dyvik and Madshus, 1985)

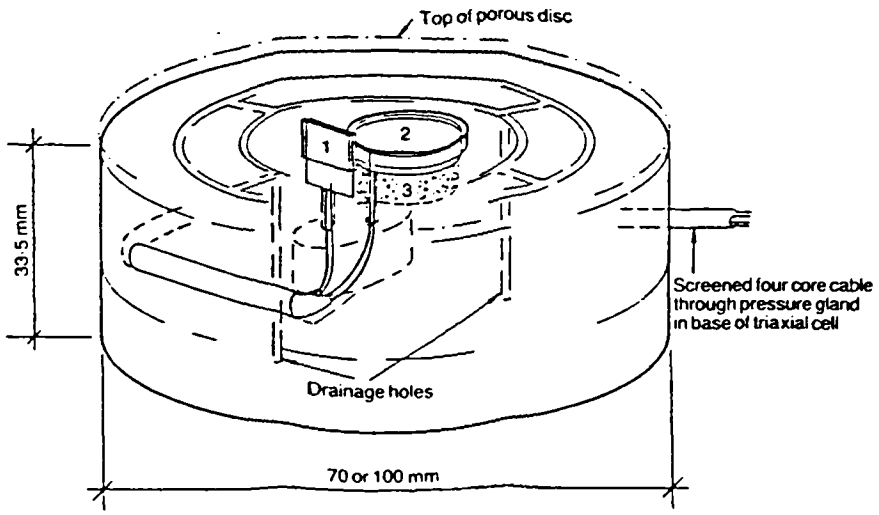

Figure 2.35 - Mounting bender element transducers into a triaxial cell (Bates, 1989)

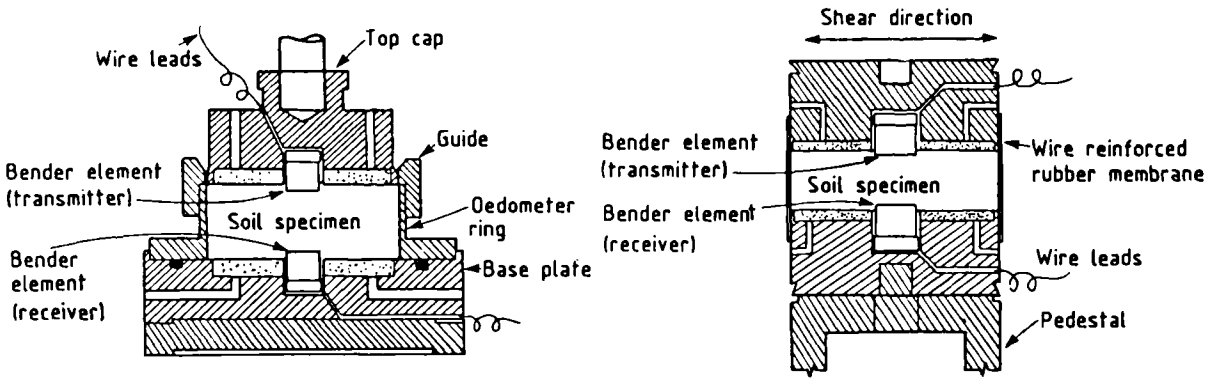

Figure 2.36 - Mounting bender element transducers into oedometer and direct simple shear devices (Dyvik and Olsen, 1989)

travel time is described in section 2.6.3 and 2.6.4.

Perhaps the first application of piezoelectric technology to geotechnical engineering was by Lawrence (1963). He used single piezoelectric crystals to generate one-dimensional compression waves through arrangements of sand and glass beads. The device was found not to be sensitive enough and was subsequently modified (Lawrence, 1965) and incorporated in the end caps of a triaxial apparatus to measure shear and compression waves through sand and clay. This was not a bender element configuration since only a single crystal was used (an applied voltage causing a torsional motion of the crystal). Since the piezoceramics were very stiff, the displacement they could produce was relatively small and similarly they were insensitive when detecting propagating waves. This stiffness is taken advantage of in the bender element configuration since a large force is produced between the two bonded piezoceramics upon displacement, making them far more sensitive. The bender element configuration was developed and used extensively at the University of Texas at Austin by Shirley and his co-workers (Shirley and Anderson, 1975, 1978; Shirley and Hampton, 1977; Shirley, 1978). They made use of the bender element design for shear wave transmission after finding it was very efficient as both a generator and a receiver of shear waves. They also noted that its mechanical impedance was similar to that of a range of soil types, and therefore provided a better degree of coupling with the soil specimen than stiffer devices such as the shear plate. A shear wave was sent as a discrete sinusoidal wave. Piezoceramic bender elements to propagate both compression and shear waves through sand were installed in a sedimentation chamber by Horn (1980). In this system, six biomorph piezoceramics were rigidly bonded together to produce a single bender element and to propagate a sinusoidal wave. Hamdi and Taylor-Smith (1982) incorporated bender elements into a variety of laboratory apparatus.

Following on from the work at the University of Austin, bender element systems were used at the University College of North Wales (Schultheiss, 1981a, 1981b, 1982, 1983; Bennell *et al.*, 1984; Bates, 1989). Piezoceramic discs for compression wave and bender elements for shear wave propagation studies were incorporated into triaxial and oedometer cells. Bates (1989) described the simultaneous measurement of compression and shear wave velocity in a triaxial apparatus by setting bender elements in the base pedestal and endcap as shown in Figure 2.35. Bender elements were also installed into a resonant column apparatus to make direct comparisons of the two forms of stiffness measurement. The bender element and resonant column were found not to agree, and the difference in the results was attributed to the different strain levels being imposed in each test (Davis, 1993).

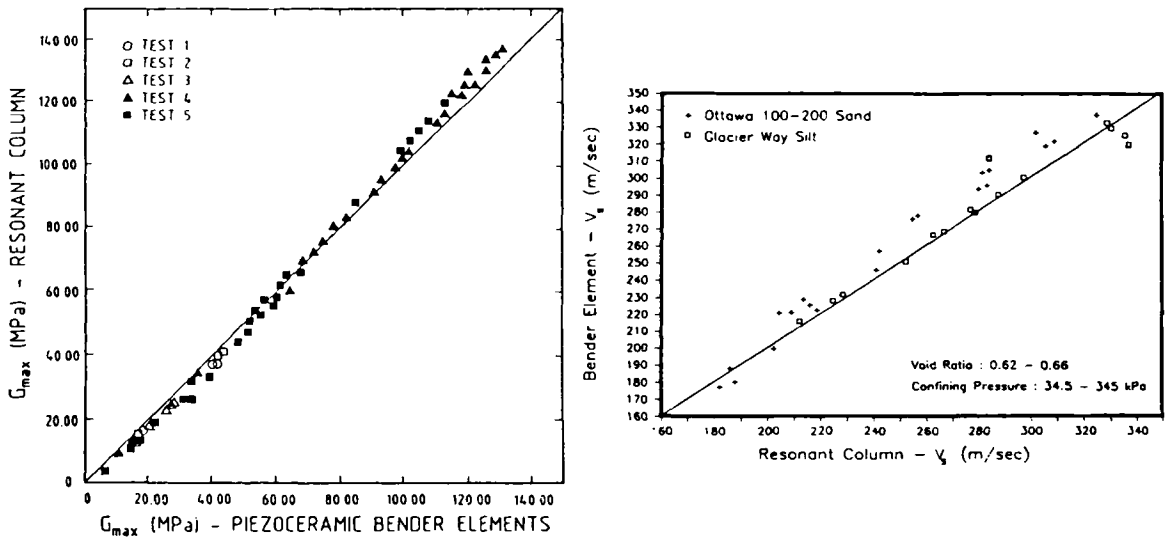

(a) (b)

Figure 2.37 - Comparison of the dynamic shear stiffness measured in resonant column and bender element tests (a) Dyvik and Madshus (1985) (b) Thomann and Hryciw (1990)

A comprehensive study of the preparation, construction, and installation of bender elements was given by Dyvik and Madshus (1985). They mounted bender element transducers into a resonant column apparatus and found that the maximum shear modulus measured in the resonant column apparatus was the same as that recorded in the bender element test if the propagation distance was taken was the tip-to-tip distance. These results shown in Figure 2.37, showed that the bender element was capable of producing G_o measurements as accurately as the resonant column apparatus and with much greater ease. Additionally, the ease of implementation into laboratory apparatus allowed concurrent static and dynamic tests to be performed. This work, carried out at the Norwegian Geotechnical Institute, was later extended to include bender element installation in oedometers and direct simple shear devices as shown in Figure 2.36. Dyvik and Olsen (1989) compared the change in G_o during consolidation using the bender element systems in the different testing apparatus, and found the stiffness to be almost identical to that measured in concurrent resonant column tests. Thomann and Hryciw (1990) also describe the insertion of bender elements into an oedometer apparatus, to record shear wave velocity measurements through cohesionless soils under K_o conditions.

Howarth (1985) described the preparation and use of a bender element testing system mounted in a triaxial cell to record dynamic stiffness properties of rock cores and compared the results with concurrent static loading measurements. Compression and shear waves were generated that passed through a steel platen which was subsequently connected by a spherical seating to the rock core itself.

An interesting application of bender elements was described by Yan and Byrne (1990). They simulated downhole and crosshole seismic-wave tests using a series of bender elements aligned horizontally and vertically as shown in Figure 2.38. Field stress conditions were maintained using the hydraulic gradient similitude method. To simulate a down-hole test, a voltage is applied to the upper bender element which transmits a shear wave to be picked up by other bender elements mounted on a rod and located in a series vertically below. The cross-hole test was produced by sending a shear pulse horizontally from one vertical rod to an adjacent one. The vertical and horizontal positioning of the bender elements could be altered as required to obtain a depth profile of shear wave velocity as would be obtained in the associated field tests.

Duffy *et al.* (1994) carried out bender element tests on unsaturated soil specimens in the triaxial apparatus. They concluded that the use of pulse wave transmission was not a useful indicator of the very small strain stiffness of specimens containing gas bubbles, since the shear wave travelled solely through the saturated matrix surrounding the bubbles, whose only effect was to slightly extend the travel path.

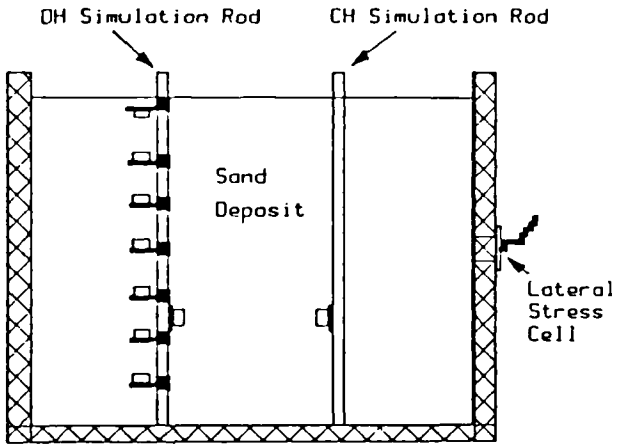

Figure 2.38 - Simulating down-hole and cross-hole seismic shear tests using bender elements (Yan and Byrne, 1990)

Gohl and Finn (1991) described the use of bender elements in centrifuge and shake table testing. They suggested that a bender element system designed to record shear wave velocities also picked up low amplitude compression wave velocity arrivals which they attributed to near-field effects (see section 2.6.4) or imperfect alignment of generator and receiver. They also presented an analysis carried out by Gohl (1990) concerning the theoretical response of a bender element receiver, due to the passing of a propagating shear wave, by considering a lumped mass model. The analysis is shown in Figure 2.39, which illustrates how the bender element response quickly reaches a maximum when the shear wave first arrives before undergoing a gradual decay as the net loading due to the ground wave reaches an approximately constant value.

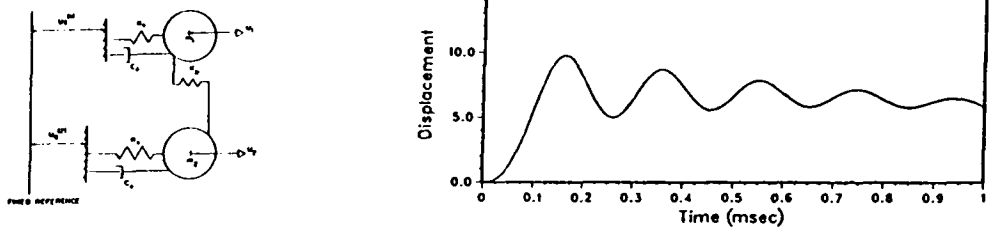

(a) (b)

Figure 2.39 - (a) Lumped mass mechanical model showing (b) theoretical bender element response to a propagating shear wave (Gohl and Finn, 1991)

De Alba and Baldwin (1991) installed bender elements entirely within the endcap of a triaxial apparatus to facilitate their use in dense or hard materials and in saturated materials (by eliminating the need to waterproof the piezoceramic). The bender elements were coupled to the soil specimen through a 2mm thick flexible polyurethane window. The coupling was not as good as it would have been if the elements had been in direct contact with the specimen, but they found that shear and compression wave propagation was monitored adequately.

Agarwal and Ishibashi (1991) describe the measurement of shear and compression wave velocities in a glass sphere assembly in a cubical triaxial device. The system required modification to the bender elements to allow suitable propagation of the compression waves since the medium was highly dispersive. The elements were designed such that the shear element could withstand up to 200V AC and the compression wave transducer up to 400-600V

AC, to generate a single pulse wave. Even with such driving voltages, it was estimated that the level of dynamic shear strain was of the order of 0.0001%.

One of the most recent and comprehensive studies of the use of bender elements was carried out by Viggiani (1992) and reported by Viggiani and Atkinson (1995a). Installing bender elements in a triaxial cell allowed the investigation of the variation of the dynamic shear modulus of fine grained soils with stress state and stress-history (Viggiani and Atkinson, 1995b).

2.6.3 Elastic wave propagation theory

The velocities of seismic waves passing through a homogenous isotropic elastic medium may be by derived from the solutions to the equations of dynamic equilibrium (Timoshenko and Goodier, 1951). The distortional response is controlled by equation 2.13, and the volumetric response by equation 2.14.

$$\rho\frac{\partial^2\gamma_{ij}}{\partial t^2} = G_o\nabla^2\gamma_{ij} \equiv G_o\left(\frac{\partial^2\gamma_{ij}}{\partial x^2}+\frac{\partial^2\gamma_{ij}}{\partial y^2}+\frac{\partial^2\gamma_{ij}}{\partial z^2}\right), \quad (ij = xy, yz, zx) \qquad \text{..... (2.13)}$$

$$\rho\frac{\partial^2\varepsilon_v}{\partial t^2} = K_o\nabla^2\varepsilon_v \equiv K_o\left(\frac{\partial^2\varepsilon_v}{\partial x^2}+\frac{\partial^2\varepsilon_v}{\partial y^2}+\frac{\partial^2\varepsilon_v}{\partial z^2}\right) \qquad \text{..... (2.14)}$$

where, G_o = Shear modulus of elasticity
K_o = Constrained modulus of elasticity
ρ = Mass density

For an elastic full space, equations 2.13 and 2.14 each produce a unique solution for a type of body wave. The distortional response, described by equation 2.13, reduces to equation 2.15, representing a distortional (shear) wave having particle motion perpendicular to the direction of propagation.

$$v_s = \sqrt{\frac{G_o}{\rho}}, \quad \Leftrightarrow \quad G_o = \rho v_s^{\,2} \qquad \text{..... (2.15)}$$

where, v_s = distortional / shear wave velocity

The volumetric response, described by equation 2.14, reduces to equation 2.16, representing a dilational, or compression, wave having particle motion parallel to the direction of propagation.

$$v_p = \sqrt{\frac{K_o}{\rho}}, \quad \Leftrightarrow \quad K_o = \rho v_p^{\,2} \qquad \text{..... (2.16)}$$

where, v_p = dilational / compression wave velocity

The subscripts, *p* and *s*, denote *primary* and *secondary* respectively. The waves are so called because the compression wave is usually significantly faster than the shear wave; thus the primary wave is the first to arrive, and the secondary wave is the second to arrive. This can be shown from the relationship between the elastic volumetric and shear stiffness shown in equation 2.17.

$$K_o = \lambda + 2G_o \quad \text{..... (2.17)}$$

$$\text{where, } \lambda = \text{Lame's constant} = \frac{vE}{(1+v)(1-2v)}$$

The ratio of the primary and secondary wave velocities can therefore be used to determine Poisson's ratio from equation 2.18.

$$v = \frac{\frac{1}{2}\left(\frac{v_p}{v_s}\right)^2 - 2}{\left(\frac{v_p}{v_s}\right)^2 + 1} \quad \text{..... (2.18)}$$

2.6.4 Additional complicating features of elastic wave propagation

Equations 2.15 and 2.16 are used routinely in field and laboratory tests to determine the shear and volumetric stiffnesses of soil. The input parameters required for the equations are the average bulk density, the length of the direct wave propagation path, and the travel time of the individual wave components.

It is the simplicity of this approach which is its attraction, and a significant advantage over the more cumbersome resonance methods. However, the interpretation of measurements may potentially be affected by the multi-phase nature of the soil, anisotropy, and the geometry of the testing apparatus relative to the wave.

IMPLICATIONS OF A MULTI-PHASE MEDIUM

Considering the multi-phase nature of soil, Biot (1956a, 1956b) presented an analysis of wave propagation through a porous homogenous isotropic elastic solid in which the pores were filled with a perfect compressible free-flowing fluid. He showed that the relative motions of the soil and liquid phases could produce a single distortional wave and two compression waves (the single phase material only being able to propagate two types, section 2.6.3). The distortional wave is produced by the inertial coupling between the soil skeleton and the pore fluid during constant volume relative deformation. The theory produces a shear wave velocity as shown in equation 2.19, after Stoll (1989).

$$v_s = b\sqrt{\left(\frac{G_o}{\rho}\right)} \quad \text{..... (2.19)}$$

$$\text{where, } b = \left(1 - \frac{\rho_f^{\,2}}{\rho m'}\right)^{-\frac{1}{2}}$$

$$\rho = (1-\beta)\rho_r + \beta\rho_f ; \beta = \text{porosity}$$

$$\rho_r, \rho_f, \rho = \text{bulk density of the soil grains / pore fluid / porous meduim}$$

$$m' = \text{complex virtual mass density (see below)}$$

The shear wave velocity for a multi-phase medium is therefore modified by the parameter b, in comparison to that through a single-phase medium. The mass term, m', is a complex value that represents an additional mass due to the dynamic viscous interaction of the fluid and soil skeletons. This value is dependent to some extent on the propagation frequency, and therefore the shear wave velocity, and hence the initial elastic shear stiffness, is also frequency

dependent. These additional terms are typically taken to be second order effects and the equation 2.15 is still applied.

The volumetric response of the multi-phase medium is given in equation 2.20 (after Stoll, 1989). There are two solutions to this equation, given by v_{p_1} and v_{p_2}, and these are known as compression waves of the first and second kind.

$$v_{p_1}, v_{p_2} = \sqrt{\frac{2(HM - C^2)}{(\rho M + m'H - 2\rho_f C) \mp \sqrt{(m'H - \rho M)^2 + 4\rho_f(\rho_f M - m'C)H + 4\rho(m'C - \rho_f M)C}}} \quad \text{..... (2.20)}$$

where, $H = \frac{(K_r - K_s)^2}{D_r - K_s} + K_s + \frac{4}{3}G$; $C = \frac{K_r(K_r - K_s)}{(D_r - K_s)}$; $M = \frac{K_r^2}{(D_r - K_s)}$; $D_r = K_r\left[1 + \beta\left(\frac{K_r}{K_f} - 1\right)\right]$

K_r, K_f, K_s = isotropic elastic volumetric stiffness of the soil grains / pore fluid / soil frame

G = isotropic elastic shear stiffness of the soil frame

A compression wave can propagate through both the solid and the fluid phases and hence the volumetric stiffness of the soil grains, the pore fluid, and the soil skeleton as a whole are included in equation 2.20.

The faster waveform is of the first kind, travelling with velocity v_{p_1}, and results from the in-phase movements of the soil skeleton and the pore fluid. When a compression pulse is applied to a saturated soil most of the energy travels through the fluid phase, since the volumetric stiffness of the soil skeleton is several orders of magnitude lower than that of either the soil grains or the pore fluid. Consequently, this first wave arrival largely reflects the volumetric stiffness of the fluid phase and the wave velocity is close to the speed of sound in water (1483m/s). Water is relatively incompressible therefore the velocity of the compression wave of the first kind is little affected by changes in pressure; a pressure increase of 1000kPa would increase the propagation speed by only 1-2m/s (Rice and Walsh, 1957)

The slower waveform is of the second kind, travelling with velocity v_{p_2}, and results from the out-of-phase movements of the soil skeleton and the pore fluid. In a saturated soil, therefore, this velocity corresponds to a compression pulse travelling through the soil skeleton rather than through the fluid phase. Because of the relatively high compressibility of the soil skeleton, the wave velocity is sensitive to changes in the confining pressure. Due to the dynamics of the viscous interaction between the pore fluid and the solid skeleton, Biot's theory implies a frequency dependence for the compression wave of the second kind which is greater than that for either of the other two waves, for which it is relatively small over a wide range of frequency.

When attempting to detect these waves, the compression wave of the first kind is generally easy to distinguish since it is the first waveform to arrive. However, the arrivals of compression wave of the second kind and the distortional wave may interfere, making their detection potentially more problematic.

IMPLICATIONS OF A POINT SOURCE OF WAVE PROPAGATION - THE *NEAR-FIELD* EFFECT

In both field (cross-hole and down-hole) and laboratory (bender element) tests, wave propagation may be idealised to wave generation from a point source and propagation through

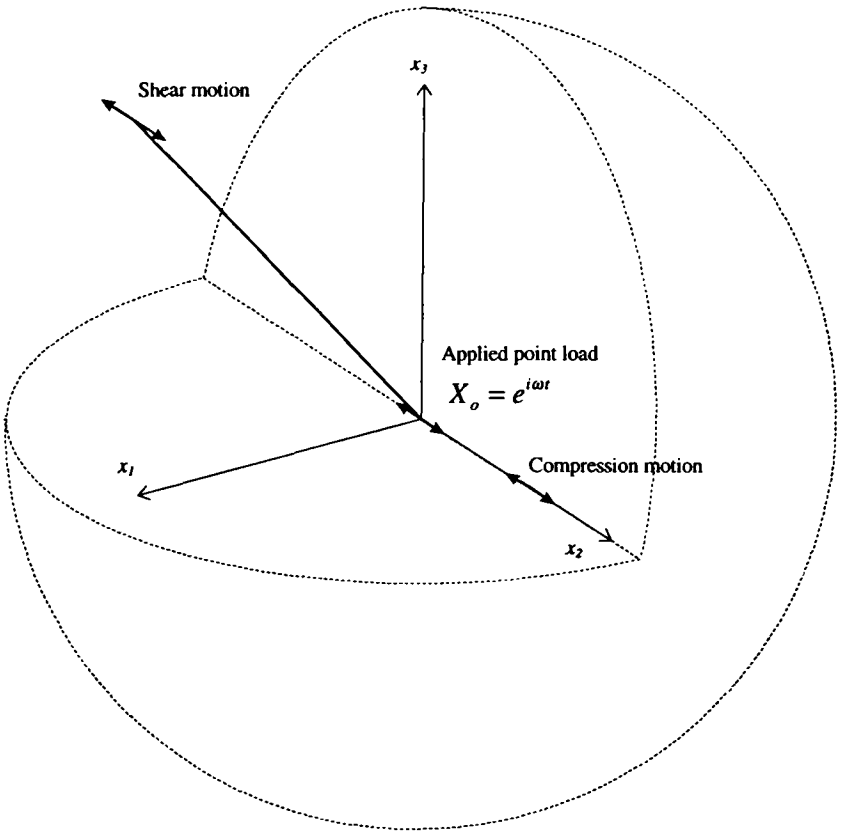

Figure 2.40 - Wave propagation from a point source in 3D space

an unconfined three-dimensional full space (Figure 2.40). The solution given by elastic wave theory in terms of the time dependent displacement with distance from the source is given by equation 2.21 (Aki and Richards, 1980).

$$u_i(\mathbf{r},t) = W_{ps} + W_p + W_s \quad \text{..... (2.21)}$$

$$\text{for, } W_{ps} = \frac{1}{4\pi\rho}\left(3\gamma_i\gamma_j - \delta_{ij}\right)\frac{1}{r^3}\int_{r/v_p}^{r/v_s} \tau X_o(t-\tau)\,d\tau$$

$$W_p = \frac{1}{4\pi\rho v_p^{\,2}}\gamma_i\gamma_j\frac{1}{r}X_o\left(t-\frac{r}{v_p}\right)$$

$$W_s = -\frac{1}{4\pi\rho v_s^{\,2}}\left(\gamma_i\gamma_j - \delta_{ij}\right)\frac{1}{r}X_o\left(t-\frac{r}{v_s}\right)$$

$$\text{where, } i = 1,2,3;\ \delta_{ij} = \begin{cases} 1 \text{ if } i = j \\ 0 \text{ if } i \neq j \end{cases}$$

$$\gamma_i = \frac{x_i}{r};\ \gamma_j = \frac{x_j}{r};\ r = |\mathbf{r}|;\ \mathbf{r} = \{x_1, x_2, x_3\}$$

This equation shows that the displacement has three components: the first term, W_{ps}, includes the shear wave velocity and the compression wave velocity; the second term, W_p, includes only the compression wave velocity; the third term, W_s, includes only the shear wave velocity. At a given time, the propagating wave displacement varies with distance from the source, r. Since the first term varies with $1/r^3$, its effect decays rapidly with distance from the source compared with the second and third terms, which decay with $1/r$. The fact that the first term is only

relevant close to the source leads to it being called the *near-field* effect (Aki and Richards, 1980; White, 1983).

The near-field effect has been investigated analytically by Sánchez-Salinero *et al.* (1986) in two and three dimensions, and their results are relevant to the interpretation of field and laboratory tests involving wave propagation. A typical analysis for the situation presented in Figure 2.40 is shown in Figure 2.41. The traces in Figure 2.41 represent the received wave due to the propagation of a single cycle of sinusoidal displacement through a homogenous linear isotropic elastic material with Poisson's ratio 0.25. The horizontal axis, representing the time record, is normalised such that the theoretical shear wave velocity is 1.0 and the theoretical compression wave velocity is 0.577. Figure 2.41(a) shows the displacement in a direction parallel to the applied displacement. It is seen that the first, and most significant, change in the displacement record occurs for a wave travelling at the compression wave velocity. However, a secondary wave arrival is seen to correspond to the theoretical shear wave velocity. This is the near-field effect and represents a wave that is travelling at the speed of a shear wave but having a longitudinal particle motion. Figure 2.41(b) shows the displacement record at a point perpendicular to the applied displacement. In this case, the major excursion of the displacement record occurs for the component travelling at the shear wave velocity, although there is a secondary component to the waveform travelling at the speed of the compression wave. Again,

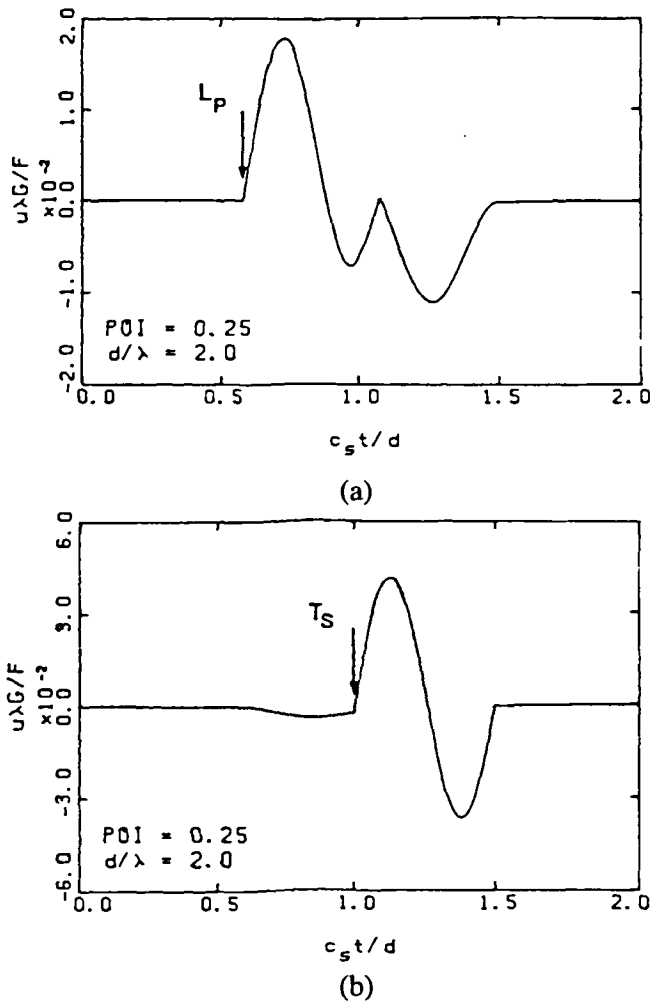

Figure 2.41 - Displacement record associated with the a single cycle sinusoidal wave generated from a point source and propagating in a three-dimensional linear isotropic elastic full space for (a) longitudinal motion, and (b) shear motion (after Sánchez-Salinero *et al.*, 1986)

this is attributable to the near-field effect, and represents a wave travelling at the speed of the compression wave but having the same particle motion as for the shear wave. The influence of the degree of damping on this type of wave motion is shown in Figure 2.42. The material in the example shown in Figure 2.42(b) exhibits 5% hysteretic damping and the effect of this is to cause the arrival of the respective wave components to be associated with a smooth change, rather than the sudden change of slope apparent for an artificial material with no damping.). This figure shows how the combination of damping and a near-field component makes the accurate identification of the shear wave arrival problematic.

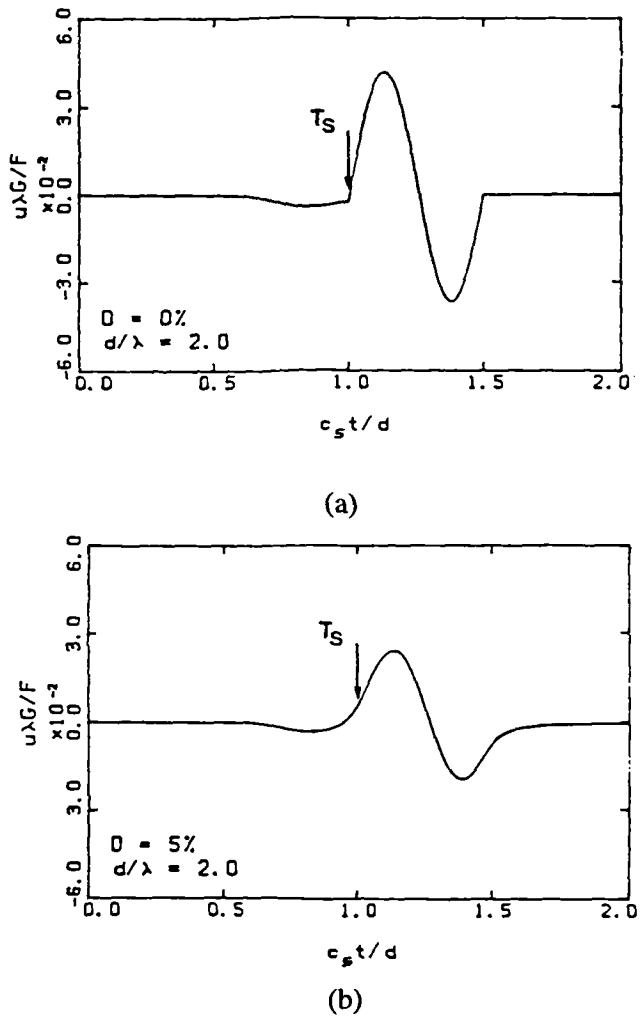

Figure 2.42 - Influence of simultaneous near-field and damping effects for (a) no damping and (b) 5% damping (Sánchez-Salinero *et al.*, 1986)

When wave arrivals are being detected, if the receiver is placed too close to the source the arrival of the shear wave may be masked by superposition of the near-field component which arrives first since it is travelling at the speed of the faster compression wave. Sánchez-Salinero *et al.* demonstrated that the influence of the near-field component on the shear wave reduced as the ratio of the source-receiver separation, d, to the wavelength, λ, increased. In Figure 2.43, for which a shear wave arrival is shown for d/λ ratios increasing from 0.3 to 16, for d/λ greater than about 4, the near-field component passes before the shear wave component arrives.

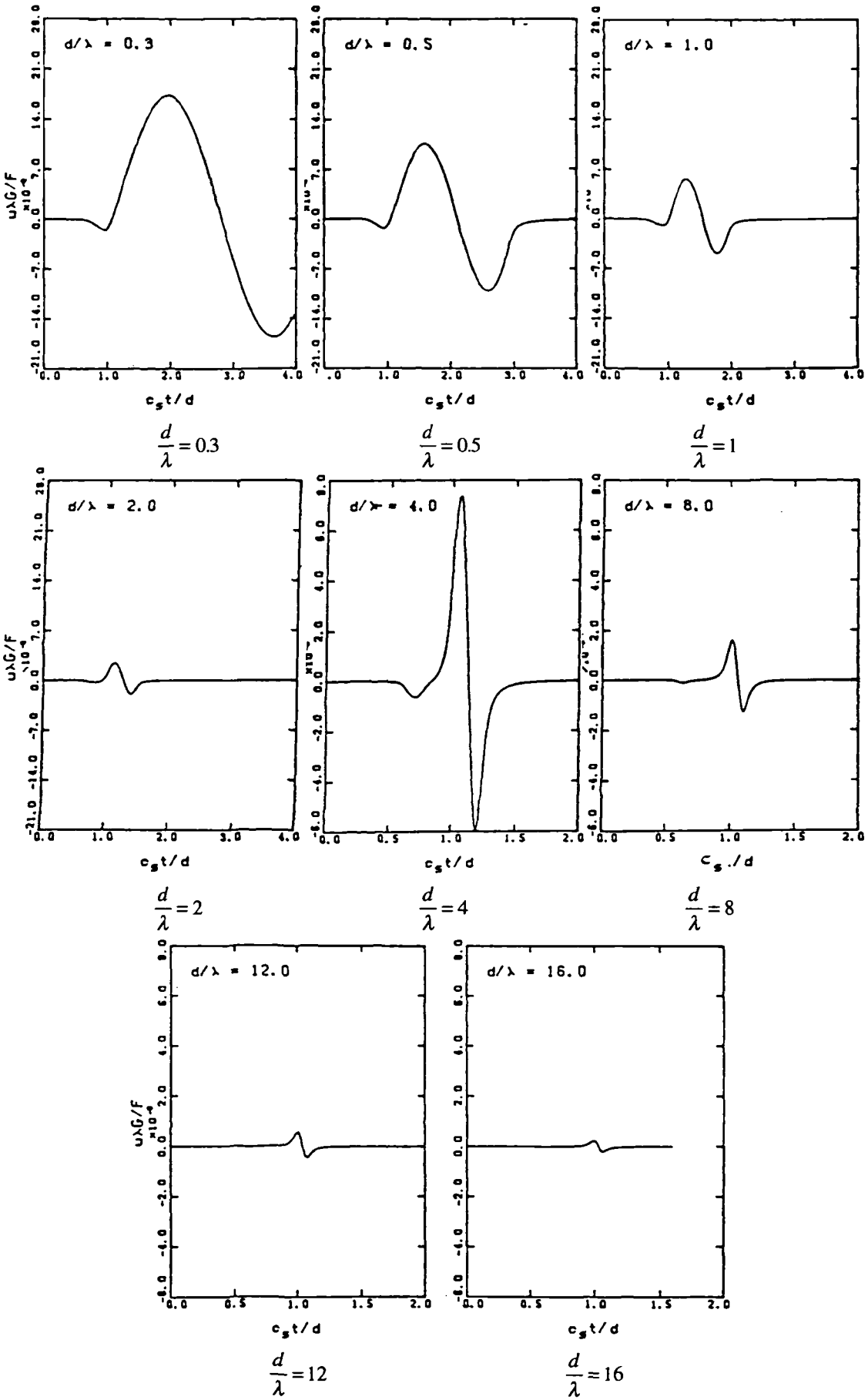

Figure 2.43 - Influence of the separation of source and receiver, *d*, and the wavelength of the transmitted signal, λ, (Sánchez-Salinero *et al.*, 1986) - note change of scale for d/λ>2

IMPLICATIONS OF AN ANISOTROPIC PROPAGATION MEDIUM

The expressions for the shear wave velocity and the compression wave velocity given in equations 2.15 and 2.16 respectively are based on the assumption of an isotropic elastic medium. The assumption of elasticity seems reasonable since the strains imposed are very small (see section 2.3) but the structural or stress-induced anisotropy is relevant regardless of strain level.

Many geological deposits, formed by uniform vertical deposition over a considerable horizontal extent, are cross-anisotropic with regard to stiffness. The theory describing this form of anisotropy is presented in Chapter 7, section 7.3. The vertical axis of symmetry implies that there are perhaps separate shear and volumetric moduli for the vertical and horizontal directions as follows:

K_{o_v}, volumetric stiffness in vertical direction
K_{o_h}, volumetric stiffness in horizontal direction

$G_{o_{vh}}$, shear stiffness in vertical plane
$G_{o_{hh}}$, shear stiffness in horizontal plane

The stress conditions and wave propagation characteristics in a cross-anisotropic soil are shown in Figure 2.44.

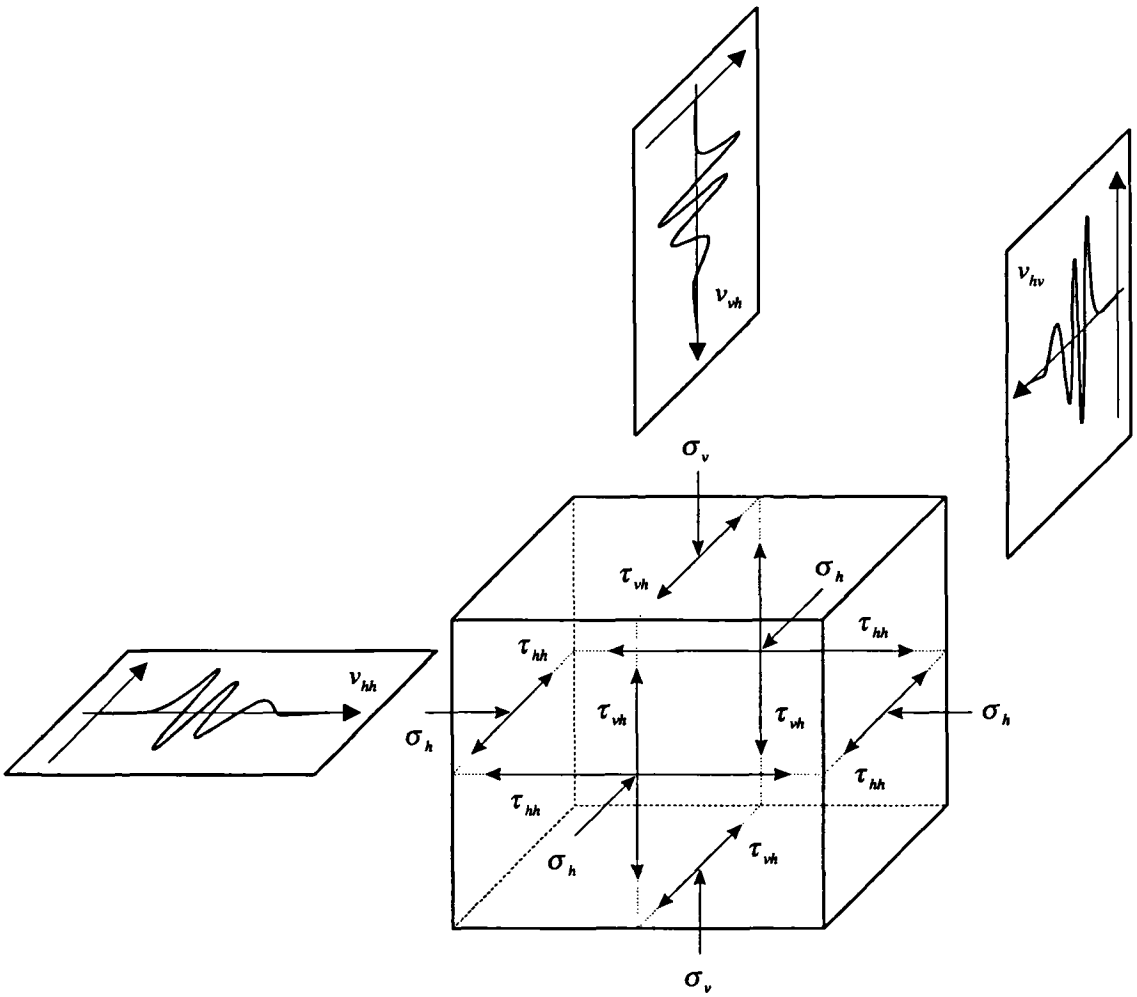

Figure 2.44 - Form of wave propagation during laboratory and field tests

In the present work, the following notation has been adopted for the velocity of a propagating wave:

v_{ij}, velocity of a wave propagating in the direction i, causing particle motion in the direction j.

As a shear wave propagates through a soil, it imposes a set of complementary dynamic shear stresses of the type shown in Figure 2.44. The type of shear stress development dictates the shear stiffness recorded for a particular test. The moduli retrieved from each type of test are given in Table 2.1.

Wave propagation velocity	Wave propagation direction	Plane of particle displacement	Cross-anisotropic elastic stiffness moduli	Examples
Distortional / shear motion				
$(v_s)_{vh}$	vertical	horizontal	$G_{vh} \equiv G_{hv}$	bender element test down-hole field test
$(v_s)_{hv}$	horizontal	vertical	$G_{vh} \equiv G_{hv}$	cross-hole test (vertically polarised)
$(v_s)_{hh}$	horizontal	horizontal	G_{hh}	cross-hole test (horizontally polarised)
Volumetric / compression-extension motion				
$(v_p)_{vv}$	vertical	horizontal	K_v	bender element test down hole field test
$(v_p)_{hh}$	horizontal	horizontal	K_h	cross-hole test

Table 2.1 - Effect of wave propagation direction in laboratory and field tests on the measurement of cross-anisotropic elastic material parameters

2.6.5 Identification of arrival times from wave propagation records

The analysis of wave propagation records is similar whether they are derived from field or laboratory tests. There are three general techniques that may be used to identify the arrival of a body wave. The three approaches have been analysed analytically and numerically by Sánchez-Salinero *et al.* (1985), applied to the interpretation of *in situ* crosshole and downhole tests by Sully and Campanella (1995), and applied to the interpretation of bender element tests (Viggiani and Atkinson, 1995a; Jovicic *et al.*, 1996).

THE 'FIRST ARRIVAL' METHOD

This is the most common technique and involves timing the interval between the initiation of the wave and the estimated point of first arrival of the wave at the receiver. The method relies on being able to accurately determine the initiation of the wave at its source, and being able to pick a precise time of arrival from the receiver trace. Sánchez-Salinero *et al.* (1985) argued that, even under ideal conditions, the presence of the near-field terms during wave propagation and

the effect of material damping (see section 2.6.4) make the identification of the first arrival both subjective and problematic. However, this technique has been used by many practitioners, particularly when there is only a single receiver. For bender element tests, the use of a stepped driving voltage for the generator element, leaves this as the only technique available. The original bender element work carried out at the University of Austin at Texas (e.g. Shirley and Anderson, 1978) used discrete sinusoidal voltage input; however the use of a square wave input was favoured by later researchers. The reasoning behind this was that the more rapid rise of the voltage applied at the generator would result in a more easily identifiable wave at the receiver (Dyvik and Madshus, 1985; Thomann and Hryciw, 1990; Bennell, 1992). The method is also analogous to using a hammer blow or explosive as a source for waves in the field. It is surprising that for bender element tests in the laboratory the use of square wave sources was dominant, since the influence of the near-field components (which are likely to be present in such tests) could have been reduced by using a source whose wavelength could be manipulated as required e.g. a sinusoidal input. This is discussed in section 6.5.2.

THE 'TIME INTERVAL' METHOD

This technique involves comparing similar points on two or more wave propagation records. This may involve comparing similar points from a series of consecutive and co-linear receivers, or comparing the generated input wave with the receiver wave in a laboratory test using a non-stepped input. The benefit of the time-interval technique is realised when the waveforms being analysed have a number of similar points available for comparison. Sánchez-Salinero *et al.* (1985) suggested possible points to choose on a sinusoidal waveform as the initial arrival, the first peak, or the point of zero crossing, as shown in Figure 2.45. For an ideal undamped waveform the travel time calculated for each point will be identical. However, for the more realistic case of a damped material the shape of the wave is less clearly defined and the location of the comparison points, particularly for the first arrival is not so well defined. The chance of determining the true travel time increases as the number of comparison points is increased.

THE 'CROSS-CORRELATION' METHOD

The cross-correlation method is a numerical technique for simultaneously matching all points on one curve to all points on another. A time shift is imposed on one of the traces, and the sum of the product of the two signal amplitudes is calculated. The greater the resultant value, known as the cross-correlation, the greater the similarity between the traces. This is repeated for a range of time shifts so that the cross-correlation may be plotted against time-shift as shown in Figure 2.46. The maximum of this function represents the interval or travel time between the two trace locations. From analytical studies of ideal pulses, Sánchez-Salinero *et al.* (1985) argued that this technique had several advantages over the visual techniques and that the travel times so calculated were generally within 1-2% of the true value, could be generated automatically, and were only slightly affected by the damping ratio. The technique was also generally to be recommended in situations were near-field components were present in the waveforms.

The cross-correlation technique is most commonly applied to field tests where the propagating wave passes two receivers in turn and, in these circumstances, has been very successful (Stokoe *et al.*, 1985; Campanella *et al.*, 1989; Campanella and Stewart, 1991; Viggiani, 1992; Sully and Campanella, 1995). Viggiani and Atkinson (1995a) discuss the technique in relation to laboratory testing using bender elements.

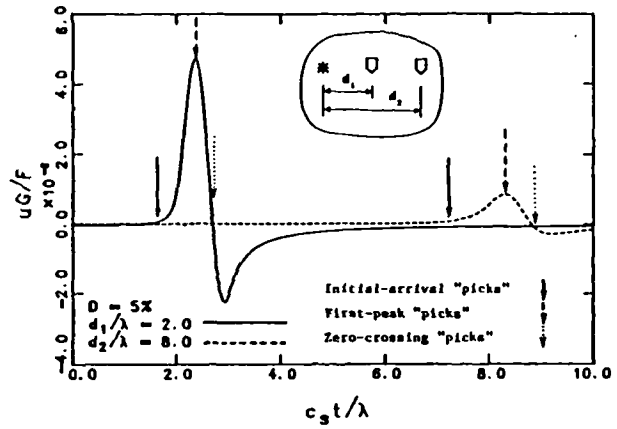

(a)

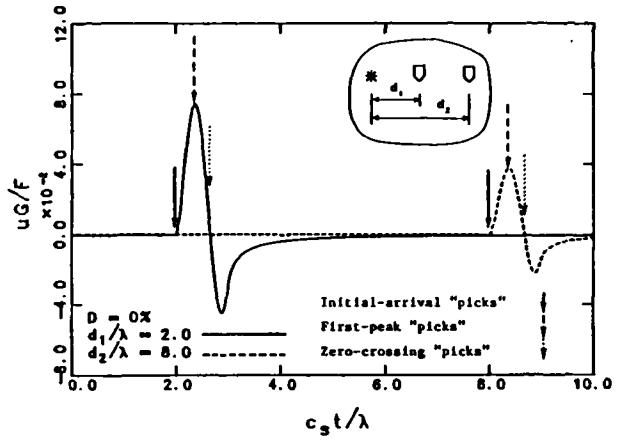

(b)

Figure 2.45 - Evaluation of travel time using the 'time-interval' method for (a) damped and (b) undamped responses of two dimensional shear motion for propagation from a point source (Sánchez-Salinero *et al.*, 1985)

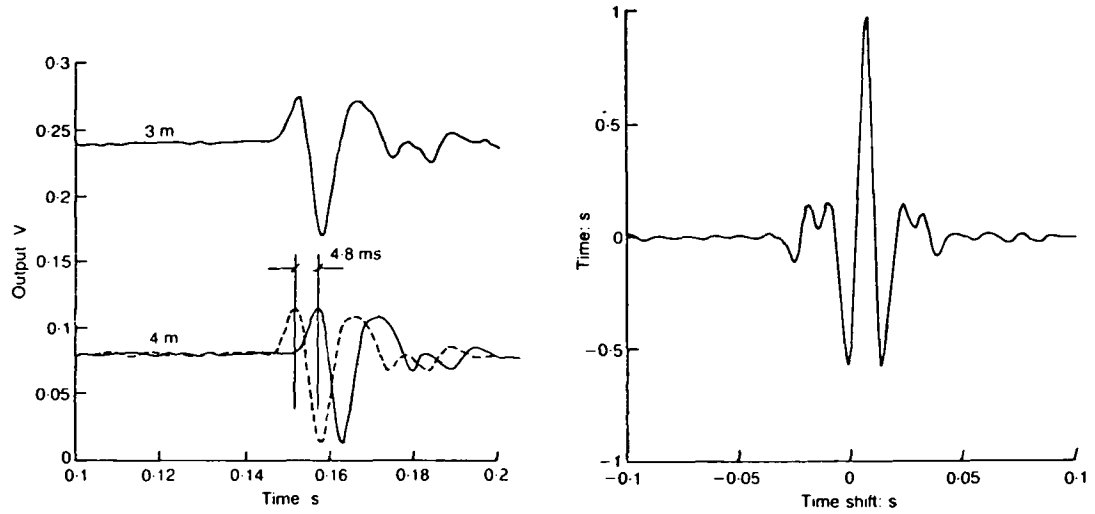

(a) (b)

Figure 2.46 - (a) two signals (caused by a single source) obtained at receivers placed 3m and 4m in a down-hole test, and (b) the cross-correlation function of the two signals normalised at its maximum value (Sully and Campanella, 1995)

2.7 Numerical modelling of soil behaviour

Soil is a complicated material. To adequately describe its constitutive behaviour, regard must be paid to its current stress and structural states, and to their development over recent and geological time scales. This may involve describing the anisotropic and time-dependent behaviour of the soil.

Modern numerical models of soil behaviour are the result of several decades of development and refinement. Early development used elasticity theory (see later in section 7.3). Such models have seen many applications in the prediction of ground deformations. Davis and Poulos (1968) and Poulos and Davis (1974) published an extensive series of closed-form linear elastic solutions to a number of common construction conditions. These could be applied quite widely using the superposition techniques applicable for linear elasticity. (Being obviously unsuitable for ultimate states, elastic deformation models were then supplemented with a perfectly-plastic failure criterion.)

Although simple to apply, it has been shown in the preceding sections that the range of application of linear elasticity is substantially more limited than previously thought. The elasticity theories proposed are perhaps best applied to the very small strain region, i.e. equivalent to only the first micron of axial displacement in a conventional triaxial test.

An early development of linear elasticity to soil came from the back analysis of field cases and from *in situ* profiles of shear wave velocities. This was the dependence of soil stiffness on the effective confining pressure.

$$G' = f(p') \qquad (2.22)$$

This is consistent with the commonly observed soil profiles in which shear stiffness increases with depth, as idealised by Gibson (1974).

Zytinski *et al.* (1978) showed that the pressure dependency of elastic soil moduli can lead to non-conservative behaviour, so that closed stress loops lead to the production of energy. In an elastic framework, an alternative formulation allows Poisson's ratio to vary while the stiffness is constant, although this leads to unreasonable negative values of Poisson's ratio. Lade and Nelson (1987) suggested the model given by equation 2.23, in which Young's modulus is proportional to both volumetric and deviatoric stresses. This model produced behaviour that was conservative.

$$E' = Mp_r'\left[\left(\frac{p'}{p_r'}\right)^2 + 6\left(\frac{1+\nu'}{1-2\nu'}\right)\cdot\frac{J_2'}{p_r'^2}\right]^{\lambda} \qquad (2.23)$$

where, M, λ are material constants
p_r' is the reference effective mean normal stress
J_2' is the second invariant of the deviatoric stress tensor

Houlsby (1985) suggested that, within the Modified Cam Clay constitutive framework (Roscoe and Burland, 1968), conservative behaviour resulted when both the volumetric and deviatoric moduli were proportional to the effective mean normal stress as shown in equation 2.24.

$$\begin{bmatrix} \delta p' \\ \delta q \end{bmatrix} = p' \begin{bmatrix} \frac{1}{\kappa} & \frac{\eta}{\kappa} \\ \frac{\eta}{\kappa} & \frac{\eta}{\varepsilon_s} \end{bmatrix} \cdot \begin{bmatrix} \delta \varepsilon_v \\ \delta \varepsilon_s \end{bmatrix} \quad \text{..... (2.24)}$$

where,

η_r is the stress ratio (q/p')
κ is the slope of a swelling line in $\ln(v)$ - $\ln(p')$ space (Butterfield, 1979)
v is the specific volume

The modelling of the dependence of soil stiffness on the current stress levels has been approached by considering the purely frictional case, and that of an assemblage of elastic spheres. The purely frictional case may be idealised as in equation 2.25 in which the stiffness is directly proportional to the effective mean confining stress.

$$G' \propto p' \quad \text{..... (2.25)}$$

Conversely, Hertz contact theories suggest that the shear modulus of an assemblage of contacting elastic spheres is described by equation 2.26 (Richart, Hall and Woods, 1970).

$$G' \propto p'^{1/3} \quad \text{..... (2.26)}$$

Viggiani and Atkinson (1995b) suggested that the degree of pressure dependency will lie somewhere between these extremes; at very small strains a soil may follow equation 2.26 more closely whilst at larger strains the purely frictional case of equation 2.25 is followed.

A general form for incorporation into constitutive models is given in equation 2.27 after Wroth and Houlsby (1985).

$$\frac{G'}{p_r} = A\left(\frac{p'}{p_r}\right)^n \quad \text{..... (2.27)}$$

where, p_r is a reference pressure (1kPa say)
included to keep the equation form dimensionless
A, n are strain dependent dimensionless parameters

Viggiani (1992) modified equation 2.27 to incorporate the influence of structural change due to previously imposed stress conditions as shown in equation 2.28.

$$\frac{G'}{p_r} = A\left(\frac{p'}{p_r}\right)^n R_o^{\ m} \quad \text{..... (2.28)}$$

where, R_o is the overconsolidation ratio
A, n, m are strain dependent dimensionless parameters

Although the equation was initially derived for the very small level of strain in dynamic tests, it was found to apply equally well at higher levels of strain. If the variation of the parameters A, n and m with strain could be determined therefore, a relatively general empirically defined constitutive model would be obtained (see Figure 2.47).

At the very small strain level, Viggiani and Atkinson (1995b) reported that equation 2.28 defined the behaviour of both heavily overconsolidated ($R_o > 20$) undisturbed specimens of London Clay, and normally consolidated reconstituted specimens of London Clay (see Figure 2.48). This suggests that the influence of the soil structure and fabric is small at very small strain levels with all structural effects being sufficiently expressed by the use of the overconsolidation ratio. This is unlikely to be the case beyond the very small strain threshold.

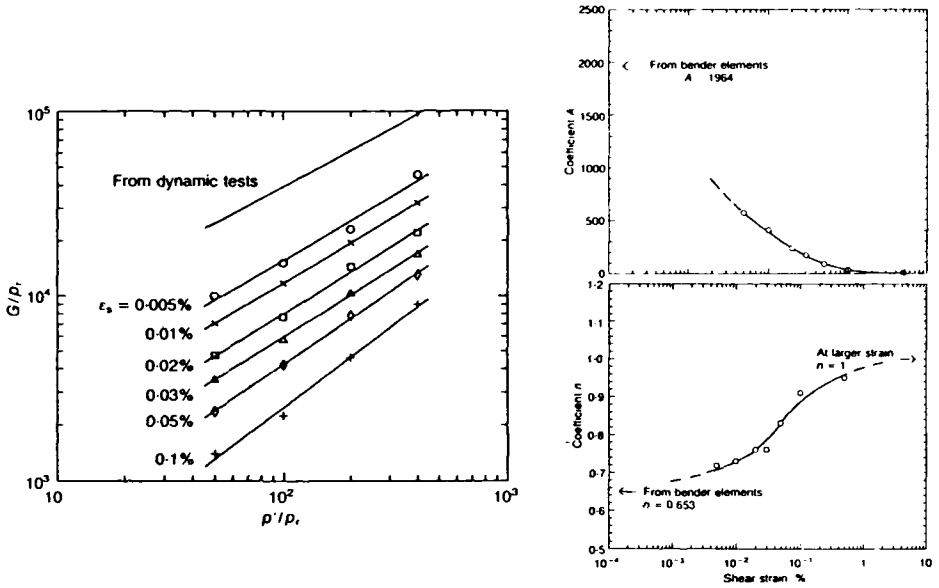

(a) (b)

Figure 2.47 - (a) Variation of shear modulus with strain and stress level and the variation of the parameters (b) A and n from equation 2.28 (Viggiani and Atkinson, 1995b)

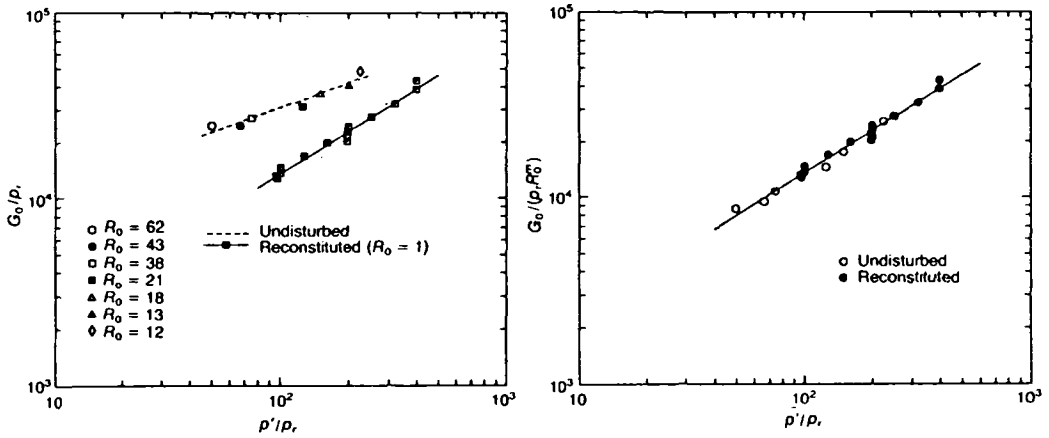

(a) (b)

Figure 2.48 - Variation of G_0' with (a) effective mean normal stress alone, and (b) additionally with overconsolidation ratio (Viggiani and Atkinson, 1995b)

Beyond very small strains, the non-linearity of the stress-strain behaviour requires a more sophisticated constitutive model than that of conventional linear elasticity. A stiffness relation that is dependent on the stress level (e.g. equation 2.28) incorporates a form of non-linearity, but a far more significant contribution to the non-linear stress-strain response is the decay of stiffness caused by progressive straining of the specimen. Shibuya *et al.* (1991b) discuss the degree and form of this non-linearity for a range of soils and weak rocks.

The incorporation of stiffness non-linearity into incremental constitutive relations has been done in two distinct ways:

1) by directly simulating empirically determined stress-strain curves, or

2) by representing the behaviour within the framework of elastoplasticity.

The implementation of constitutive relations based on the representation of a variation of stiffness that has been determined experimentally requires only a suitable mathematical formulation for curve-fitting the stress-strain response. Such models have proved to be very popular, being straightforward to implement and to understand, while also being capable of adequately representing the material response at both laboratory and field scale (see section 2.3). These models are fundamentally elastic so that increments of strain are directly proportional to increments of stress. There are a very large number of non-linear elastic models in the literature. The first strain-dependent constitutive relation, and probably the most well known is the hyperbolic relation (Kondner and Zelasco, 1963; Duncan and Chang, 1970). This may be used to represent a typical triaxial test stress-strain curve as in equation 2.29.

$$q = \frac{\varepsilon_s}{a + b\varepsilon_s} \qquad (2.29)$$

The constants a and b are determined easily from triaxial test data by plotting ε_s/q against ε_s and calculating the intercept and slope of the best fit straight line. Tatsuoka and Shibuya (1992) provided a review of the numerous non-linear relations that are based on strain dependent hyperbolic functions. They concluded that if constant parameters are used, the previously used equations are only valid for a limited range strain. However, they also found that equation 2.30 is able to fit observed stress-strain relations from a wide variety of geotechnical materials over a relatively large strain range.

$$\sigma = \sigma_e + \frac{\varepsilon - \varepsilon_e}{\frac{1}{c_1(\varepsilon)} + \frac{(\varepsilon - \varepsilon_e)}{c_2(\varepsilon)}}, \quad \sigma \geq \sigma_e, \varepsilon \geq \varepsilon_e \qquad (2.30)$$

where, σ_e = stress at the linearity limit

ε_e = strain at the linearity limit

$c_1, c_2 = f(\varepsilon)$

Jardine *et al.* (1986) proposed a periodic logarithmic function which has been subsequently modified for deviatoric and volumetric tangent stiffness (Jardine *et al.*, 1991) as shown in equation 2.31.

$$\frac{G'}{p'} = \frac{d}{d\varepsilon_s}\left(\varepsilon_s\left[A + B\cos\left(\alpha \log_{10}\left(\frac{\varepsilon_s}{C}\right)^{\gamma}\right)\right]\right)$$
$$\frac{K'}{p'} = \frac{d}{d\varepsilon_v}\left(\varepsilon_v\left[A + B\cos\left(\alpha \log_{10}\left(\frac{\varepsilon_v}{C}\right)^{\gamma}\right)\right]\right) \qquad (2.31)$$

As the degree of non-linearity of the stress-strain relation from experimental data increases the complexity of the fitting equation correspondingly rises. It is a mistake to judge the complexity

of the resulting model on the number of parameters required for these equations. If a suitable method is available for defining the parameters from test data then the number of parameters is of no consequence.

The drawback of any such approach is that the experimentally determined stress-strain curve is modified to some degree depending on the mathematical limitations of the fitting procedure. Also the transformation of apparently irregular experimental data into a smooth curve could blur aspects of the soil stiffness response. Stallebrass (1990a) pointed out that no experimental evidence is available to show that the stress-strain response of a soil should form a smooth curve.

An alternative to mathematically describing the experimental data in their entirety is to adopt some form of interpolation; this could simply involve linear interpolation between data points or possibly the use of interpolation polynomials or spline functions. The use of spline functions has been discussed by Desai (1971) and is perhaps the most adaptable as the resulting curve would be able to model post-yield strain softening behaviour or the progression from a compressive to a dilative volumetric response.

Whatever form of non-linear function is used, the stiffness relations must be mathematically consistent when applied to practical problems (Jardine *et al.*, 1991). It is most important that the relation fits the small strain range well, since it is this that will dominantly affect the ground response around engineering structures (Burland, 1989; section 2.3).

The calculation of stiffness parameters from individual experimental stress-strain curves is not trivial and is discussed in section 5.6. For modelling purposes, however, it is perhaps easier to derive and to fit a mathematical relation to secant stiffness data. The description of secant stiffness may be translated to one of tangent stiffness (being more suited to incremental numerical techniques) as follows:

$$G'_{sec} = \frac{\Delta q}{\varepsilon_s}$$

$$\text{since } G'_{tan} = \frac{dq}{d\varepsilon_s},$$

$$G'_{tan} = \frac{d}{d\varepsilon_s}\left(G'_{sec} \cdot \varepsilon_s\right) \quad \text{..... (2.32)}$$

where, G'_{sec} is the secant deviatoric stiffness

G'_{tan} is the tangent deviatoric stiffness

An equally important consideration is the choice of variable used to control the stiffness. Jardine (1985) took the larger absolute value of the major principal strains; Jardine *et al.* (1986) used the shear strain and the volumetric strain for the shear stiffness and volumetric stiffness respectively (see equation 2.31); Simpson *et al.* (1979) defined a kinematic yield surface defined as a sphere in $(\varepsilon_x + \varepsilon_y,\ \varepsilon_x - \varepsilon_y,\ \gamma_{xy})$ space, where ε_x is the horizontal strain, ε_y is the vertical strain and γ_{xy} is the shear strain, and it would be possible to use the radius of such a sphere as a generalised strain parameter. A stiffness relation may also be defined in terms of changes in stress rather than strain. Richardson (1988) argued that such a definition is preferable since stress is an absolute value and strain is defined relative to a datum of the start of the test and is subject to any errors accumulated at this stage. An average stress or strain increment may also be used as shown in equations 2.33 and 2.34.

$$\varepsilon_{gen} = \sqrt{\left(\varepsilon_s^2 + \varepsilon_v^2\right)} \quad \text{..... (2.33)}$$

$$\sigma_{gen} = \sqrt{\left(\Delta p'^2 + \Delta q^2\right)} \quad \text{..... (2.34)}$$

The non-linearity may also be represented using a combination of stress and strain parameters. Burland (1989) argued that incremental strain energy provides the most generalised strain parameter as shown in equation 2.35.

$$\varepsilon_{gen} = U = \sum_0^{\varepsilon_1}(\sigma'_1 - \sigma'_{1_o})\delta\varepsilon_1 + \sum_0^{\varepsilon_2}(\sigma'_2 - \sigma'_{2_o})\delta\varepsilon_2 + \sum_0^{\varepsilon_3}(\sigma'_3 - \sigma'_{3_o})\delta\varepsilon_3 \quad \text{..... (2.35)}$$

where $(\sigma'_{1_o}, \sigma'_{2_o}, \sigma'_{3_o})$ defines the initial stress state and $(\sigma'_1, \sigma'_2, \sigma'_3)$ defines the new state.

This equation may also be written in terms of deviatoric and volumetric behaviour, as in equation 2.36, since the stress and strain invariants are defined so as to satisfy the work condition.

$$\varepsilon_{gen} = U = \sum_0^{\varepsilon_v}\Delta p'\,\delta\varepsilon_v + \sum_0^{\varepsilon_s}\Delta q\,\delta\varepsilon_s \quad \text{..... (2.36)}$$

where $\Delta p'$ and Δq are the changes in effective stress.

The theoretical development of constitutive soil models involving plasticity has generally followed those used for modelling the deformation response of metals. The initial application of plasticity theories in soil mechanics was carried out by Drucker *et al.* (1957). This led to the first unified theories of soil behaviour which incorporated the volumetric and deviatoric loading responses of soil within the critical state framework (Schofield and Wroth, 1968; Atkinson and Bransby, 1974; Wood, 1990). The success of plasticity theory in modelling soil behaviour is due to its ability to represent, at least qualitatively, a number of key features of the response of which elastic theories are incapable.

The formulation of a plasticity model requires only the three basic assumptions of (i) a yield criterion, (ii) a flow rule, (iii) a hardening rule. These are incorporated in equation 2.37 for an elastoplasic model.

$$\begin{aligned}\delta\sigma &= \boldsymbol{D}\cdot\delta\varepsilon \\ &= \left(\boldsymbol{D}_e - \boldsymbol{D}_p\right)\cdot\delta\varepsilon\end{aligned}$$

where, $\boldsymbol{D}$ is the elastoplastic stiffness matrix
$\boldsymbol{D}_e$ is the elastic stiffness matrix
$\boldsymbol{D}_p$ is the plastic stiffness matrix

$$D_p = \left[1 - \frac{D_e \frac{\partial Q}{\partial \sigma} \left(\frac{\partial F}{\partial \sigma} \right)^T}{\left(\frac{\partial F}{\partial \sigma} \right)^T D_e \frac{\partial Q}{\partial \sigma} - \left(\frac{\partial F}{\partial h} \right)^T H \frac{\partial Q}{\partial \sigma}} \right] D_e \quad \text{..... (2.37)}$$

where,

F is the yield function, $f(\sigma, h)$

Q is the plastic potential, $g(\sigma, h)$

H is a hardening function which modifies with plastic strain such that $dh = Hd\varepsilon_p$

The most popular of the plasticity models are based on the principles of critical state soil mechanics, e.g. the Modified Cam Clay model (Roscoe and Burland, 1968). Within the basic critical state framework the soil response within the state boundary surface is assumed to be purely elastic and although slightly non-linear, is not strain level dependent. A significant development was that of the bounding surface models (Dafalias and Popov, 1975; Dafalias and Herrman, 1980, 1982a, 1982b, 1986; Dafalias, 1986). In bounding surface theory, plastic strains are incorporated within the state boundary surface by mapping each stress state to a corresponding point on the state boundary surface. A smooth transition from elastic to plastic behaviour is then obtained by relating the plastic modulus at the current stress state to that at the mapped image point upon the state boundary surface and incorporating this within the hardening rule. This is shown is shown schematically in Figure 2.49. Manipulation of the mapping rule led to realistic predictions of experimental results but for monotonic loading only. The non-linearity at small strains was captured satisfactorily but the features of soil behaviour attributed to changes in stress path direction could not be adequately represented.

The introduction of nested yield surfaces within a kinematic hardening framework manages to model the increase of stiffness experimentally obtained when there is a change in the stress path direction. It also takes account of the fact that a soil element in equilibrium under a set of stresses will initially exhibit a relatively stiff and possibly elastic response and that plastic strains will develop only gradually.

An early, simple implementation of kinematic yield surfaces for soil behaviour was the non-linear elastic Model L.C. (Simpson *et al.*, 1979). In this model, the elastic region was cross-anisotropic. A kinematic yield surface was defined in strain space about the current strain level such that up to a small limiting strain level the stiffness was ten times larger than that beyond this level. This was a pragmatic attempt at reproducing the high initial stiffness reported in experimental work and the small strain levels recorded in the field (see section 2.3).

The development of kinematic yield surfaces for elastoplastic models was initially carried out for metal behaviour (Mròz, 1967; Iwan, 1967) but the work was extended to their application to soil behaviour (e.g. Mròz *et al.*, 1978, 1979; Hashiguchi, 1985). The use of many surfaces inevitably involves numerous model parameters. This led to the formulation of a relatively simple two-surface model within the critical state framework. This so-called 'bubble' model (Al Tabbaa, 1987; Al Tabbaa and Wood, 1989) requires only two parameters in addition to the five required for Modified Cam Clay and is shown schematically in Figure 2.50. The inner yield surface encloses a region of isotropic purely elastic behaviour. As the stress state moves to intercept the yield surface plastic deformations are predicted using a mechanism similar to the bounding surface models in which an image point is located on the state boundary surface.

As the stress state moves, so the yield surface both translates and expands. All parameters for the two-surface model could be determined from a single multi-stage triaxial test.

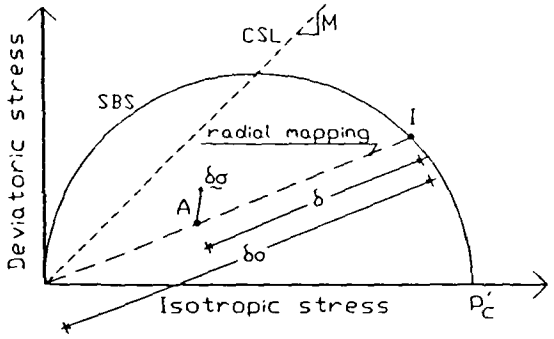

Figure 2.49 - Bounding surface plasticity

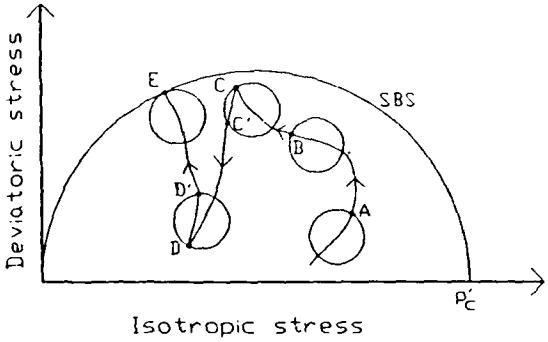

Figure 2.50 - Two-surface kinematic hardening 'bubble' model (Al Tabaa and Wood, 1989)

The translation of the kinematic surfaces effectively gives the soil model a memory of its stress history. The orientation of the inner yield surfaces is dependent on the previously imposed stress path and consequently the stress-strain behaviour depends on the degree of rotation of the subsequent stress path. Although Cam Clay models do take account of the degree of overconsolidation, for overconsolidated soils particularly, the orientation of the inner yield surfaces within the state boundary surface provides a much more precise definition of the stress history.

The 'bubble' model was further developed by Stallebrass (1990b) who included a third surface within the state boundary surface. This was following an experimental programme that showed the soil's memory of previous loading history extended far beyond that of the inner elastic region. The third surface was therefore called the 'recent-history' surface and is shown in Figure 2.51. The geometry of the extra surface required an additional parameter; however all eight parameters could be determined from conventional laboratory tests. The model was shown to be able to describe the key features of the experimentally determined behaviour within a relatively simple framework. The model has now been implemented in the finite element program CRISP, and has been applied to boundary value problems (Stallebrass *et al.*, 1994).

The numerical modelling of soil behaviour has developed to the stage where it is now challenging experimentalists to determine the parameters that are required to fully define some of the current models. This would suggest that a graduated approach to modelling soil behaviour should be adopted in which increasing levels of complexity are incorporated until a solution is obtained to the required accuracy. One approach uses a unified model (*g*UTS) which adopts a single framework for the response of the whole range of soil types and soil states (Crouch and Wolf, 1994a, Crouch *et al.*, 1994). This represents a modular approach in that although 32 parameters are required to fully define the model, the number of parameters required depends on the complexity of the problem and reduces to Modified Cam-Clay (Roscoe and Burland, 1968) in its simplest state. The model developed from bounding surface plasticity models (Dafalias and Herrmann, 1986) but included a number of novel modifications. The bounding and plastic potential surfaces are constructed of three curves meeting at common tangents, allowing great versatility in specifying its shape. Also, the point of reference for referring the current stress point to the bounding surface is allowed to move from the

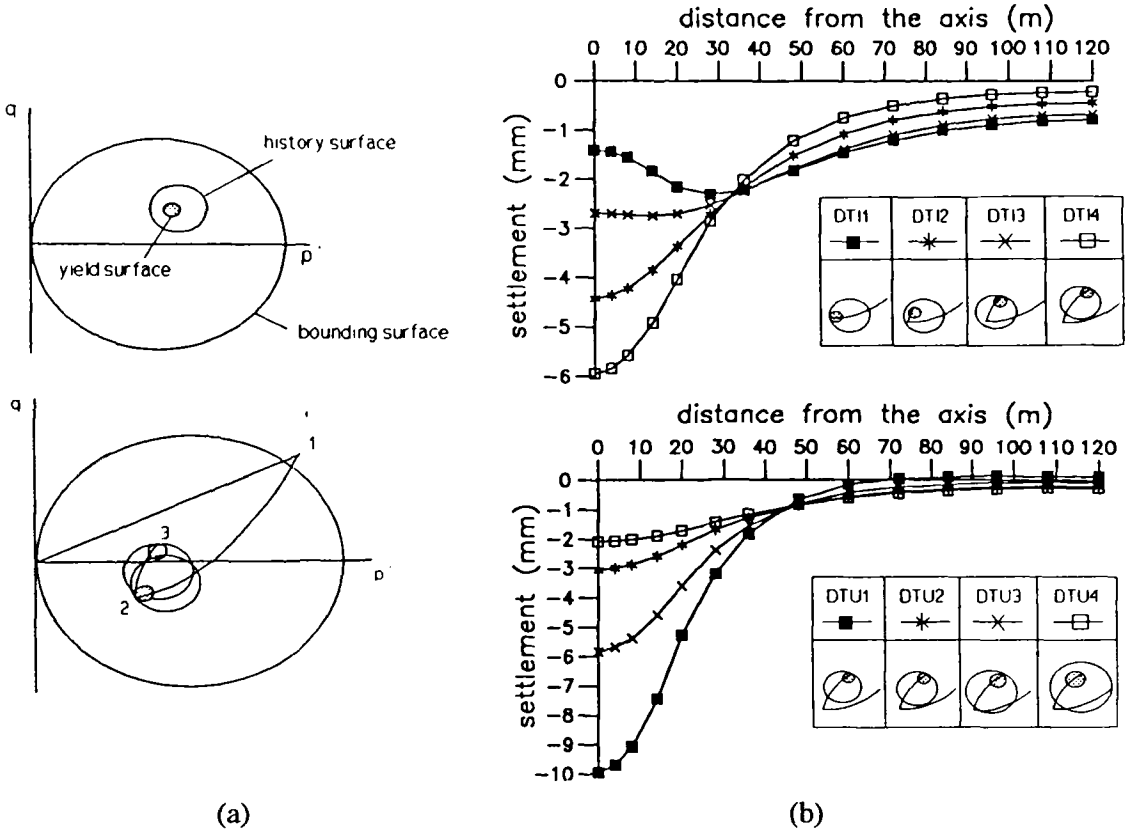

Figure 2.51 - (a) A three-surface kinematic hardening model, the modelling of overconsolidation, and (b) the effect of modelling the recent stress history on settlement profiles of a deep tunnel (Stallebrass *et al.*, 1994)

hydrostatic axis for stress states in the heavily overconsolidated region allowing continuous plastic strains to be modelled during cyclic loading. The model has been validated against an extensive series of experimental data and was shown to perform well (Crouch and Wolf, 1994b), and is currently being applied to field problems (Crouch, 1996).

Whittle and Kavvadas (1994) argued that, due to the complexity of soil behaviour, it was not possible to develop a completely generalised model for all soils. Rather, a model should be tailored to the specific requirements of a problem. Whittle (1993) described the MIT-E3 model which was formulated specifically for normally to moderately overconsolidated clays. The model follows a closed, symmetric hysteresis loop during unloading and utilises bounding surface plasticity to develop plastic strains as the stress state approaches the normal consolidation line during reloading. The model has been shown to adequately predict the laboratory behaviour of London Clay and Boston Blue Clay specimens with an overconsolidation ratio less than 8 (Whittle, 1993; Whittle *et al.*, 1994), and the behaviour of a deep excavation in Boston Blue Clay (Whittle *et al.*, 1993)

A very different approach to modelling the non-linear and path dependent behaviour of soil was proposed by Simpson (1992). His BRICK model was based on a physical analogue of a man pulling bricks attached to him by strings, as shown in Figure 2.52. As the man walks in one direction he gradually drags behind him an increasing number of bricks. If he changes direction, a number of the bricks will stop moving, and only until he has walked a certain distance in the same direction will all the blocks once again be dragged behind him. The analogy with soil behaviour is that the room the man is walking in is strain space, and the movement of a brick represents plastic straining. Initially, as no bricks are moving, the behaviour is both stiff and elastic. As the number of bricks being dragged increases, the ratio of plastic to elastic strain

increases while the stiffness falls. This simple model was initially developed to model the small strain effects in stiff clay, but it has since been found to reproduce a wider variety of soil responses (Ng and Lings, 1995).

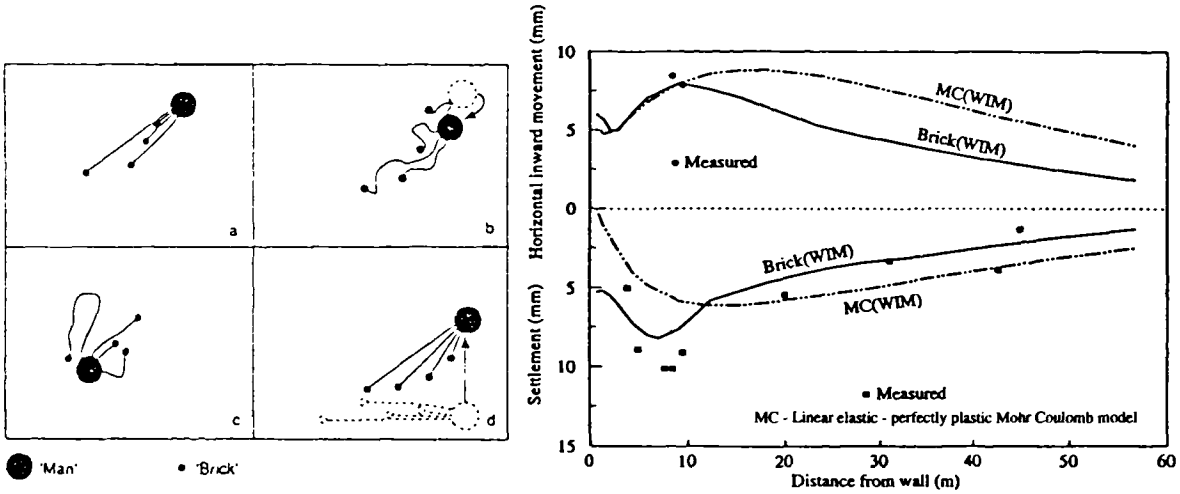

(a) (b)

Figure 2.52 - (a) A physical analogue describing the brick model (Simpson, 1992) and (b) the model's application to retaining wall behaviour (Ng and Lings, 1995)

During any analysis, an appropriate response for each soil element must be modelled, depending on its location. This may be achieved by regarding the small strain soil behaviour as essentially inelastic resulting in yielding and hardening within kinematic yield surfaces which expand and translate inside the state boundary surface, as proposed for example by Mròz *et al.* (1979), Al-Tabbaa and Wood (1989) and Atkinson and Stallebrass (1991). In such models the stiffness response of each soil element caused by a change in loading depends on the previous stress history. This history is provided through the model input parameters or developed during the numerical analysis. Alternatively, for empirical non-linear elastic models the input parameters may be varied on the basis of the stress path being followed and the results of appropriate stress path tests. Fourie *et al.* (1986) suggested that for retaining wall analyses, triaxial compression tests and triaxial extension tests should be used to specify appropriate non-linear stiffness parameters for the soil behind the excavation and in front of the wall respectively. Similarly, Jardine *et al.* (1991) suggested that the soil mass can be divided into generally *active* or *passive* zones for which non-linear elastic properties derived from triaxial compression or extension tests could respectively be specified.

3. Elstow Site Investigation

3.1 Introduction

The site investigation at Elstow, Hertfordshire formed part of the pre-application site study carried out by the Nuclear Industry Radioactive Waste Executive (UK Nirex Ltd.) to select a suitable site for the construction of a near surface repository for low level nuclear radioactive waste. Three other sites, Bradwell, Fulbeck and Killinghome were also considered and investigations were carried out here simultaneously.

Mott MacDonald Consulting Engineers (MM), then Mott, Hay and Anderson, were appointed by the Generation Development and Construction Division of the Central Electricity Generating Board (CEGB) on behalf of Nirex following the issuing of a Government Special Development Order. The appointment, announced on 10 June 1986, included the design, supervision and interpretation of the geological, geotechnical and hydrogeological investigations at the site.

The physical aspects of the ground investigation were carried out by Norwest Holst Soil Engineering Limited (NHSEL), appointed by the CEGB on 1 August 1986, to the instruction of MM. The investigation included the construction of a trial excavation, 10m deep, 105m long and 35m wide (50m long and 10m wide at its base).

Access to the site was delayed until 19 September 1986 due to the action of protesters and works eventually started on 14 October 1986. The excavation commenced on 18 March 1987 and continued until 1 May 1987 when all site investigation work was cancelled. Following advice from Nirex and due largely to public pressure, the Secretary of State for the Environment announced in the House of Commons that Nirex would cease its investigation of sites for a near surface repository for low level nuclear waste. MM were instructed to suspend all work and leave the site at the earliest opportunity. Before this date, a large part of the site work had been carried out and it was estimated that the excavation would have been completed with a single extra day's work. The majority of the planned laboratory testing, further *in situ* testing and the medium to long term monitoring of the installed instrumentation was still to be carried out.

It was realised that this trial excavation could provide an invaluable resource for future works on similar materials and required further analysis. With this foresight, and to ensure the short term stability of the excavation sides, the monitoring of instruments continued for a further three months until 1 August 1987 when remedial work to reinstate the Elstow site commenced. It was not possible to leave the excavation open since this controversial project had to be seen publicly to terminate. Prior to the suspension of work only limited interpretation of the

investigation had been carried out and no further work was carried out until 1990. Rudrum (1990) presented and analysed the majority of the NHSEL laboratory test data and all the piezometer data of pore water pressure fluctuations; he partially analysed the inclinometer and extensometer data which described the ground displacement response. These results will be outlined again as part of the present assessment of the site response and extended to include analyses of the remaining laboratory data and a more complete analysis of the vertical and horizontal ground displacement data.

This chapter contains the details of the site investigation and the partial analysis carried out on the data obtained before the suspension of works (Mott MacDonald, 1989; Norwest Holst Soil Engineering Limited, 1988; Rudrum, 1990). An overview of the literature regarding the geology of the site, particularly the dominant stratum of Oxford Clay is included. The details of the Elstow excavation, the interpretation of the instrumentation data, and the initial attempts at numerically modelling the response are presented.

3.2 Scope of the investigation

The Elstow site investigation was designed to cover the following aspects:

- the drilling of boreholes
  - to obtain high quality borehole samples for visual examination and laboratory testing
  - for the performance of *in situ* tests and geophysical studies
  - for the installation of instrumentation
- the excavation of small trial pits to determine near surface conditions and to provide high quality block samples of the Oxford Clay for small strain stress path testing and other laboratory tests
- a programme of experimental earthworks involving the construction of a trial excavation, a trial embankment, and numerous smaller embankments designed to investigate weathering
  - to investigate the mechanical and hydraulic behaviour of the ground due to excavation, loading and compaction, by monitoring with extensive instrumentation
  - to perform *in situ* tests
  - to obtain soil samples, including high quality block samples from depths greater than accessible by trial pitting
  - for visual examination of subsurface conditions, especially any large scale features which may affect the ground behaviour response
- geophysical work involving determination of dynamic shear moduli and a seismic survey to link borehole information and to locate structural discontinuities within the ground
- *in situ* geotechnical testing comprising standard penetration tests, self boring pressuremeter tests, dilatometer tests and plate bearing tests
- hydrogeological testing and monitoring of groundwater conditions

3.3 Site description

3.3.1 Location and land use

The site of the Elstow trial excavation, shown in Figure 3.1, is approximately 5km south of the centre of Bedford close to the town of Stewartby.

With the exception of the earthworks blast bunds, the ground is generally flat but nevertheless slopes from around 40mAOD in the south east and south west of the site to around 30mAOD in the north east of the site over a distance of approximately 1km. The trial excavation was situated in the north east of the site.

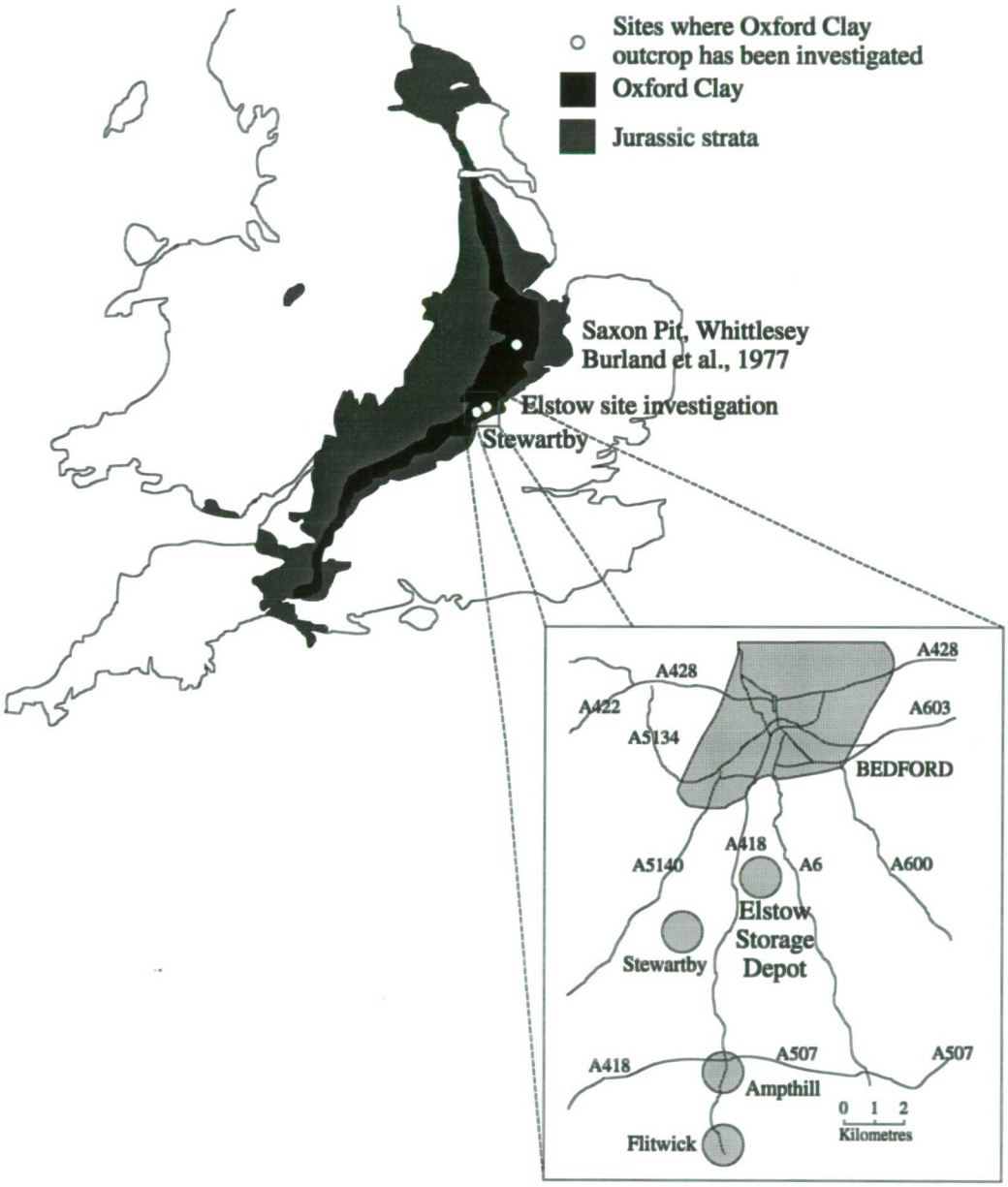

Figure 3.1 - Present location of the Oxford Clay and Jurassic Strata in England (after Jackson and Fookes, 1974) in relation to the location of the Elstow site investigation

The site is owned by the CEGB and is called the Elstow Storage Depot due to its original use as an agricultural storage depot on an area of arable farmland although this is now largely discontinued. During the second world war a munitions factory was constructed and blast

protection, consisting of earthwork embankments, was created around the buildings. A significant number of these building remain today as part of a light industrial and trading estate, although part of the factory site has been reclaimed as farmland.

The London Brick Company has extensively worked the surrounding area for the Lower Oxford Clay which is used in the brick making process. The clay pits extend to the base of the clay seam which in this area is 12-15m below the surface. A number of the pits are presently active with the remainder either flooded and used for recreation, used for the disposal of domestic, commercial and industrial wastes or simply abandoned and unused. Sand and gravel extraction takes place 1km north of the site from the drift deposits above the Oxford Clay.

3.3.2 Site geology

A desk study was carried out by the British Geological Survey (BGS) on behalf of Nirex (Nirex, 1985) to study the geology and hydrogeology of the area. The hydrogeological aspect, including the determination of the flow paths and travel times through the various strata, was obviously important due to the nature of the intended disposal project but will only be briefly summarised here.

At the time of the original site investigation no recent 1:50000 BGS map of the area had been produced and, although this map is currently being prepared, it remains unavailable (BGS, 1994).

The general stratigraphic succession of the area was originally described by Arkell (1933) and later by Callomon (1968) so the site was known to consist of superficial drift deposits of variable thickness and composition (ranging from sand and gravel through sands to silt and clays) overlying the Jurassic succession which was thought to extend to a depth of approximately 160m to the Palaeozoic basement rocks (although only proved to a depth of 69m). These were conjectured to be of Carboniferous or Devonian strata.

The information derived from the desk study was used to initiate and complement the ground investigation carried out by NHSEL on behalf of MM at the Elstow Storage Depot. This investigation revealed the site geological succession shown in Figure 3.2.

OXFORD CLAY

It was anticipated that the ground deformations associated with the excavation would be dominated by the response of the Oxford Clay and so investigations were concentrated there.

The Oxford Clay has been described in detail by Callomon (1968). A deposit of the Upper Jurassic, the Lower Oxford Clay encountered at the Elstow site occupies the Middle Callovian together with the top sub-zone of the Lower Callovian. These strata were deposited in a relatively stable marine environment leading to the thick sequences of bituminous shales, shaley clays and calcareous clays present over a large area of England.

The Oxford Clay comprises weathered and slightly weathered zones overlying the green-grey unweathered clay. The Oxford Clay deposits at the Elstow site were seen to increase in thickness from 14m to 24m from the northern end to the southern end of the site although local to the trial excavation the thickness was relatively constant at 11m.

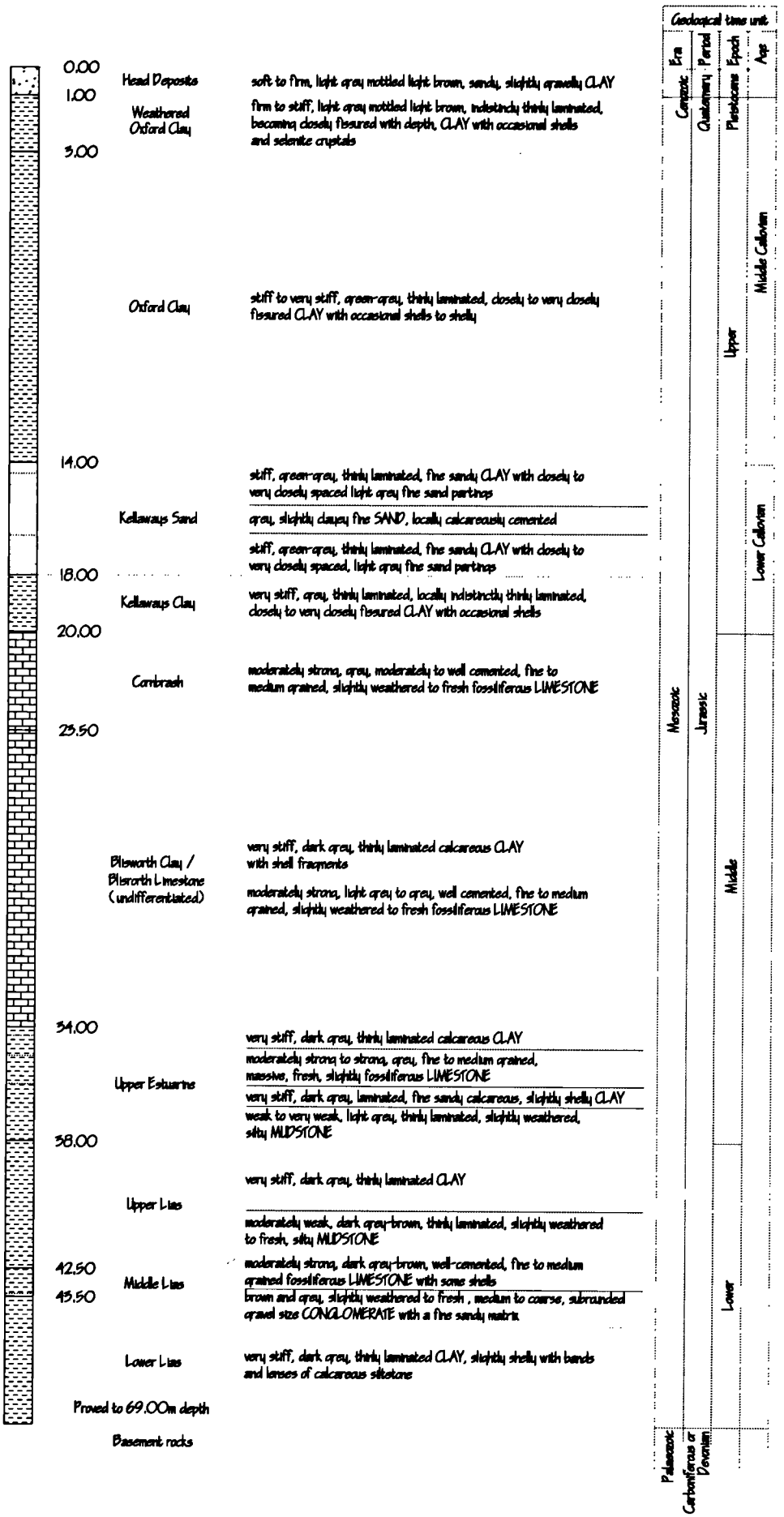

Figure 3.2 - Soil profile and strata descriptions at Elstow site

The green-grey unweathered Oxford Clay is heavily overconsolidated due to the overburden pressure exerted in the past by great depths of overlying material. Jackson and Fookes (1974) estimated that approximately 500m of overlying material has been removed in the past and the clay is consequently stiff to very stiff. It is heavily fissured and strongly horizontally laminated. The Jurassic strata regionally dip at approximately 1° to the south-east but it is known that the strata are dislocated by a number of faults (Parry, 1972). The exposures created in the Oxford Clay for brick making purposes have revealed numerous vertical joints (Parry, 1972, Burland *et al.*, 1977).

WEATHERED OXFORD CLAY

The combined thickness of the weathered and slightly weathered zones of the Oxford Clay varied between 1m and 7m across the site, but local to the trial excavation it was between 2m and 3m. The green-grey unweathered clay weathers to a light mottled grey-brown colour and it contains occasional selenite crystals.

A study of the weathering characteristics of Oxford Clay was compiled by the BGS (Milodowski *et al.*, 1985) with reference to the site's intended use as a nuclear waste repository.

KELLAWAYS BEDS

The Kellaways Beds are the gradual and locally very variable transition between the Oxford Clay and the lower limestones (Callomon, 1968). The upper Kellaways bed, the Kellaways Sand consists of 4-4.5m of variable fine to medium sands and sandy clays. Locally the strata becomes 'Kellaways Rock', areas of soft sandstones with occasional concretionary masses up to 3m across, known as 'doggers', which are calcareously poorly or well cemented. The lower Kellaways bed is the Kellaways Clay which consists of 1.5-2m of a very stiff, thinly laminated, closely to very closely fissured clay.

CORNBRASH

The uppermost limestone stratum, the Cornbrash, was seen at the Elstow site to be of variable nature and thickness but with an average thickness of 3-3.5m. The deposit was seen to contain numerous erosion surfaces.

BLISWORTH SERIES

The Blisworth Series is an undifferentiated sequence of limestone and clay strata which were encountered in thicknesses of between 6.0m and 14.5m. The first significant clay bed below the Cornbrash was taken as the upper boundary of the Blisworth Series, although this was not always clear. The Blisworth Clay consists of a very stiff, dark grey, thinly laminated calcareous clay. The Blisworth Limestone consists of hard, sometimes massive, limestone comprised of fine to coarse grained units which were locally argillaceous. Throughout the series there are varying amounts of fine shell detritus and occasionally large shell fragments.

UPPER ESTUARINE SERIES

At the Elstow site the first grey clay or mudstone band was taken to show the Upper Estuarine series underlying the Blisworth strata. The Upper Estuarine series constitute the lowest formation of the local Great Oolite Series (Horton et al., 1974). They are predominantly clay and mudstone and are known to contain a group of calcareous beds, the Upper Estuarine Limestone. The clays were recorded as becoming darker in colour with increasing depth and varied in thickness from 4.0m, generally, to 12.0m, maximum.

LIAS

Prior to the site investigation little borehole information was available relating to the Lias strata but a few deep boreholes were commissioned as part of the investigation. The Upper Lias encountered beneath the Upper Estuarine was seen to comprise dark grey clays and mudstone containing limestone bands. The top of the deposit was stained light grey or orange brown. The deposit was generally less than 5m thick and locally absent. The Middle Lias is a conglomeratic limestone locally comprised of calcareous siltstones and sandstones. It is also locally absent but is generally about 1.0m thick. The Lower Lias was proved to a depth of 69m in the vicinity of the excavation and comprises very stiff, dark grey clays with phosphatic siltstone nodules and bands. The base of the Lower Lias was found at 94m depth from a borehole in another part of the site.

BASEMENT ROCKS

The Palaeozoic basement rocks were encountered beneath the Lias up to the extent of the deepest boreholes at 180m depth. This was one of the deepest bores carried out in the region and revealed red brown and locally grey green mudstones, siltstones and sandstones of uncertain age. Palaeotological work to date these materials was carried out by the BGS but provided no conclusion as to their origin.

3.4 Material properties

The laboratory test data produced during the site investigation has been analysed previously (Rudrum, 1990) and is reproduced here in summary for reference purposes.

3.4.1 Previous studies

The Oxford Clay and the associated near surface Jurassic strata are an extensive geological unit outcropping over a large area of England (see Figure 3.1) and consequently there is a large body of literature concerned with their geological characteristics. However, in contrast to the London Clay, the Oxford Clay outcrop has received relatively little geotechnical attention to date.

A summary of the standard material properties quoted in the literature is given in Table 3.1. This table also includes the average values recorded during the Elstow investigation from the laboratory tests described in section 3.4.2.

Only two of these studies make reference to the stiffness of the Oxford Clay. Burland *et al.* (1977) recorded the vertical undrained Young's modulus of specimens trimmed from block samples as increasing from 20MPa to 150MPa over a depth of approximately 20m.. The ratio of Young's modulus to undrained shear strength was relatively constant with depth at about 100. These stiffness measurements were taken from the initial slope of conventional triaxial tests without small strain instrumentation. O'Brien *et al.* (1992) reported two undrained unconsolidated triaxial tests in which local measurements were made on specimens obtained by rotary coring. These tests are summarised in Figure 3.3.

The anisotropy of the Oxford Clay has been investigated in terms of strength (e.g. Parry, 1972; Russell *et al.*, 1978) but only by Burland *et al.* (1977) in terms of stiffness. For the tests described above, the moduli determined from horizontally orientated specimens were generally about twice those for vertical specimens.

Reference	Bulk unit weight (kN/m^3)	Water content (%)	Liquid limit (%)	Plastic limit (%)	Clay fraction (%)	Activity	c_u (kN/m^2)	c' (kN/m^2)	ϕ' (°)
	17-18.5	*25-32*	*52-70*	*23-33*	*30-35*	*0.69-0.91*		*25-40*	*21-32*
Elstow site investigation	*17.7*	*28.5*	*60*	*29*			*20-66*		*26*
Parry, 1972		20-40	65-75	20-30			95-165	25	29.5
Jackson, 1973			52-69		47-66	0.4-0.5			
Jackson and Fookes, 1974		22-24	62-70	25-33	50-70	0.5-0.75		59-89	29-32
Burland et al., 1977	19.9	17-25	50-65	22-25	>55		50-1200	0-180	21-36
Cripps and Taylor, 1981			45-75		30-70				
Crabb and Atkinson, 1991			60	32				0	25
O'Brien et al., 1992							200-250		

Table 3.1 - Summary of material properties from Elstow site investigation and literature

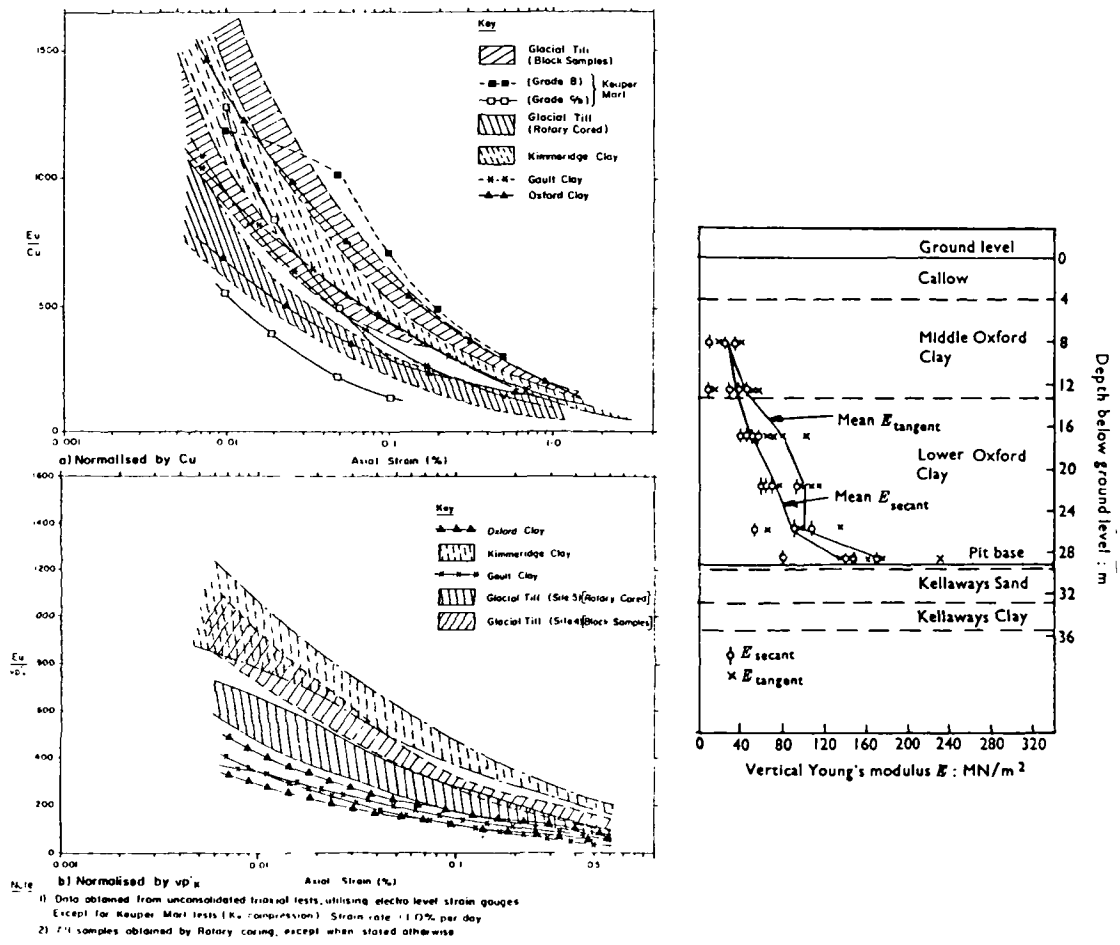

(a) (b)

Figure 3.3 - The stiffness of Oxford Clay from previous studies: (a) O'Brien *et al.* (1992), (b) Burland *et al.* (1977),

3.4.2 Initial laboratory testing

Although a comprehensive suite of testing was envisaged, only a limited amount had been carried out before the site investigation was suspended. The majority of completed tests were carried out on Oxford Clay samples with relatively few on the lower strata. The testing consisted of:

CLASSIFICATION TESTS - these consisted of moisture content tests, liquid and plastic limit tests, and particle size distributions for samples taken during installation of the piezometers and in a limited number of additional boreholes at the trial excavation site.

CONVENTIONAL TRIAXIAL TESTS - a limited number of quick undrained tests, consolidated drained and consolidated undrained tests were carried out on 38mm and 100mm diameter specimens. The specimens for these tests came from boreholes T1-T4 at the trial excavation site and from borehole T5 beneath the trial embankment (see Figure 3.23 and Figure 3.15 respectively).

The results of these standard laboratory tests are shown in Figure 3.4 to Figure 3.8 and summarised in Table 3.1.

LOCALLY INSTRUMENTED TRIAXIAL TESTS - a series of eight consolidated undrained triaxial tests were carried out on 100mm diameter, 200mm long specimens of weathered and unweathered Oxford Clay. The tests were carried out on a computer controlled hydraulic stress path cell which incorporated local strain instrumentation (Yung, 1987). The data from these tests were not analysed before the suspension of work and are included with the current testing programme results in Chapter 5.

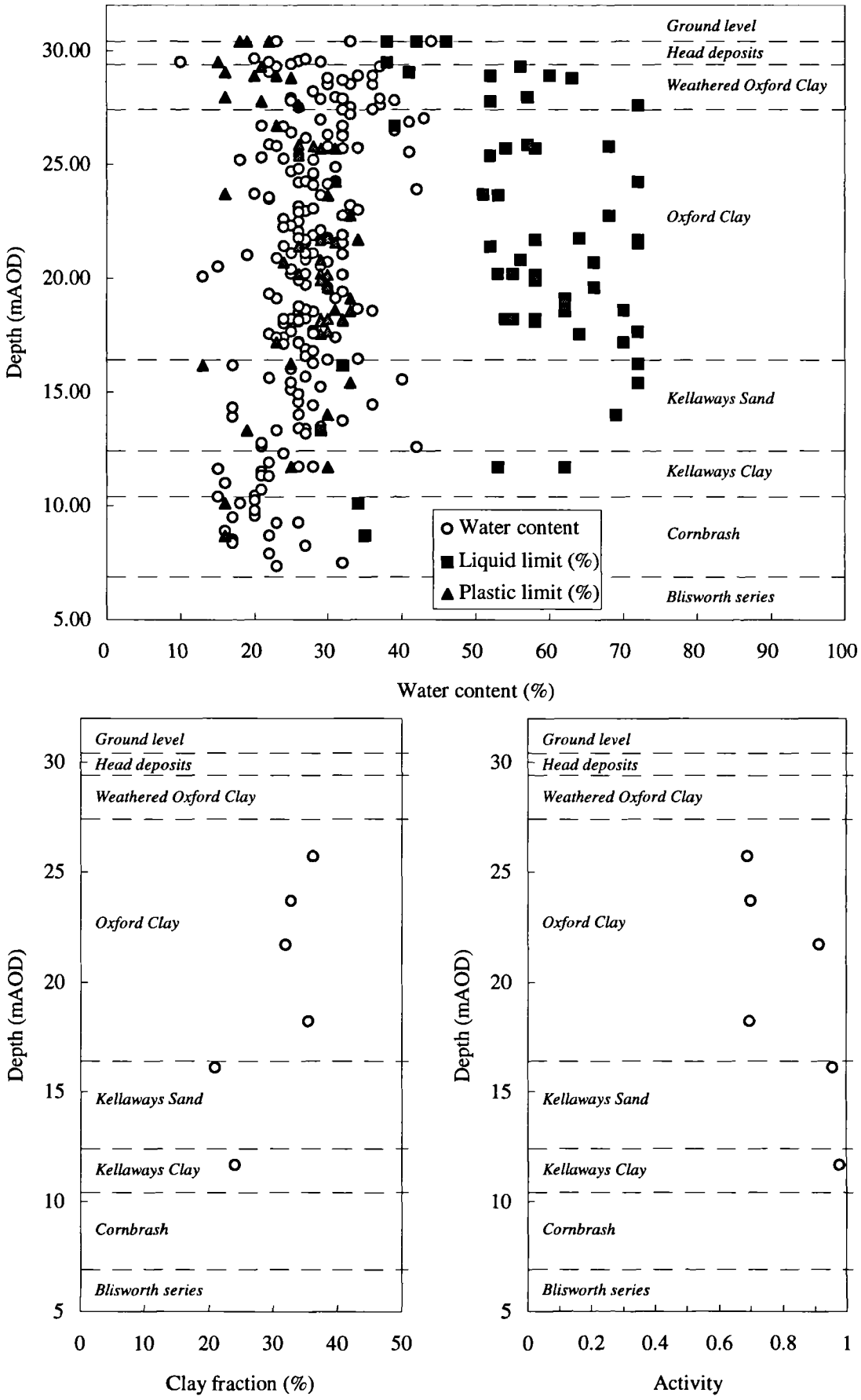

Figure 3.4 - Variation of index properties, clay fraction and activity with depth

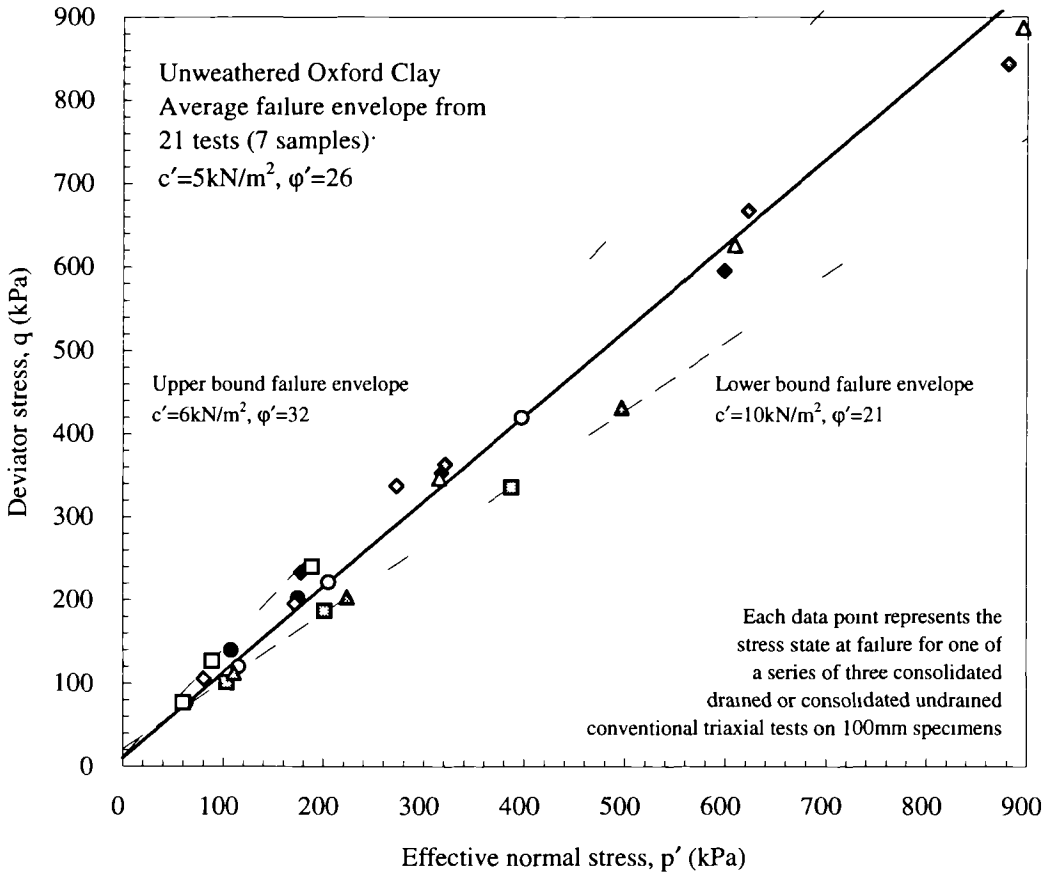

(a)

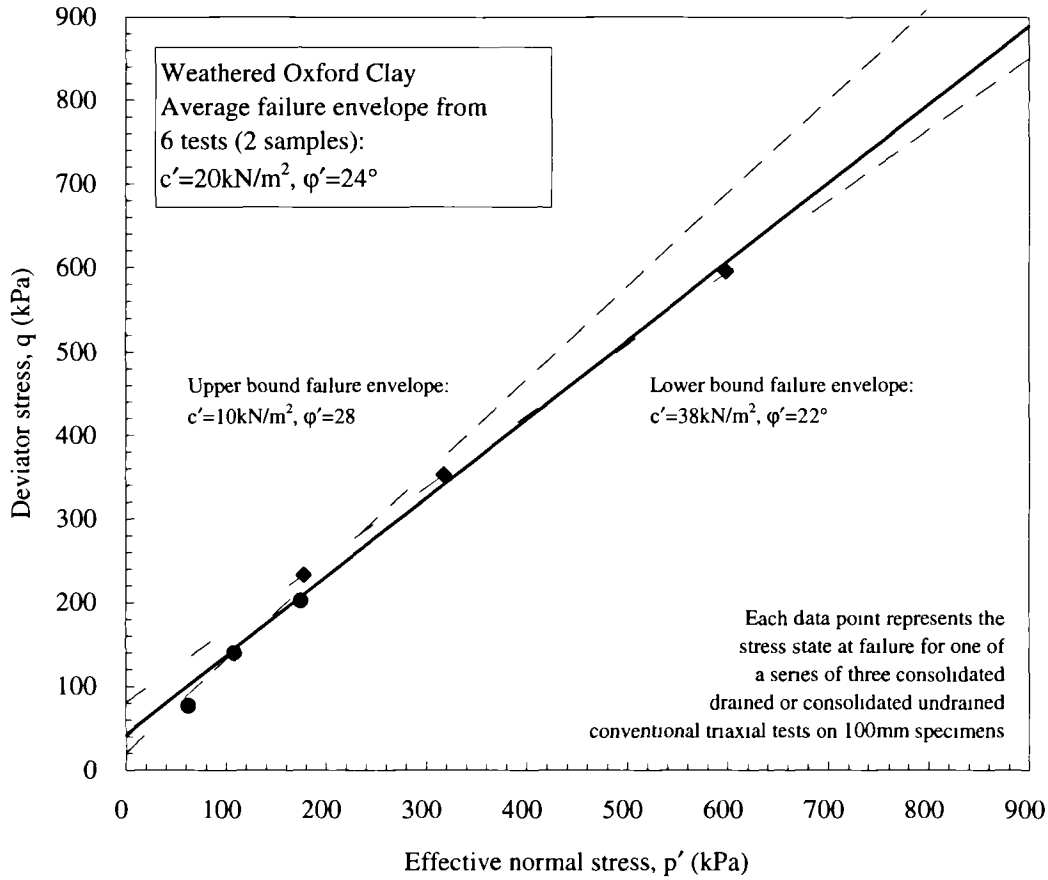

(b)

Figure 3.5 - Stress state at failure for conventional triaxial tests on (a) unweathered and (b) weathered Oxford Clay

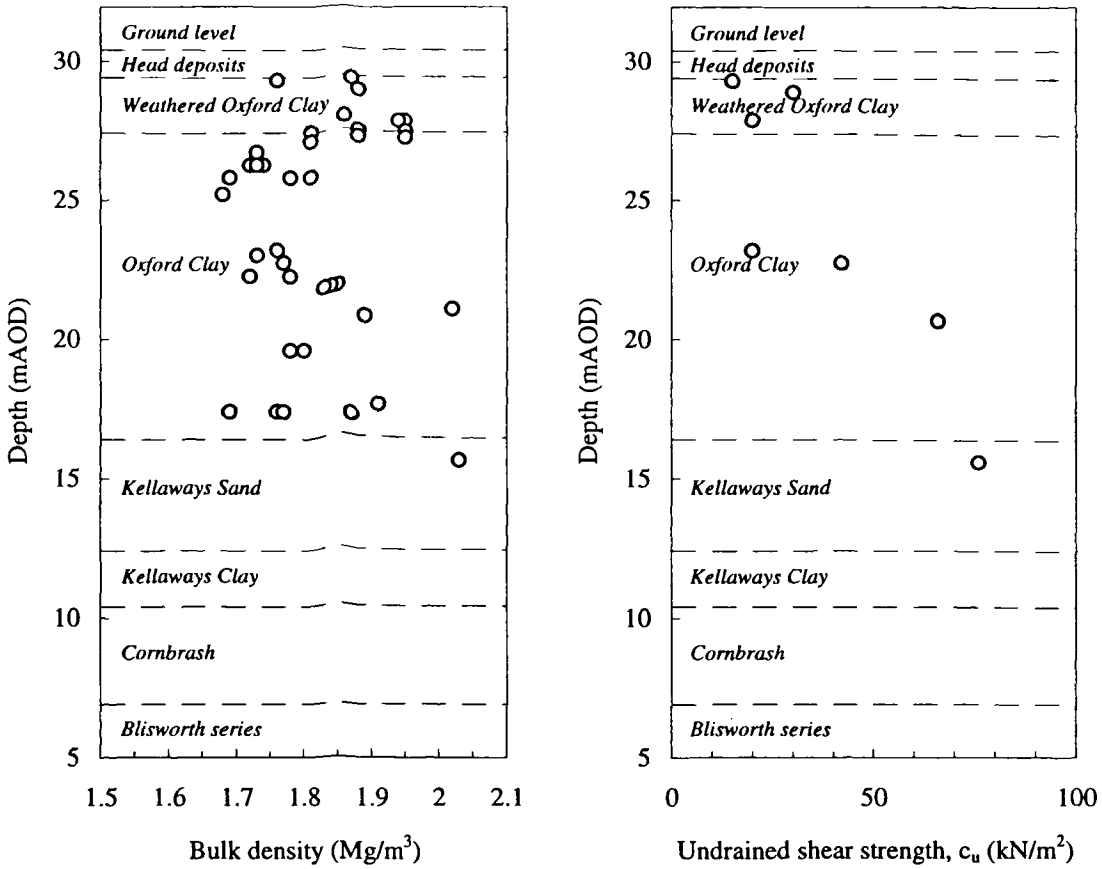

Figure 3.6 - Variation of bulk density and undrained shear strength with depth

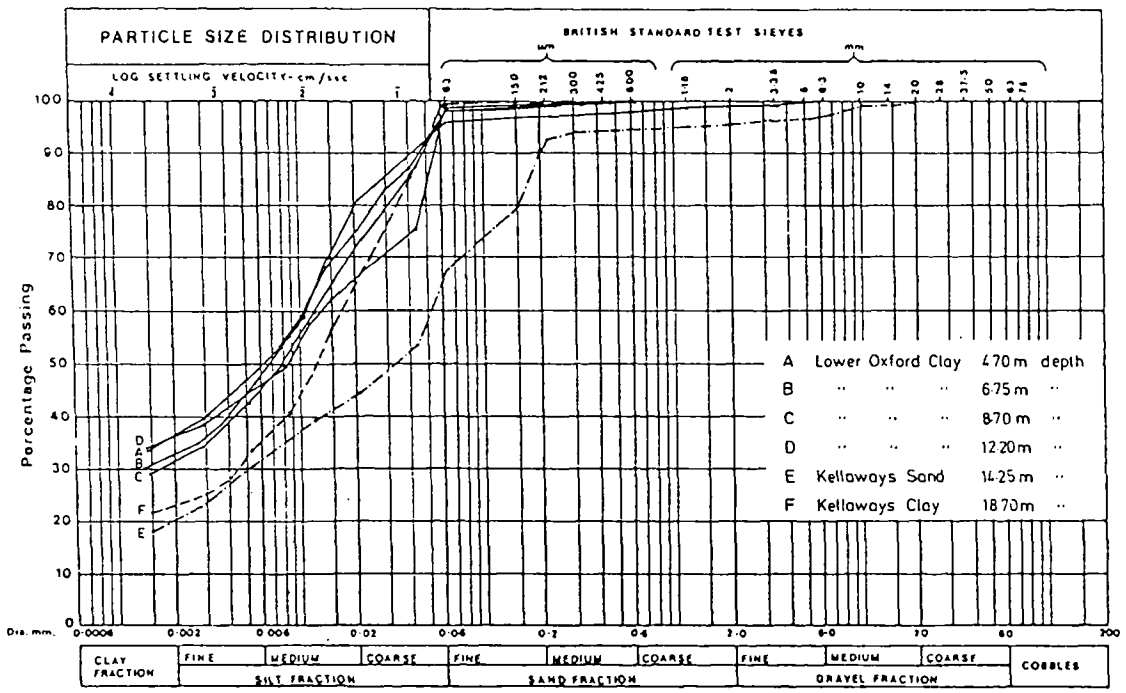

Figure 3.7 - Site investigation particle size distribution curves (after Rudrum, 1990)

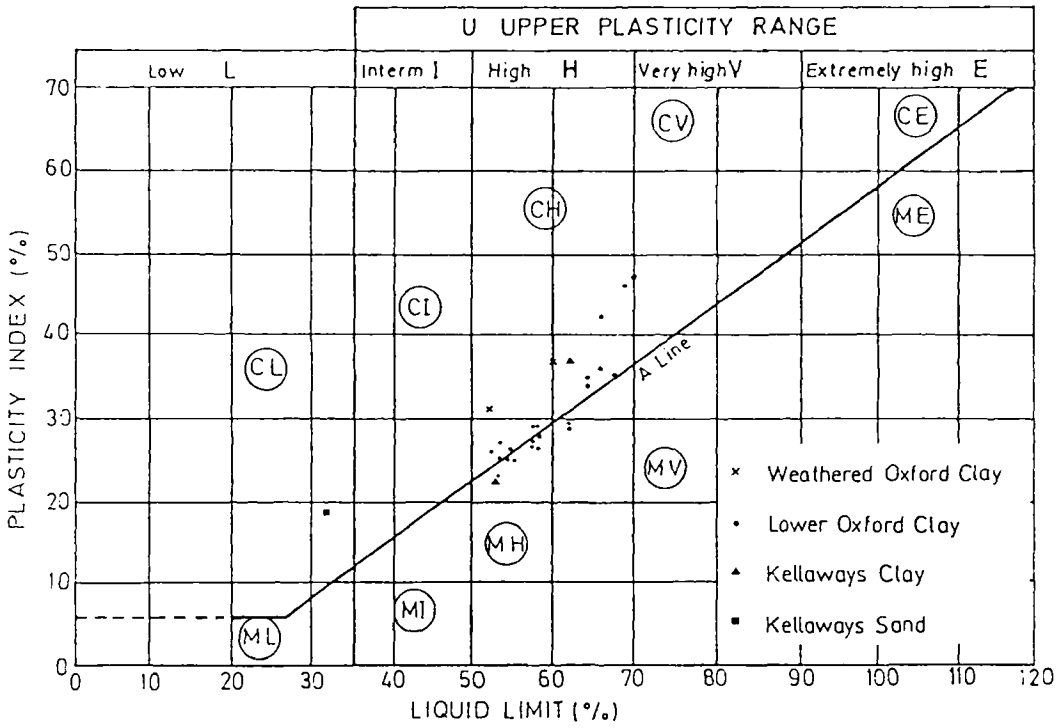

Figure 3.8 - Casagrande soil classification for Elstow strata (after Rudrum, 1990)

3.4.3 *In situ* tests

PRESSUREMETER TESTING

At Elstow, two types of pressuremeter were used to cope with the range of materials encountered:

- The Cambridge *In situ* self-boring pressuremeter, the Camkometer
- The Cambridge *In situ* direct strain measuring high pressure borehole dilatometer

The Camkometer was designed to be used in soft ground conditions, but it has also been applied to stiff clay sites (O'Brien *et al.*, 1992). At Elstow the Camkometer was intended for use in the Oxford Clay and Kellaways Beds, although a limited number of tests were attempted in the Blisworth Strata.

In total, 65 tests were carried out with only a 57% success rate. Severe problems were encountered during the self-boring phase in which 65% of the failures occurred. These were typically due to the pyritised shell bands within the Oxford Clay, the cemented sands within the Kellaways Beds, and the gravel within the head deposits being impenetrable to the cutting shoe. Additionally, in some cases poorly formed borehole walls led to uneven expansion stresses and consequent bursting of the membrane.

The successful tests were typically stress controlled during the stiff, small strain response, before transferring to strain control as failure was approached. Three unload-reload loops were also incorporated in the majority of tests. The 'lift-off' method (Mair and Wood, 1987) was applied to estimate the *in situ* stress condition, which was determined for each of the instrument's three strain arms. Where possible, unload-reload loops were performed

immediately following the lift-off pressure, at approximately 5% strain and prior to final unloading at the end of the test.

In the stiffer deposits the dilatometer was used. This instrument was designed for very stiff clays, dense sands and weak rocks. The 76mm diameter testing pocket is carefully preformed on the assumption that disturbance due to boring is less critical in such deposits. The general arrangement and testing strategy was similar to that for the self-boring pressuremeter, although the tests were purely stress controlled and proceeded in increments up to a maximum allowable pressure of 20MPa. Initially, several tests failed due to uneven membrane expansion in fractured strata or where softer clay beds were present, and subsequently the borehole core was examined beforehand to provide a uniform testing site. In total 21 successful tests were achieved out of the 37 attempted. Examining the borehole core prior to testing has perhaps incorporated a bias into the results such that the horizontal *in situ* stress measured is likely to be an upper bound result.

The pressuremeters and dilatometers were calibrated before each test by expanding the probe inside a rigid thick-walled steel cylinder to determine the instrument compliance.

The *in situ* horizontal stress and the *in situ* shear moduli are directly relevant parameters for predicting the ground response at Elstow. The *in situ* total horizontal stress data, Figure 3.9, show a wide scatter in the individual strain arm readings, although there is a definite trend of increasing stress with depth. The Camkometer and Dilatometer data are combined to show the variation to below the Blisworth series. Individual strain arm readings are only available for the Camkometer which show the limited depth to which the instrument could be applied.

In Figure 3.10 the shear moduli obtained from the unload-reload loops are plotted as individual readings for each loop and as the average for a particular test. A trend of increasing shear modulus with depth is observed and is most clearly defined for the Camkometer tests within the Oxford Clay. The degree of scatter increases significantly in the results of the Dilatometer tests carried out below the Kellaways strata. The trend is still perhaps of increasing modulus with depth, although the scatter in the averaged readings is of the order of 1000MPa.

The total vertical stress and the hydrostatic pore water pressure distributions are relatively straightforward to determine at the Elstow site and these may be combined with the *in situ* horizontal stress measurement to calculate the coefficient of earth pressure at rest, K_o'. Previously, the strain arm readings were considered individually, showing no clear variation of K_o' with depth and values ranging between 1 and 16 (Rudrum, 1990). The data were therefore reinterpreted using the average results from each test to give the *in situ* stress variation and the corresponding variation in K_o' shown in Figure 3.11. The average value of K_o' increases from 4 to 10 with depth through the Oxford Clay. The ratio reduces to 6 at the base of the Cornbrash and increases again to 9 through the Blisworth series.

During geological unloading the vertical stress in the ground reduces at a faster rate than the horizontal stress and eventually the ratio of horizontal stress to vertical stress is such that passive failure results. This limiting condition is defined following Rankine's method in equation 3.1 to determine the maximum allowable horizontal stress.

$$P'_h = \left(\frac{1+\sin\phi'}{1-\sin\phi'}\right)\sigma'_v + 2c'\sqrt{\left(\frac{1+\sin\phi'}{1-\sin\phi'}\right)} \quad \text{..... (3.1)}$$

P'_h = horizontal effective stress at passive failure
σ'_v = vertical effective stress in the ground

The implied value of K'_o is calculated, using the parameters shown in Figure 3.5, and presented in Figure 3.12 including the effect of variation in the degree of cohesion. It is clear that the measured *in situ* stress exceeds the theoretical maximum value unless the cohesion term has a significant influence.

Several empirical relationships have been proposed relating K'_o to overconsolidation ratio. One which is widely used was given by Mayne and Kulhawy (1982). For the idealised case of overconsolidation resulting purely from the removal of overburden, with no subsequent reloading, the relationship is given by equation 3.2.

$$K'_o = (1-\sin\phi')(OCR)^{\sin\phi'} \quad \text{..... (3.2)}$$

$OCR = \frac{\sigma'_{vm}}{\sigma'_v}$, σ'_{vm} is the maximum past vertical effective stress

Further empirical relationships are provided by Wroth (1975, 1976). He suggested two alternative relationships. Equation 3.3 was suggested to apply up to an overconsolidation ratio of 5 and equation 3.4 for higher overconsolidation ratios.

$$K'_o = OCR\,K'_{nc} - \frac{\nu'}{1-\nu'}(OCR-1) \quad \text{..... (3.3)}$$

$$m\left[\frac{3(1-K'_{nc})}{1+2K'_{nc}} - \frac{3(1-K'_o)}{1+2K'_o}\right] = \ln\left[\frac{OCR(1+2K'_{nc})}{1+2K'_o}\right] \quad \text{..... (3.4)}$$

where, $K'_{nc} = 1-\sin\phi'$
$m = 0.022875\,\mathrm{PI} + 1.22$,
PI is the plasticity index in %

A similar and more straightforward alternative to equation 3.4 was proposed by Parry (published in Britto and Gunn, 1987) and is shown in equation 3.5.

$$K'_o = K'_{nc}(OCR)^{\phi'} \quad \text{..... (3.5)}$$

Using the geological history referred to in section 3.3.2, an average bulk density of 2Mg/m^3 and an angle of shearing resistance of between 25° and 30°, the variation in K'_o and OCR with depth predicted by the Mayne and Kulhawy relation is presented in Figure 3.12. The variation in K'_o with depth predicted by either equation 3.4 or 3.5 is broadly similar to that of equation 3.2. Again the comparison with the measured results is poor and the general trend with depth is reversed.

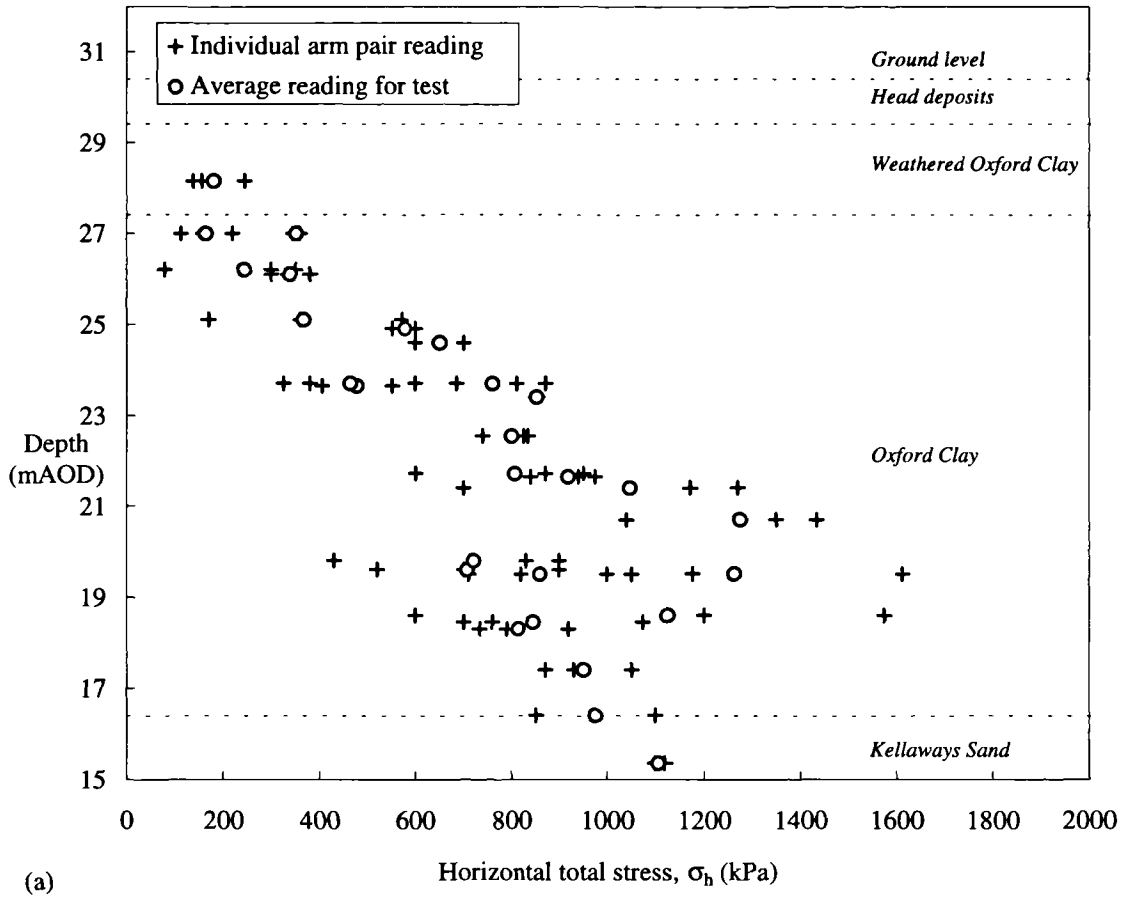

(a)

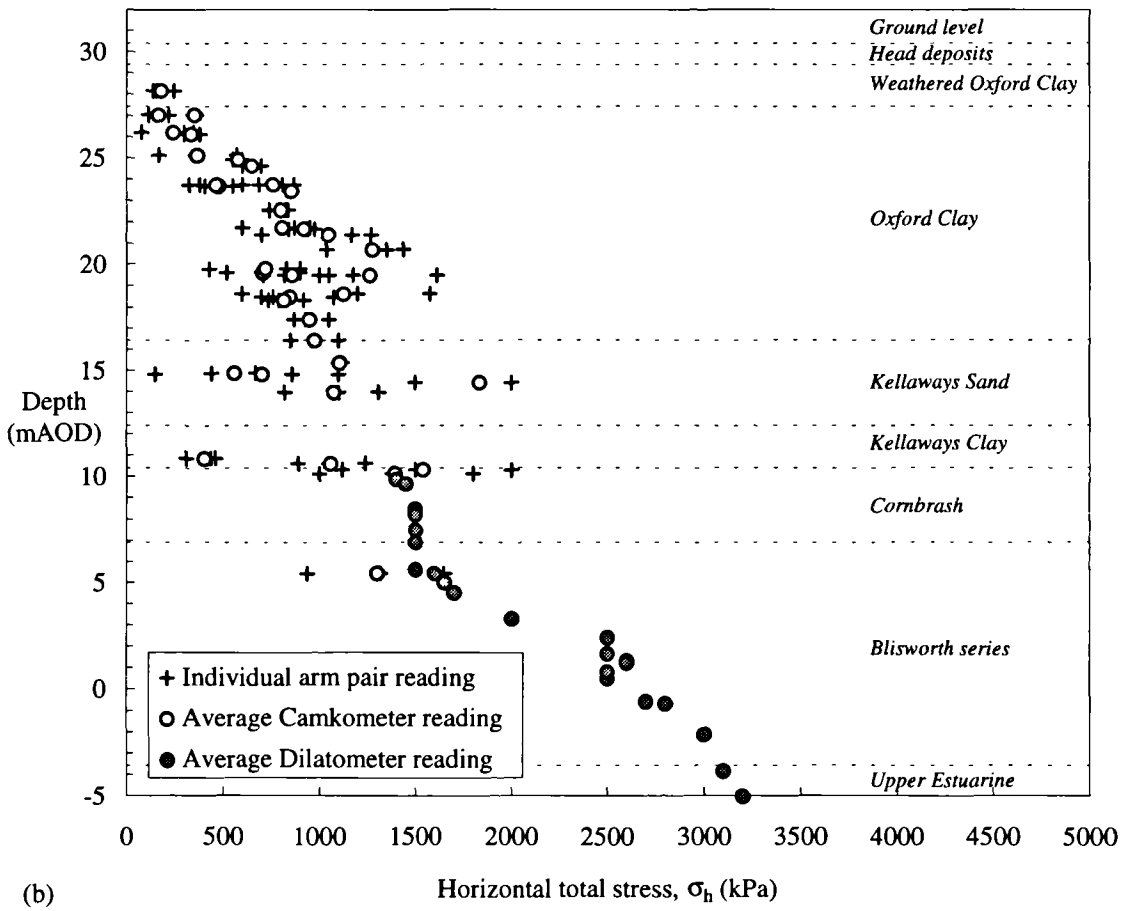

(b)

Figure 3.9 - *In situ* measurements of horizontal total stress

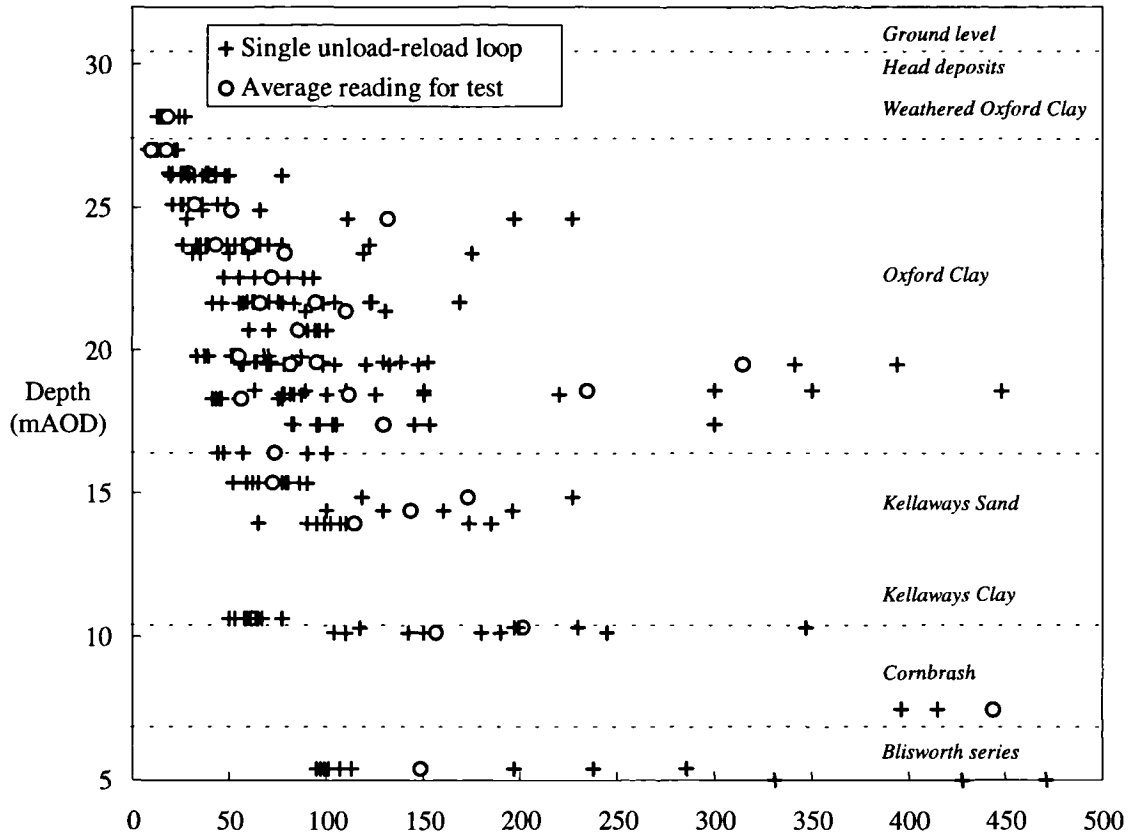

(a)

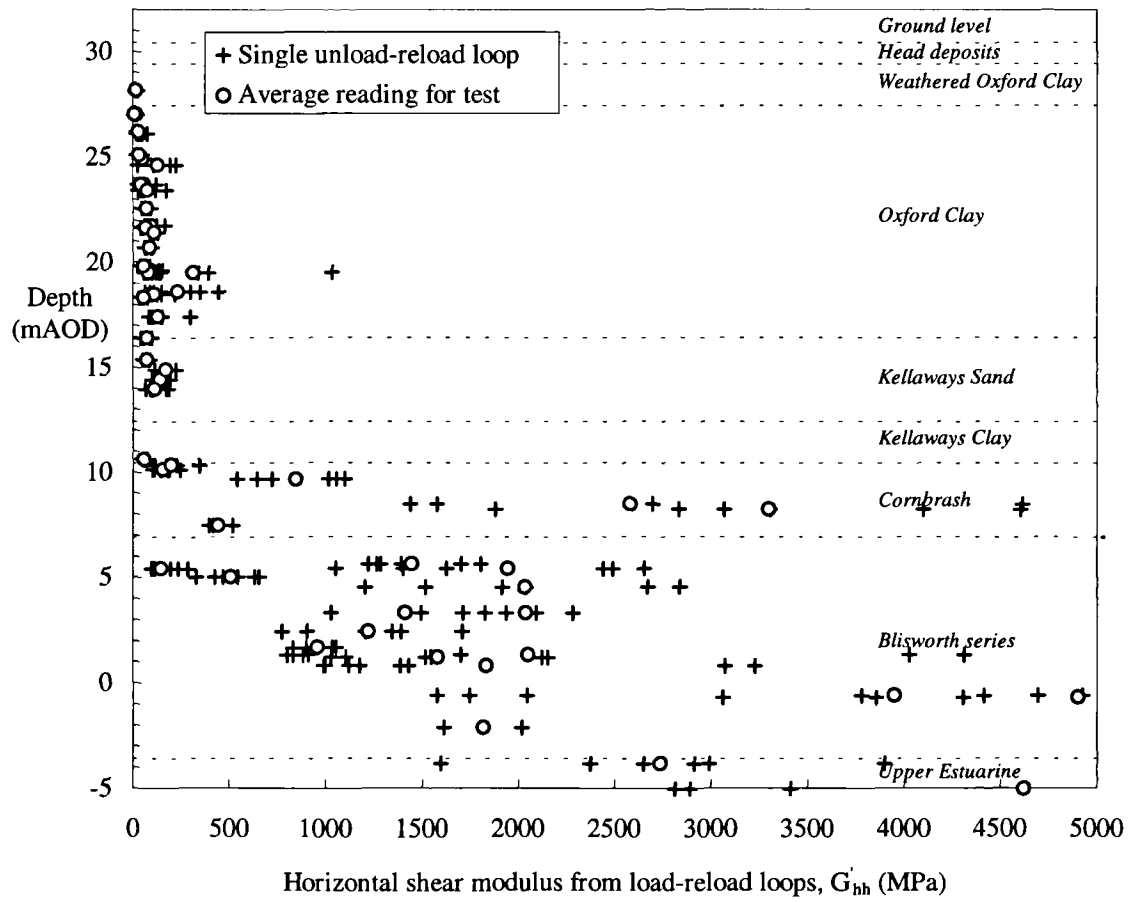

Figure 3.10 - *In situ* measurements of horizontal shear modulus

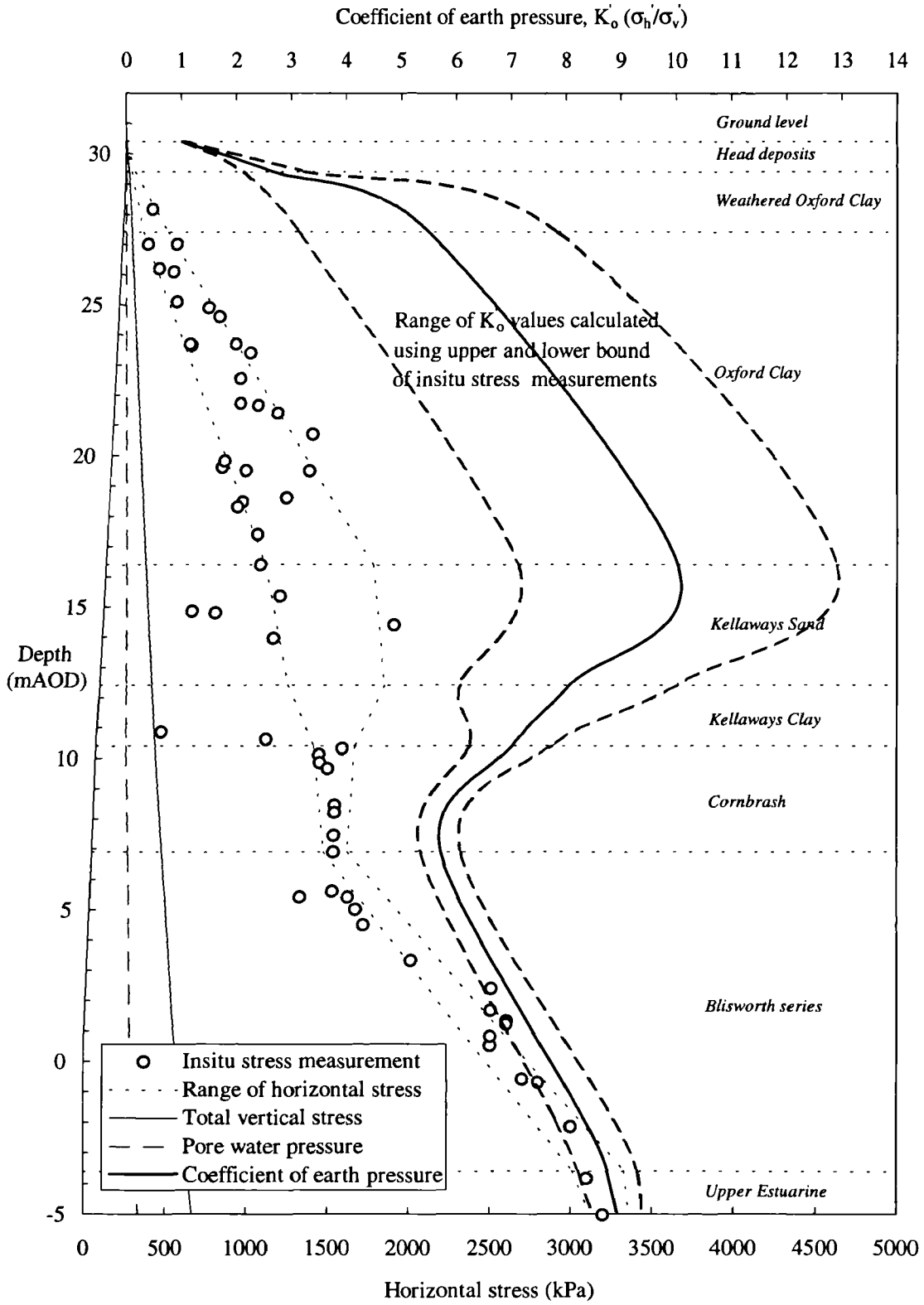

Figure 3.11 - Variation of *in situ* stress and earth pressure coefficient with depth

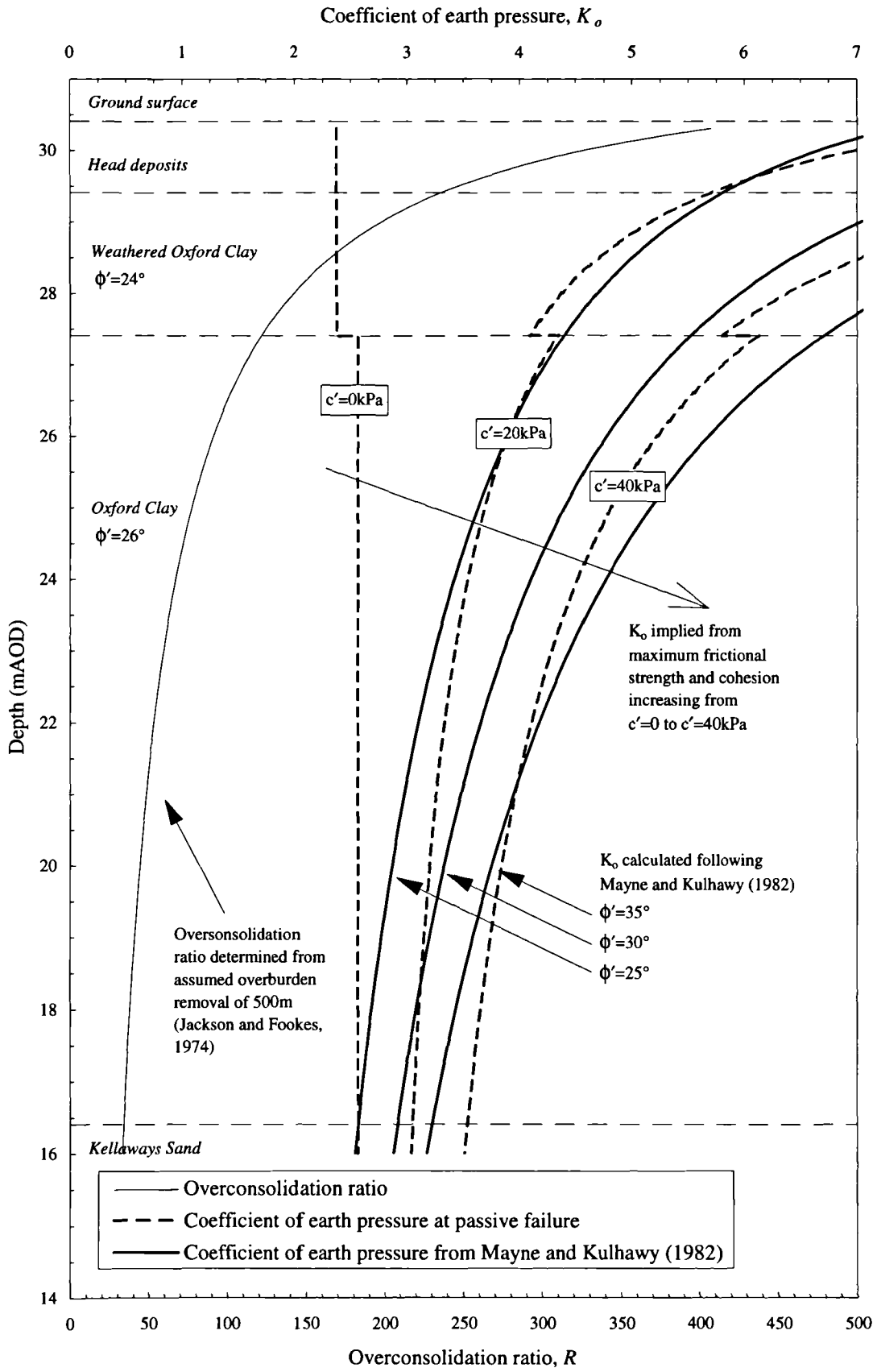

Figure 3.12 - Interpreted variation of overconsolidation ratio and coefficient of earth pressure with depth

PLATE LOADING TESTS

A series of 4 plate loading tests was carried out as excavation progressed to investigate the variation in the soil properties with depth.

The data (applied load against vertical plate displacement) were analysed by NHSEL to BS 5930 specifications to determine values of Young's modulus from initial loading and from unload-reload loops (see Table 3.2).

The interpretation of plate loading tests to determine deformation moduli is not straightforward. The boundary conditions are ill-defined and the strain field is based on elasticity theory. Marsland and Eason (1973) installed instrumentation below the loading plate, allowing an approximate calculation of the strain level during testing and more clearly defining the non-linearity of soil stiffness.

Test No.	Depth	E_i	E_1	E_2	E_u	E_y
	(m)	(MPa)	(MPa)	(MPa)	(MPa)	(MPa)
1	0.45	16.88	22.06	18.75	18.75	3.75
2	2.85	-	-	-	14.00	10.00
3	4.85	13.75	29.81	18.35	13.27	5.00
4	7.15	29.40	72.00	27.50	-	-
Constant rate of penetration test on tests number 3						
3	4.85	52.14	-	-	27.41	8.80
Failure load = 590kN, at 9% strain.						

E_i: Initial modulus; E_1, E_2: Reload moduli
E_y: Yield moduli; E_u: Final unloading modulus

Table 3.2 - Deformation properties derived from plate loading tests

PERMEABILITY TESTS

A series of 39 permeability measurements using constant and variable head tests were carried out in the 10 Casagrande piezometers at the trial excavation. It was hoped to repeat these tests following excavation to determine the change in permeability following stress relief. Such information would have been invaluable when considering the field instrumentation results presented in Chapter 4 but, due to the suspension of works, such a comparison could not be carried out. The results of these tests, as determined by NHSEL, are summarised in Table 3.3.

Strata	Number of tests	Minimum permeability (m/s)	Maximum permeability (m/s)	Average permeability (m/s)
Oxford Clay	4	1.09×10^{-10}	1.07×10^{-9}	**6.0×10^{-10}**
Kellaways Sand	12	1.69×10^{-8}	6.75×10^{-7}	**3.1×10^{-7}**
Cornbrash	11	6.08×10^{-9}	3.07×10^{-8}	**1.4×10^{-8}**
Blisworth strata	11	1.41×10^{-8}	4.62×10^{-8}	**3.4×10^{-8}**

Table 3.3 - Summary of *in situ* permeability tests

3.4.4 Geophysical testing

SEISMIC REFRACTION SURVEYS

Seismic refraction techniques are used to locate boundaries in the ground between materials having different seismic velocities.

The seismic waves can penetrate to 30m so it was anticipated that a seismic survey would establish the thickness of the drift materials, the thickness of the weathered and unweathered Oxford Clay, the depth to the top of the Kellaways Sand, the depth to the top of the Cornbrash strata and the location of any faults or infilled channels. However, the survey met with only limited success. This was mainly due to the low energy input produced by using a lead slug propelled into the ground as a seismic source.

Variable and low velocities were encountered in the upper layer of material at the site and it was not possible to detect any discrete geological boundaries, the depth of the drift materials or the depth of the weathered zones. The second layer interpreted from the seismic data extended from the weathered Oxford Clay to beneath the Kellaways beds. The distinction between the Oxford Clay and Kellaways Sand should have been clear, as the latter is considerably stiffer and consequently has a greater seismic velocity. However, the thickness of the Kellaways Sand and its depth of occurrence were such that the arrival of seismic waves from this stratum was masked by reflected waves from deeper, stiffer strata which arrived first. The lower boundary of this zone was interpreted as the top of the Cornbrash, but could only be detected to an accuracy of ±4 to 10m and so the expected small scale faulting (of the order 2m throw) could not be established.

Although as a survey of ground structure this technique did not prove particularly useful, it did produce shear wave velocity measurements in the upper deposits which were incorporated into the initial finite element analyses (see section 3.8).

CROSS HOLE SEISMIC SURVEY

In a cross hole seismic survey the travel time of compression and shear waves is measured between two points.

It was thought that the clay deposits would be cross-anisotropic and to verify this an L-shaped array of boreholes was adopted to assess the similarity in moduli between the two wings of the L. The layout of the borehole array is shown in Figure 3.13. The boreholes were spaced at 5m intervals which was considered short enough to limit the refraction caused by multi-layered strata. The boreholes were drilled to 30m depth to provide measurements down to and including the Blisworth strata. Verticality surveys of the boreholes were carried out to provide an accuracy of ±3% of the separation distance at any given depth.

Since the exact instant of seismic wave initiation could not be accurately determined, the transmitter was placed in one of the outer boreholes and the wave travel time recorded between two other boreholes in line. Testing was therefore carried out with a transmitter in either E5, G1 or G4 and receivers in the remaining boreholes of the array.

Compression waves generally travel more quickly than shear waves and may therefore mask the arrival of the latter. For shear wave measurements it is necessary to use a source which maximises the ratio of shear wave energy to compression wave energy. A shear hammer was used as the transmitter with the shear wave arrivals recorded by three-component geophones clamped to the borehole lining. An airgun was used to initiate compression waves which were recorded by hydrophones immersed in water filled boreholes. A seismic record was then obtained by activating the seismic source and recording the resulting output from the receivers placed at the same depth in the adjacent boreholes.

Although compression wave measurements were made successfully at all test locations, it was not always possible to determine the instant of shear wave arrival and the quality of the data subsequent to the compression wave arrival was often poor. The combination of continued refraction of the compression wave and the choice of an unsuitably short seismograph record, in order to maximise resolution, often prevented recognition of the shear wave arrival.

The primary distinction between shear waves and compression waves on the seismic trace was intended to be the reversal of shear waves following a reversal of the shear hammer impact direction. It was found, however, that the compression waves as well as the shear waves apparently reversed polarity. This is consistent with the first wave arrival being exclusively composed of near-field terms (see section 2.6.4) since these reverse in polarity when the direction of the impulse is changed (see later in section 6.5.2).

Of the thirty tests carried out, nine produced data from which shear wave arrivals could be determined at the two receiver boreholes; eight readings provided a shear wave arrival at the nearest borehole and the velocity computed was therefore less accurate; the remaining tests only produced compression wave arrival times.

The variation in the dynamic shear modulus with depth was calculated from the interpreted shear wave velocity using equation 2.15, and is shown in Figure 3.14. It may be noted that the scatter in the data increases markedly below the Kellaways strata (i.e. below about 20m depth). This is possibly due to increased refraction effects in the compression wave, caused by the

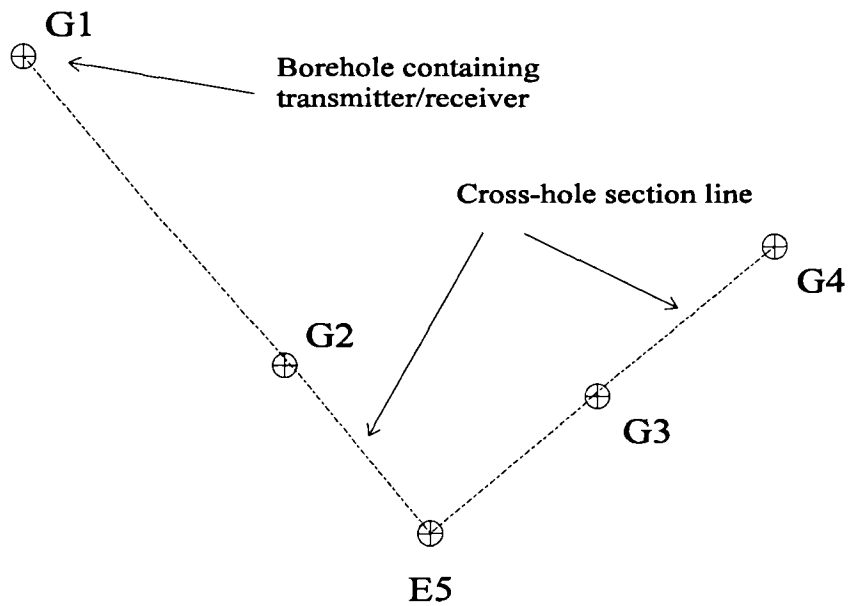

Figure 3.13 - Location of boreholes and section lines for geophysical survey using cross-hole technique

reduced strata thickness at these depths, further masking the shear wave arrival.

The compression wave and shear wave measurements may be used to calculate Poisson's ratio. However, for a saturated medium, the fluid is relatively incompressible compared to the soil skeleton and since the rate of loading in a dynamic event is high the soil behaviour remains undrained and the compression wave first arrival is likely to have travelled via the pore water. The compression wave velocities were in fact close to 1500m/s, the velocity of wave propagation in water, and the computed Poisson's ratios were close to 0.5.

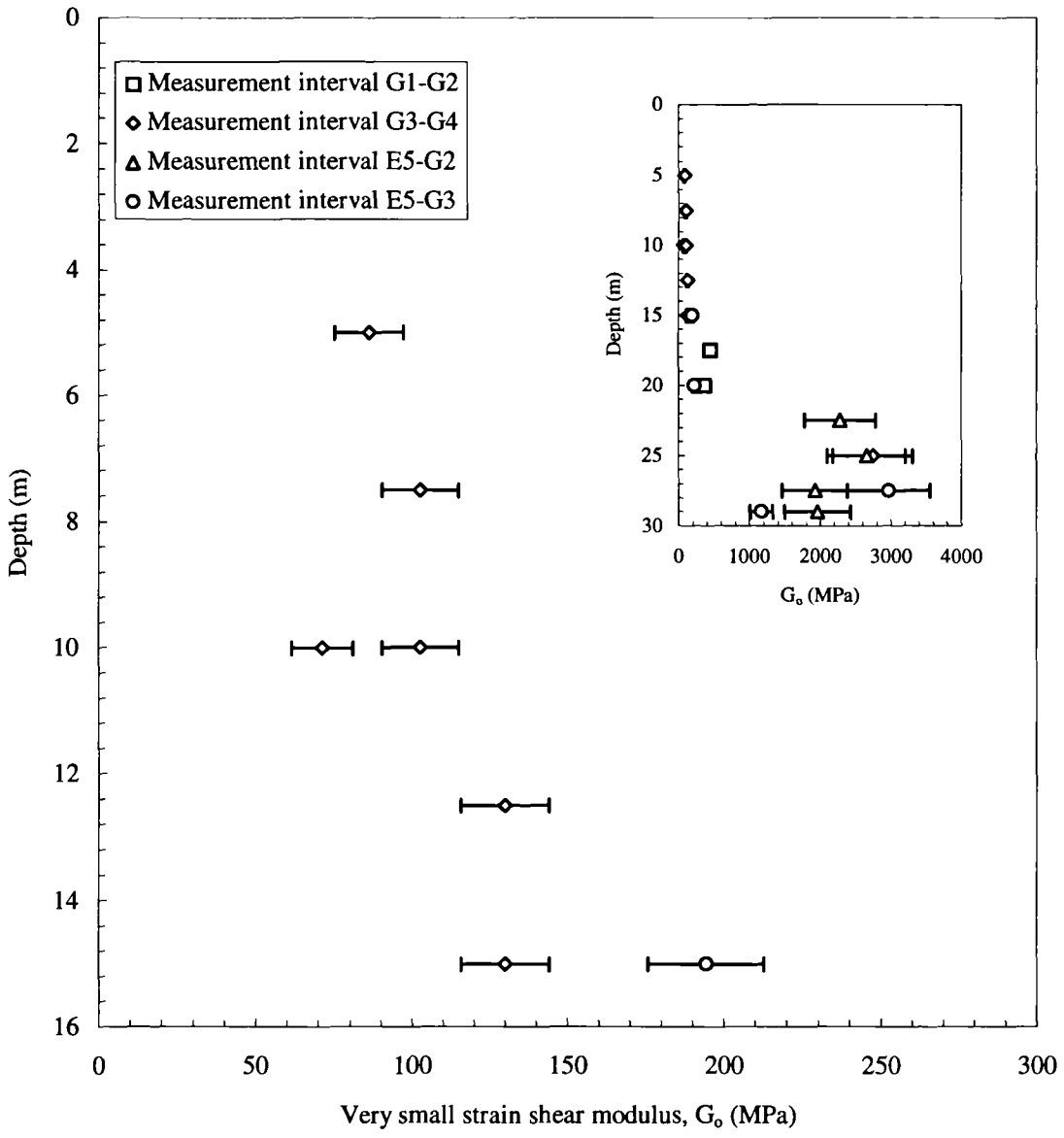

Figure 3.14 - Variation of very small strain shear modulus, G_o, with depth, measured by the cross-hole geophysical survey

3.5 Earthwork details

It was believed that at Elstow the strata likely to be affected by the construction of a shallow repository contained a large scale macrofabric (see section 3.3.2). With such structural features, it was possible that the mass behaviour could not be determined through laboratory testing of relatively small specimens taken from boreholes or trial pits or through the *in situ* tests on slightly larger volumes. It was considered that the best way to investigate the mechanical and hydrogeological ground response was to carry out a trial excavation with dimensions approximating any future repository construction.

A trial excavation was constructed on a scale to achieve stress changes in the ground comparable to those produced by the construction of a prototype shallow repository. This required the excavation to be 10m deep and to have a base width of 10m. To allow simpler interpretation of the instrumentation data the excavation base length was to be such that plane strain conditions existed around the main instrumented section. Preliminary computer modelling (see section 3.8) suggested that a base length of 50m would be adequate. The overall shape of the excavation was dictated by access requirements, the requirement to minimise damage to the surrounding farmland and the overall stability of the excavation. This led to a 1 in 4 access ramp and side slopes of 1 in 1 in the unweathered Oxford Clay and 1 in 2 in the weathered upper zone, with a 1m wide bench between the two slopes at a depth of 3m. This produced overall dimensions of the excavation at ground level of 104m long by 38m wide and involved the removal of 15,000m^3 of material.

The excavated material was used in the following ways:

- To construct a trial embankment which was hoped to,
  - allow a large scale test of the response of the Oxford Clay to surcharge load
  - allow field testing of the excavated material as potential backfill
- To construct a number of small stockpiles, some protected, the remainder left unprotected, to assess the effect of weathering on the Oxford Clay

The trial embankment was 6m high and took the form of a 120m long elongated pyramid, 10m wide at the peak, 38m wide at the base, with end slopes of 1 in 5 and 1 in 15, and side slopes of 1 in 2. Only limited instrumentation was placed beneath the embankment, so the ground response is difficult to interpret and has not been attempted here.

The layout of the site with the locations of the trial excavation, the trial embankment and the various stockpiles of excavated material is shown in Figure 3.15.

It was hoped that the trial excavation and the associated instrumentation would allow an assessment of the *in situ* stress conditions and provide a quantitative measure of the ground movements and pore water pressure response over the short, medium and long term. From the geotechnical standpoint, it is unfortunate that the project had such a short time scale, as the weathering effects could not be investigated and only the short term ground response could be assessed.

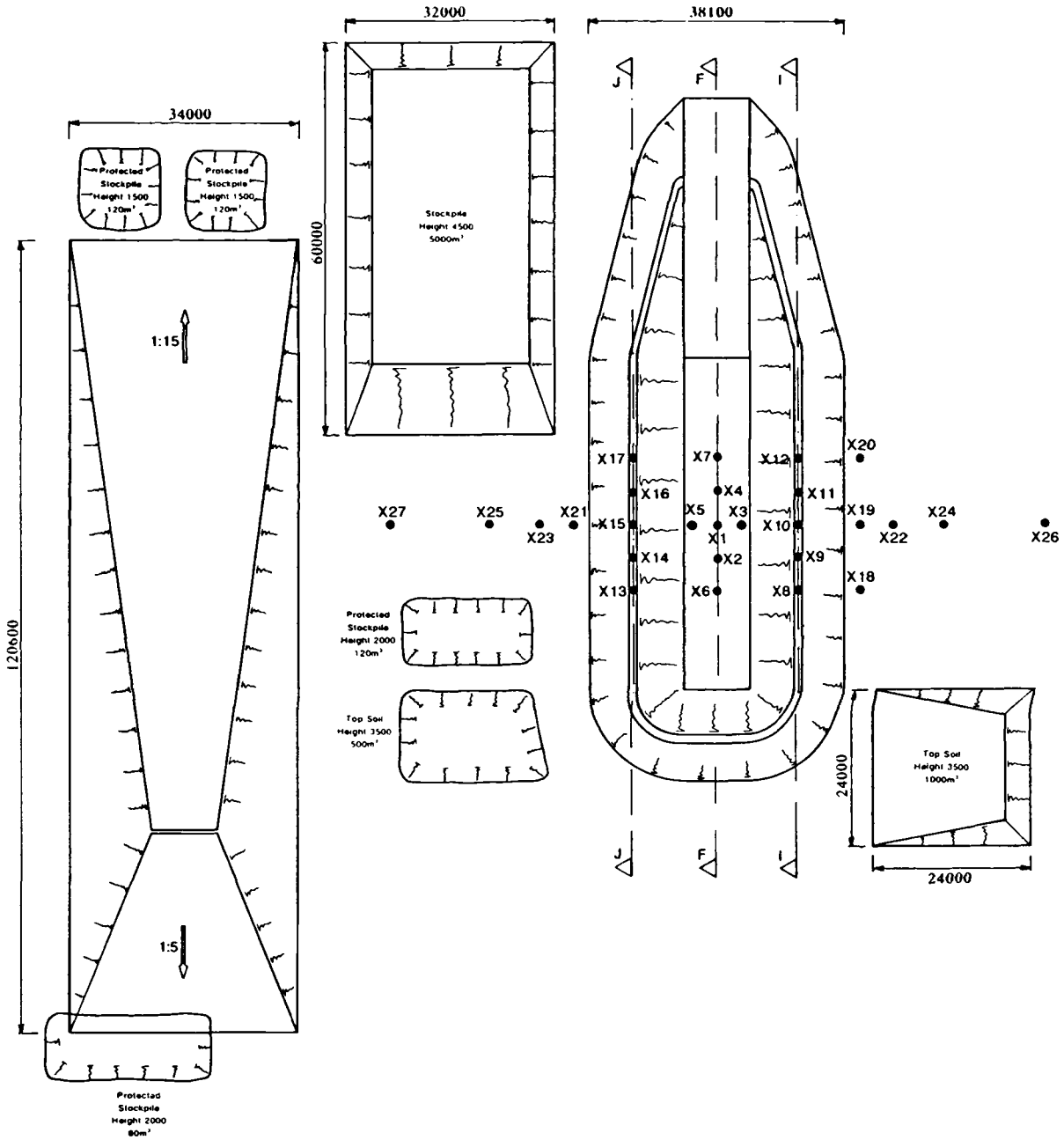

Figure 3.15 - As constructed plan view of experimental trial excavation, trial embankment and earthworks stockpiles

3.5.1 Description of excavation works

The site earthworks started on 18 March 1987 with topsoil being stripped across the site and the excavation commencing the following day. The excavation proceeded to the required depth of 10m in stages of 3m, 2m, 2.5m and 2.5m. Each stage was substantially complete before excavation progressed to the next level. The first three stages were completed on 28 March, 2 April and 4 April respectively. At this stage, when the excavation was 7.5m deep, there was a break of three weeks to carry out a series of plate bearing tests (see section 3.4.3) and to allow the logging and sampling within the excavation to catch up with the earth moving operation. After this time the work continued for a further five days until the suspension of all site investigation works on 1 May 1987 (see section 3.1). The excavation had been completed to its full depth of 10m over 75% of the base area.

The detailed earthworks records maintained by NHSEL allowed the construction excavation sequence to be determined (Rudrum, 1990) and this is reproduced in Figure 3.16 and Figure 3.17.

The progress of the excavation can be seen in the sequence of figures from Figure 3.18 to Figure 3.22.

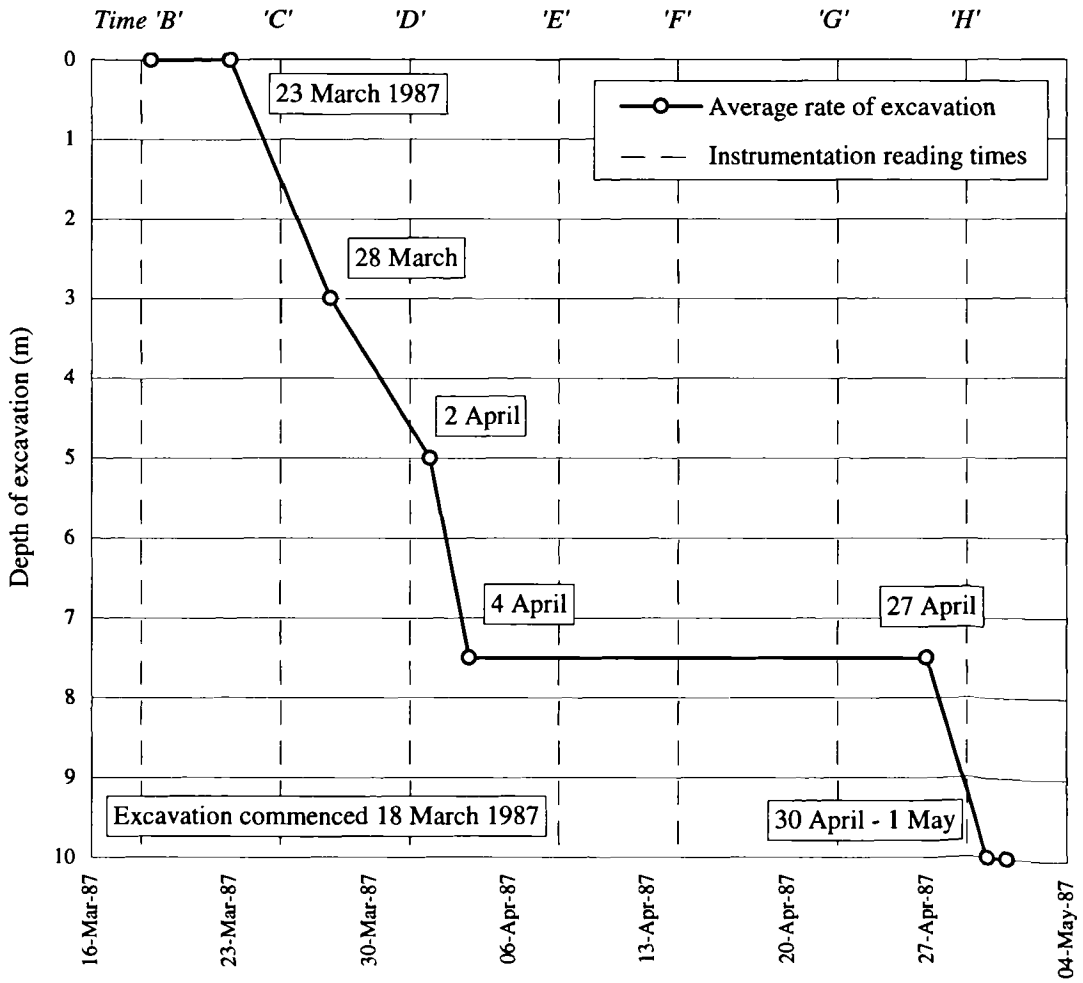

Figure 3.16 - Excavation sequence from site records (after Rudrum, 1990)

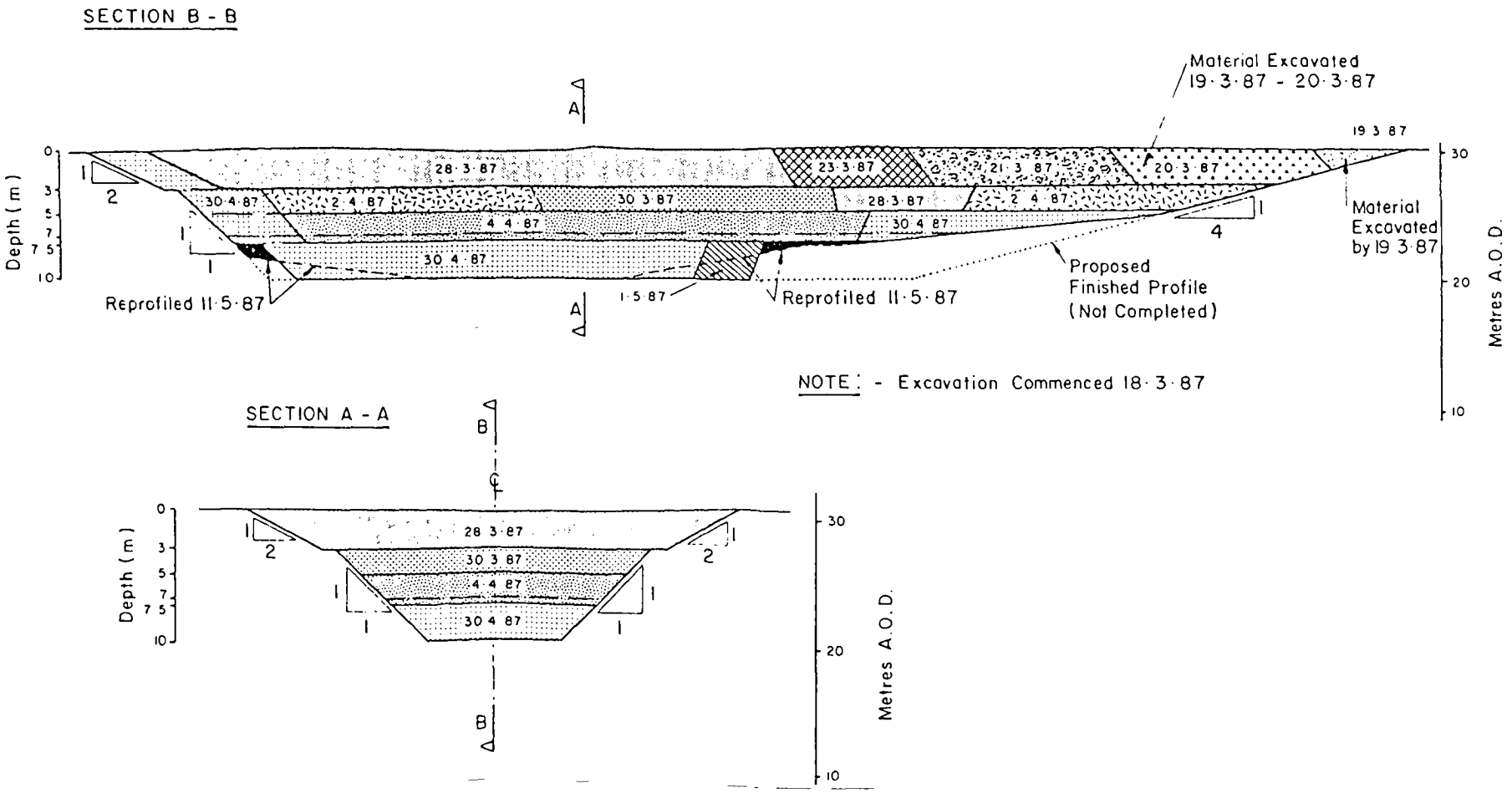

Figure 3.17 - Figurative excavation sequence determined from site records (after Rudrum, 1990)

Figure 3.18 - View from south-west showing excavation at 5m depth (2 April 1987)

Figure 3.19 - View from south-west showing excavation from 5m to 7.5m (3 April 1987)

Figure 3.20 - View from south-west showing excavation from 7.5m to 10m around instrument locations (30 April 1987)

Figure 3.21 - View from south-west showing stage of excavation at suspension of works and trial embankment in background (5 May 1987)

Figure 3.22 - View from south-west prior to backfilling excavation (31 July 1987)

3.6 Field instrumentation used at the Elstow excavation

An extensive array of instrumentation comprising inclinometers, extensometers and piezometers was installed to monitor the horizontal movement, vertical movement and the pore water pressure response respectively caused by the trial excavation.

The location of all the instrumentation is shown in Figure 3.23. The distribution of instruments across the site was based on preliminary elastic finite element analyses of the excavation (see section 3.8).

The displacement monitoring equipment was arranged to measure the distribution of movements and to prove that no movement took place where none was expected. Figure 3.23 shows the main instrumented section of the excavation and the instrumentation installed along parallel offsets designed to verify the assumption of plane strain.

The piezometers were concentrated in the areas were there was expected to be maximum unloading or shear stress development. In view of this the piezometers were located in clusters below the base of the excavation, below the edge of the excavation base and below the 1m wide bench, two thirds of the way up the excavation side slopes. The pore pressures were measured using twenty five acoustic (vibrating wire) instruments, numbered P1 to P25, and ten Casagrande piezometers, numbered P51-P60. Each of the piezometers was installed in a separate borehole with five holes at each of the seven piezometer group locations to provide a vertical distribution of the ground water response. The acoustic piezometers were chosen for their relatively fast response time compared with the Casagrande type. However the long term reliability of the acoustic instruments was held in doubt, so the Casagrande instruments were installed as a back-up system. The Casagrande piezometers also allowed *in situ* permeability testing.

The piezometer tips consisted of a cylindrical porous ceramic element with a pore diameter 60μm and a permeability of $3x10^{-4}$ m/s. They were installed in 150mm diameter boreholes

within 1-2m long sand cells. The sand cells were isolated at the top and at the bottom, where not located at the base of the borehole, using a 1m long hydrated bentonite pellet seal. The borehole was grouted to within 1m of the ground surface.

The monitoring of pore pressures beyond the excavation crest was carried out by 4 Westbay Multiport Piezometers, D22-D25, shown in Figure 3.23. These piezometers were designed to measure the ground water response at a number of levels in the same instrument by using inflatable packers between levels. Unfortunately these piezometers proved unreliable due to leakage between piezometer ports and have not been analysed (Rudrum, 1990). Due to the failure of the multiport piezometers, the piezometric response beyond the excavation crest is unknown.

The instruments used to measure ground displacements within the excavation were located at offsets of approximately 0m, 4.5m, 12.5m, 19m, 25m, 35m and 50m on either side of the excavation centreline. The main method used was a combined extensometer/inclinometer borehole installation. This allowed the three dimensional displacement field to be determined at each of these locations. In the four most remote installations, only inclinometers were installed as it was thought that vertical displacements would be negligible in this area.

All but one of extensometers used were magnetic probe devices, combined with the inclinometers and numbered X1-X23. A single multiple rod extensometer was installed, numbered R1.

The magnet extensometer system (Burland et al., 1972) consists of a number of circular ('ring' or 'spider') magnets axially magnetised and permanently fixed in positions at the locations in the ground where the vertical movement is to be measured. These magnets are able to slide on a central access tube within the borehole and, using a sensor to record their position with time, a record of the rate and amount of vertical displacement at that location can be obtained.

At each installation between six and eight magnet positions were installed with the lowest, the 'base' magnet, taken as a fixed datum from which all the other magnet positions were measured. The instruments were surveyed a number of times before the commencement of excavation to obtain a set of average distances between the base magnet and the magnets above which could be used as a datum for further readings.

The accuracy of this system, assuming the securing method is effective, depends on the accuracy to which the location of the magnets may be sensed. In this case the accuracy is approximately ±1mm, the limit to which the steel tape could be used. This is the most basic sensing method and was thought to be sufficient for the degree of movement expected. Burland et al. (1972) and Smith and Burland (1976) outline a number of more sophisticated techniques capable of resolving to 0.1mm.

The multiple rod extensometer (R1) was installed to provide a backup to the magnet extensometers in case unexpectedly large movements took place which would cut off the access tubes and prevent further monitoring. It was of more robust construction and consisted of four rods, anchored in grout at depths of 3m, 11m, 24m and 55m respectively, which each extended to a reference point at the hole collar. The borehole was grouted with each rod separated from the grout by a close fitting plastic sleeve. The movement of each rod was recorded with displacement transducers fixed to the reference head and acting on the end of each rod. This ought to have provided a measurement system with a resolution of 0.01mm. However, the measured vertical displacements were an order of magnitude lower than the magnet extensometer measurements. It was thought that either the initial calibration of the system was

inaccurate or the calibration was inappropriately applied. Therefore, the rod extensometer displacements were not interpreted further.

The inclinometer tubes were surveyed using a Soil Instruments MK IV biaxial inclinometer which detects changes in verticality using two force balanced accelerometers within the 0.5m gauge length probe. The biaxial probe allowed measurements to be taken in two perpendicular directions simultaneously and had a maximum negotiable curvature of 3.5m radius. Probe readings were recorded from the base of the access tube upwards at 0.5m intervals. The use of the biaxial probe allowed horizontal displacement profiles to be inferred for both the in-plane and out-of-plane directions.

As for the extensometer magnets, the inclinometer tubes were surveyed several times before the earthworks began to determine an initial deformed profile which could act as a datum. This set of base readings was calculated as the mean deviation from the vertical from a minimum of six surveys per instrument (NHSEL, 1988).

The calibration of the readout system was carried out regularly and the accuracy of the inclinometer probe was checked daily using a wall mounted reference frame. The inclinometer system has a measurement resolution of 0.1mm but the system accuracy depends on the installation depth, since errors accumulate as the probe traverses the length of the borehole.

The majority of the boreholes containing displacement instrumentation were 25m deep and passed through the Oxford Clay stratum and Kellaways Beds. These strata are relatively deformable and were thought most likely to be the ones affected by the excavation. The underlying Cornbrash formations are much stiffer and were thought suitable to provide a datum for the displacement measurements. The strata below the Kellaways Beds, being remote from the excavation, were expected to experience only small stress changes and consequently little recordable deformation. At the base of the excavation, however, three combined extensometer/inclinometer installations extended through the Blisworth Series and the Upper Estuarine to bed in the Lias strata at a depth of 60m to provide a check on any deep seated movements. Similarly, the piezometer tips were concentrated in the Oxford Clay, but there were installations in all strata down to and including the Lias.

The instrument readings taken at the trial excavation were specified on a daily basis by the supervising engineer with regard to the likely change in the magnitude of the readings and access requirements. It was essential that the instrumentation remained undamaged as the excavation progressed and so excavation took place around the instrument locations. Bulk excavation was carried out to within 1m of an instrument cluster and the remainder removed more carefully. This was initially done by hand but proved time consuming, so later the soil was carefully trimmed using a small 0.3m bucket attached to a backhoe excavator, which was equally effective. This method generally proved successful, but when the isolated column of soil surrounding an instrument reached about 3m in length it became unstable and, if toppled, would break the instrument tube contained within it. This caused no problems with the combined extensometer/inclinometer installations, since the tubing tended to bend and break leaving the active recordable length below the excavation base unaffected. The acoustic piezometer installations were unaffected, since the cables were protected and did not break. On the other hand Casagrande piezometers were affected if the level of water in the installation was above the excavation base level. An attempt was made to overcome this problem by installing Druck pressure transducers, but the transducers were in short supply and proved ineffective.

The interpreted inclinometer, extensometer and piezometer records are presented in Chapter 4

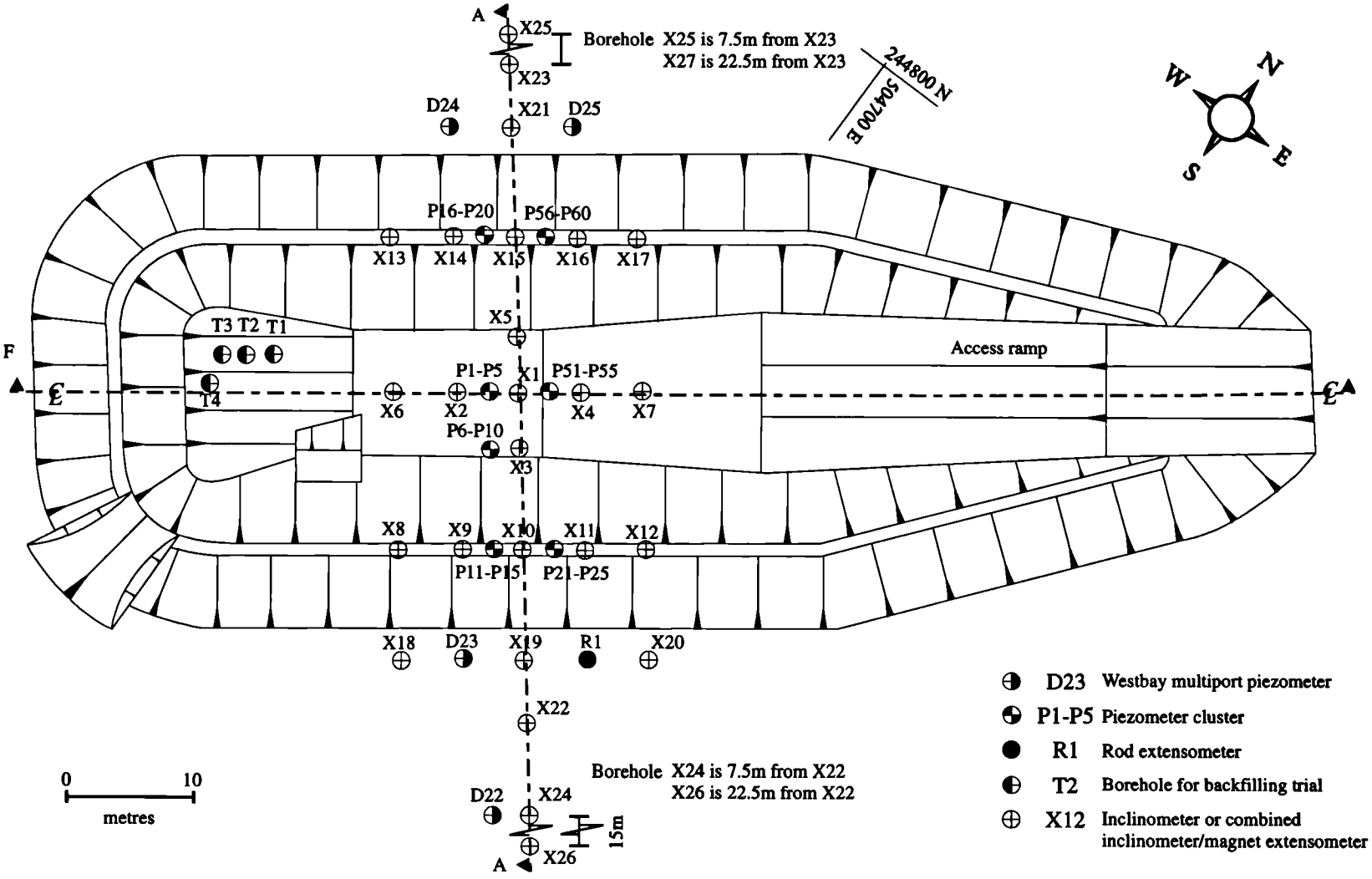

Figure 3.23 - Plan view of Elstow trial excavation with instrument locations

3.7 Aspects of site investigation to determine the ground structure

3.7.1 Introduction

One of the principal concerns of the Elstow site investigation was with the groundwater flow regime, both before and after construction of a repository. The investigation therefore was required to describe not only the composition of the ground, but most importantly its structure and fabric as this would critically affect the degree and pattern of groundwater flow.

3.7.2 Trial pits (logging and sampling)

A suite of trial pits was designed to investigate and sample the near surface deposits, specifically the Head Deposits, any Alluvial or Glacial Deposits, any Made Ground and the underlying weathered Oxford Clay.

Particular attention was paid to the logging of discontinuities within the clay soils. In the weathered and unweathered Oxford Clay fissure spacing was noted. Sub-vertical desiccation cracks were present in the Head Deposits and weathered Oxford Clay; their spacing and surface nature was described using standard terms defined during the investigation. Within the Head Deposits shear surfaces were noted and those with greater than an arbitrary 0.5m exposed length were individually described and plotted on the face logs and their orientations were recorded.

The trial pits were excavated nominally 1m wide, 3 to 5m long and 3.8m to 4.5m deep with a bench at one end to assist access.

Several of the trial pits remained dry, but there was often a seepage of ground water either from the granular Head Deposits, from the fissured clay towards the base of the pit, or from intercepted land drains. The pits were periodically pumped dry, although in none of the pits was continuous pumping required.

Of the 19 trial pits scheduled, nine were carried out before the suspension of works. In the immediate vicinity of the trial excavation, four trial pits were carried out in association with a series of plate loading tests. These trial pits were logged in similar detail, but also included the logging of prominent fissures in the unweathered Oxford Clay, since they penetrated to a greater depth. These fissure details have been incorporated with those logged on the excavation profiles and included in Figure 3.26.

Early on in the trial pitting programme it was established that high quality undisturbed block samples could be successfully taken and at a similar time it was realised that the quality of the cored samples (taken with the triple tube Mazier type core barrels - see section 3.7.4) was not as good as had been hoped. It was therefore decided to place a greater emphasis on obtaining block samples to provide undisturbed specimens for laboratory testing.

Block samples were taken in six of the trial pits at intervals to cover the full range of cohesive material types identified within the trial pit after logging. Trial pits with significant water seepage were avoided due to the difficulty this would have created in sampling.

A trial pit block sampling operation is shown in Figure 3.24. The benched end of the trial pit was extended and widened into a battered excavation to provide safe access for the taking of the samples. The deepest samples taken in this manner were from nearly 4m depth resulting in an excavation approximately 7m square at the surface. Once the bench and any side trenches

had been excavated to within 0.3m of the proposed sample location, the block of soil was trimmed by hand. In the softer Head Deposits and weathered Oxford Clay the samples were cut by spade, various hand tools or cheesewire. In the stiffer slightly weathered Oxford Clay the samples were cut by chainsaw With the sample isolated on all four sides, but still attached at the base, the top of the sample was marked with a North arrow, a sample label added and then the whole covered in aluminium foil and cheesecloth which was liberally impregnated with paraffin wax. A further sample label was embedded in the wax. A four sided wooden box was placed over the sample and the gap between sample and box filled with an expanding polyurethane foam. The wooden lid was fixed in place and the excess foam was allowed to exude through holes in the lid. Once set the surplus foam was cut off and a further label attached to the lid and a North arrow was also usually drawn on. The base of the sample was cut off by cheesewire or spade and then trimmed down by hand, and further foil, waxed cheesecloth and foam were added before the base lid of the box was fixed in position.

Figure 3.24 - Block sampling in a trial pit at the Elstow excavation

3.7.3 Trial excavation (logging and sampling)

The trial excavation permitted the detailed logging of the fabric and structure of the Oxford Clay, and the overlying weathered deposits, and the taking of relatively large 'undisturbed' samples.

It was decided that the lateral and vertical variation in the ground conditions could be determined by logging several isolated profiles at intervals along the excavation faces Five stepped profiles were therefore specified for detailed logging as shown in Figure A.1, Appendix A. The profiles were approximately 5m wide and excavated in 1.5m steps to provide easily accessible vertical faces. These steps were removed after logging when excavating the final excavation side slopes.

The faces were excavated near vertical or slightly inclined to aid stability. There were no significant failures of the logging faces during the course of the works and only minor spalling occurred. Slight groundwater seepages were experienced from the excavated faces, but few persisted for many days after excavation A notable exception to this was from a 'blocky' clay

(a)

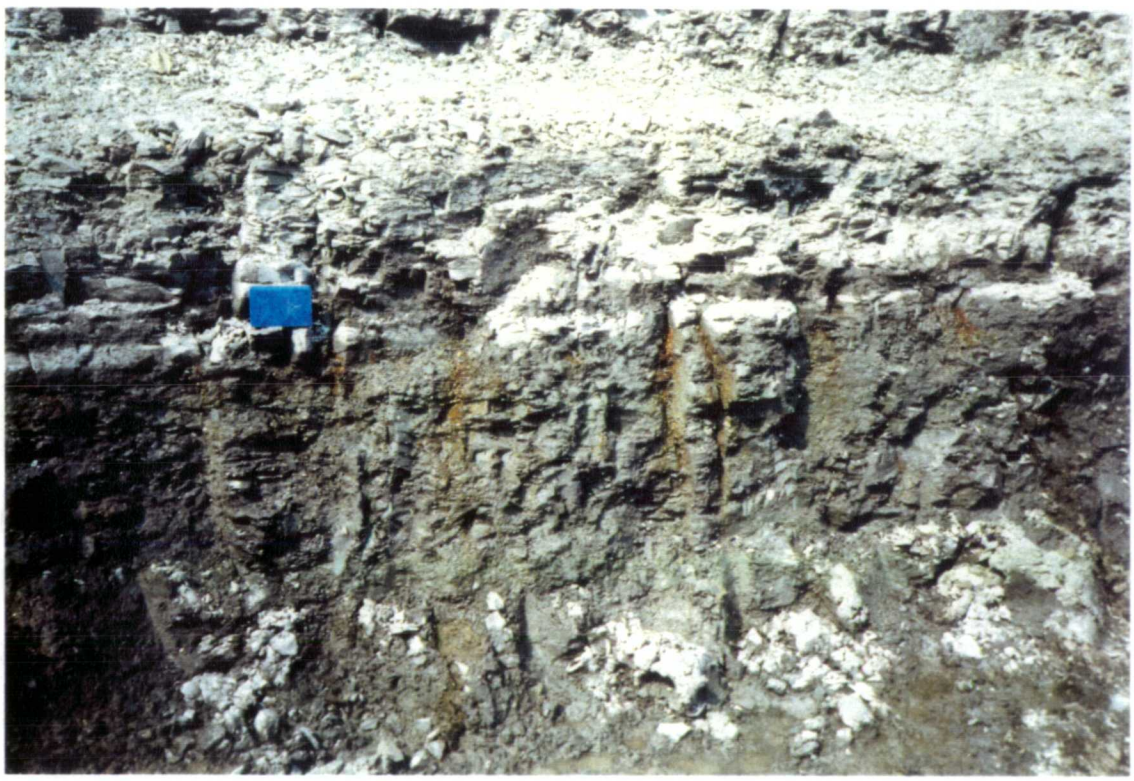

(b)

Figure 3.25 - (a) View of northern side of excavation showing seepage at about 5m below ground level; (b) close-up view of seepage from pyritic bands

bed between two pyritic bands at about 26m AOD as shown in Figure 3.25.

The logging profiles taken of the excavation sides during construction provide a valuable record of the structure and composition of the ground. The descriptions associated with the five profiles are presented in Appendix A.

The lithology, fabric and discontinuities within the Head Deposits and the weathered Oxford Clay were logged in the same manner as in the trial pits (see section 3.7.2). As little unweathered Oxford Clay had been seen in the trial pits the descriptive scheme for this material required some development in the trial excavation. Several types of fissuring, varying in orientation, surface nature and extent were noted and separately described. The Oxford Clay was then sub-divided on the basis of variation in the nature of fissuring and the shell content. A number of very shelly, often pyritic, laterally continuous beds were found and these proved to be useful horizon markers. Prominent, generally medium to widely spaced, planer and sub-vertical fissures were observed in most of the sub-divisions, and individual fissures of greater than 0.5m exposed extent were measured and described. The bearings and orientations of these larger fissures are plotted in Figure 3.26. This shows that majority of the fissures are sub-

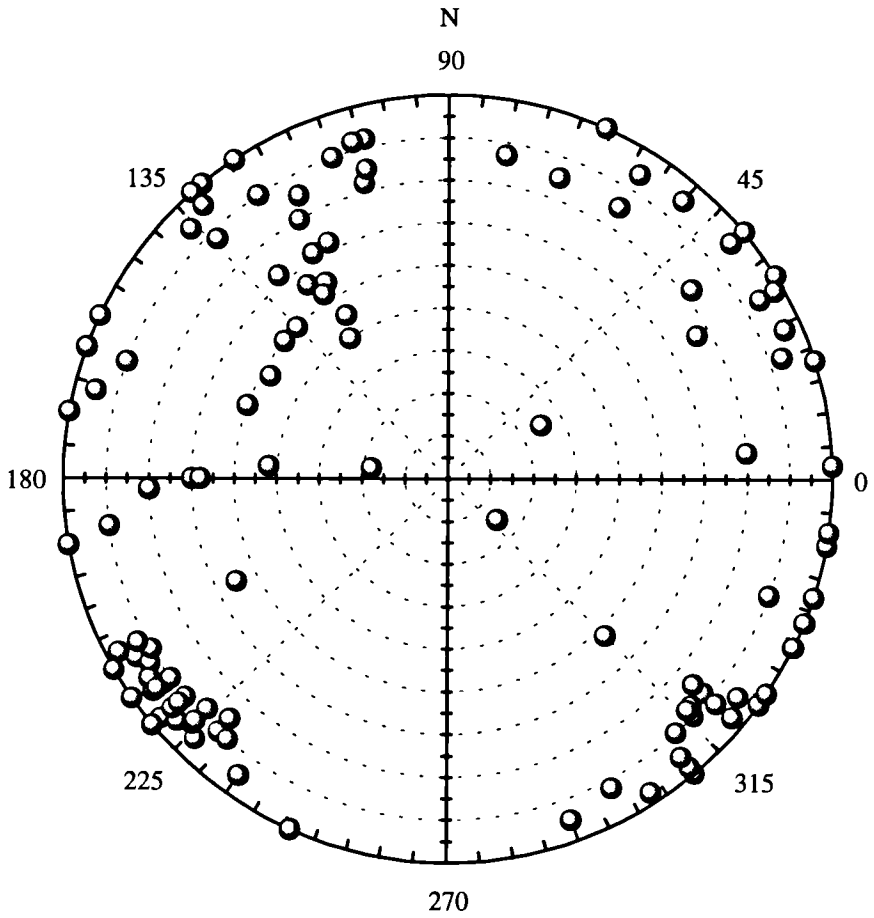

Each circle represents a single fissure record. The orientation is given on the outside scale and the fissure dip angle measured as radius with the outside edge representing 90° (vertical) and the centre representing 0° (horizontal)

Figure 3.26 - Orientation and inclination of prominent fissures (greater than 500mm extent) recorded on profile records of excavation sides

vertical and that they tend to run from north west to south east (aligned with the axis of symmetry of the excavation) and orthogonally to this.

It was appreciated that the groundwater flow within the Oxford Clay might essentially be fissure flow, and that any patterns to the orientation, nature and/or extent of fissures might have an influence on directional permeability. It was therefore decided to carry out a more detailed fissure survey at three or four locations within the trial excavation. At each survey location one end of the bench was to be hand trimmed to isolate an approximate 1m cube of soil. Mott MacDonald commenced a fissure survey of one such cube of unweathered Oxford Clay, but it was discontinued since the task proved very time consuming and after 2 man days approximately only one third of the metre cube had been destructively logged and 130 readings taken.

Block samples were taken along two profiles at opposite ends of the excavation to provide a lateral and vertical spread of material sampled. Sample pairs for the preparation of horizontally and vertically cut laboratory test specimens were taken at nominally metre intervals for the full depth of the excavation in both profiles. The sampling method used was similar to that previously carried out in the trial pits (section 3.7.2). The bench for each sample pair was not excavated until the day of sampling to minimise drying-out and stress relief of the sampled material.

Most of the excavation profile block sampling took place adjacent to the logged faces of profiles P1 and P4 (see Figure A.1). Block sample pairs were recovered at approximately 1m centres in both profiles, although the vertical spacing was somewhat erratic at times. It proved difficult to obtain samples at the greatest depth attempted on profile P4. Due to traces of moisture on the fissures and probable stress relief of the ground, the samples were very fragile at this depth and one or two were lost when they fell apart along fissures during preparation. At P4 no attempt was made to sample the pyritised bands and this contributed to the uneven steps in the depth sequence of the samples. At P1 an attempt was made to sample the pyritised bands using a chain saw, but this was unsuccessful. A further attempt was to be made using a disc cutter but this was not carried out due to the suspension of the works.

3.7.4 Borehole investigations

The use of percussive boring techniques was ruled out because the percussive effort would cause excessive disturbance to the sample and allow the opening up of fissures in the clay strata. Also, the hard pyritised bands within the clay and the very stiff limestone strata beneath the Kellaways strata would not have been readily penetrated by such techniques.

Rotary coring was therefore adopted. However, it was anticipated that the consequence of using a drilling fluid would be to cause disturbance to the sample. In an attempt to prevent water from coming in contact with the sample, triple tube rotary coring with a Mazier type core barrel was used. In this type of barrel, the sample is contained within a solid plastic inner tube fitted with a spring loaded cutting shoe. The inner tube can, therefore, advance beyond the cutting bit to an extent depending on the resistance of the material being drilled. The seven months of drilling included 100 cored boreholes totalling 3200m. The majority of the boreholes were 25-75m deep, but one extended to 160m depth (see section 3.3.2).

Although the Jurassic strata were known to be both extensive and laterally relatively uniform, the regional dip of approximately 1° to the south east was intersected by faulting systems which could possibly dislocate the strata at the Elstow site (see section 3.3.2).

An additional series of investigative boreholes was drilled in areas where it was thought, based on initial interpretation of the site investigation data, that specific structural or geological features such as faults could possibly exist. Such areas were investigated using lines of vertical and inclined boreholes, but no evidence of faulting was discovered.

3.8 Numerical analyses performed as part of the site investigation

A series of numerical analyses carried out as part of the Elstow site investigation are described in a Mott MacDonald Internal Report (MM, 1987). Initially the GEA (General Earth Analysis) program was used to carry out a series of linear elastic analyses. This program was developed at Cambridge University for the analysis of linear elastic and Cam Clay soil models following the requirements of the Department of Transport. The program CRISP was then used to combine plasticity effects with the linear elasticity. CRISP was modified to incorporate a non-linear isotropic elastic perfectly plastic model, designed to suit the heavily overconsolidated ground at Elstow.

The purpose of these analyses were to make a prediction of the likely ground displacements and pore pressure changes in the vicinity of the excavation to help with the positioning of the instrumentation prior to the commencement of works.

The numerical analyses carried out at the time of the site investigation are discussed alongside the current analyses in Chapter 8.

4. Ground response due to excavation

4.1 Introduction

In this chapter the instrumentation data from the Elstow site investigation described in Chapter 3 are presented and interpreted to describe the overall ground response following excavation. The frequent records of the inclinometer, extensometer and piezometer data allowed the development of the displacements and excess pore water pressures to be determined, both during excavation and during the subsequent three month period prior to the excavation being backfilled.

The excavation dimensions were designed to provide plane strain conditions around the central instrumented section (see Figure 3.23). The extent of the plane strain response was investigated by examining the out-of-plane displacements (perpendicular to the major axis of the excavation) at the inclinometer installations. The degree of symmetry of the ground movements and pore water pressure changes could be evaluated since the instruments were installed along specific section lines.

The combination of both vertical and horizontal displacements allowed the ground strains to be estimated. The volumetric response of the Oxford Clay strata was calculated and the validity of assuming a constant volume response was tested.

4.2 Interpretation of instrumentation data

4.2.1 Introduction

Extensive monitoring of the trial excavation was carried out. The instrument locations in relation to the excavation plan were shown in Figure 3.23. The instruments were set out along a series of sections running parallel and perpendicular to the major axis of the excavation. These sections are shown again in Figure 4.1, labelled such that sections A and F represent the main instrumented section and the major axis of the excavation respectively. The distribution of instruments allowed the degree of symmetry in the excavation response to be evaluated. The instrumentation data were considered along section lines F to R to examine these symmetries.

Data are available, in varying degrees of detail, from 11 March 1987 to 23 July 1987 and an average excavation response has been calculated from particular clusters of readings. This

provides a series of snapshots of the excavation response during and after construction. These times, labelled A to S, are shown in Table 4.1. (Times B to H are also shown in Figure 3.16.)

	Date			Excavation depth (m)		
Name	From	To	Average	From	To	Average
A	9-Mar-87	13-Mar-87	11-Mar-87	0	0	0
B	16-Mar-87	21-Mar-87	18-Mar-87	0	0	0
C	23-Mar-87	28-Mar-87	25-Mar-87	0	3	1.5
D	30-Mar-87	3-Apr-87	1-Apr-87	3	5	4
E	6-Apr-87	11-Apr-87	08-Apr-87	7.5	7.5	7.5
F	13-Apr-87	16-Apr-87	14-Apr-87	7.5	7.5	7.5
G	21-Apr-87	24-Apr-87	22-Apr-87	7.5	7.5	7.5
H	27-Apr-87	1-May-87	29-Apr-87	7.5	7.5	7.5
I	5-May-87	8-May-87	06-May-87	10	10	10
J	11-May-87	13-May-87	12-May-87	10	10	10
K	20-May-87	22-May-87	21-May-87	10	10	10
L	27-May-87	29-May-87	28-May-87	10	10	10
M	1-Jun-87	5-Jun-87	3-Jun-87	10	10	10
N	9-Jun-87	12-Jun-87	10-Jun-87	10	10	10
O	16-Jun-87	16-Jun-87	16-Jun-87	10	10	10
P	30-Jun-87	2-Jul-87	1-Jul-87	10	10	10
Q	8-Jul-87	9-Jul-87	8-Jul-87	10	10	10
R	15-Jul-87	16-Jul-87	15-Jul-87	10	10	10
S	23-Jul-87	24-Jul-87	23-Jul-87	10	10	10

e.g. The excavation displacement field at Time 'H' is defined using the measurements from the various instruments between 27 April 1987 and 1 May 1987 but is defined as being the condition at 29 April 1987 when the average excavation depth was 7.5m

Table 4.1 - Times during the site investigation when instrumentation data are available

For the inclinometer and extensometer data, therefore, an average response was determined from a series of closely spaced readings at the same instrument location, combined with similar responses from those instruments along the same section line (F to S) as shown in Figure 4.1. The greater the number of instruments along the section, the greater the confidence in the calculated average. Consequently, the average response along sections F, I, J, and K is expected to be more accurate than along the other sections where there are only single instruments (sections L, M, N, O, P, Q, R). The reading frequency was higher prior to the suspension of works (time I) and 3 to 5 consecutive readings for each instrument could be averaged. However, for the remainder of the monitoring period the readings were taken less frequently and generally the average reading represents a single reading or, for time M, two consecutive readings.

The inclinometer data are shown in subsequent as either 'In-plane' or 'Out-of-plane' readings. These represent measurements which are, respectively, perpendicular to, and parallel to the major axis of the excavation (Section F). The sign convention used is such that a positive reading represents a horizontal displacement to the north-west for in-plane readings and to the north-east for out-of-plane readings. The out-of-plane measurements are subject to greater reading errors than the in-plane measurements since the inclinometer sensor guide wheels are

sprung to hold the device firmly in the in-plane direction, possibly allowing greater flexibility of movement out-of-plane (see section 3.6).

The extensometer data are presented in figures showing the displacements of magnets at approximately similar elevations within each of the longitudinal section lines shown in Figure 4.1 (the variation of the magnet elevations about the average is generally less than 0.5m). An average vertical displacement at each elevation is also included in the figures. The sign convention used is such that heave is represented by a positive reading.

A representative sample of the instrumentation data is presented following the written discussion (section 4.2.2), although the complete set of data is given in Pierpoint (1996b).

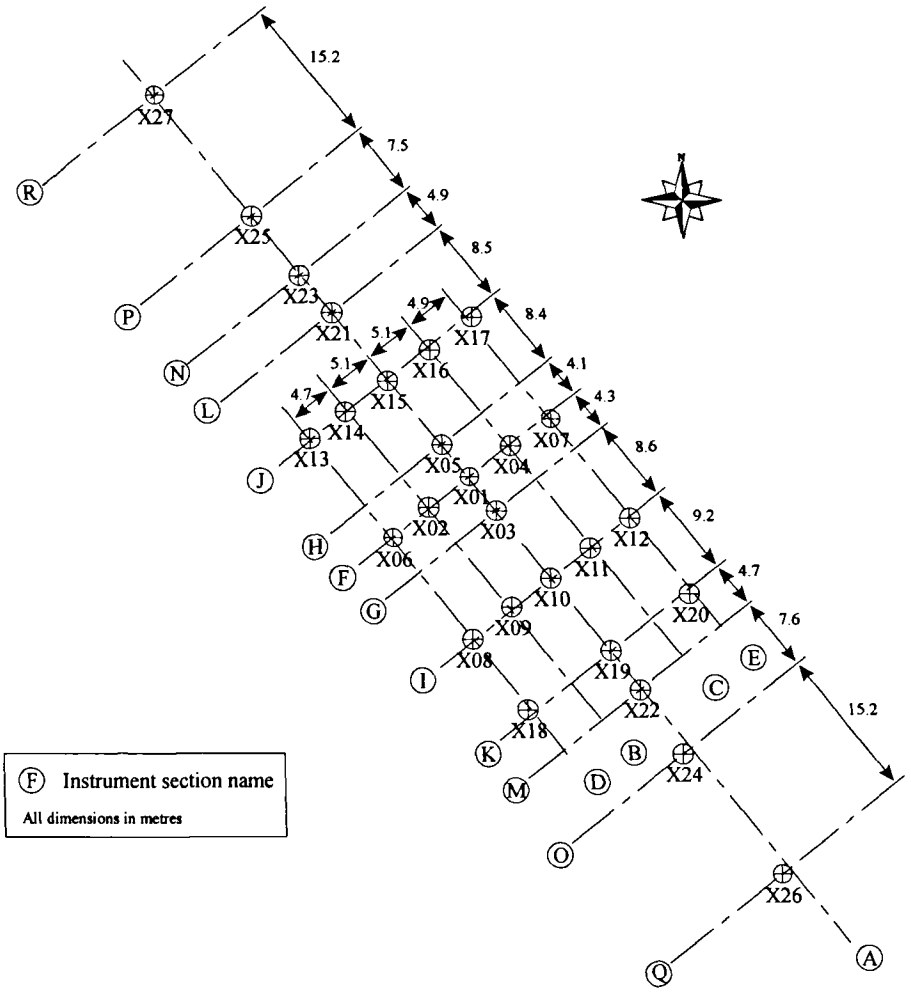

Figure 4.1 - Plan view of excavation with as constructed locations of instrumentation boreholes and cross-section definitions

4.2.2 Interpretation of vertical and horizontal displacement data

SECTION F

Section F is located at the centre of the excavation base (see Figure) and, from south west to north east contains instruments X06, X02, X01, X04 and X07 at approximately 5m intervals evenly spaced about the main line of instrumentation (Section A).

Instruments X01 and X02 extend to 60m below original ground level whereas instruments X06, X04 and X07 only extend to 25m. The deeper instruments are founded in the Lower Lias and the shallower instruments at the base of the Cornbrash (see Figure 3.2). Inclinometer data from

these instruments are shown in Figure 4.2 for a time prior to the start of excavation. In this figure, the deeper instruments record far greater displacements than the shallower instruments. It was also found that successive readings for the deeper instruments were not repeatable, varying by as much as 10mm at the surface. The large recorded displacements are probably due to the cumulative measurement errors over the much larger length of the deeper tubes and are not thought to reflect to the true ground response. To allow comparison of the inclinometer records from across the excavation, a false datum for deeper instruments has been taken at the base level of the remaining instruments. The data shown in Figure 4.2 are re-interpreted and shown with the new datum for the deeper instruments in Figure 4.3. Similarly, Figure 4.4 and Figure 4.5 show the inclinometer response along section F for a time after excavation (Time K).

The average horizontal displacement response, shown in Figure 4.6, suggests that the in-plane displacement was minimal below 1m depth. The larger displacements recorded for the top 1m of the instrument are possibly attributable to local effects at the excavation base or physical disturbance to the instrument top during excavation. The out-of-plane readings shown in Figure 4.3 and Figure 4.5 are representative of those recorded throughout excavation and do not indicate any developing movements. The magnitude of movements recorded prior to excavation are as large as those recorded following excavation suggesting that, to within the accuracy of the instrument, the out-of-plane movements were negligible.

The magnet extensometer measurements are not affected by cumulative reading errors to the same extent as the inclinometer data suggesting that the deeper instruments could be compared directly with the shallower instruments. Instruments X01 and X02 both recorded 7mm of heave at the base of the Blisworth Series following excavation to 7.5m depth. This initial heave is evident at all magnet positions above this point but was largely recovered at the lower magnet positions during the 3 week pause in earthworks before excavation continued from 7.5m to 10m depth. It was not expected that displacements of this magnitude should take place at the base of a stiff deposit, 25m below the base of a 10m deep excavation and they were considered erroneous. The readings at magnet 5 in the deeper instruments have therefore been used as (zero displacement) base readings for interpreting the readings from magnets 1 to 4.

Figure 4.7 shows the extensometer response at each of the upper 5 magnet positions for instruments X06, X02, X01, X04 and X07 along Section F. There is generally an increasing heave during the fairly continuous period of excavation to 7.5m. During the 3 week pause in earthworks the vertical displacement remains essentially constant until excavation continues to 10m depth when the heave is reinitiated (during excavation from 7.5m to 10m the excavation passes the elevation of the upper magnet positions). The ground continues to heave until approximately the end of June 1987, two months after the excavation was completed. The ground heave is concentrated in the Oxford Clay, with a maximum average displacement of 20-25mm recorded in the clay and 5-10mm recorded in the Kellaways Sand.

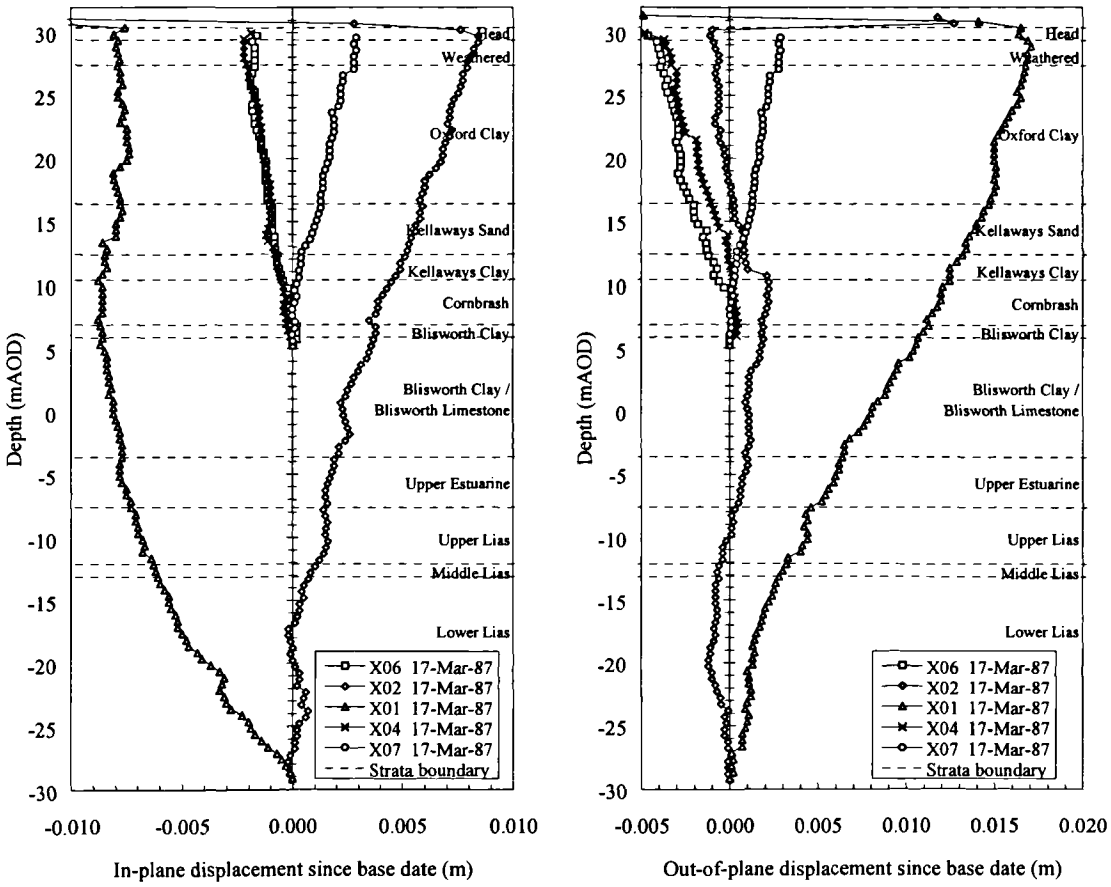

Figure 4.2 - Full depth inclinometer data for section F, Time 'B'

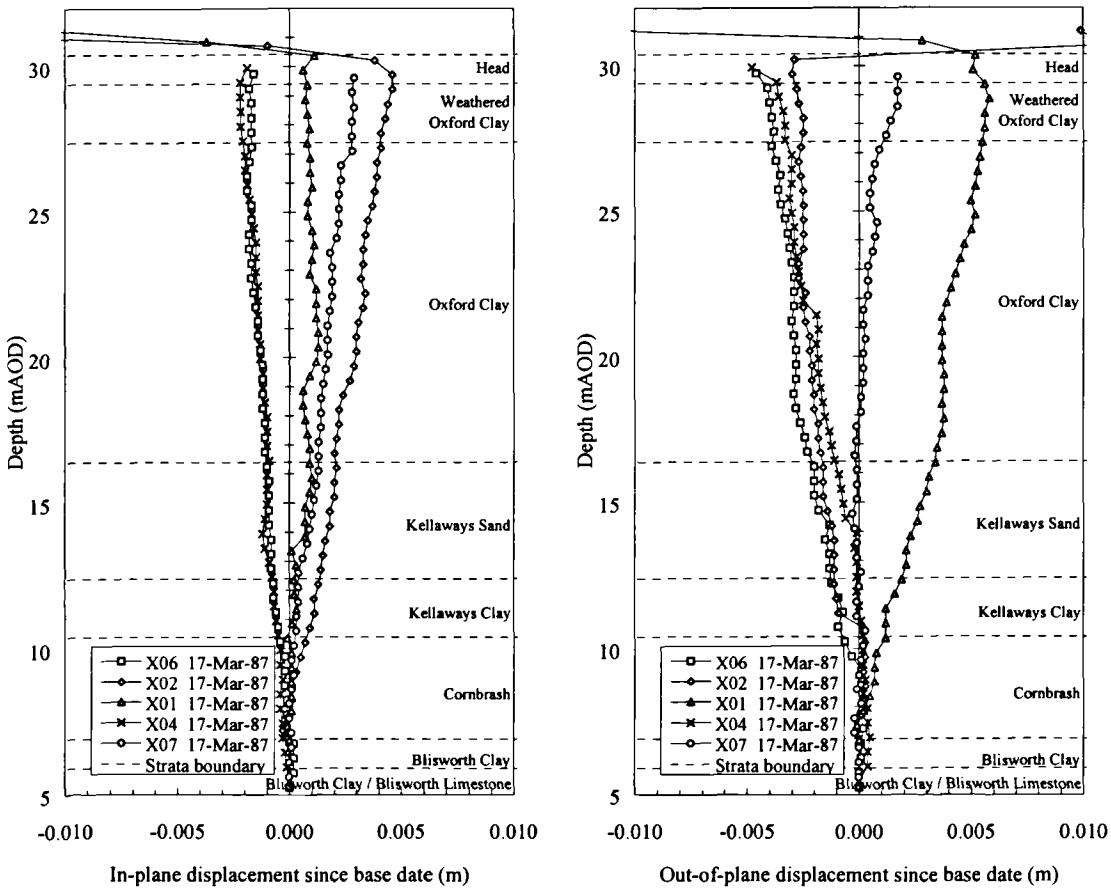

Figure 4.3 - Inclinometer data with reset datum for section F, Time 'B'

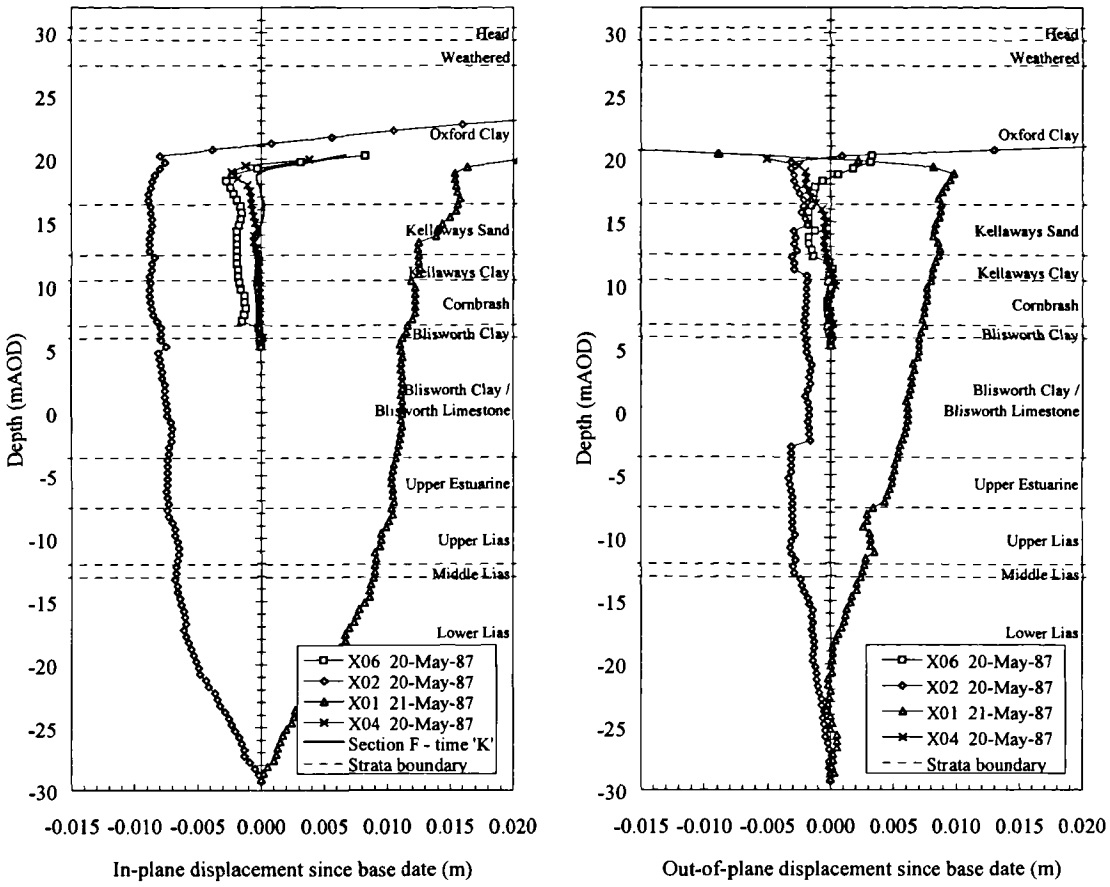

Figure 4.4 - Full depth inclinometer data at section F, Time 'K'

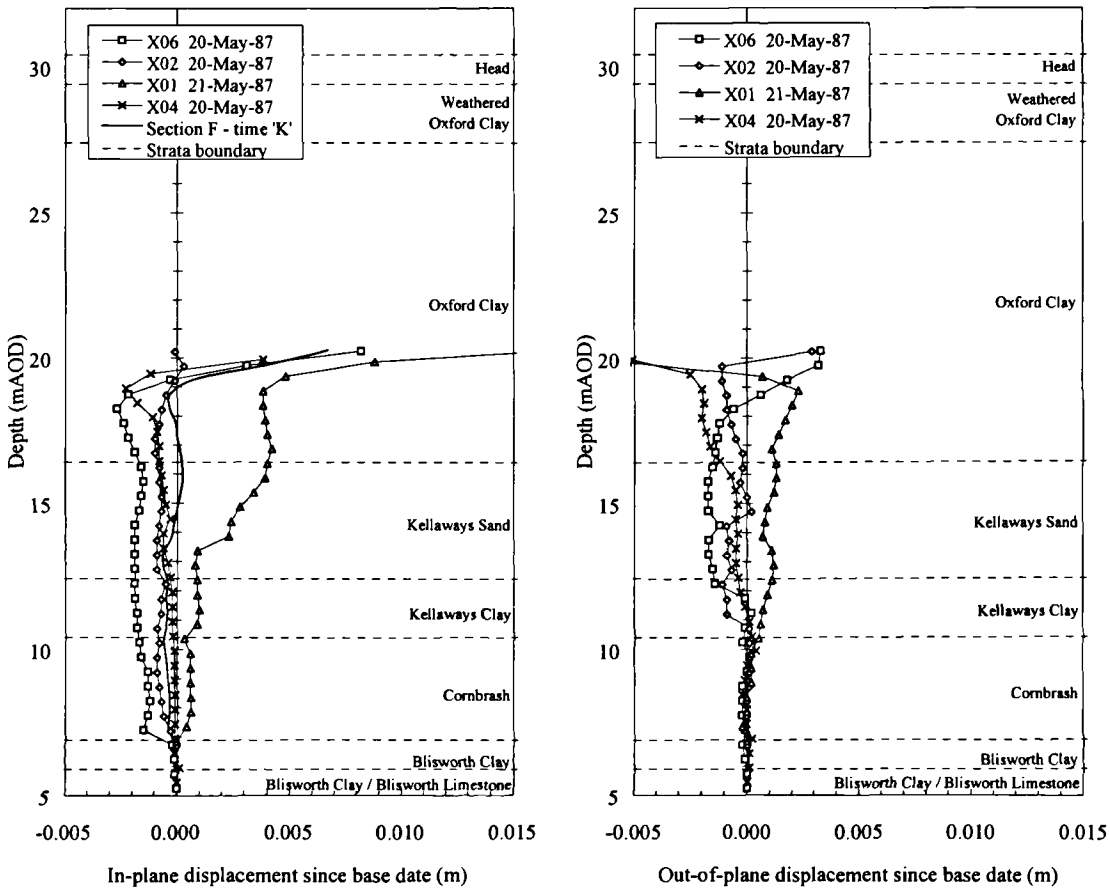

Figure 4.5 - Inclinometer data with reset datum at section F, Time 'K'

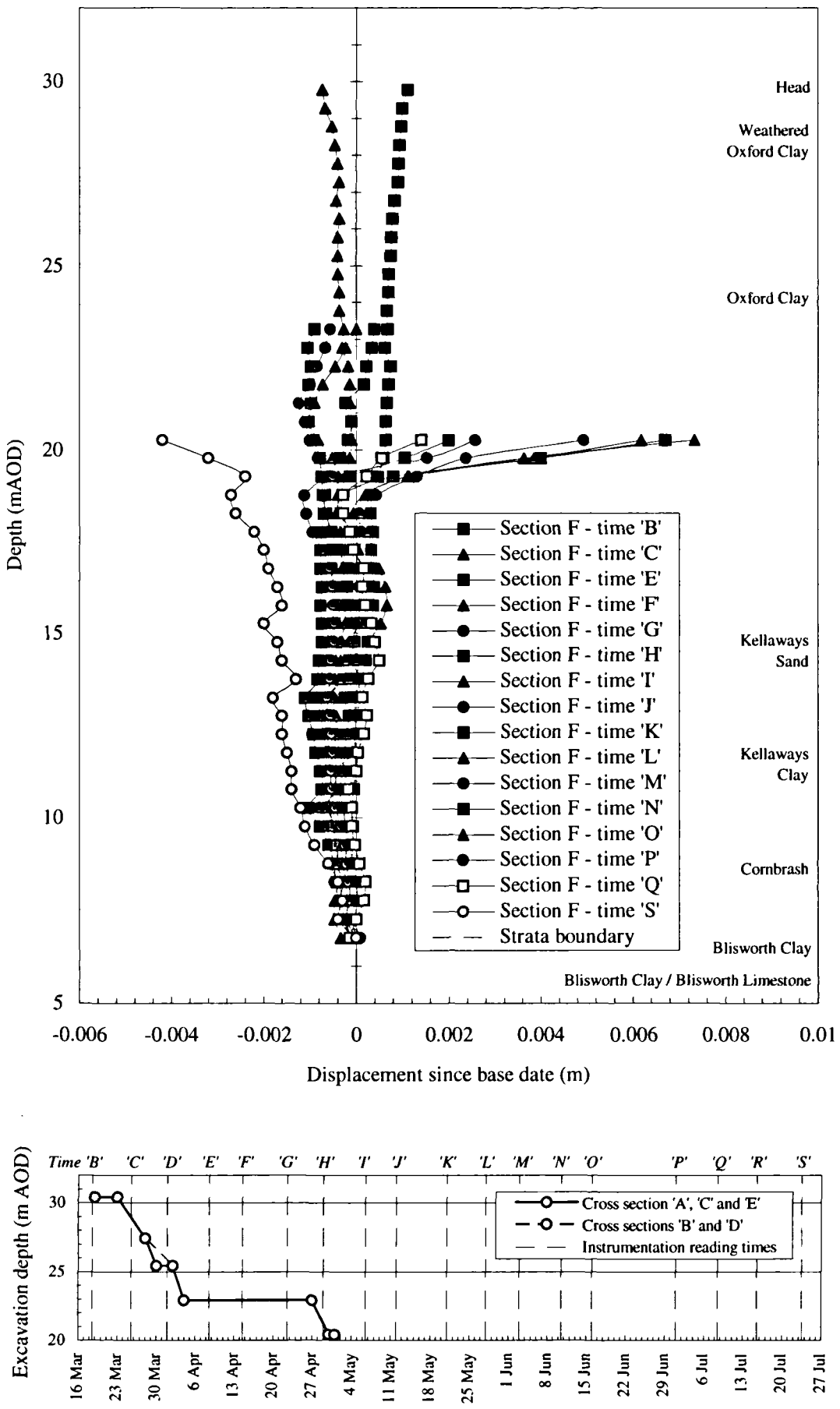

Figure 4.6 - Average inclinometer profile with time at section F

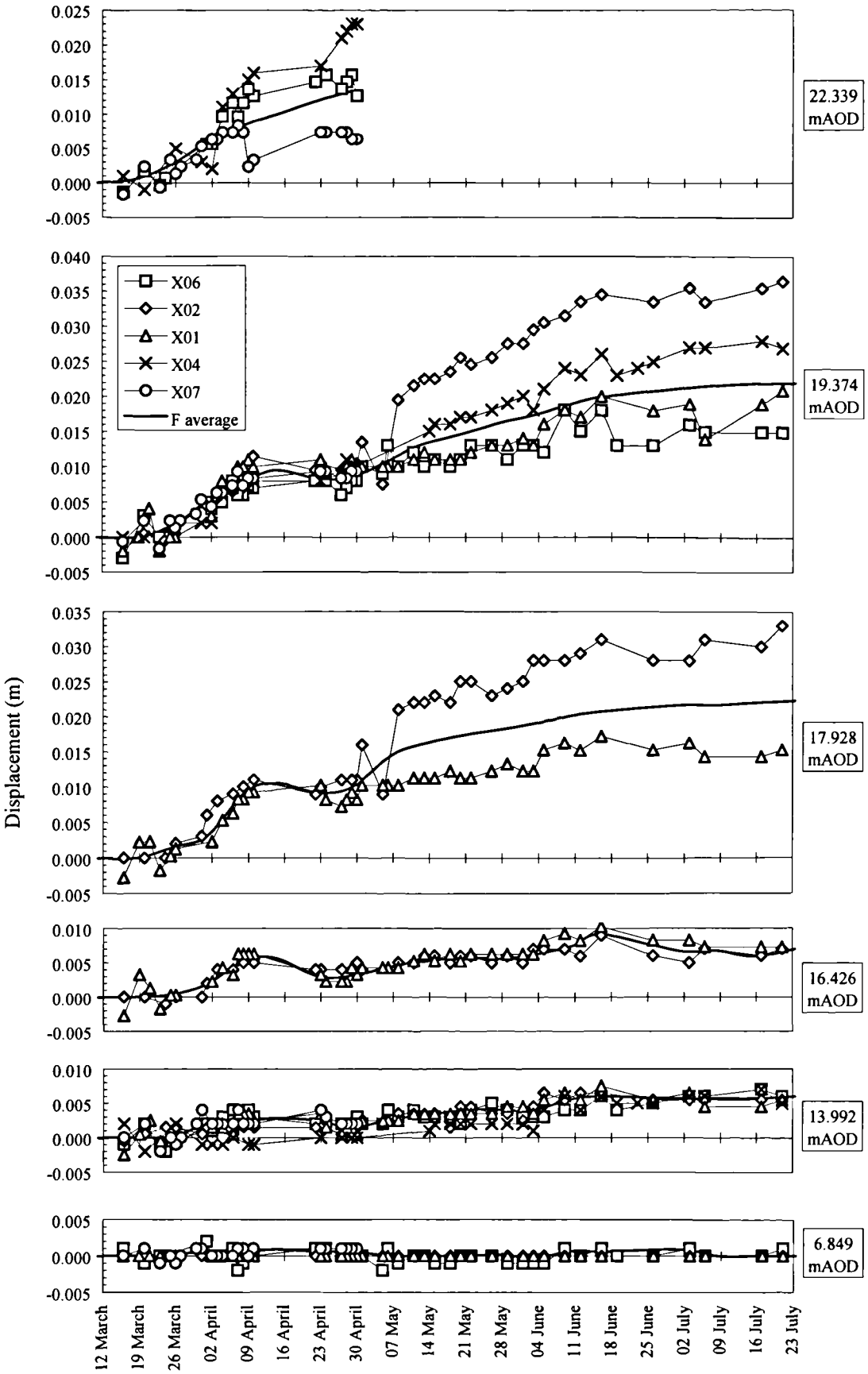

Figure 4.7 - Vertical displacement records for discrete elevations from extensometer installations along section F

SECTIONS G AND H

Sections G and H contain just one instrument each, X03 and X05 respectively, and are located approximately 4.5m from the excavation centreline at the base of the final excavated side slopes. Section G is to the south east and section H is to the north west as shown in Figure 4.1.

Although a complete set of inclinometer readings is available for section H, section G readings are only available until the beginning of May when instrument X03 was damaged. The average in-plane response is shown in Figure 4.8 and Figure 4.9. The individual readings taken at section H for times I to K are shown in Figure 4.10. Instrument X03 extended to 60m depth and suffered the same measurement difficulties as instruments X01 and X02 on Section F. The readings were therefore taken from a datum set by the base of the shallower instruments at 25m depth.

The readings at times B and C were taken prior to excavation, although both sections show an already deformed profile. These readings were therefore taken as the base readings when interpreting subsequent measurements. The out-of-plane movement for each instrument was generally small and within ±1mm although a maximum of 5mm to the south west was recorded in the top 1.5m.

During the 3 week suspension of work at 7.5m excavated depth, both sections show a horizontal displacement within the Oxford Clay of approximately 4mm towards the excavation centreline. The magnitude of movements in the underlying Kellaways Sand was similar. The readings for section G at time H show anomalous readings and these are thought to be erroneous as the associated out-of-plane readings at this time were uncharacteristically large. The displacement profiles in the top 2m of the instruments are also possibly erroneous due to mechanical disturbance and were not considered accurate. Following excavation to full depth the inclinometer response at section H, shown in Figure 4.9, is not definitive, although it perhaps shows up to 2mm of further movement concentrated within the Oxford Clay

Turning to vertical displacements (Figure 4.11), instrument X03 showed an implausible 6mm of movement at 60m depth in the Lower Lias. As with section F, in order to compare the vertical displacement at X03, which extends to 60m depth, with the displacement at X05, which extends to 25m depth, the X03 magnet readings are interpreted using magnet 5 as a datum (Figure 4.11). During excavation to 7.5m there was an associated heave of 8-10mm within the Oxford Clay with half this amount at the top of the Kellaways Sand. At the end of the monitoring period a maximum heave of 8-10mm was recorded in the Oxford Clay, 4-6mm of heave within the Kellaways Sand, and almost no movement beneath the Cornbrash.

The comparison of instrument X03 with X05, Figure 4.11, suggests symmetry about the excavation centreline.

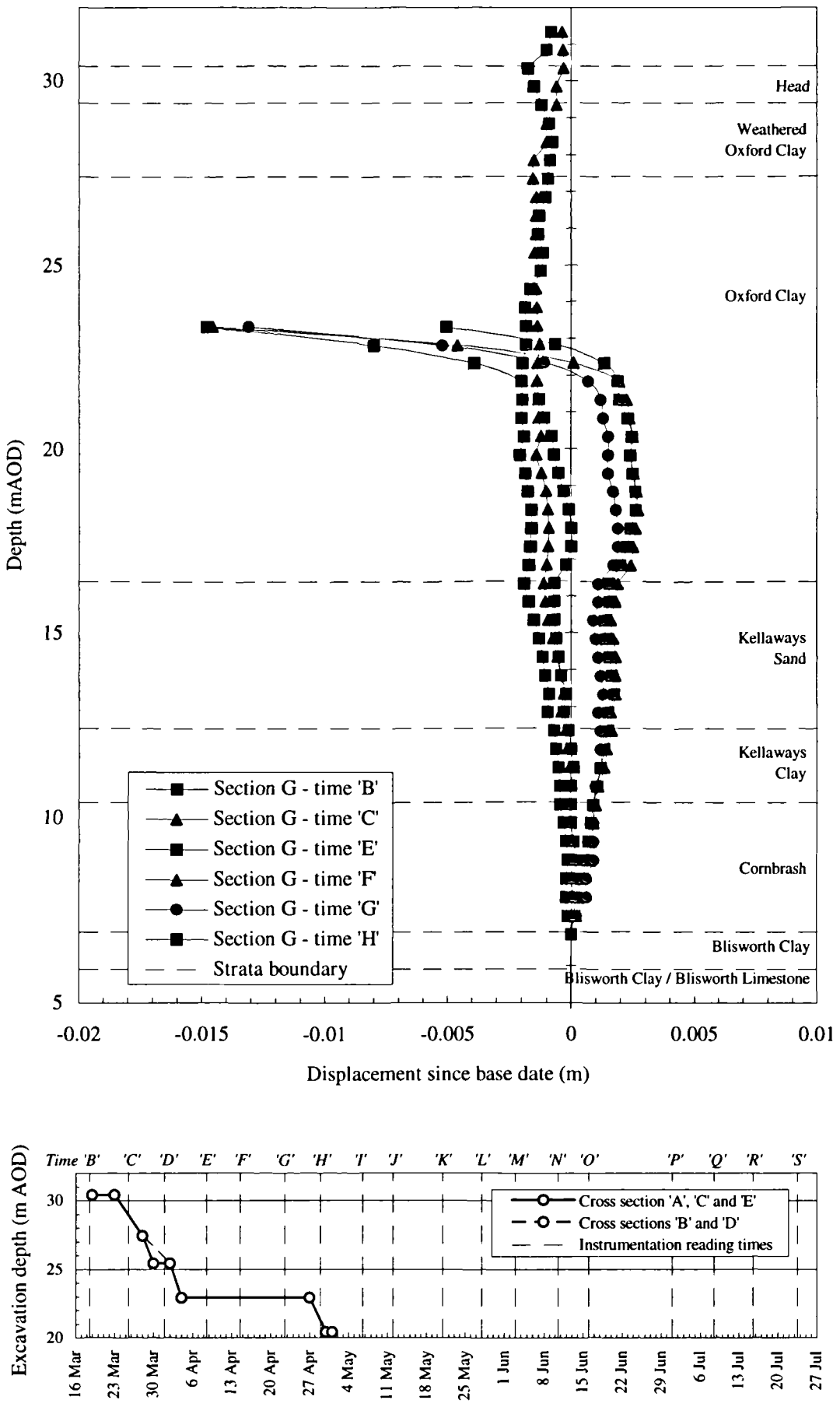

Figure 4.8 - Average inclinometer profile with time at section G

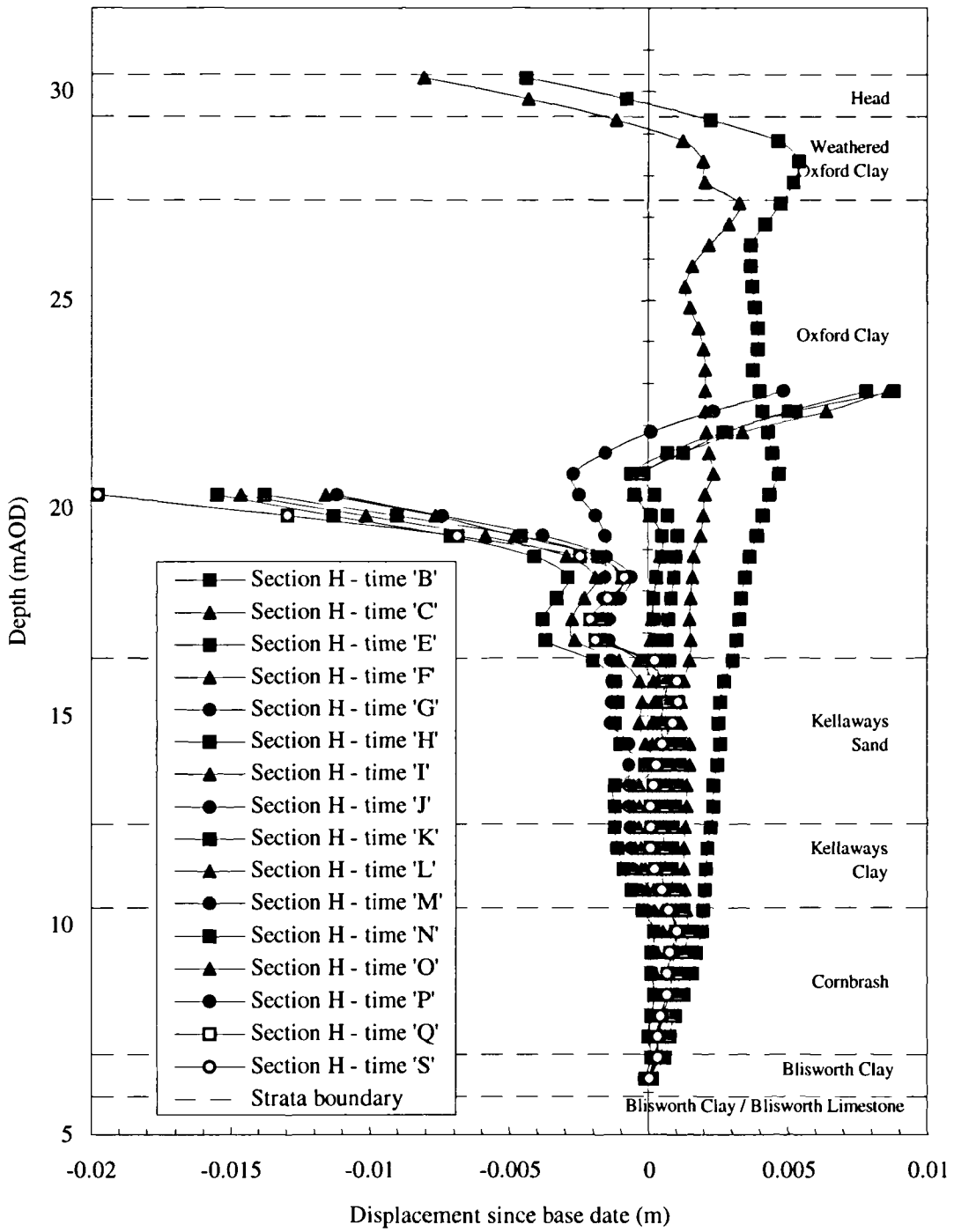

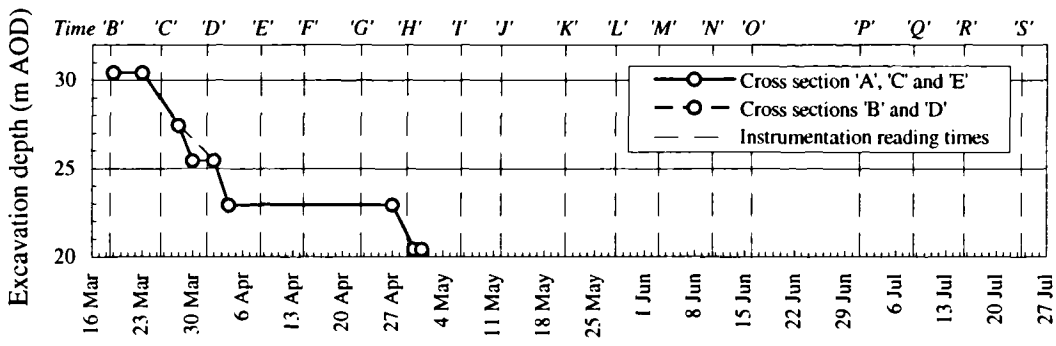

Figure 4.9 - Average inclinometer profile with time at section H

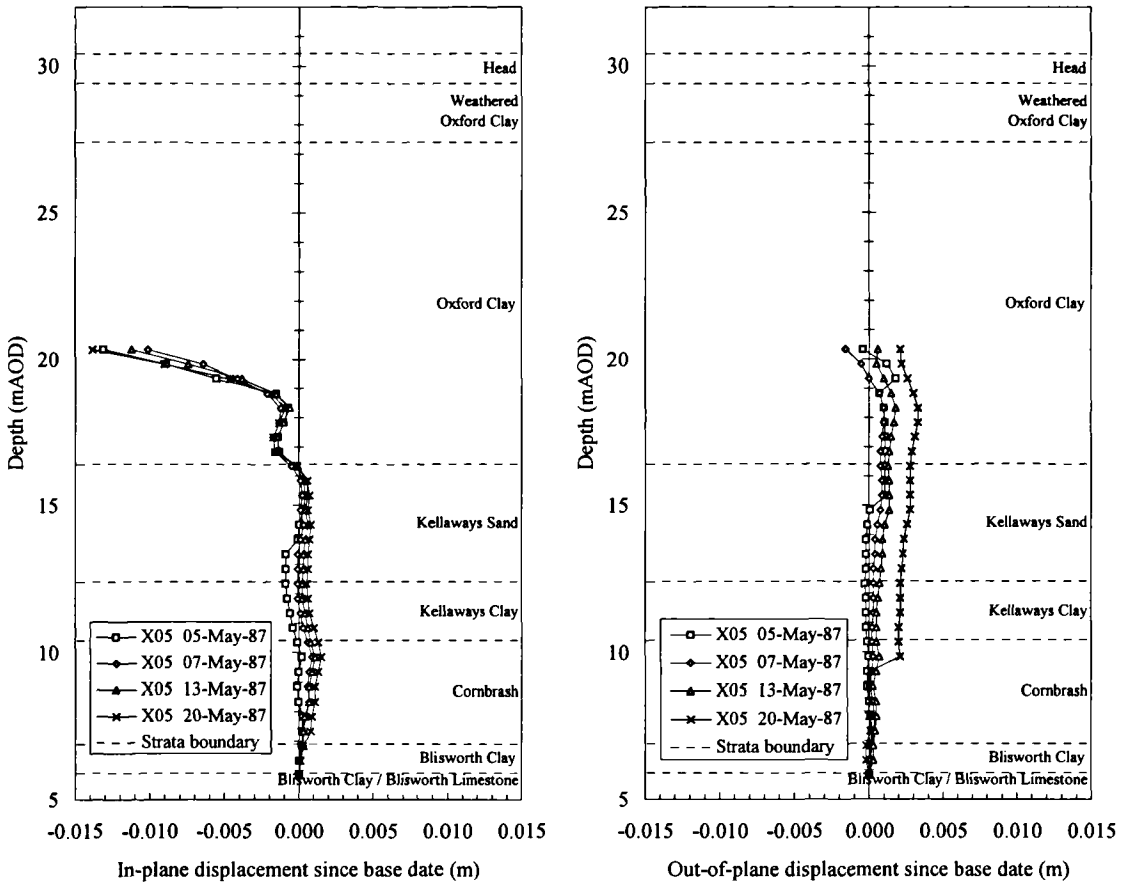

Figure 4.10 - Inclinometer data at section H , Times 'I'-'K'

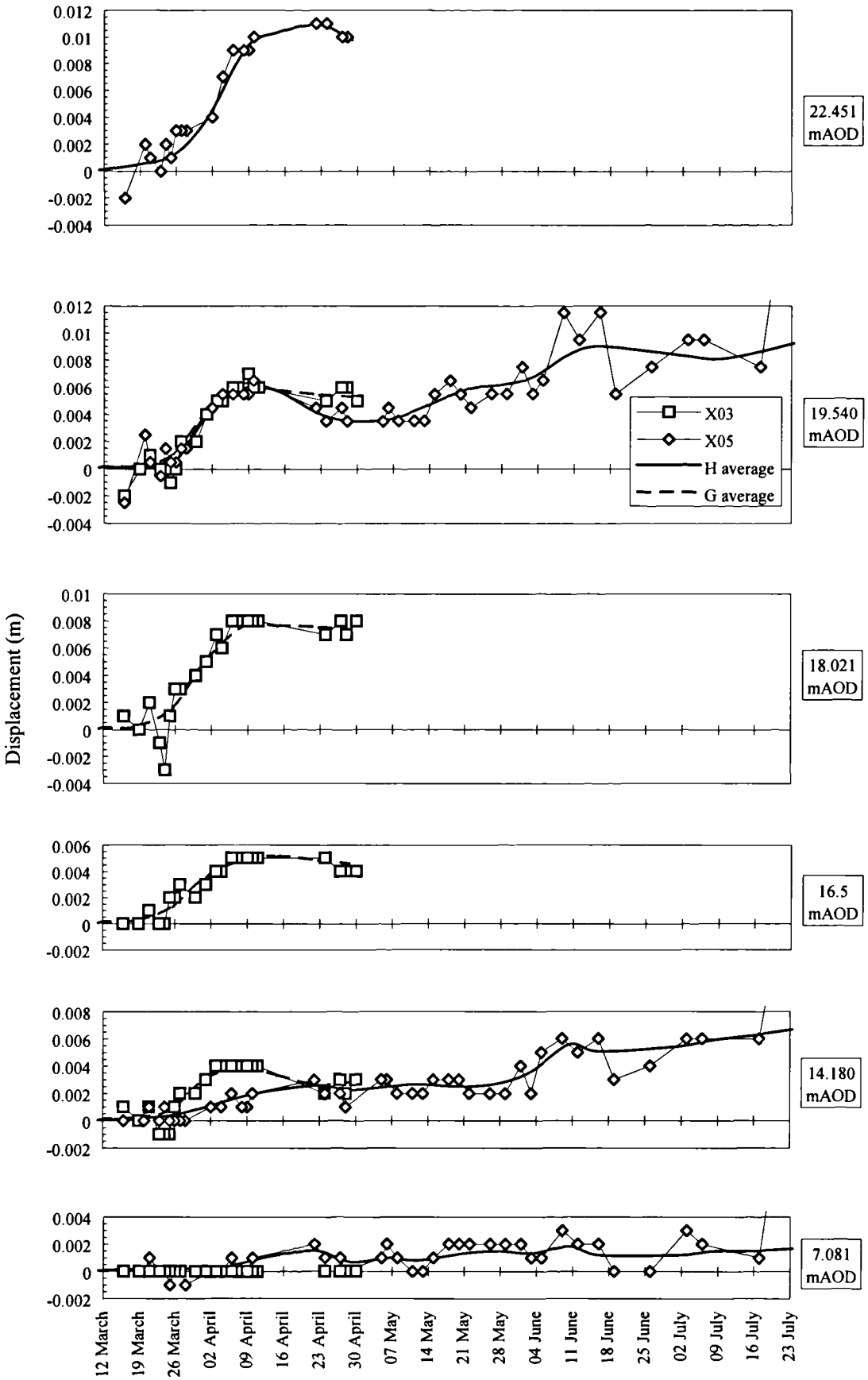

Figure 4.11 - Vertical displacement records for discrete elevations from extensometer installations along sections G and H

SECTIONS I AND J

Sections I and J are located on the excavation berm, two thirds of the way up the side slopes, on the south east and north west faces respectively. They provide the most complete set of displacement data in that there are five instruments along each section which were read frequently.

Section I consists of instruments X08, X09, X10, X11 and X12 located as shown in Figure 4.1. The average in-plane horizontal displacement is shown in Figure 4.12.

Along section I, the in-plane horizontal displacements of instruments X08, X09, X10 and X12 are broadly consistent, as shown for time K in Figure 4.14. However, the readings from X11 are very different. Also, the corresponding out-of-plane displacements for X11 are greater than for the other instruments. The inclinometer readings for instrument X11 are therefore considered erroneous and are not included in Figure 4.12 or subsequent analysis. The out-of-plane readings for times O and R are very scattered, possibly indicative of an erroneous response, and the in-plane readings show no clear pattern between the instruments leading to problems in interpreting an accurate average.

Section J consists of instruments X13, X14, X15, X16 and X17 located as shown in Figure 4.1. The average in-plane horizontal displacement is shown in Figure 4.13.

The progress of excavation is reflected in the inclinometer records through times E, F and G. Horizontal movement is generated throughout the Oxford Clay and directed towards the excavation. These movements are significantly greater above the current level of excavation, highlighting the importance of horizontal stress relief. After excavation to 10m depth the distinction in the displacement profile at the excavation base is less marked as the sloping sides of the excavation cause the stress relief at the face to be more remote. Time M clearly shows the response: no displacement in the Cornbrash; up to 1mm deflection developing in the Kellaways Clay; returning to zero at the Kellaways Sand/Oxford Clay boundary; and generally movement restricted to the Oxford Clay.

The maximum horizontal displacement is attained very shortly after excavation to 10m and is sustained thereafter. By time J (11-13 May) no further trend of movement is evident.

The horizontal displacement is generally slightly greater for section J than section I, approximately 5mm greater at 25mAOD for example. The individual readings within the section are again consistent, as shown for the time K response in Figure 4.15.

The vertical displacements recorded along both sections I and J (Figure 4.16 and Figure 4.17 respectively) suggest that plane strain conditions existed for 25m either side of the main line of instrumentation. Comparing sections I and J it is seen that, to within the accuracy of the instruments, symmetry may be assumed. The general form of displacement is repeated at both locations but, although the response at section I is fairly similar to that at section J at all levels, the section J response is more clearly defined.

The overall extensometer response is as expected. Initially, the ground heaves as the ground above is excavated. As excavation continues the zone of unloading decreases in extent (see later in section 8.8). When the excavation level reaches and then passes the instrument location, the magnets are affected by loading rather than unloading. This is seen in settlement being initiated between 30 March and 9 April.

This settlement continues to develop through the construction rest period, during excavation from 7.5m to 10m and on until mid- to late May at which time there is a second period of heave

lasting until mid June. This effect is seen at all magnets within the Oxford Clay and must therefore be considered a genuine effect, although the reason for it is not clear. The development of the heave is relatively rapid, matching that during excavation.

After this second period of heave, in mid June, a second period of settlement is recorded at the magnets within the Oxford Clay. Again, these movements are seen at all instruments in sections I and J, and must therefore be considered a genuine effect, although an explanation is not apparent, and it is unfortunate that monitoring did not continue to observe how this effect continued.

Possible explanations for the second periods of heave and settlement following the completion of excavation may be linked to environmental factors. Unfortunately, the weather monitoring station which was installed on the site did not provide any useful data. The measuring tape for recording the locations of the extensometer magnets was not made of invar steel and, consequently, the vertical displacements recorded were possibly affected by temperature changes.

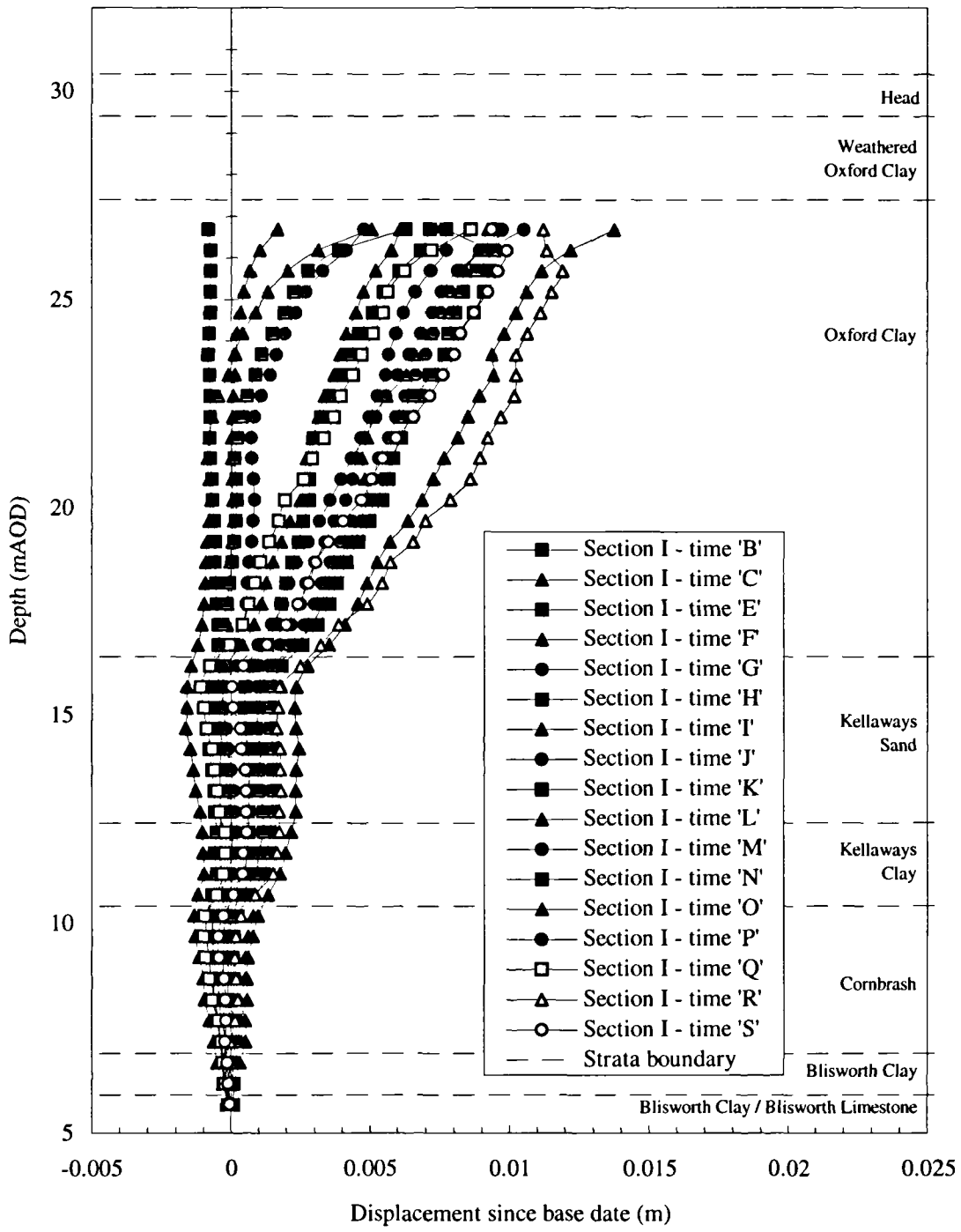

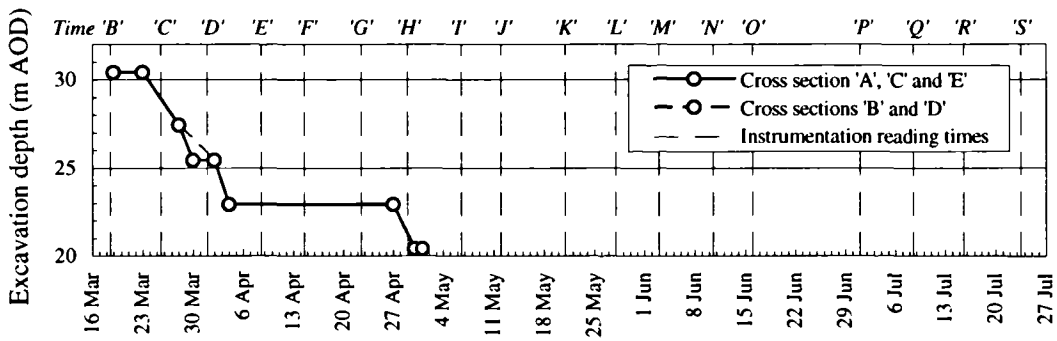

Figure 4.12 - Average inclinometer profile with time at section I

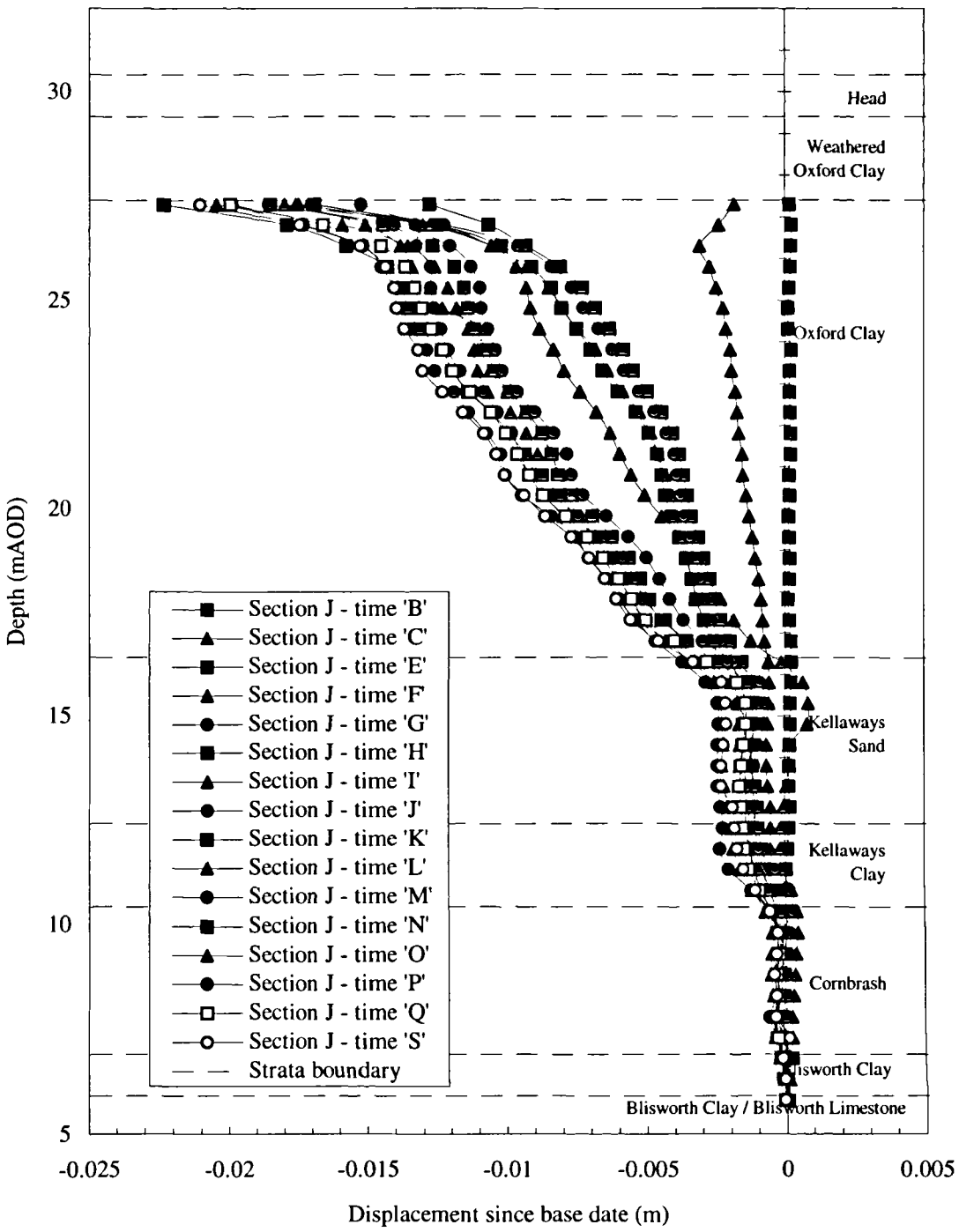

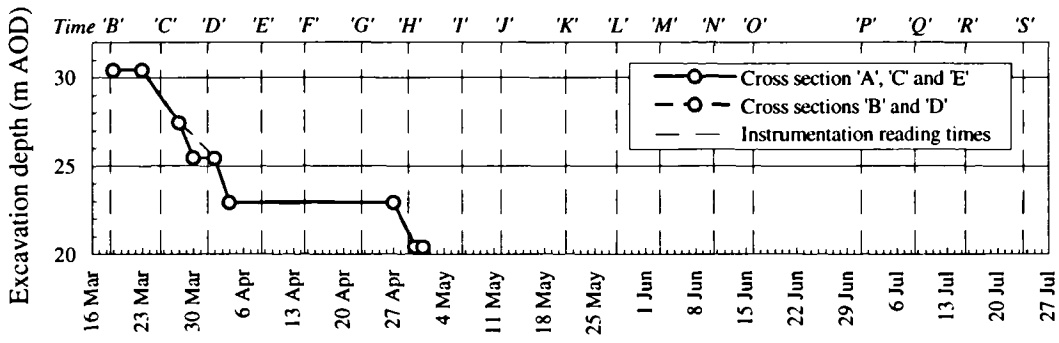

Figure 4.13 - Average inclinometer profile with time at section J

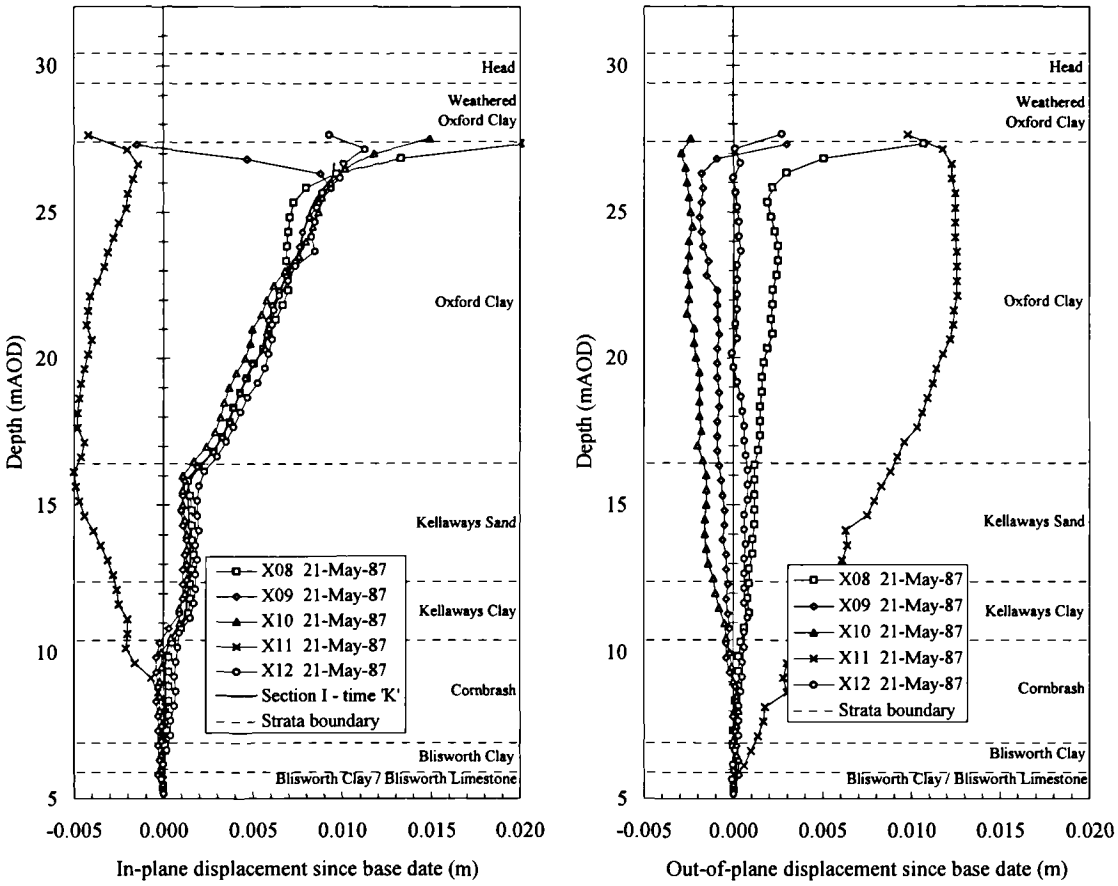

Figure 4.14 - Inclinometer data at section I, Time 'K'

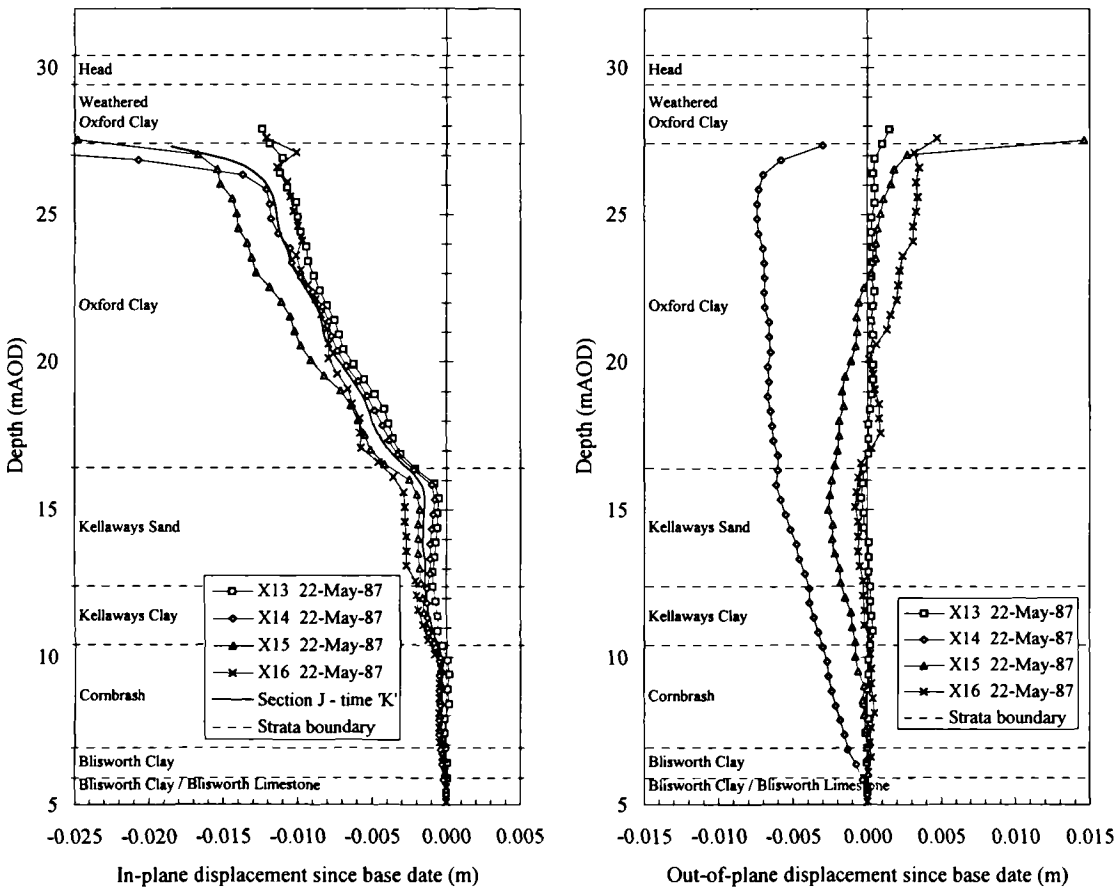

Figure 4.15 - Inclinometer data at section J, Time 'K'

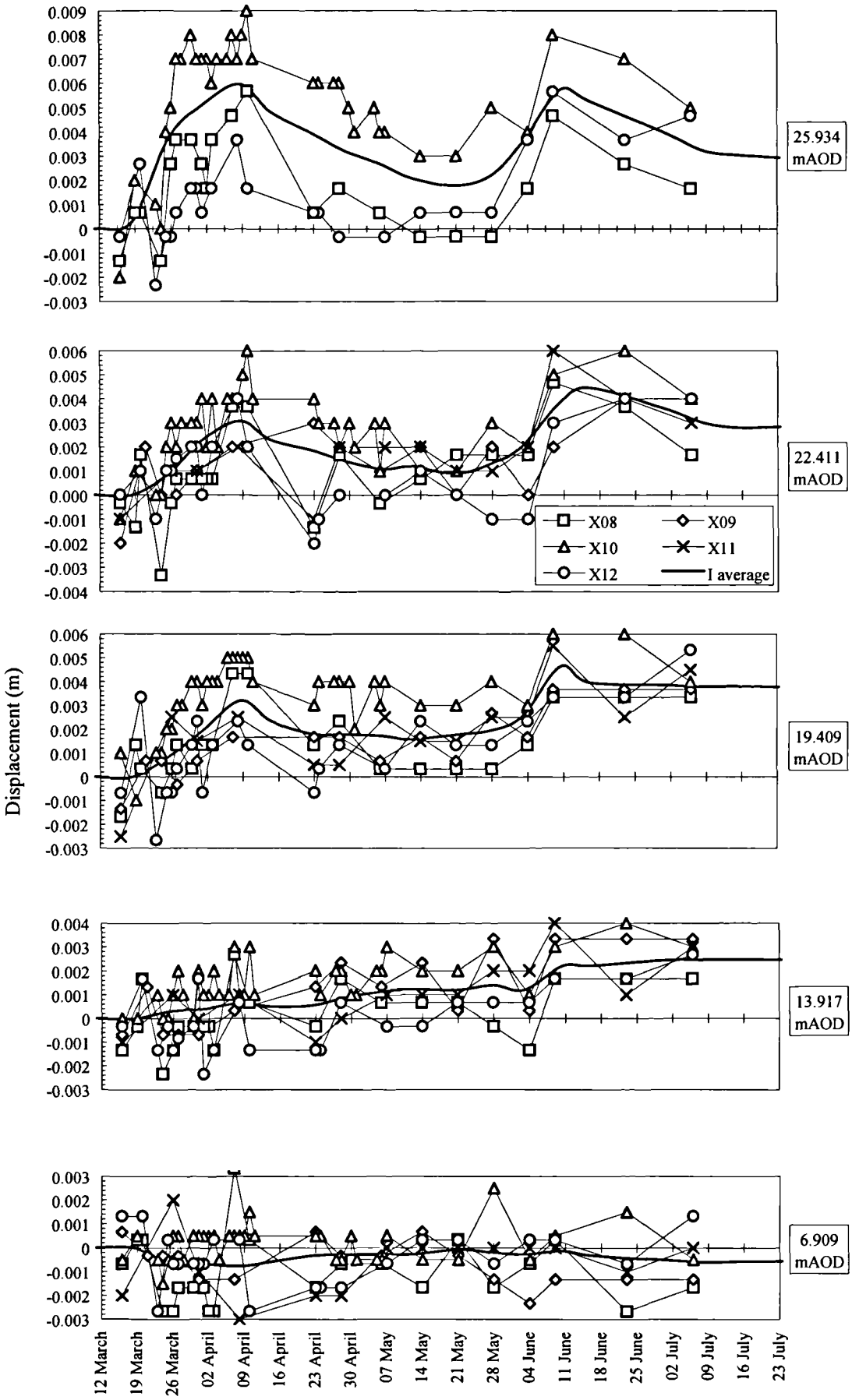

Figure 4.16 - Vertical displacement records for discrete elevations from extensometer installations along section I

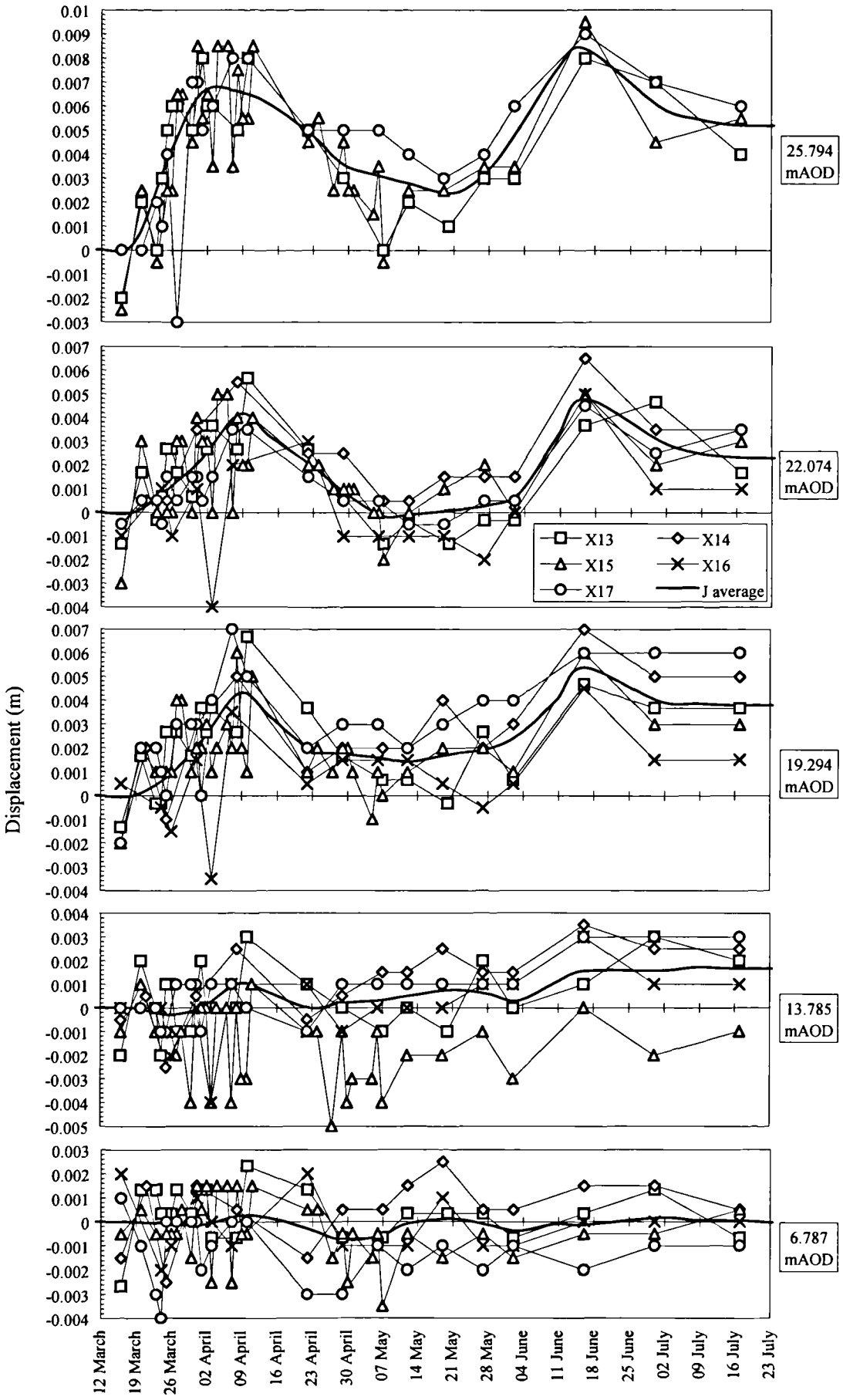

Figure 4.17 - Vertical displacement records for discrete elevations from extensometer installations along section J

SECTIONS K AND L

Sections K and L are located just beyond the excavation crest, approximately 19.5m from the excavation centreline. Section K contains three instruments, X18, X19 and X20, spaced at 10m intervals and symmetrical around the main instrumented section (section A). Section L contains only a single instrument, X21, located diametrically opposite X19 on section A.

The average in-plane horizontal displacement at sections K and L is shown in Figure 4.18 and Figure 4.19 respectively. The in-plane horizontal displacement at these locations is generally small, with a maximum displacement in the range 5-8mm. In this range the accuracy of the inclinometer is an even more important factor than for sections closer to the centreline where displacements are larger. In such circumstances, it is unfortunate that only a single instrument was positioned along section L. However, the displacements recorded at X21 lie within the bounds recorded for instruments X18, X19 and X20 along section K, as shown in Figure 4.20, suggesting that the response was consistent.

Considering the average in-plane response along section K shown in Figure 4.18, the general pattern shows displacement being concentrated once again in the Oxford Clay. The maximum displacement is seen at time P, with a near surface displacement of 7mm towards the excavation. The readings during July show a reduction in the displacement magnitude to 4mm at the end of monitoring.

The in-plane single inclinometer response at section L shown in Figure 4.19, is generally similar to that at section K. The maximum horizontal displacement recorded near the ground surface was 6-8mm.

When considering the vertical displacement at these sections shown in Figure 4.21, a notable feature is the sympathy between the responses at section K and at section L, demonstrating symmetry. Also, the magnet displacements at similar levels at section K are almost identical, to within the accuracy of the instrument, implying that plain strain conditions probably exist in this region.

As expected, all the instruments record settlement from the onset of excavation. This continues to produce a settlement of 13mm near the surface of the Oxford Clay. At the end of May, there is a period of heave followed by a period of settlement, which appears to reflect the behaviour observed at sections I and J, although an explanation for these later readings has not been found.

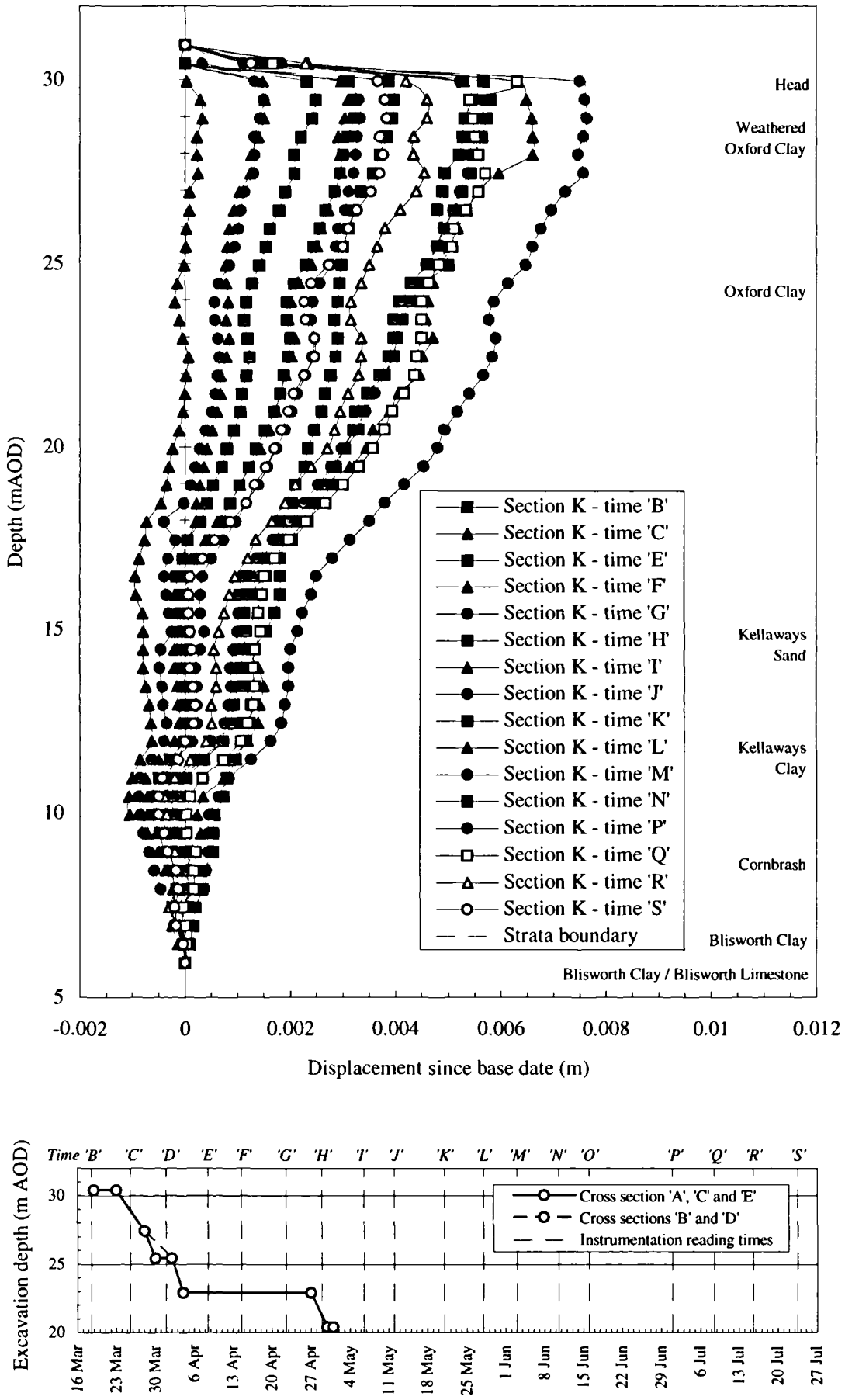

Figure 4.18 - Average inclinometer profile with time at section K

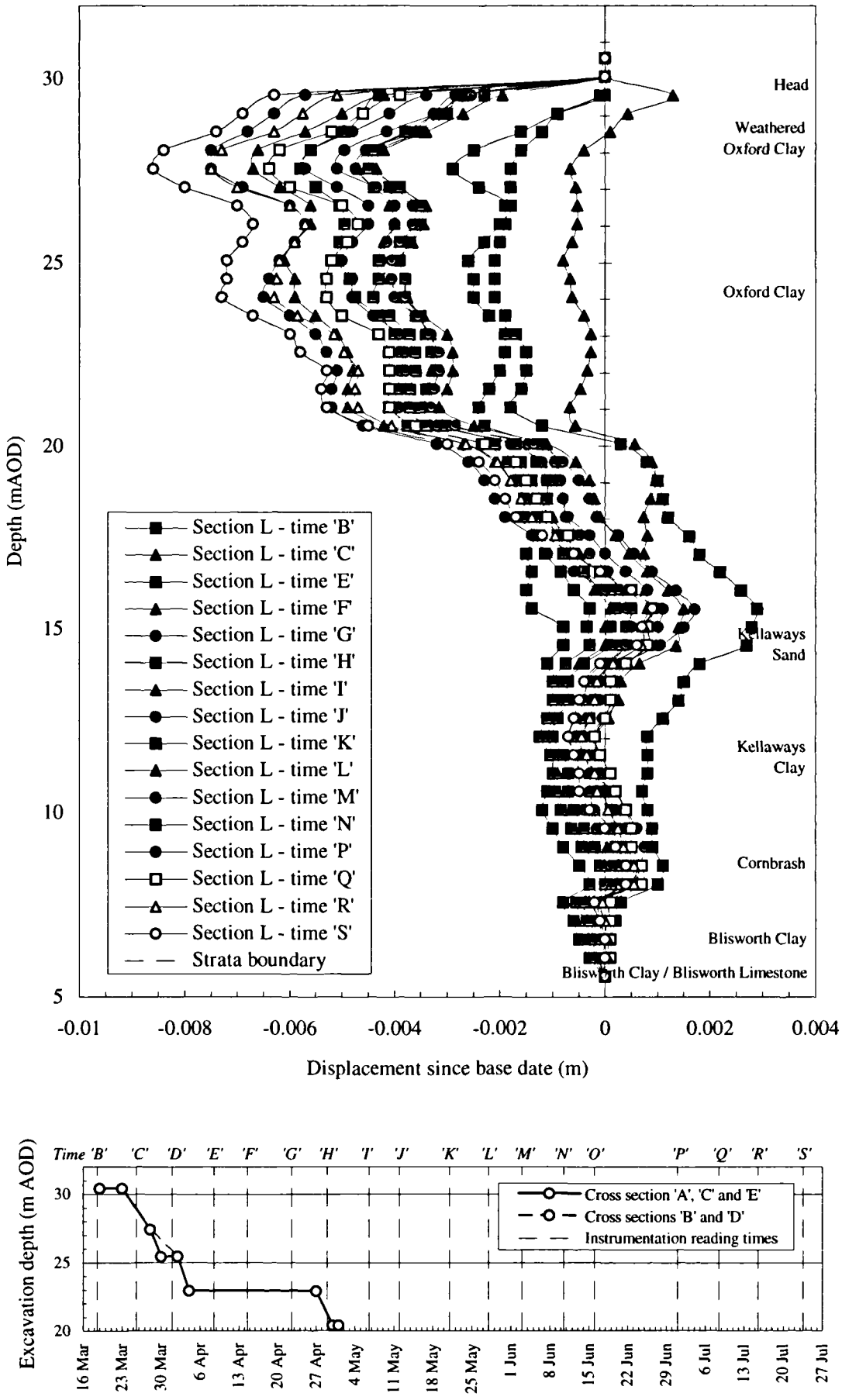

Figure 4.19 - Average inclinometer profile with time at section L

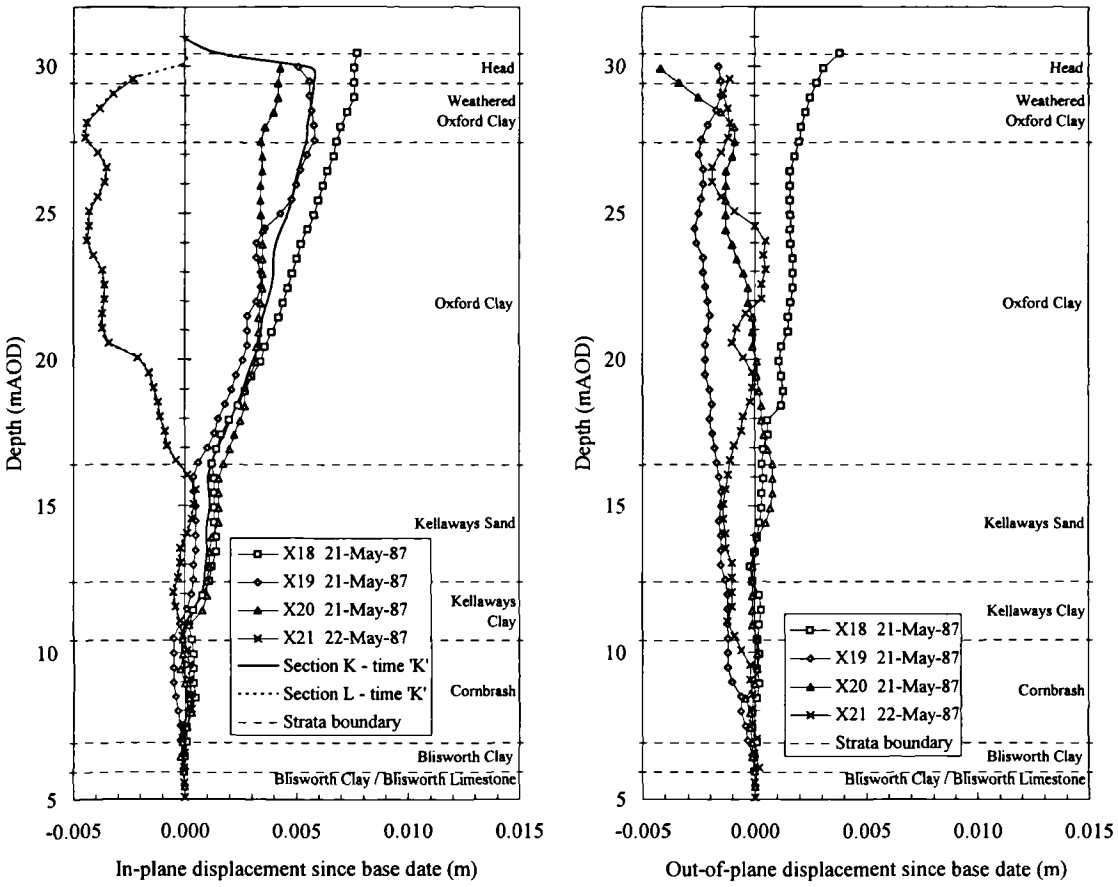

Figure 4.20 - Inclinometer data at sections K and L, Time 'K'

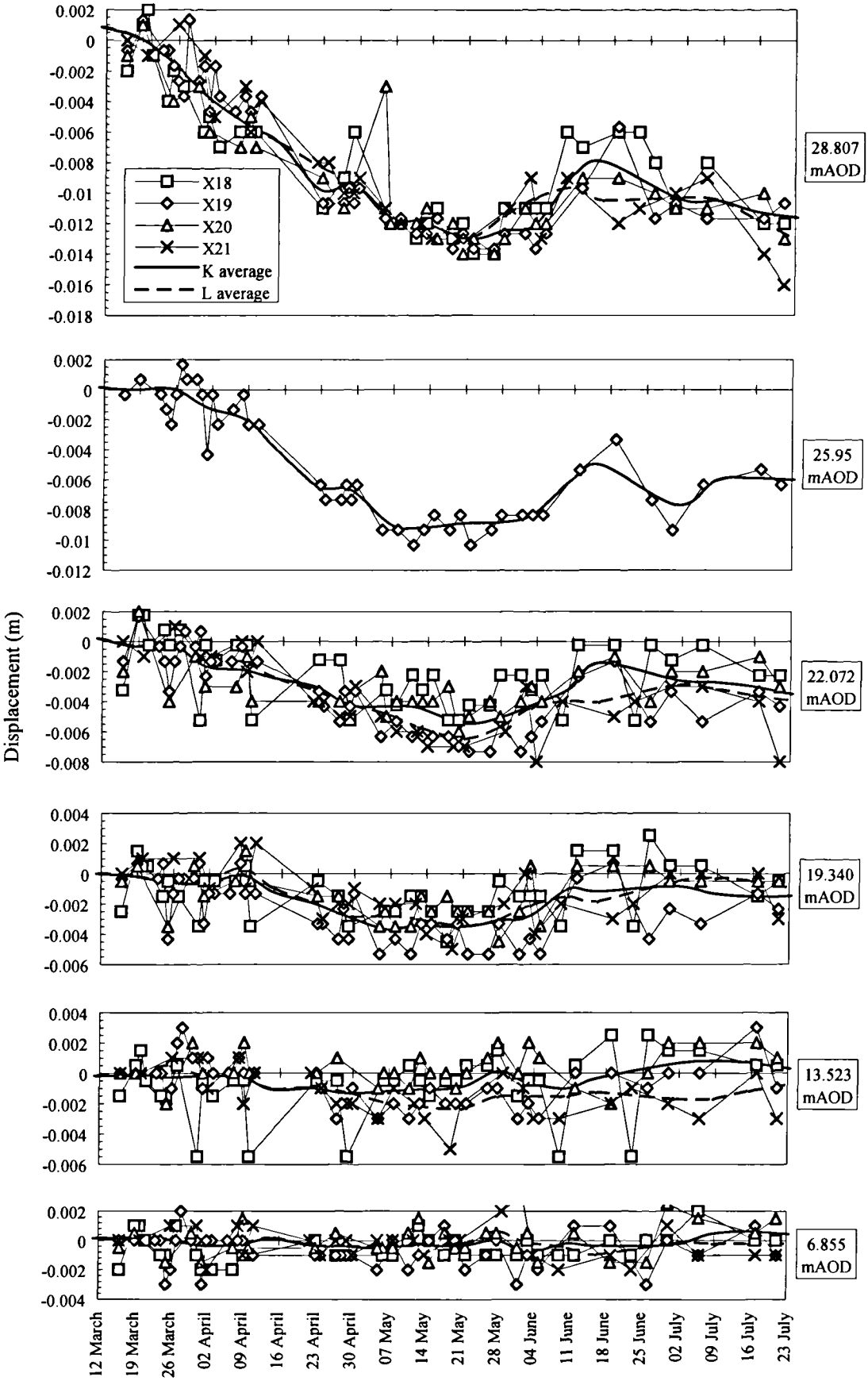

Figure 4.21 - Vertical displacement records for discrete elevations from extensometer installations along sections K and L

SECTIONS M AND N

Sections M and N contain single instruments, X22 and X23 respectively. They are located on the main instrumented section approximately 7.5m from the excavation crest. This section provides the limit at which inclinometer and extensometer readings are available at the same instrument locations.

Since only single instruments are available, the average displacement for a particular time is based on consecutive readings from the same instrument (see section 4.2.1), although it can be seen that there is a very high degree of repeatability between consecutive readings (Figure 4.22).

Results for section M, shown in Figure 4.23, required significant interpretation when considering the raw data. Relatively large horizontal displacements were apparently recorded in the Kellaways Sand at X22 which were not recorded at X23. It was decided that these were unrealistic since they were directed away from the excavation, in the opposite direction to those recorded at the adjacent sections of K and O (see below). The readings at time B, prior to excavation, also show a deformed shape suggesting that the initial base reading was erroneous. The out-of-plane measurements below the Oxford Clay were also large which is indicative of possible tube alignment or reading problems. It was decided that the readings below the Oxford Clay were erroneous and the displacement record was therefore zeroed at the base of the Oxford Clay. Following adjustment, the readings suggest up to 4mm of movement towards the excavation within the Oxford Clay.

The results for section N, shown in Figure 4.24, have also been modified to correct the anomaly in all readings at 14mAOD within the Kellaways Sand. The readings at time B (which are shown unaltered) have been used as the datum for the subsequent readings. The general form of

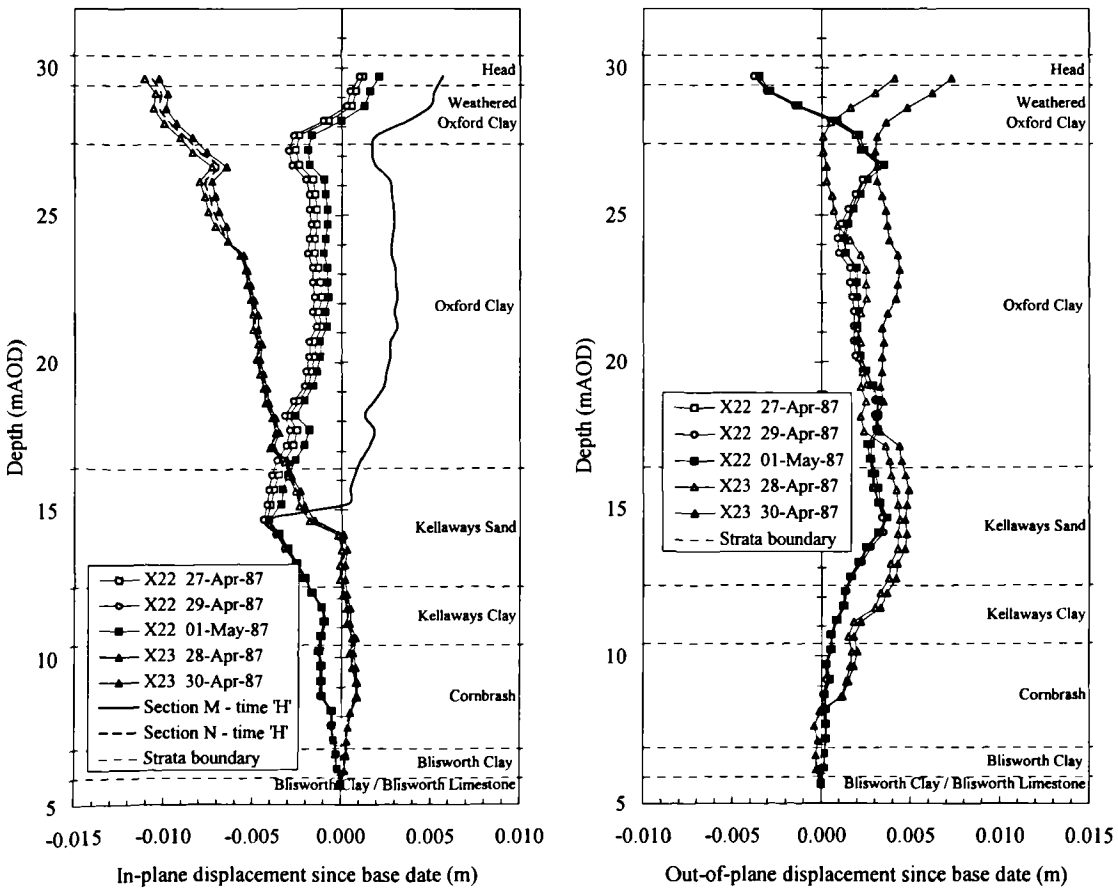

Figure 4.22 - Inclinometer data at sections M and N, Time 'H'

horizontal displacement shows 1 to 2mm movement occurring in the Kellaways Sand, and approximately 6mm in the Oxford Clay. Although there is not a clear trend, there is some evidence to suggest an increase in displacement with time. However, there is very little development following the completion of the excavation.

The modifications required to the inclinometer profiles complicate any absolute comparison of the two sections' responses. However, considering just the Oxford Clay, it is seen that the development of horizontal displacement is similar for both sections.

The vertical displacements recorded at X22 and X23 are similar to those at sections K and L in both form and magnitude. The agreement between results from sections M and N, shown in Figure 4.25, is not as good as between sections K and L, but is generally to within ±1mm, which is close to the reading accuracy of the extensometer magnet system.

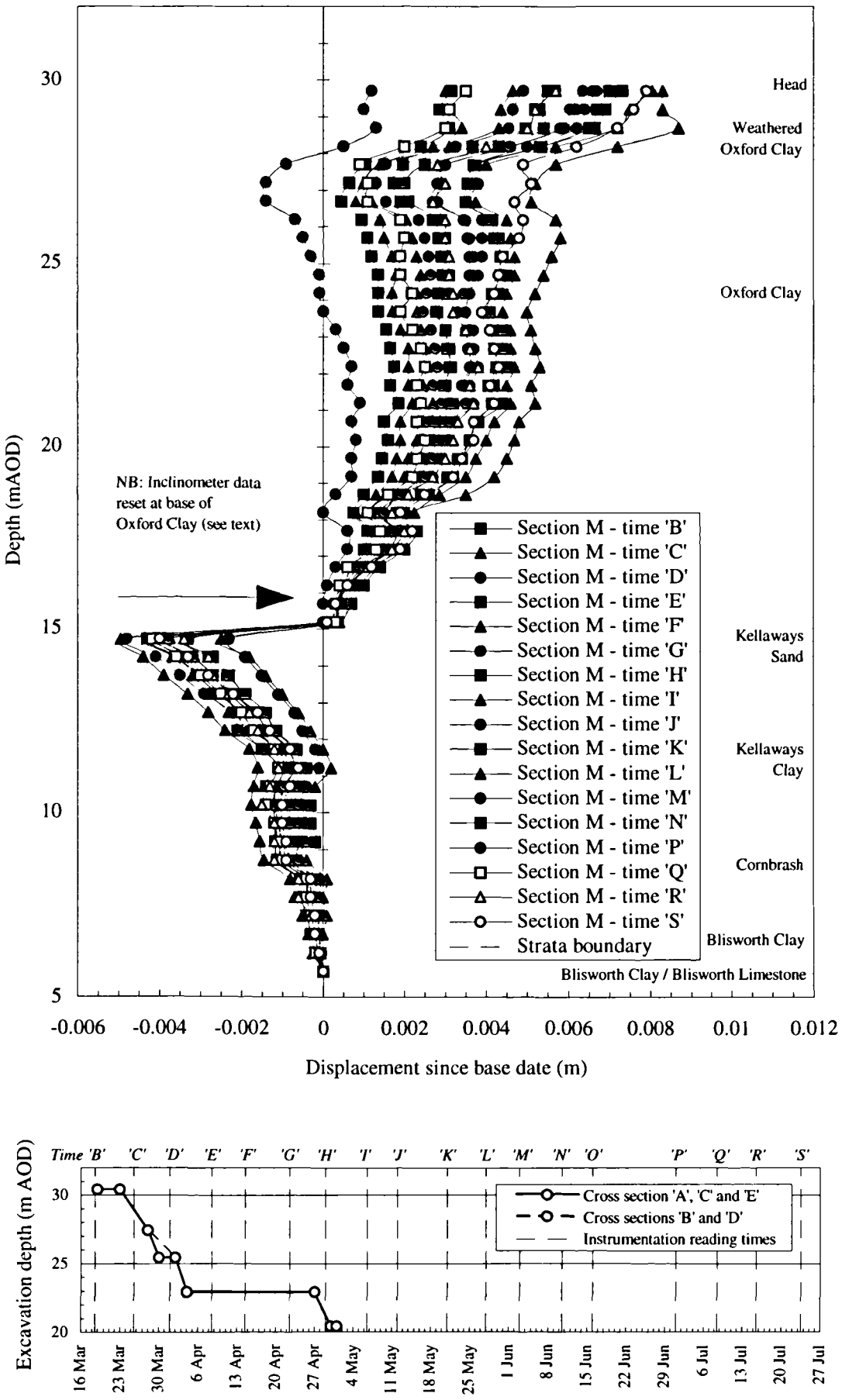

Figure 4.23 - Average inclinometer profile with time at section M

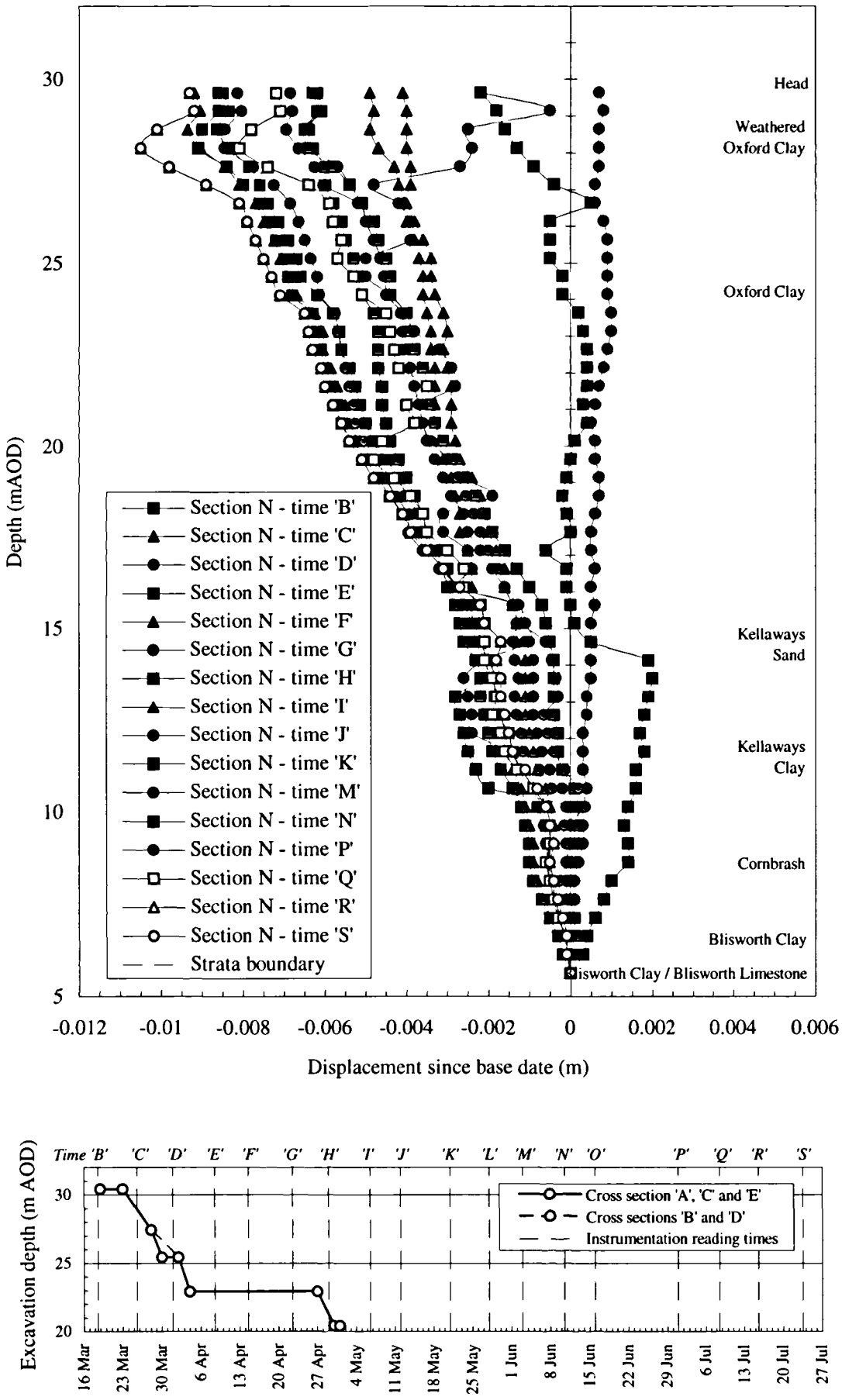

Figure 4.24 - Average inclinometer profile with time at section N

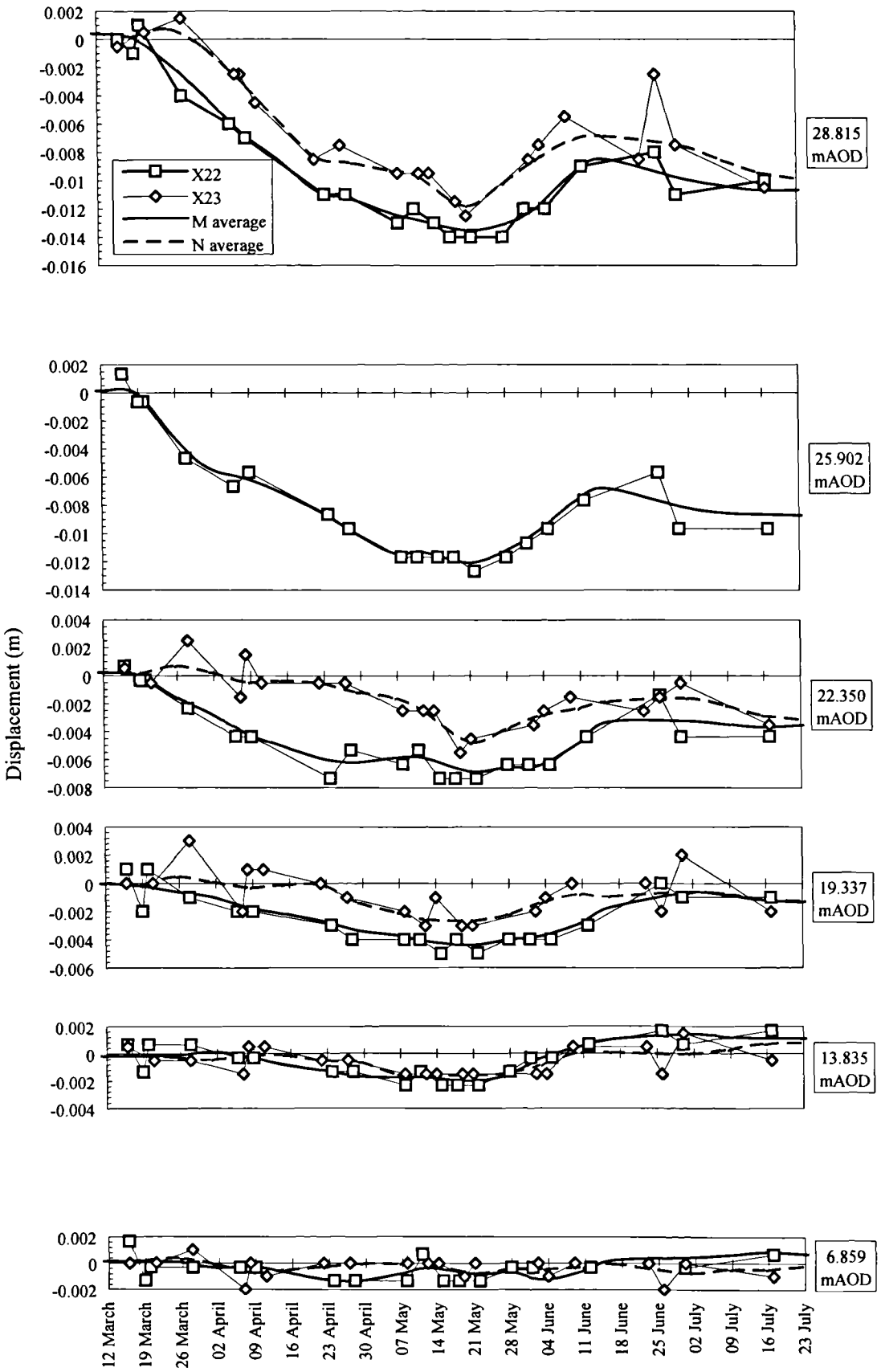

Figure 4.25 - Vertical displacement records for discrete elevations from extensometer installations along sections M and N

SECTION O AND P

Sections O and P each contain single instruments, X24 and X25 respectively, which monitored lateral movement only. The instruments are located on the main instrumented section approximately 35m from the excavation centreline.

The instrument to the north west, X25, is equidistant from the excavation and a 4.5m high stockpile of removed earth and so could perhaps be expected to experience greater out-of-plane movement than X24 which is unaffected by any additional earthworks. However, out-of-plane measurements at both locations were negligible as shown for time H in Figure 4.26.

The average horizontal displacement response is shown for sections O and P in Figure 4.27 and Figure 4.28 respectively. The initial base reading for section O was apparently erroneous since at time B, prior to excavation, 2mm movement was recorded at the base of the Kellaways Sand. The time B readings have again therefore been used as a datum for section O. The section P results have been zeroed at the same time for consistency. In both figures, the time B reading is shown unaltered.

For both sections, the horizontal displacement is directed towards the excavation. At the top of the Oxford Clay the magnitude of the movement is approximately 2 to 3mm. The similarity in the section O and P response suggest that symmetry still exists at this distance from the excavation.

It is noted that significant horizontal displacements are recorded at a distance which is three times the depth of excavation measured from the excavation centreline (see below).

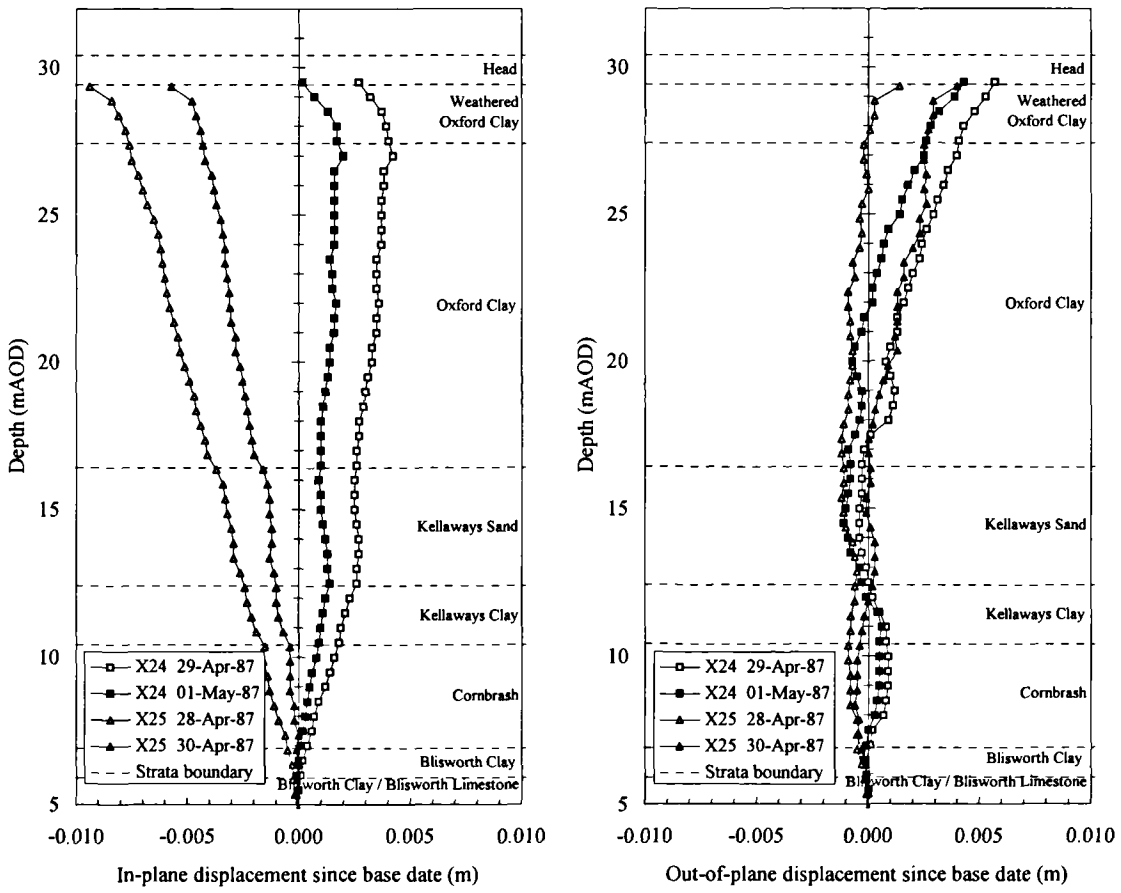

Figure 4.26 - Inclinometer data at sections O and P, Time 'H'

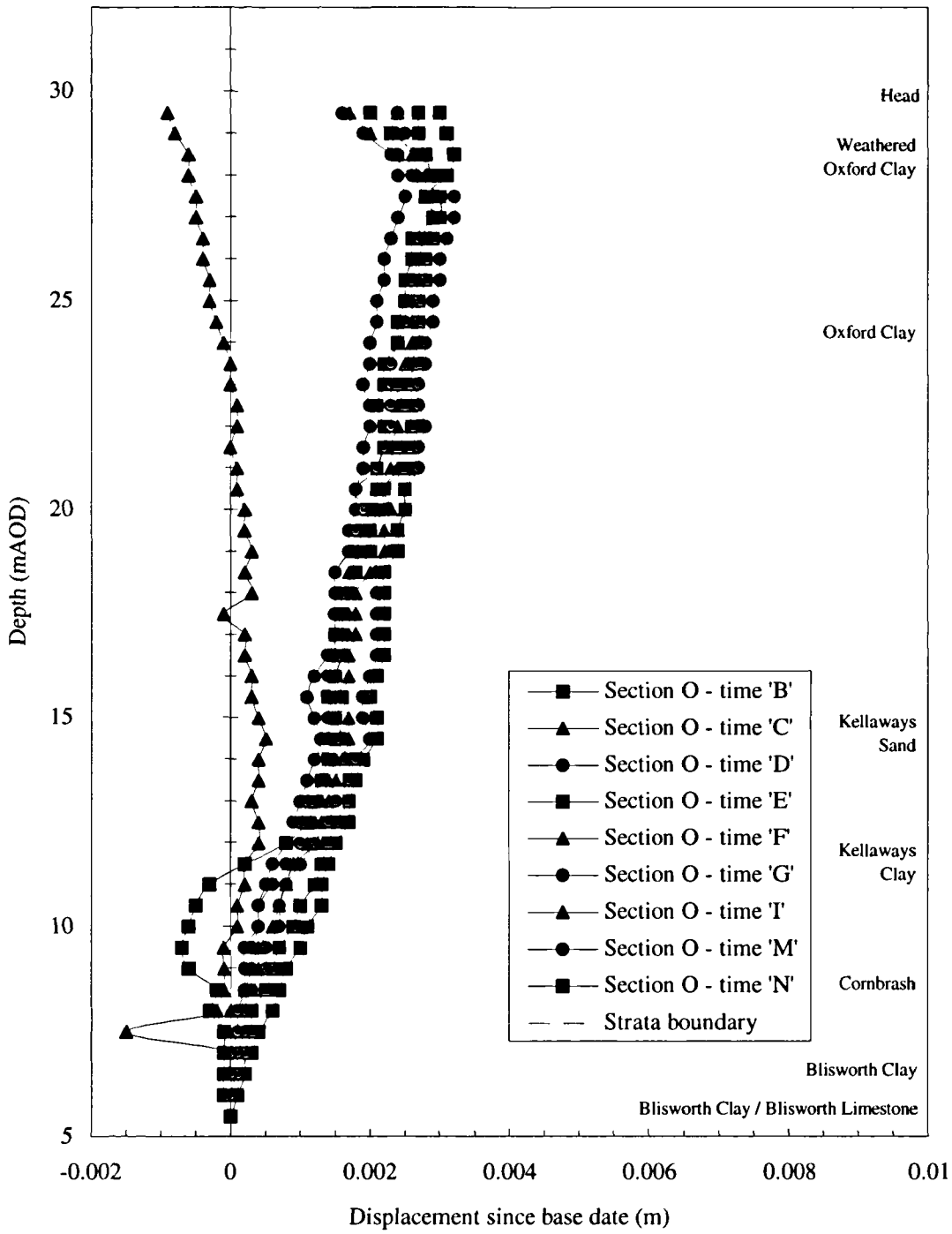

Figure 4.27 - Average inclinometer profile with time at section O

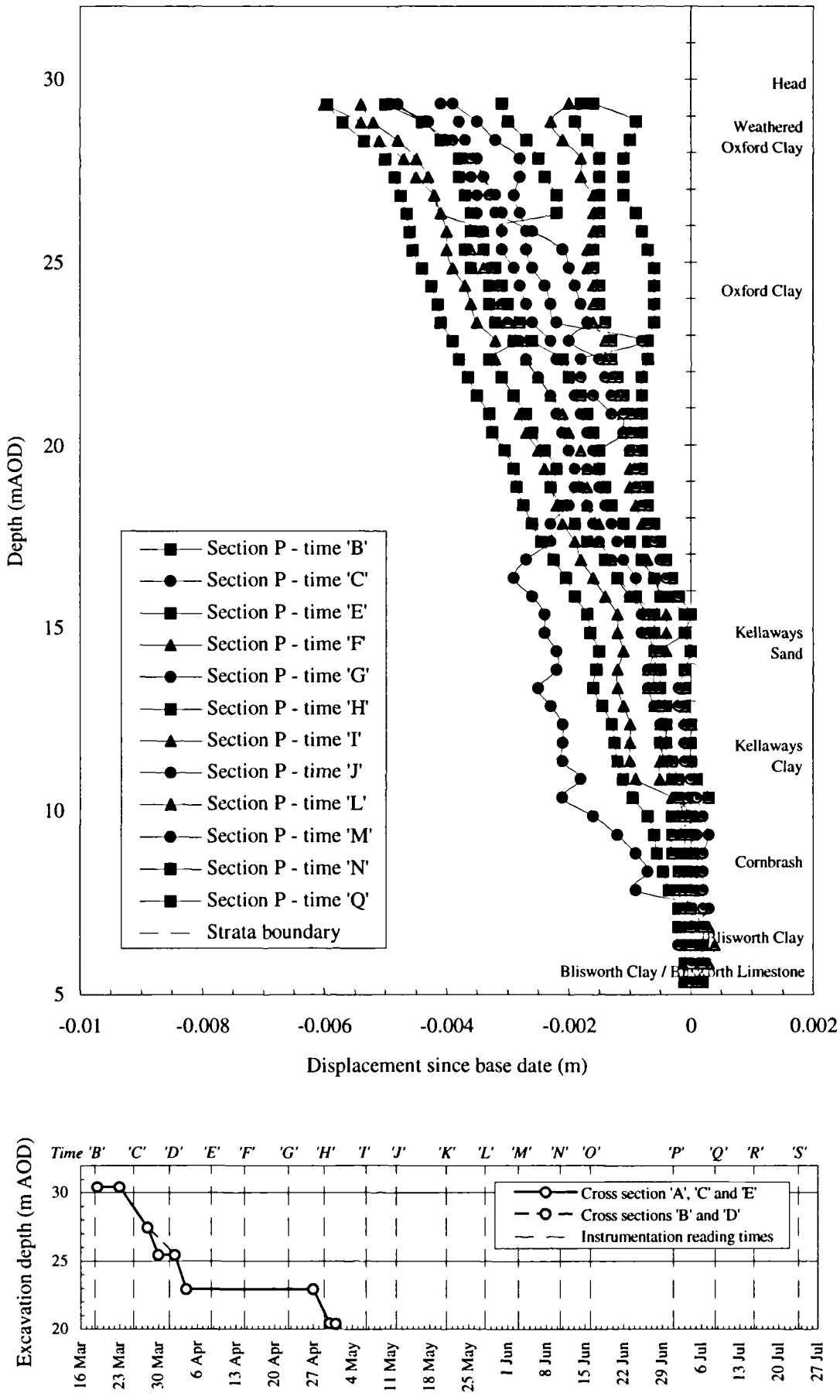

Figure 4.28 - Average inclinometer profile with time at section P

SECTION Q AND R

Sections Q and R each contain single instruments, X26 and X27 respectively. The instruments are located on the main instrumented section approximately 50m from the excavation centreline and measured only lateral movement.

The instrument to the north-west, X27, is closer to one of the earth stockpiles mentioned above than to the trial excavation and so could perhaps be expected to be affected as much by these constructions as by the trial excavation. The out-of-plane response at time S, shown in Figure 4.29 indicates no evidence of this but X26 is apparently affected by large out-of-plane displacements. The average horizontal displacement records for section Q (Figure 4.30) do not show a consistent response. The relatively large displacements recorded prior to excavation, at time B, suggest that the base readings were possibly erroneous. However, the readings at time B have not been used as a datum because of the scatter in all the subsequent readings at this position. Although the results indicate slight movement towards the excavation, the quality of the data is poor.

The inclinometer readings for X27 are easier to interpret than those of X26. The in-plane displacement is directed towards the excavation and increases with excavation depth. The maximum displacement was attained immediately after excavation work was complete with a surface lateral movement of about 2 to 3mm towards the excavation. The proximity of the trial embankment (Figure 3.15) would account for a proportion of this movement. It is questionable whether the zone of influence of the excavation extends to this distance, which is five times the depth of excavation from the excavation centreline. At the Saxon Pit, Burland *et al.* (1977) noted that the limit of the excavation influence was about three times the depth of excavation and attributed this to the presence of the stiffer Kellaways Sand strata.

In summary, at these locations the limit of the effectiveness of the inclinometers has been reached and the data obtained must be considered either erroneous or of questionable significance. The single inclinometer installations are not capable of providing accurate data for such small ground movements.

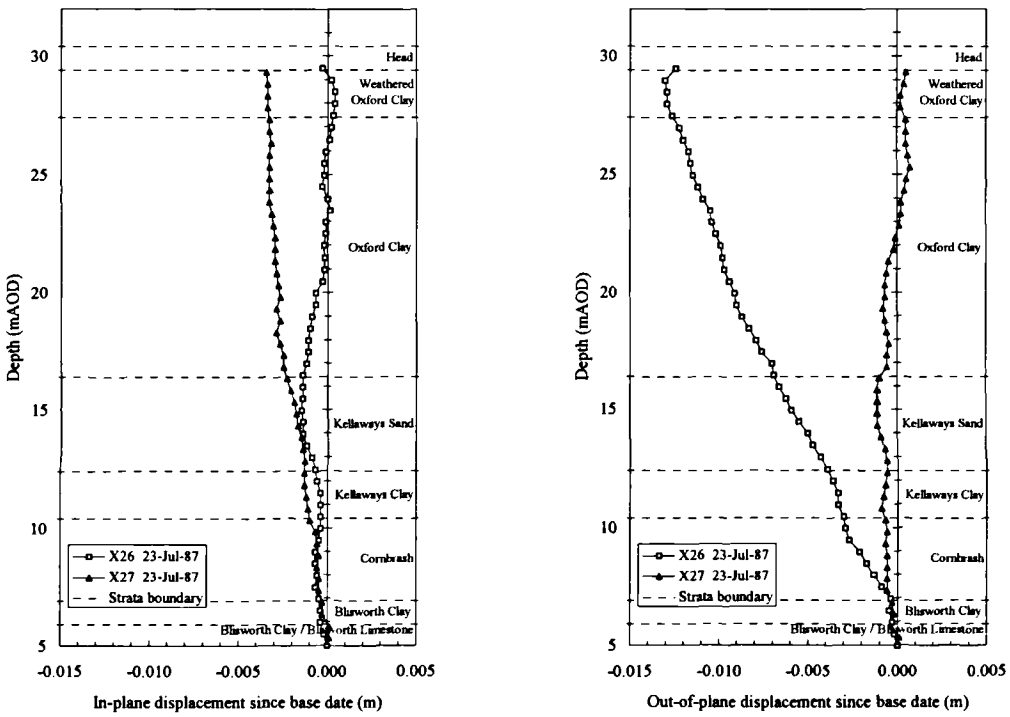

Figure 4.29 - Inclinometer data at section Q and R, Time 'S'

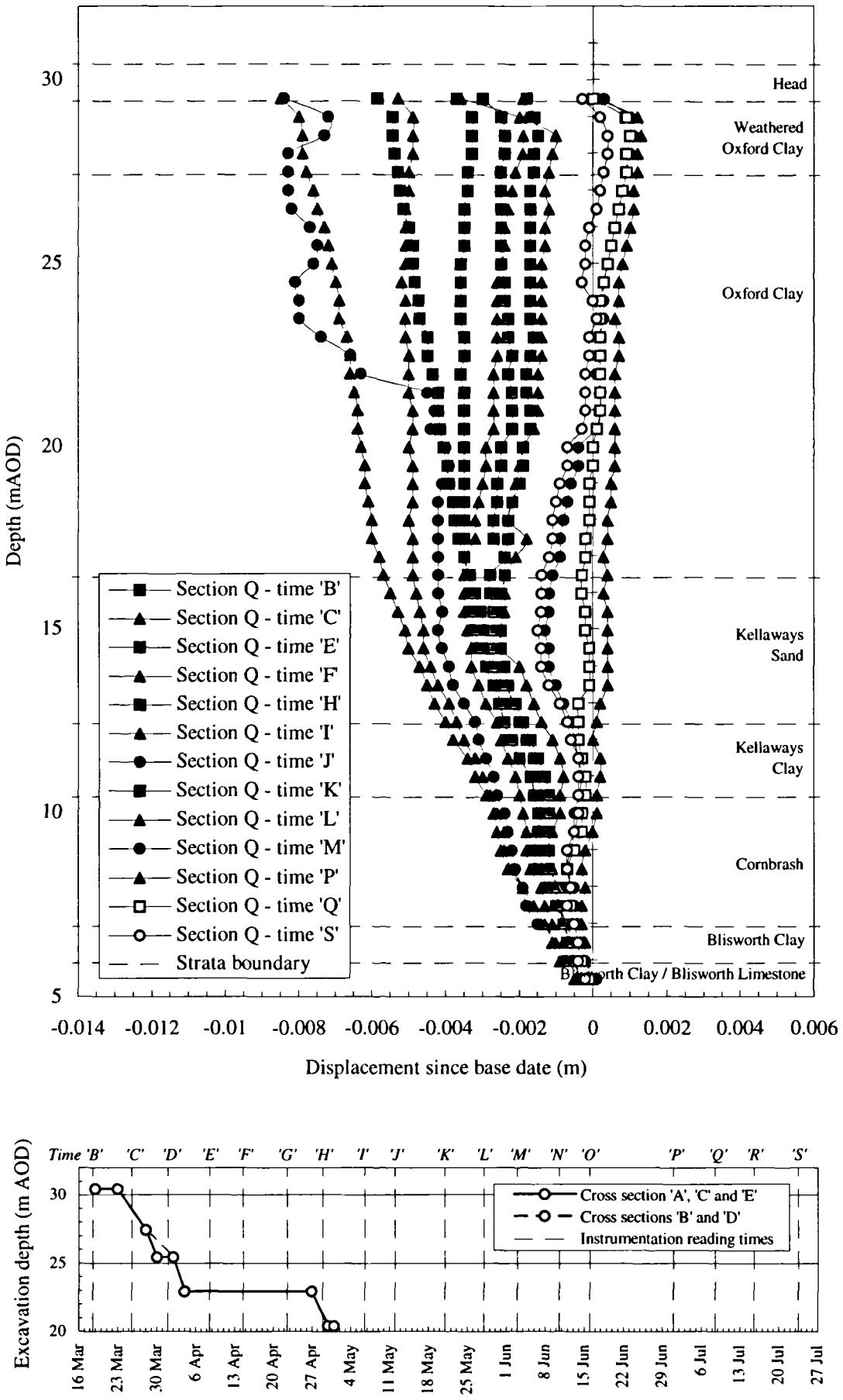

Figure 4.30 - Average inclinometer profile with time at section Q

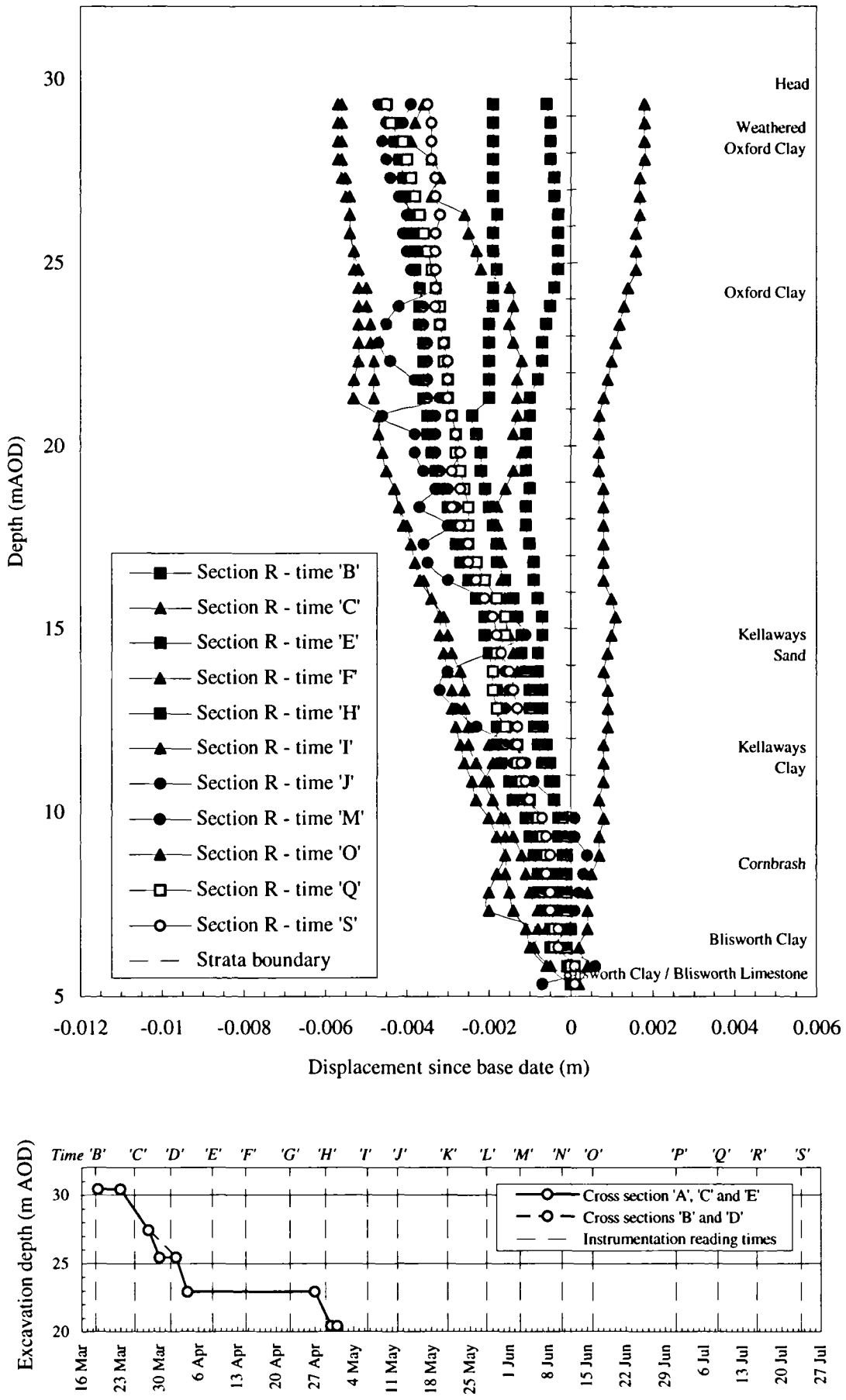

Figure 4.31 - Average inclinometer profile with time at section R

4.2.3 Deformation response

Extending the work of Rudrum (1990), the data obtained from the inclinometer and extensometers have been combined to describe the overall ground response due to increasing excavation depth and following completion. Combining the vertical and horizontal displacement data provides the necessary information required to plot displacement vectors which are shown for groups of average readings at various stages during the monitoring period in Figure 4.32 to Figure 4.34.

These figures show the general pattern of displacement and also provide a convenient basis for comparison with numerical analysis (see later in section 8.10).

The general pattern of displacement is consistent with that expected. Figure 4.32 shows the response during the excavation in which horizontal displacements dominate at the excavation sides and vertical displacements dominate at the excavation base and beyond the excavation crest. As excavation progresses, the displacement vectors at the sides of the excavation rotate from vertical to horizontal whereas those beyond the excavation crest rotate from horizontal to vertical. Figure 4.33 shows the response up to one month following the completion of excavation in which the vectors rotate slightly in the opposite direction to that during excavation. The vectors at the excavation sides rotate slightly to the vertical, and beyond the excavation crest they rotate slightly to the horizontal. During this time the magnitude of the displacements generally increases only slightly throughout the excavation although there is a significant movement at the excavation base. The final period of monitoring (Figure 4.34) shows the magnitude and orientation of the vectors to be relatively constant. The magnitude of displacement at the excavation base, however, is still increasing.

The displacement vectors show that the greater proportion of the movements had taken place immediately following completion of the excavation. Only at the excavation base were the displacement vectors indicate continuing movement.

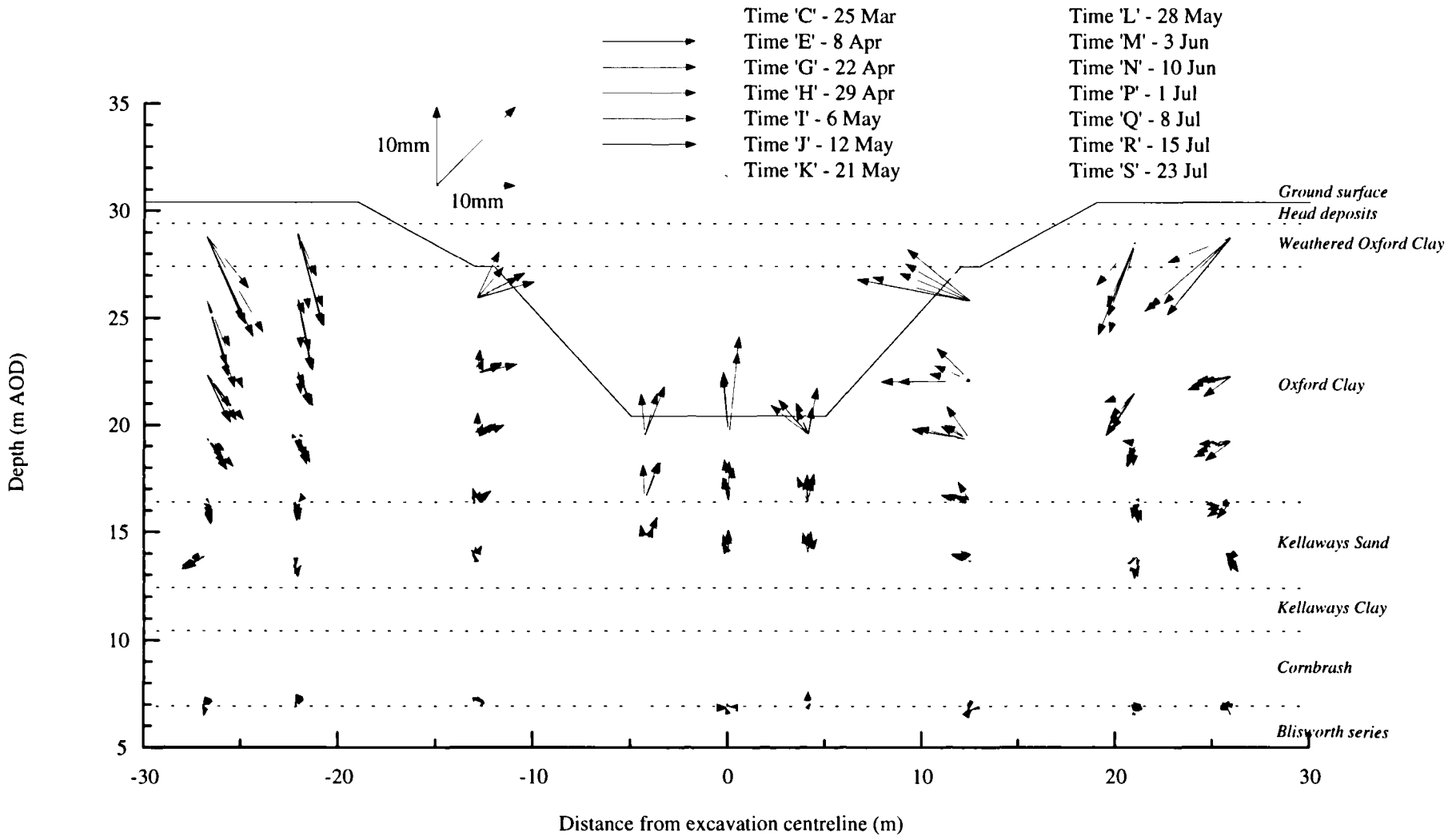

Figure 4.32 - Displacement vectors for excavation cross-section from time 'C' to time 'J'

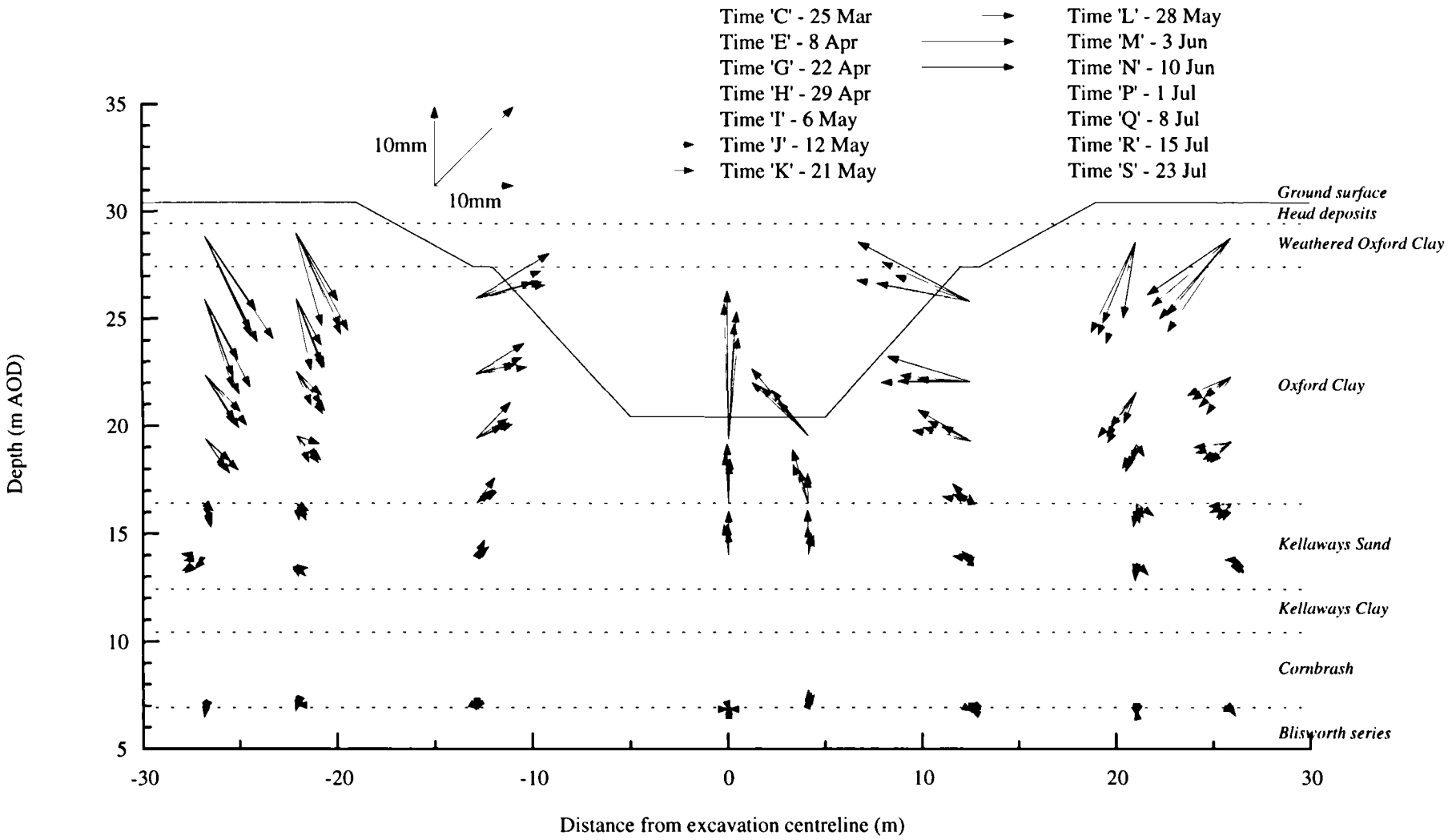

Figure 4.33 - Displacement vectors for excavation cross-section from time 'J' to time 'N'

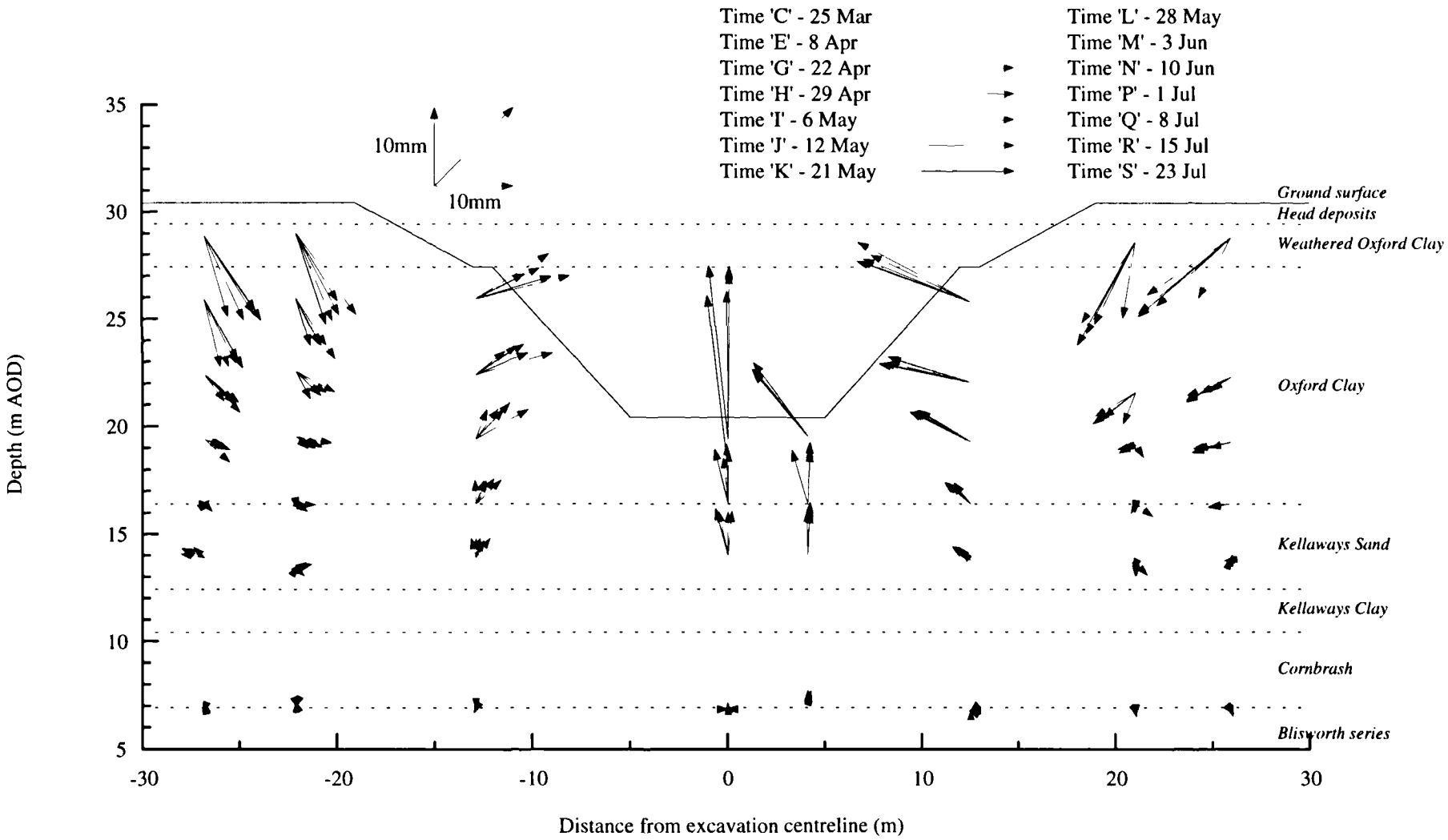

Figure 4.34 - Displacement vectors for excavation cross-section from time 'N' to time 'S'

4.2.4 Interpretation of the piezometric response

A previous interpretation of the instrumentation data from the piezometer clusters in the vicinity of the excavation has been carried out (Rudrum, 1990). The main conclusions from that analysis will be briefly outlined in this section.

At Elstow, the piezometers were arranged in clusters of five instruments, to record the pore pressure change at five depths beneath the centre of the excavation base, at the toe of the excavation slope and beneath the berm on the excavation sides. The interpreted data are presented in Figure 4.36, Figure 4.37 and Figure 4.38 and a summary of information for each instrument is given in Table 4.2.

INITIAL PORE PRESSURE DISTRIBUTION

The initial pore pressure distribution is shown in Figure 4.35.

Hydrostatic conditions exist in the Lower Oxford Clay with a projected water table level at approximately 29.6mAOD, 0.9m below the average ground level.

The pore pressures are less than hydrostatic within the Kellaways, Cornbrash and Blisworth strata, suggesting that these strata underdrain the Lower Oxford Clay. At the time of the

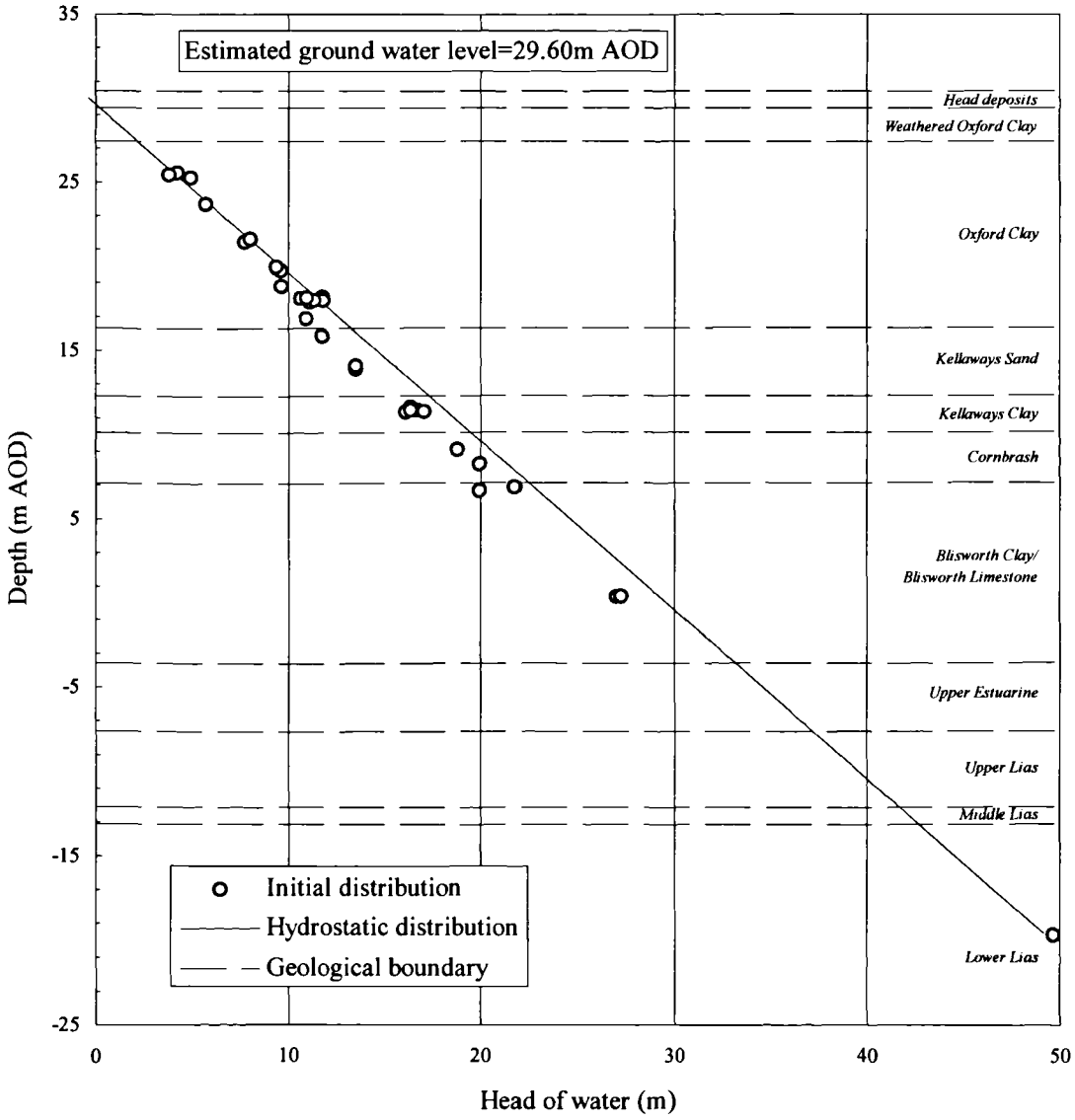

Figure 4.35 - Initial pore water pressure distribution

excavation Anglian Water Authority were actively pumping from these strata for water supply purposes.

PORE PRESSURE CHANGES DUE TO EXCAVATION

The interpreted piezometer records in Figure 4.36 show that, as expected, the pore pressure changes are closely related to the excavation sequence. After an initial drop in piezometric level, there is typically a slight recovery over a period of 2-3 weeks, but it is thought that this is due to a short term redistribution of stresses local to the instrument and not a reflection of the overall excavation drainage response. It is seen that although vertical stress relief provides the major effect (see for example instrument P1), instruments P16 to P20 show that lateral stress relief also contributes to the pore pressure response.

Once excavation was complete, the piezometers continued to fluctuate until the end of May 1987, after which time every piezometer recorded an approximately constant response until the end of the monitoring period. As expected on the basis of the *in situ* permeability measurements ($k=1x10^{-9}$ to $1x10^{-10}$ m/s), the dissipation of excess pore water pressure during this time within the Oxford Clay and the Lower Lias was negligible. However, the lack of dissipation in the Kellaways, Cornbrash and Blisworth strata was not expected. The Kellaways Sand recorded the highest permeability from in-situ tests ($k=1.6x10^{-8}$ to $6.8x10^{-7}$ m/s), but even within this stratum pore water pressure dissipation was not seen to take place. Although these more permeable strata were thought to be underdraining the Oxford Clay, the amount of silt and clay present as secondary constituents within the sand seemed to be inhibiting the flow over such a time period.

The comparison between the initial and the final interpreted piezometric levels is presented for each cluster of instruments in Figure 4.37 and also in Table 4.2.

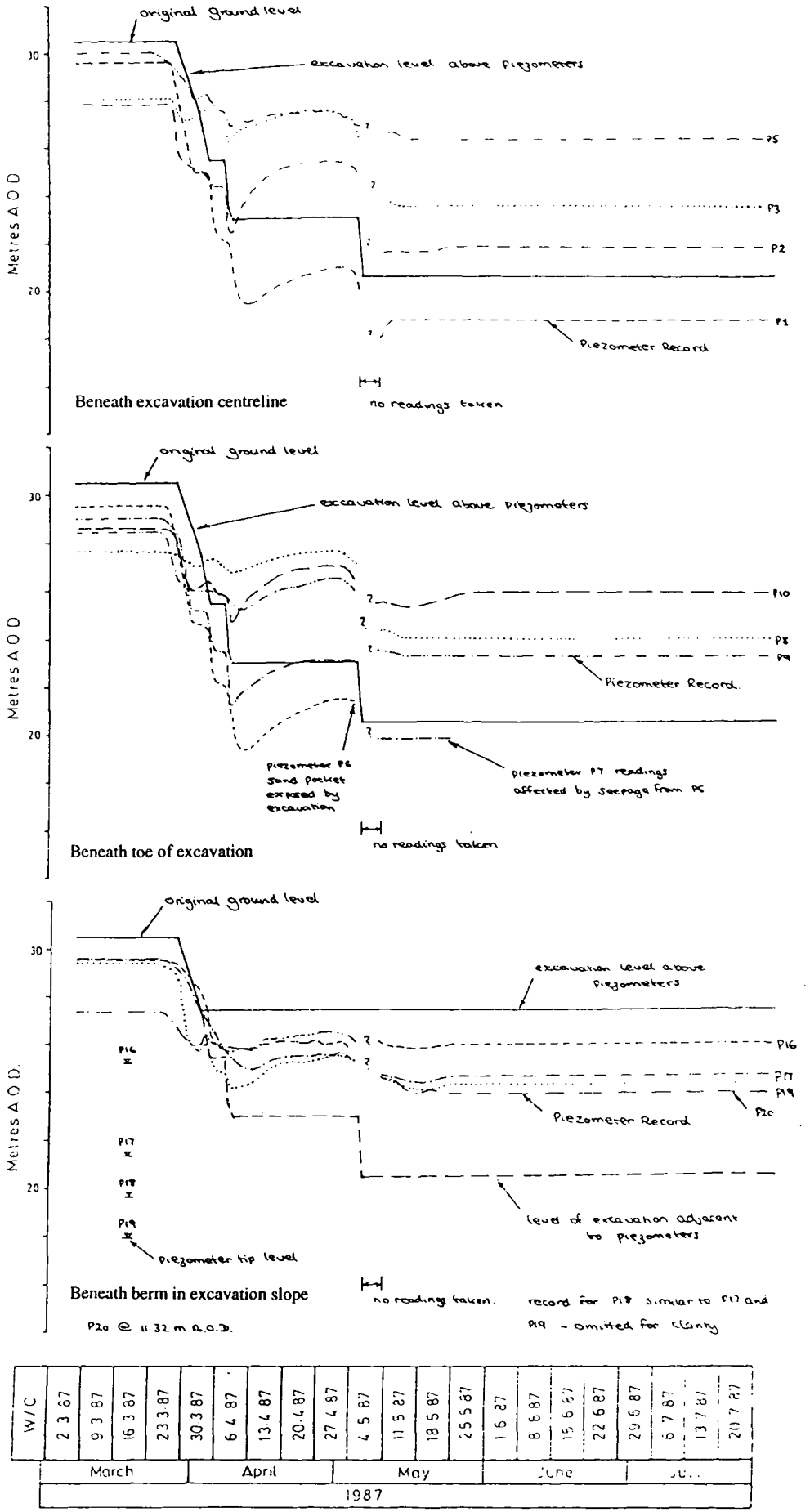

Figure 4.36 - Interpreted piezometer records (after Rudrum, 1990)

Piezometer instrument number	Stratum	Elevation of Tip (m AOD)	Distance from centre line (m)	Depth below ground surface (m)	Initial head of water (m)	Final head of water (m)	Change in head (m)	Change in pore pressure (kPa)
P1	O.C.	18.80	0.00	-11.61	9.65	-1.20	-10.85	-106
P2	O.C.	16.88	0.00	-13.53	10.92	4.87	-6.05	-59
P3	K. Clay	11.45	0.00	-18.96	16.70	12.05	-4.65	-45
P4	Blisworth	6.68	0.00	-23.73	19.92			?
P5	L. Lias	-19.67	0.00	-50.08	49.67	45.97	-3.70	-36
P6	O.C.	19.89	4.50	-10.52	9.41			?
P7	O.C.	17.87	4.50	-12.54	11.13	1.93	-9.20	-90
P8	K. Sand	15.87	4.50	-14.54	11.73	8.13	-3.60	-35
P9	K. Clay	11.37	4.50	-19.04	17.03	11.93	-5.10	-50
P10	Blisworth	6.86	4.50	-23.55	21.74	19.14	-2.60	-25
P11	O.C.	25.56	12.50	-4.85	4.24	0.74	-3.50	-34
P12	O.C.	21.56	12.50	-8.85	8.04	3.04	-5.00	-49
P13	O.C.	20.08	12.50	-10.33		3.72		?
P14	O.C.	18.14	12.50	-12.27	11.76	7.46	-4.30	-42
P15	K. Clay	11.64	12.50	-18.77	16.36	13.16	-3.20	-31
P16	O.C.	25.25	-12.50	-5.16	4.95	1.45	-3.50	-34
P17	O.C.	21.42	-12.50	-8.99	7.73	2.88	-4.85	-47
P18	O.C.	19.74	-12.50	-10.67	9.61	4.56	-5.05	-49
P19	O.C.	17.98	-12.50	-12.43	11.82	6.62	-5.20	-51
P20	K. Clay	11.32	-12.50	-19.09	16.08	12.68	-3.40	-33
P21	O.C.	25.45	12.50	-4.96	3.80	0.30	-3.50	-34
P22	O.C.	21.59	12.50	-8.82	8.01	3.61	-4.40	-43
P23	O.C.	19.94	12.50	-10.47	9.36	4.26	-5.10	-50
P24	O.C.	17.96	12.50	-12.45	11.34	6.94	-4.40	-43
P25	K. Clay	11.44	12.50	-18.97	16.36	13.36	-3.00	-29
P51	O.C.	18.08	0.00	-12.33	10.62	2.62	-8.00	-78
P52	K. Sand	13.91	0.00	-16.50	13.49			?
P53	Cornbrash.	8.26	0.00	-22.15	19.94			?
P54	Blisworth	0.38	0.00	-30.03	27.02			?
P55	U. Lias	-9.37	0.00	-39.78				?
P56	O.C.	23.67	-12.50	-6.74	5.73	1.43	-4.30	-42
P57	O.C.	18.13	-12.50	-12.28	10.97	6.42	-4.55	-44
P58	K. Sand	14.11	-12.50	-16.30	13.49	10.29	-3.20	-31
P59	Cornbrash.	9.11	-12.50	-21.30	18.79	17.09	-1.70	-16
P60	Blisworth	0.41	-12.50	-30.00	27.24	26.59	-0.65	-6

Table 4.2 - Locations of piezometer instruments and change in pore pressure due to excavation

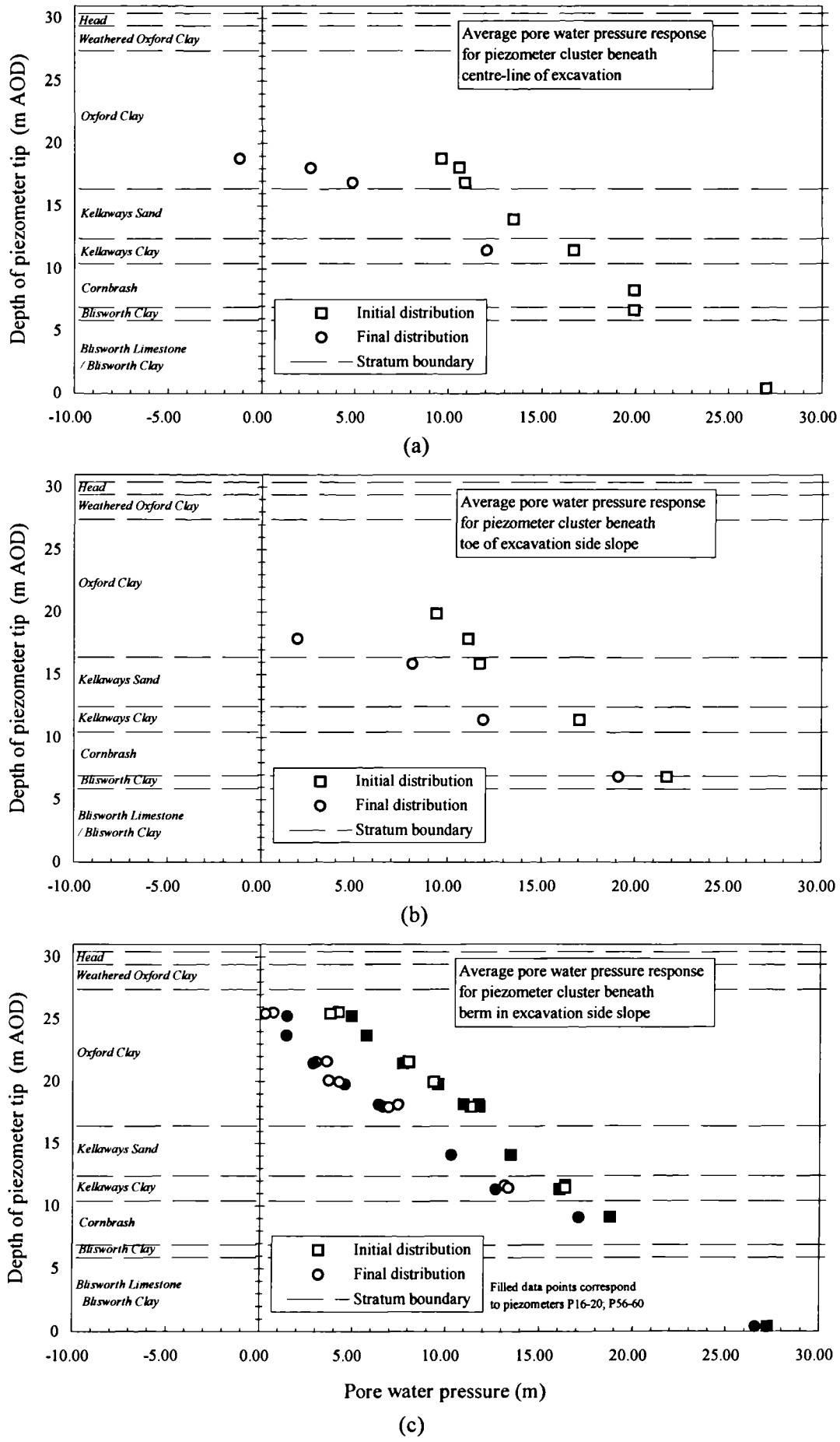

Figure 4.37 - Pore water pressure distribution before and after excavation

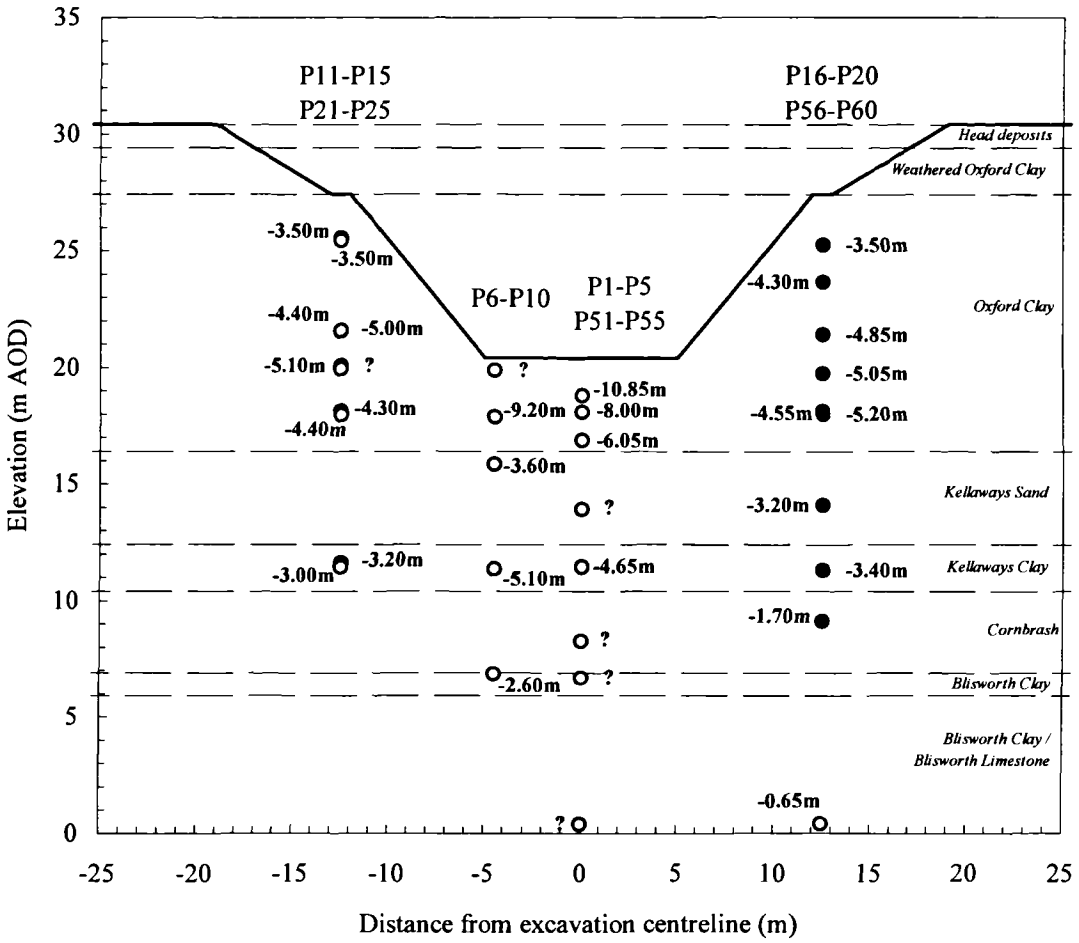

Figure 4.38 - Change in pore water pressure head at 23 July 1987 due to excavation

4.2.5 Plane strain and excavation symmetry

The scale and dimensions of the Elstow excavation were designed to ensure that the central cross-section would deform under plane strain conditions and that the ground response would be symmetrical about the excavation centreline.

Validity of the plane strain assumption implies an absence of out-of-plane movements in the vicinity of the main instrumented section. As discussed in section 4.2.2, the inclinometers generally supported this assumption.

The validity of the assumption of symmetry may be assessed for both plane lateral movement (Figure 4.14; Figure 4.15; Figure 4.20; Figure 4.22) and for vertical movements (Figure 4.7; Figure 4.11; Figure 4.16; Figure 4.17; Figure 4.21; Figure 4.25). In terms of ground movements, the excavation dimensions were sufficient to ensure that symmetry existed for 25m on either side of the main instrumented section, and at least up to 30m either side of the major axis of the excavation. The symmetry is also shown in the magnitude and orientation of the displacement vectors shown in Figure 4.32 to Figure 4.34.

The piezometric response shown in Figure 4.37 and Figure 4.38 also demonstrates a symmetry which extends at least to the berms in each side of the excavation.

4.3 Volumetric response of excavation

4.3.1 Introduction

It has been shown that the pore water pressure regime around the excavation remained substantially unaltered following the immediate response due to excavation. This implies that the soil behaviour was undrained.

The absence of volume change may be verified from the displacement characteristics of the excavation. Surface profile measurements, extending to the far field, can be analysed as shown in Figure 4.39. For an undrained, and therefore constant volume response, in the saturated soil the volumes A and B swept out per unit length should be the same under plane strain conditions.

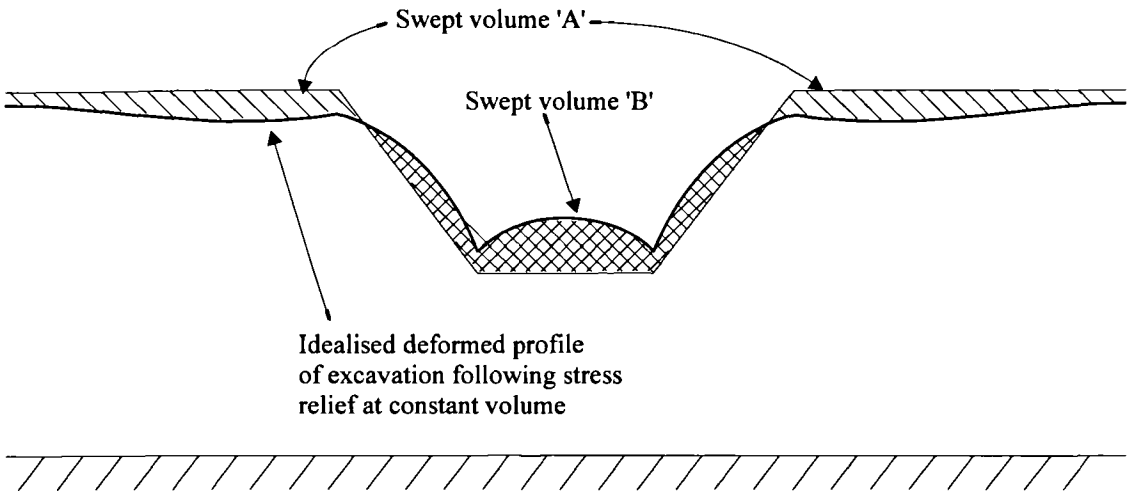

Figure 4.39 - Diagrammatic representation of heave and settlement volumes

This technique has been adapted so that it can be applied to the instrumentation data at the Elstow excavation.

In the absence of suitable surface profile measurements, an alternative approach must be adopted. The inclinometer data provide continuous horizontal displacement profiles and these may be combined with the discrete data from the extensometer magnets to set up a coarse grid of elements across the excavation cross-section as shown in Figure 4.40.

The calculation of volume changes and strains within each element is described in the next section.

4.3.2 Calculation of volume changes and strains from ground displacement data

The volumetric response of each element shown in Figure 4.40 is broken down into its vertical and horizontal components, as shown in Figure 4.41. The volume change at each element boundary is calculated and summed using a compression positive sign convention. The volume change along vertical boundaries is calculated as the area swept out by the curve of horizontal displacement measured by the inclinometers. The volume change along horizontal boundaries is calculated as the area swept out by the interpolation of the vertical displacements at element corners measured by the extensometers. This process is carried out automatically by a spreadsheet program written in Microsoft VisualBasic for Applications.

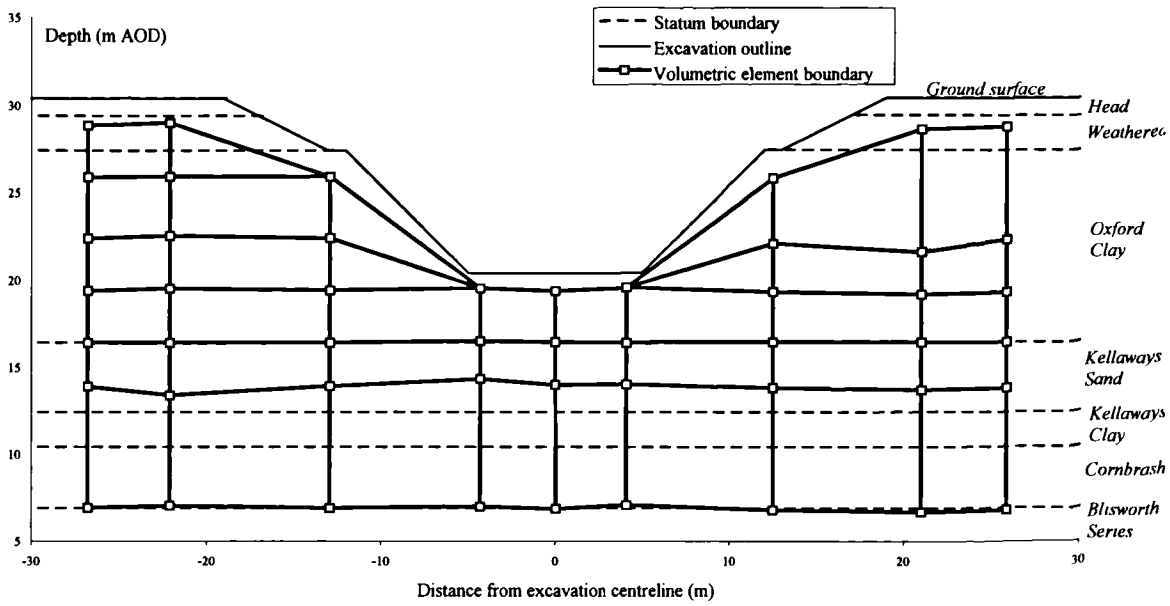

Figure 4.40 - Definition of elements across excavation cross section

The elements may be considered in isolation or in combination. The change in element area may be used directly to calculate overall or average volumetric strains. The ratio of the horizontally swept volume to the vertically swept volume may indicate the general form of the movements. The accuracy of this method depends not only on the accuracy of the displacement data, but also on the size of the element relative to the gradient of strain.

As described in section 4.2.1, the instrumentation monitoring period has been divided into clusters of instrument readings to provide time sections, labelled A to S, during and after excavation at which the ground displacement response is interpreted (see Table 4.1). Where sufficient data are available, the volumetric strain at each stage can be calculated for each element of soil defined in Figure 4.40.

Studying the volumetric strains calculated for individual elements, it proved difficult in the present case to see the general trends of volume change since they were masked by inaccuracies. The quality of the calculation improves when the grid elements are combined as this provides a larger reference volume and reduces the relative magnitude of measurement errors. Combining strips of elements together is an effective method for eliminating the errors in inclinometer measurement, since the errors at adjoining boundaries cancel each other out during the volume summation.

The volumetric strains for strips across the excavation can be seen in Figure 4.42. Although there is a degree of scatter in the data, the general response is of volumetric expansion at the base of the excavation, volumetric compression in the area surrounding the excavation, and a transition zone which deforms at approximately constant volume at the excavation sides. The degree of compression seems to have been approximately constant during the monitoring period after the earthworks ceased. The volumetric expansion at the base of the excavation developed during the period of excavation and was relatively constant from this point until mid-June. However, from this point until the end of the monitoring period additional expansion was recorded at the base of the excavation.

The effect of combining several strips is shown in Figure 4.43. Unfortunately the instrument data at section G is only available up to the end of excavation, on 1 May 1987, meaning that the overall volumetric behaviour of the excavation must be deduced from the behaviour of only the north western side of the excavation by combining strips from section F to section N. This

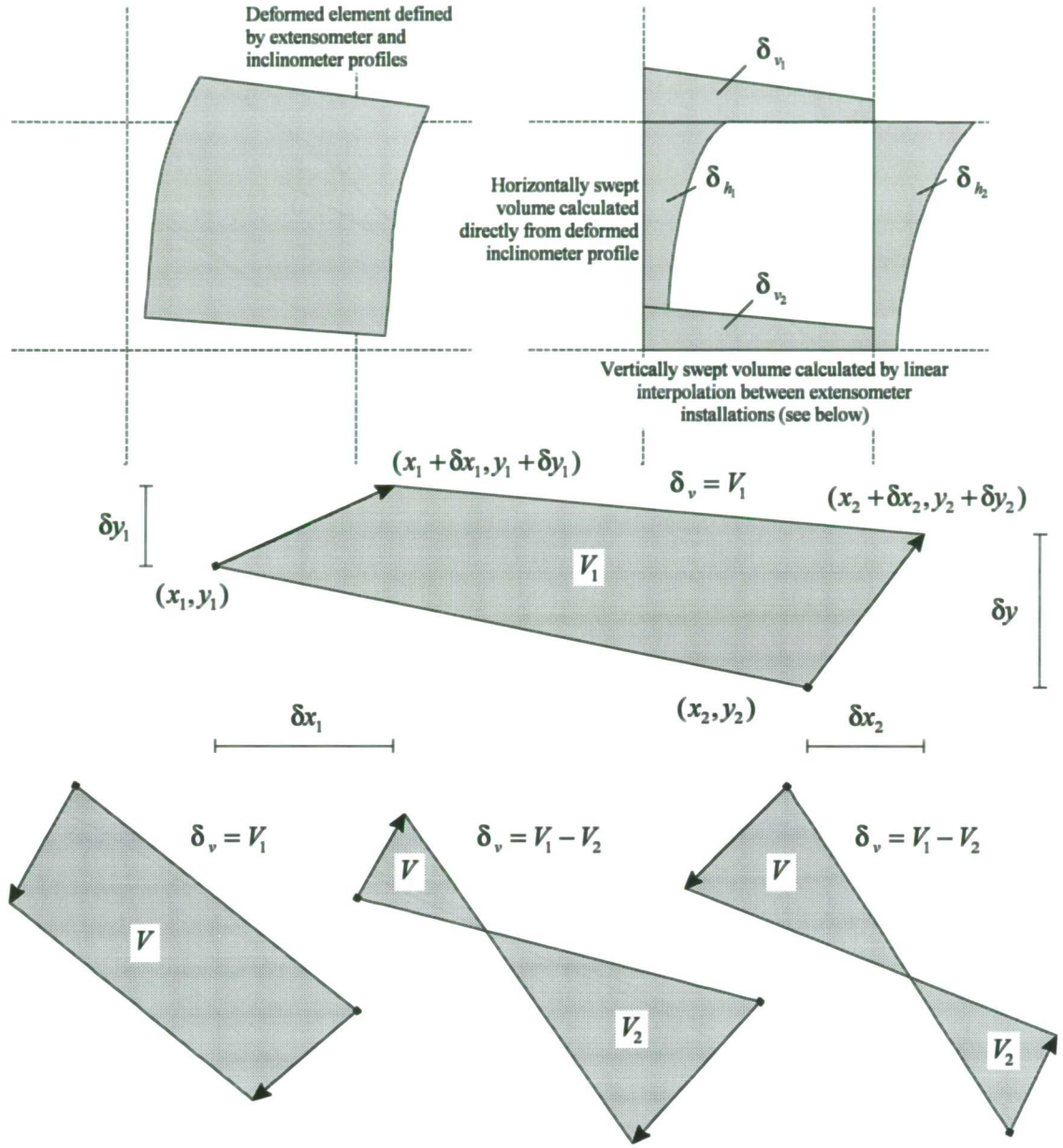

Figure 4.41 - Approximation used to calculate volumetric strain around excavation

suggests that the volumetric expansion at the base of the excavation is balanced by compression beyond the excavation crest. Thus, although the overall deformation response of the excavation is at constant volume, this is not due to uniform constant volume behaviour.

4.3.3 Discussion of the volumetric ground response due to excavation

Volume changes in a saturated medium are assumed to be explained solely by migration of water through the soil i.e. by the processes of consolidation and swelling. However, the intact permeability of the clay would not allow this over the short time scale considered here. This view is supported by the piezometer data which show no evidence of changes in the pore water pressure regime with time following excavation (see section 4.2.4).

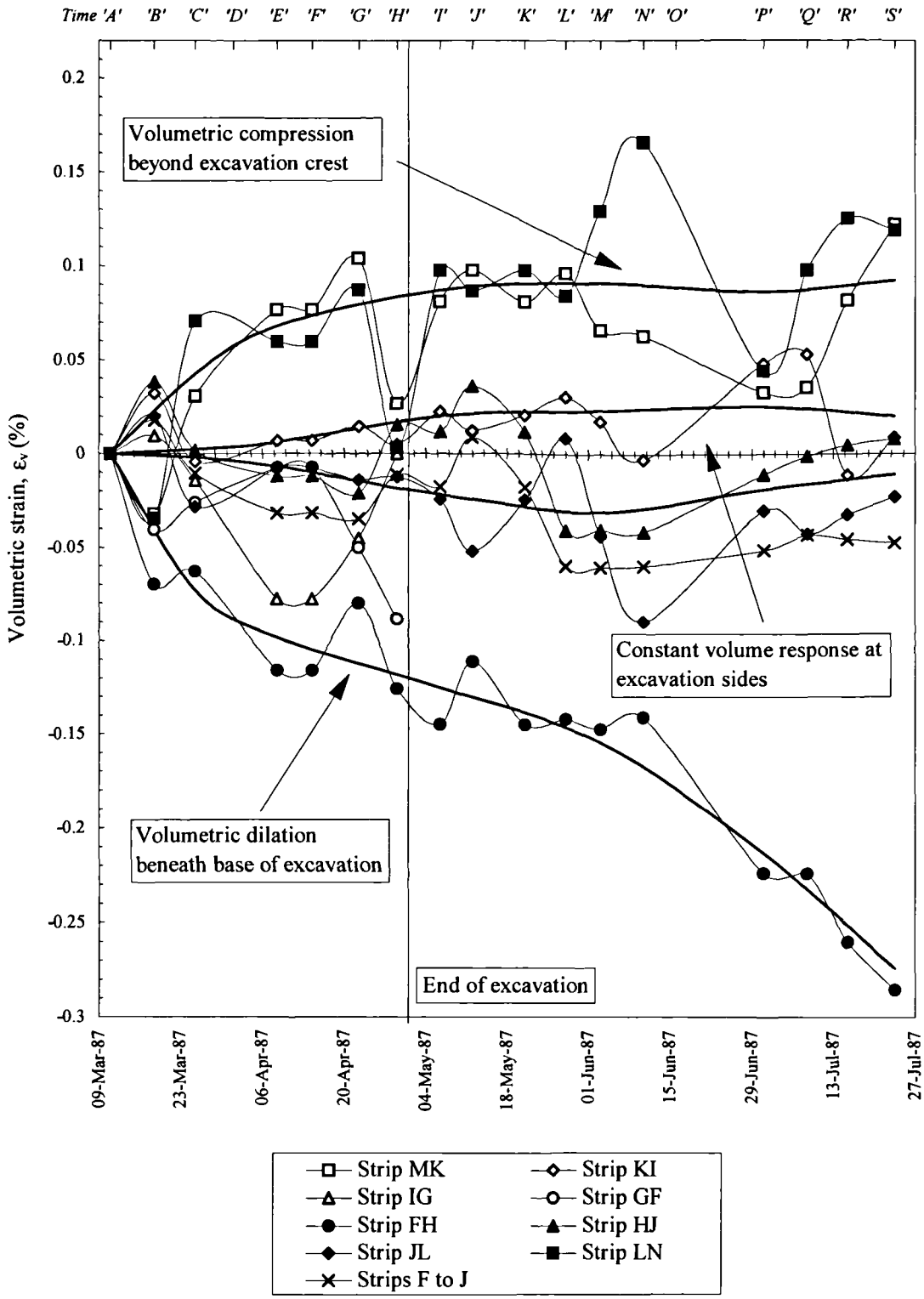

Figure 4.42 - Variation of volumetric strain of strips across excavation cross-section

In the field fissures are generally closed and are often only evident after unloading due to stress relief caused by excavation or sampling. The total stress relief at the base of excavations may induce negative pore water pressures in intact blocks of clay. Fissures in the intact clay will be forced open following stress relief if the negative pore water pressure induced in the intact material is not maintained across the discontinuity.

A negative pore water pressure was recorded at the base of the excavation on the excavation centreline at instrument P1 (see Figure 4.37(a) and Table 4.2). The instrument is 1m below the base of the excavation and recorded a negative excess pore water pressure of -1.2m head of water. All the remaining piezometers recorded a positive pore water pressure. Instrument P6 (installed at an elevation similar to instrument P1) was exposed during excavation to 10m, although prior to this was following a similar trend and magnitude of pore pressure change as at instrument P1. The ability of the piezometers to record negative pore water pressure relied on the sand cells into which they were installed, being able to maintain the suction. It is unlikely that the water in the sand pocket could have maintained a suction much greater than 10kPa. Consequently, cavitation is likely to have occurred in the sand cell, and the recorded negative pore water pressure may not reflect the magnitude of suctions in the ground. It is possible, therefore, that fissures and other discontinuities would have opened, in a region extending to 2m below the base of the excavation. This would have lead to volumetric expansion and additional vertical displacements being recorded in this region.

The magnitude of volumetric compression calculated in the Oxford clay beyond the crest of the excavation is less than that of the corresponding expansion at the base. The magnitude is also comparable with the accuracy of the technique and, therefore, may be unreliable. However, such a zone of volumetric compression could be explained by a flow of water towards the excavation. It is possible that, at upper levels, fissures and discontinuities would have been open prior to excavation. The effect of the excavation may have been to draw water from such fissures, causing them to close. This would have produced compressive strains and additional settlement in this area. Such compressive volumetric strains may also have been produced by the consolidation of the more permeable silt, sand and pyritic bands within the Oxford Clay. The most significant seepage into the excavation was noted from a pyritic band at 5m depth (see Figure 3.25). The influence of such seepage could have been assessed from the piezometric

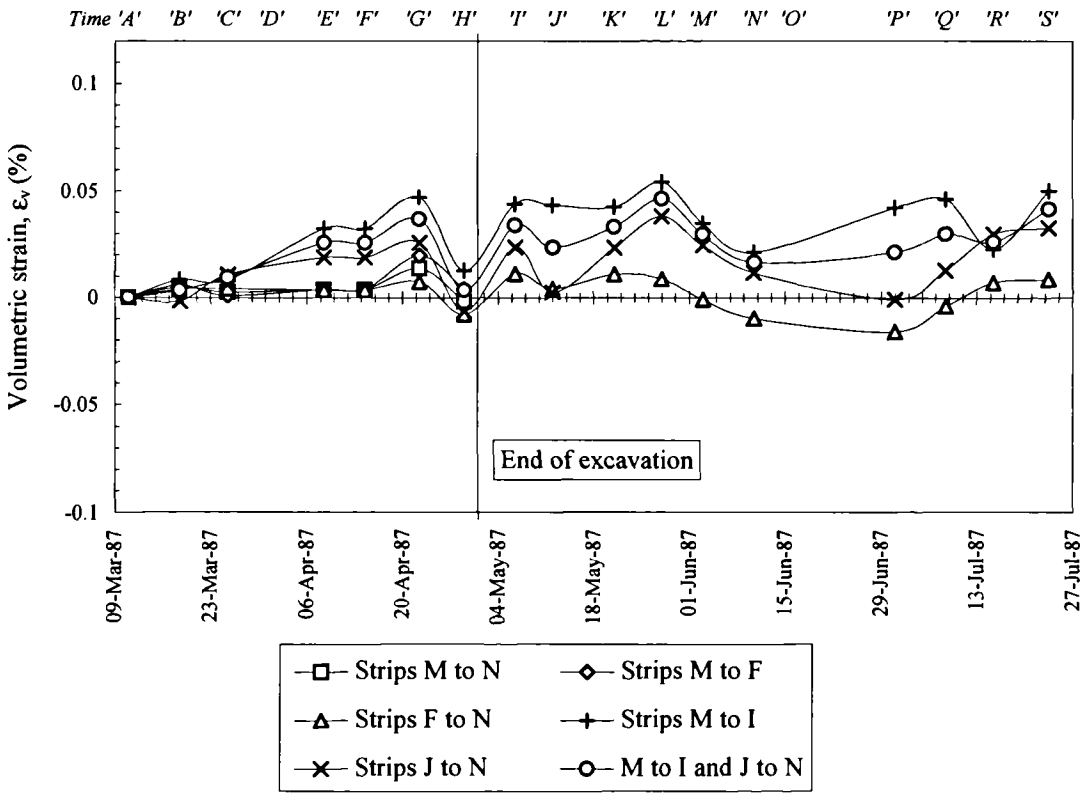

Figure 4.43 - Volumetric strain of combinations of strips of excavation elements

response in this region, but unfortunately, no piezometer data are available beyond the excavation crest.

Such conclusions are hard to verify without carrying out detailed measurements of the discontinuity system prior to and subsequent to excavation. One approach might be to record the fissure size in block samples obtained from across the site. This would obviously be a very labour intensive process and perhaps a flawed method due to the stress relief experienced during sampling. An attempt to provide a quantitative description of the macro structure of the Oxford Clay during excavation was attempted at Elstow (see section 4.2.4), although it was only partially successful due to the suspension of works. A more practical alternative might to be to compare *in situ* permeability measurements before and after excavation. If the permeability increased at the base of the excavation this would provide evidence for the opening of fissures as flow paths. Such measurements were planned during the Elstow excavation, but were not carried out due to the suspension of works.

An alternative explanation of the volume changes might be sought in the effect of a large scale feature within the Oxford Clay providing a drainage path or a shear surface. At the Saxon Pit (Burland *et al.*, 1977) the horizontal stress relief associated with the deep excavation resulted in a shear surface forming and propagating along the base of the pit. At the Saxon Pit (Burland *et al.*, 1977) it was found that "*contrary to assumptions made at the beginning of the investigation, there is no evidence to suggest that the presence of major joints or fissures other than bedding planes directly affect the pattern or magnitude of movement of the main clay mass*". At Elstow, no evidence of large scale faulting was found prior to excavation and the instrumentation response does not show any concentration of displacement to associate with a major shear surface.

There is relatively little work published on the volumetric ground response due to excavation. Cole and Burland (1972) describe limited ground surface and retaining wall profile measurements in a large excavation in London Clay for Britannic House using methods described in Burland and Moore (1972) and Cheney (1973). A more extensive layout of instrumentation was adopted for the construction of the House of Commons underground car park (Burland and Hancock, 1977). A major monitoring program was also carried out in Oxford Clay during the excavation of the 29m deep Saxon Pit (Burland *et al.*, 1977). However, in none of these cases were volume strains calculated.

Burland *et al.* (1979) summarised the response of London Clay due to excavation, concentrating on continuum behaviour of an intact mass of clay during the short term (constant volume response) and with time (following drainage and dissipation of excess pore water pressures). Such categorisation of behaviour could be expected to be less applicable to the more heavily over consolidated Oxford Clay, in which the greater degree of fissuring, and abundance of discontinuities generally, may have an increased influence.

5. Experimental methods and analysis techniques

5.1 Introduction

The experimental work performed as part of this research project was required to determine data to be used in a numerical model capable of predicting the ground movements and pore water pressure changes associated with the excavation at Elstow described in Chapter 4. For such analyses the *in situ* stress-strain response of the soil had to be determined from specimens tested in the laboratory. The particular aspects of the soil response it was thought necessary to capture were:

- the non-linearity in the stiffness response
- the structural and stress-induced anisotropy
- the effect of the *in situ* stress regime
- the effect of the recent and overall stress histories

These complicated and inter-related effects had to be ascertained from a limited supply of soil samples and the laboratory tests were so designed to maximise the information produced from each test. Although it was realised that this placed a greater importance on each individual specimen, the quality of specimens trimmed from block samples was high and so made this approach feasible. The sample preparation techniques are described, including the use of a band saw to very quickly obtain a high quality triaxial test specimen from a stiff, fissured material.

A method of testing the triaxial specimens was devised, which involved a multi-stage stress path technique and quantified the stress dependent non-linear and anisotropic nature of the stress-strain response of the Oxford Clay. The testing method is described, as is the computer controlled triaxial stress path equipment used to carry out the tests. The existing apparatus incorporated local strain measurement devices, and these were supplemented with the development of a bender element system to enable stiffness to be investigated over a wider range of strain.

5.2 Sampling procedures and storage

5.2.1 Elstow excavation block samples

During the site investigation at Elstow, as the trial excavation progressed a number of block samples were taken, as described in section 3.7.2. At the time of the suspension of works, only limited testing had been carried out on the block samples. However, an opportunity for future high quality testing was realised, and a number of the samples were transported to the University of Sheffield where they were stored unopened from August 1987 until the start of the experimental programme described here, in January 1992. A description of each block sample, showing the stratum it was retrieved from and its depth is given in Table 5.1.

Identification Number	Depth (m)	Description	Condition on opening
E/EX11 29.140 /BL	1.360	W.O.C.	Good
E/EX9 29.185 /BL	1.315	W.O.C.	Good
E/EX16 24.845 /BL	5.655	O.C.	Dried out
E/EX17 24.910 /BL	5.590	O.C.	Good
E/EX20 26.845 /BL	3.655	W.O.C./O.C.	Dried out
E/EX14 26.690 /BL	3.810	O.C.	Dried out
E/EX22 23.341 /BL	7.159	O.C.	Dried out
E/EX15 25.640 /BL	4.860	O.C.	Good
E/EX19 24.069 /BL	6.431	O.C.	Dried out
E/EX21 24.970 /BL	5.530	O.C.	Dried out

Table 5.1 - Block samples retrieved from the Elstow excavation (W.O.C - weathered Oxford Clay, O.C. - unweathered Oxford Clay)

When the block samples were opened, it was immediately clear which ones had been stored effectively, for several had dried significantly. This had lead to fissures opening, revealing extensive crystallisation. There was also evidence of biological growth on a number of the samples. As the protection was removed from a block sample, its surface was checked for splits and openings, although, only one of the dried out samples showed such clear damage. Once the soil was revealed, moisture content tests were performed on the block's outer layers for comparison with similar tests performed during sampling.

For 'perfect' sampling, it is hoped that the suctions developed following the removal of total stress can be maintained. If the suctions within the sample cannot be maintained, the fall in the mean effective stress may allow the sample to swell in the presence of free water and fissures within the specimen to open. Alternatively, for a heavily fissured soil such as Oxford Clay, cavitation may occur at the fissure surface, again allowing them to open. Such stress relief and opening of fissures would put a stress onto the protective material perhaps sufficiently high to break the seal, allowing further drying of the specimen. If the initial sealing methods were adequate, preventing the fissure opening, the sample would have a greater probability of remaining in good condition. The degree of block stress relief is clearly related to the depth from which the samples are taken. Costa Filho (1986) suggested that block samples could not be taken in London clay at depths below 6m without the disturbance due to stress relief being too great.

5.2.2 Kempston Pit block samples

It was realised that there were insufficient samples from the Elstow site of suitable quality for testing. Additionally, the few samples which still appeared to be in good condition had been stored for an extended period and this would always be an additional complicating factor in interpreting the stress-strain response of the soil. Consequently, it was decided to carry out a further block sampling operation to provide fresh samples of Oxford Clay. Enquiries were addressed to the London Brick Company which had several active pits in the area. The closest pit to the Elstow site was the Kempston Pit, situated 500m away. Although this was the closest available location for sampling, the average dip of the Oxford Clay (1°) would change the strata levels by approximately 7m over this distance. Pragmatically, it was nevertheless decided to take block samples at Kempston.

The block sampling operation took place on the current active face at the site, shown in Figure 5.1a, which was inclined at approximately 60° to the horizontal. It was acknowledged that the stress relief of such an element of soil would not be the same as that followed by an element at the base of an excavation. The excavation process required 1 week to travel along the face of the slope, and this was a similar length of exposure to that prior to sampling during the Elstow excavation. Initially, a berm was cut into the slope, approximately 1m from the base of the pit, to provide a working platform (Figure 5.1b). Using a spade and hand tools a cube of soil of side length 400mm was formed by cutting into the ledge (Figure 5.2). The single cube of soil was then separated into two, roughly equal parts using a trimming knife (Figure 5.3). A spade was eased under each section of the block in turn, and, with slight downward pressure to the handle, the block was separated from its base. Each section was transferred to a wooden base and then sealed with cling film. This sealing was only a temporary measure to prevent drying during transport to the University of Sheffield where a more permanent sealing was performed. During transport, the samples were supported on all sides by polystyrene blocks and cloth, to prevent damage. The permanent sealing applied at the laboratory consisted of additional layers of cling film before the samples were wrapped in a wax impregnated muslin gauze. Further coatings of wax were applied as required. Each block was carefully turned upside down and the base sealed in the same way. The smaller of the two blocks was reopened the following day to prepare a specimen for testing (see section 5.5.1). The block identification is given in Table 5.2.

Identification Number	Elevation (mAOD)	Description	Condition on opening
KEMP/BL/1	21.5	O.C.	Good
KEMP/BL/2	21.5	O.C.	Good

Table 5.2 - Block sample retrieved from Kempston pit (O.C. - unweathered Oxford Clay)

(a)

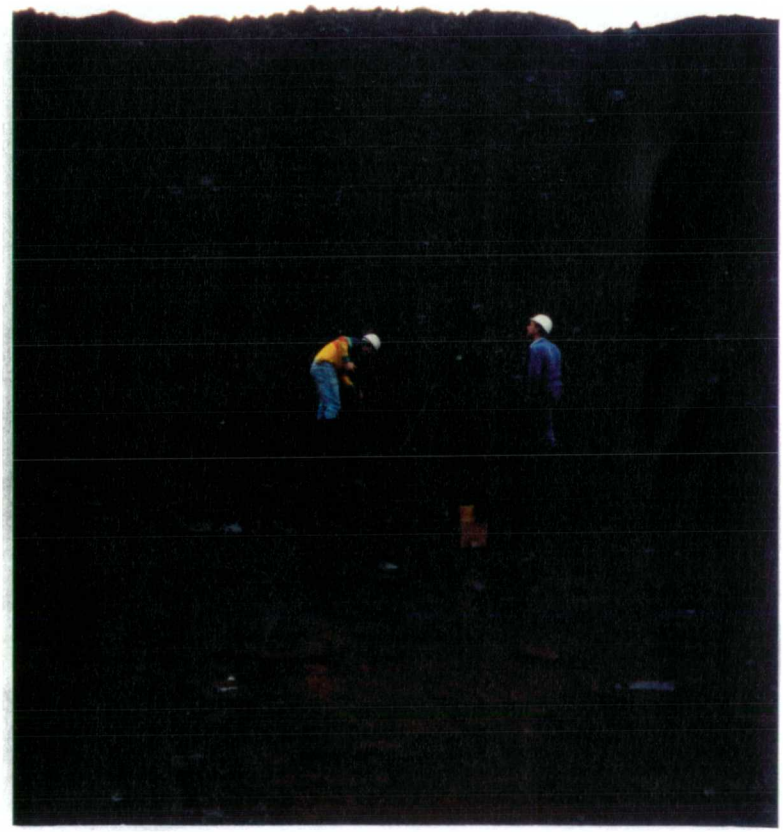

(b)

Figure 5.1 - The Kempston Pit slope at which the block sampling operation took place (a) from side elevation, and (b) in front elevation showing creation of ledge at base of slope to retrieve sample.

Figure 5.2 - Preparing slope and digging block sample clear of slope

Figure 5.3 - Splitting of block sample into two before sealing and transporting back to the laboratory

5.3 Testing methodology

5.3.1 Requirements of the testing programme

The experimental programme was required to quantify the stress-strain behaviour of the Oxford Clay to a degree which would justify a prediction of the ground response following excavation at the Elstow site.

The testing programme was developed to allow investigation of those factors which were thought to have the greatest influence on the stress-strain behaviour of the soil. From much published work on other overconsolidated clays (see section 2.4) and from the initial suite of tests carried out on the Oxford Clay at the time of the Elstow excavation (see later in section 6.2), it was clear that a non-linear stress-strain response could be expected. Its investigation would require the recording of small strains and, therefore, the use of high quality local instrumentation (see section 2.5.2). Another feature of the initial tests on the Oxford Clay was the structural anisotropy of the stiffness response (Hird *et al.*, 1987). The small strain Young's modulus from specimens trimmed horizontally from block samples was more than twice that recorded from vertically trimmed specimens. It was considered that such an anisotropic stress-strain response would have significant influence due to the nature of the stress-relief imposed by excavation.

A wide range of soil types, including overconsolidated clays, demonstrate a stress-path direction dependent stiffness characteristic (see section 2.4.2) which is a function of the overall stress history of the soil., This would clearly be of consequence for the excavation analysis considered here, since the stress paths experienced by elements of soil around the excavation would depend on their location. A further effect of stress-history is that of relatively recently imposed changes (see again section 2.4.2). The amount of reloading following stress relief due to overburden removal was assumed to be minimal for this site. However, there remained the possibility of changes in the stress path direction during excavation caused by the excavation sequence (discussed later in section 8.6).

As well as stress history, the current effective stress regime may influence the stress-strain behaviour (see sections 2.4.2 and 2.7). Assuming that a representative effective stress profile for the Elstow site could be determined, the variation with stress level, or depth, of the influencing factors described above, would be required.

In addition to the fundamental factors influencing the soil stress-strain behaviour, a number of practical requirements were also considered in the design of the testing programme. As described in section 5.2.1, the clay from the Elstow site had been stored for a number of years and, although the storage techniques were thorough, the samples were not initially intended to be kept for such a period. Quantifying the effect of storage on the clay specimen was therefore a requirement. The use of specimens trimmed from block samples obtained from the Kempston Pit partly addressed this problem, but also raised the issue of differences between the Elstow and Kempston Pit strata.

5.3.2 Testing strategy

An attempt was made to reinstate the *in situ* stresses on the specimen. The Oxford Clay strata at Elstow is very heavily overconsolidated due to the removal of an estimated 500m of overburden (see Figure 3.12, and section 3.3.2). The *in situ* horizontal stresses derived from field tests were thought unreasonably high (see Figure 3.11), as it was likely that the clay was at, or close to, the passive failure state for most of its extent. Reinstating the *in situ* stresses would therefore

involve bringing the soil to passive failure before attempting a test. Passive stress relief tests have been described by Burland and Fourie (1985), but these were not thought appropriate for the current work since it would not be possible to derive stiffnesses of the constitutive matrix as described below. Therefore, an initial stress state was chosen conservatively so that excessive strains were not imposed on the specimen during the reconsolidation process. The initial vertical stress was calculated from the bulk unit weight of the clay (see Figure 3.6) and an assumed ground water level (see Figure 4.35). The initial horizontal stress was calculated from the K_o' value consistent with a purely frictional passive failure angle (see Figure 3.11). In the absence of extension test data, the active and passive failure angles were assumed to be the same giving an average frictional angle of failure for unweathered Oxford Clay of approximately 26° (see Figure 3.5). When determining an initial stress state for a test, a passive frictional strength of $\phi' = 25°$ was chosen as a conservative estimate, although the specimen was monitored during application of these stresses to prevent excessive straining. The recent stress history of the specimen was approximated with a constant q stress path approaching the initial stress point by decreasing p' as shown in Figure 5.5. In early tests the initial stress state was first approached directly, with a constant p' stress path from an isotropic stress state, before increasing p' on a constant q path. The recent stress history path was then applied. In later tests, the recent stress history path was preceded by a constant p' stress path with q decreasing from an isotropic stress state in which p' was approximately 100kPa greater than in the initial stress state.

To describe the small strain stiffness non-linearity explicitly, it was decided to carry out stress paths from the initial stress state which would define the parameters of the compliance equation discussed in section 2.2, and presented again as equation 5.1

$$\begin{bmatrix} \delta\varepsilon_v \\ \delta\varepsilon_s \end{bmatrix} = \begin{bmatrix} \frac{1}{K'} & \frac{1}{J'_{qv}} \\ \frac{1}{J'_{ps}} & \frac{1}{3G'} \end{bmatrix} \cdot \begin{bmatrix} \delta p' \\ \delta q' \end{bmatrix} \quad \text{..... (5.1)}$$

The coupling between deviatoric and volumetric components of the specimen deformation requires that stiffness moduli be determined from stress paths along which either the deviatoric stress or the effective normal stress is held constant.

A series of constant p' and constant q stress paths from the initial stress state (p_i', q_i) were used to decouple the deviatoric and volumetric responses as shown in Figure 5.4. For a constant p' test,

$$J'_{qv} = \frac{\delta q}{\delta \varepsilon_v} \text{ and } G' = \frac{\delta q}{\delta \varepsilon_s} \quad \text{..... (5.2)}$$

so that J'_{qv} and G' can be obtained from plots of deviator stress versus volumetric strain and shear strain respectively. In a constant q test,

$$J'_{ps} = \frac{\delta p'}{\delta \varepsilon_s} \text{ and } K' = \frac{\delta p'}{\delta \varepsilon_v} \quad \text{..... (5.3)}$$

so that J'_{ps} and K' may be independently determined.

Similar testing strategies were employed by Yudhbir and Khan (1980), and Atkinson *et al.* (1989).

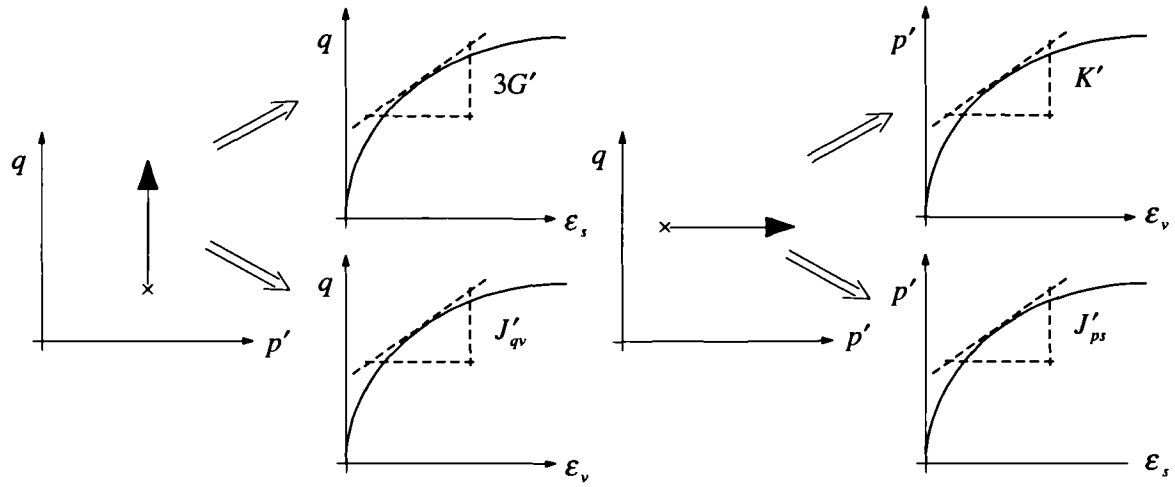

Figure 5.4 - Determination of stiffness moduli from triaxial stress path tests

To take account of the influence of stress path direction, each stiffness parameter was required for both increasing and decreasing stress levels. The 4 stress path probes required to fully define the stiffness characteristics in triaxial stress space are shown in Figure 5.5.

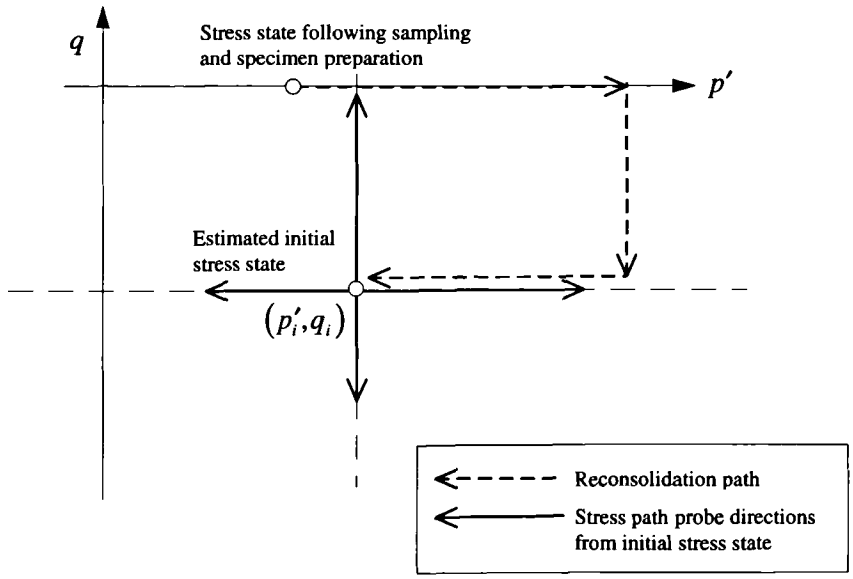

Figure 5.5 - Reconsolidation path and subsequent stress path probes designed to obtain the specimen's *in situ* stiffness characteristics

It became clear, early on in the testing programme, that there would be a very limited supply of Oxford Clay block samples from which suitable triaxial specimens could be obtained (see section 5.2.1). It was decided, therefore, to attempt to maximise the information which could be obtained from each specimen by carrying out a series of cyclic loading paths such that all 4 required stress path probes could be performed on the same specimen. However, due to time restrictions and a limited number of specimens, the constant q stress path with decreasing p' was not investigated from the estimated initial stress state. After one of the stress path probes was performed, the specimen was returned to the initial stress state by reversing the loading direction, and retracing the approach path as shown in Figure 5.6. In this figure, a stress probe

has been carried out from the initial stress state, O, along path OB. The specimen is then returned to the initial stress state through stress paths BO-OA-AO, allowing a second stress probe, OC, say, to be followed.

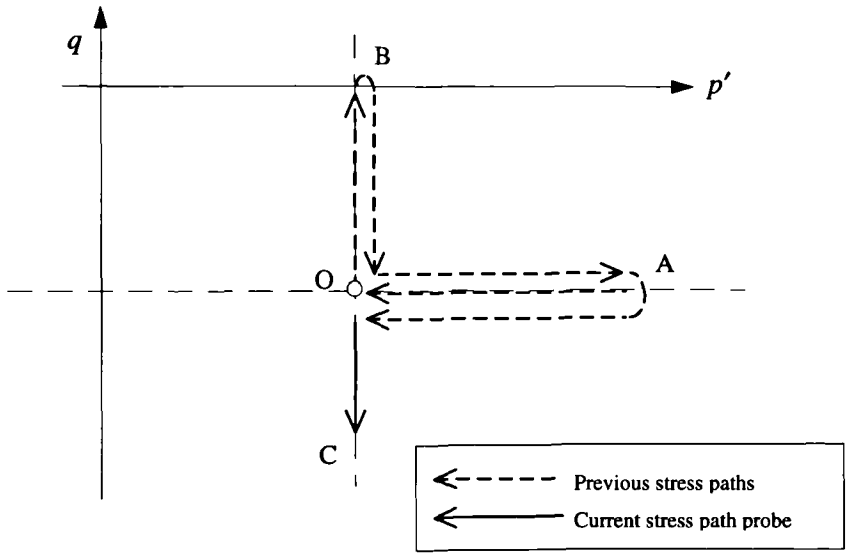

Figure 5.6 - Cyclic stress path loading used in multi-stage tests

Although in principle, such cycling of stress paths could be continued indefinitely, providing a complete description of the stiffness response with a degree of redundancy, there are a number of drawbacks to the approach:

- Potentially, the most significant drawback, is that the cycling of stress paths disturbs the structure of the clay to such an extent that the resultant stiffness response is not representative of the true behaviour. Such degradation of the specimen may be detected by incorporating repeat paths within the same test. If any consistent reduction in stiffness between such paths is evident, the technique would clearly be unsuitable. Although it may be expected that such stress paths would inevitably cause significant mechanical disturbance to the specimen, the stress changes involved may be less than those the soil would have been subjected to during sampling.
- For the tests described here, the initial stress state of the specimens was close to passive failure. Consequently, stress path probes bringing the specimen closer to this line would, inevitably, cause rapid strain development before failure. Such paths were selected to be the final stress path followed, bringing the specimen to failure. Only the previous stress paths, in the quarter of q-p' space furthest from passive failure, were repeated.
- For clay specimens, the rate of loading along both constant p' and constant q stress paths must be very small to prevent pore water pressure development (see later in section 6.4.7). Such multi-stage tests, therefore, take a long time and, although providing much information from a single test, require great confidence in the quality of specimen. In the present case, it was not possible to test a larger number of specimens, although the specimens available were thought to be of high quality, justifying the extended testing periods.

As a working hypothesis, it was assumed that the soil response to a stress probe in any direction from an initial stress state, (p_i', q), could be simulated by using the stiffness parameters obtained along the bordering constant p' and constant q stress path directions. In order to verify this hypothesis, a diagonal stress path in p'-q space was incorporated into the testing

strategy. The sequence of stress paths chosen is shown figuratively in Figure 5.7. In this figure, the final path (to failure) is a constant p' path (although this final path could also be a constant q path no such paths were carried out). Numerous multi-stage configurations were considered, but the chosen configuration provided a balance of repeated stress paths, a diagonal path, and the required stress probes. As discussed later, in sections 7.5.3 and 8.8, although the Elstow excavation would generally be considered a monotonic unloading problem, the construction produced reversals in the loading direction beneath the excavation's sloping sides as excavation progressed. These recent stress history effects were incorporated into the multi-stage test through the 180° and 90° changes in the stress path direction. Although the recent stress history effect has been investigated experimentally for reconstituted soils (see section 2.4.2), less is known about its influence on natural soils. The testing programme allowed the effect of the most recent stress history to be quantified for Oxford Clay.

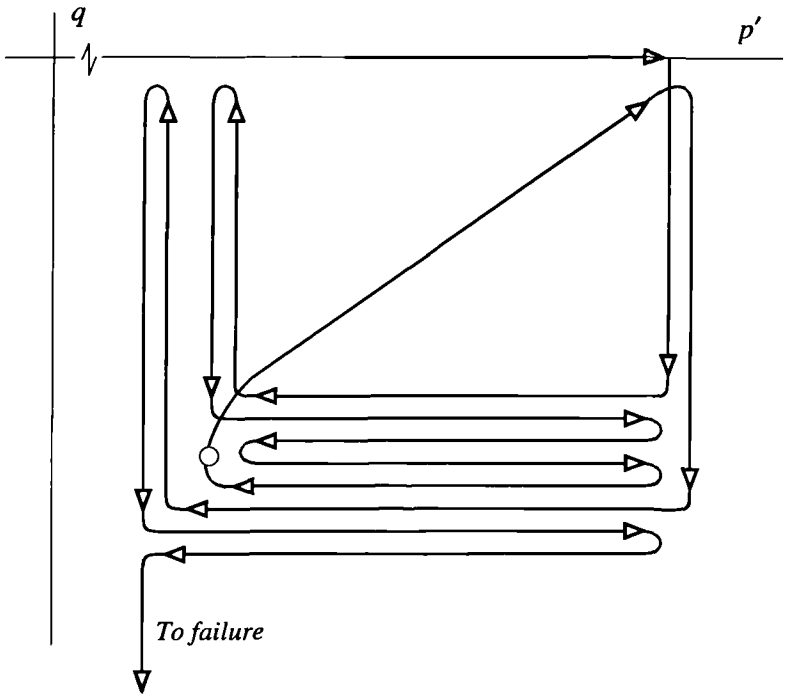

Figure 5.7 - Stress path testing using the multi-stage technique

It was unfortunate that this work could not be conducted immediately following the Elstow site investigation, assuring the quality of the block samples. The small number of block samples, and the effect of the extended storage time, required additional specimens to be tested from the nearby Kempston Pit. Identical multi-stage stress path tests were carried out on specimens trimmed from block samples obtained at each site to highlight any differences in the stress-strain response of the two materials.

The variation of the stiffness parameters around the Elstow excavation, and with depth, required the influence of stress level on the stress-strain response to be evaluated. This was incorporated into the testing programme by carrying out identical multi-state stress path tests at different values of effective mean normal stress. For the anisotropic stress state at the Elstow site, the influence of p' and q would, ideally, be considered separately. This would require repeated tests in which either p' or q of the initial stress state would be varied while keeping the other constant. It was thought, however, that it was more important to retain the initial anisotropic stress state close to the passive failure line and determine the influence of confining stress by carrying out multi-stage tests at different initial p', rather than to vary the initial deviatoric load. The dependence of the very small strain shear modulus on the current stress

level was also quantified during each multi-stage test through performing bender element tests (see section 5.7) along each stress path.

5.3.3 Time dependent aspects of testing

The triaxial test loading rates determined from the traditional Bishop and Henkel (1962) approach based on estimated times to failure are not applicable to the stress path tests considered here. A comprehensive study of the loading rates in stress path tests was carried out by Cherrill (1990), and these techniques were used to provide an estimate of the required testing rate. The calculation of loading rates is related to the coefficient of consolidation and a typical calculation is included later in section 6.4.7. Additionally, the stress path apparatus incorporated a miniature pressure transducer, which recorded the pore water pressure at the mid-height of the specimen, and this was used directly to assess the rate at which a stress path could be carried out and still be considered drained. A nominal loading rate of 1kPa/hour for axial stress was chosen following Cherrill (1990). However, although this was the slowest practical loading rate due to the limited time available, it was found that stress paths carried out at this rate still led to development of excess pore water pressures (see again section 6.4.7).

A second aspect of time dependent effects is the influence of the residual strain rate within a specimen at the end of a (total) stress path caused either by dissipation of generated excess pore pressure or by soil creep. The residual strain rate must be low enough for its effect on the subsequent stress path response to be negligible. It was found during the testing programme that the influence of the holding period between stress paths had a significant influence on the subsequent stress-strain behaviour. Other researchers have dealt with this by keeping the holding period constant (Richardson, 1984; Stallebrass, 1990a; Jardine , 1992) and assuming that the effect is similar for each stress path. This is not strictly true if the residual straining is directional and the stress path direction is varying, as in the current scheme. Then its effect must be essentially removed rather than assumed constant. Initially, a standard holding period of 24 hours was allowed between stages, but this was found to be unsuitable for the low testing rates involved and it was realised that up to 72 hours was required. The influence of the holding period is discussed later in section 6.4.7.

5.4 Stress path testing apparatus

5.4.1 Introduction

The experimental investigation of the stress-strain response of the Oxford Clay was carried out using computer controlled triaxial stress path testing apparatus. The testing equipment consisted of two, almost identical, Bishop and Wesley (1975) type stress path cells for testing 100mm diameter specimens.

One cell, Cell 1, was developed by Hajj (1990), and another, Cell 2, was commissioned during the current work. The Cell 2 apparatus is shown in Figure 5.8.

The pressure supply to the apparatus was provided by a 1MPa capacity air compressor through which a steady 700kPa could be supplied through an air pressure regulator. The pressure supply to the cell was controlled through a system of electrical stepper motors which could be controlled manually or, more usually, automated through computer control. The cells were fitted with standard instrumentation, consisting of a load cell and pressure and displacement transducers. This equipment was supplemented with high resolution local instrumentation to measure strains directly on the specimen so that they were free of the bedding, seating and compliance effects recorded by the externally mounted displacement transducers (see section 2.5.2). Additionally, bender element equipment, for transmitting and receiving seismic waves, was installed in each apparatus.

Figure 5.8 - Stress path cell, Cell 2, during a test

The system was continually maintained during the experimental programme to ensure the accuracy of both measurement and control. The triaxial instrumentation was calibrated between stress path tests to determine if there was any drift of the electrical characteristic. The long term and short term stability of the transducer's output was similarly checked. It was generally found that the conventional instrumentation behaved well; any changes in the calibrations were slight and the electrical stability was good. Greater care was required with the proximity transducer system, however, and the procedures employed are described in section 5.4.7.

The following sections describe the instrumentation and the calibration procedures. Further details are provided by Hajj (1990).

5.4.2 Electrical equipment for transducer monitoring

All logging and control of the stress path equipment was carried out using IBM compatible personal computers; each cell required a dedicated computer.

The apparatus featured both AC and DC transducers, and digitally controlled stepper motors. This required a range of interfaces to the computer.

The working resolution of the transducers was determined by the precision with which the interface equipment could convert the, otherwise infinite, analogue resolution of the transducers into digital form. For example, for both cells 1 and 2, the pressure transducers were connected to an Analogue Input Unit (AIU) manufactured by MC-Computers, Berkshire, England (type 2014). Internally, these devices are 8-bit but, through on-board averaging over several frequency cycles, a 12-bit conversion is obtained such that over the ±5V range, the 2^{12} divisions produce a minimum step of 2.5mV. With this system, a 700kPa range pressure transducer, at a suitable gain, could be read to a resolution of 0.17kPa.

The proximity transducers were driven by AC and, consequently, required a separate analogue to digital conversion interface. For Cell 1, a System 16 unit, manufactured by Sangamo, West Sussex, England, was used, which provided a 12-bit conversion without averaging. To achieve a higher resolution for the proximity transducers on Cell 2, a 14-bit D100 unit, manufactured by Sangamo, was used.

The stepper motor control required a digital signal to produce a step in the required direction (increasing pressure or decreasing pressure). The stepper motors were controlled on both Cell 1 and Cell 2 by DADIO digital output cards, manufactured by Brainbox, connected directly to the computer.

5.4.3 General calibration procedures

The details of the calibration procedure varied with the particular transducer type, although a similar general framework was employed in each case. The existing computer programs for the calibration process were found to be inadequate and these were subsequently re-written.

Prior to calibration, the system was switched on for a sufficient period to ensure all transducers and controllers had warmed up sufficiently. This generally involved monitoring the transducer response for a number of hours.

Immediately prior to calibration, the transducer input voltage was set to the required level (generally 5V or 10V) using a digital voltmeter calibrated against a fixed supply. The ambient room temperature was also recorded. These readings were re-taken following calibration, and the calibration repeated if the change was possibly significant.

Generally three complete cycles of pressure, displacement, load, or volume were performed and the response was analysed immediately to determine a suitable calibration equation and to ensure the transducer was both sufficiently precise and accurate. If the data were unsatisfactory, the calibration was repeated and, if there was no improvement, the transducer was replaced.

Specific calibration details are included in the following sections, and a summary of the calibration accuracy and resolution of each transducer is given in Table 5.3. The calibration accuracy was calculated statistically as the standard error of the calibration data from appropriate fitting equation.

				Cell 1 / Cell 2	
Name	Parameter	Make	Range	Standard error of calibration	Resolution
Pressure transducer	Cell pressure	Druck / Bell & Howell	0 to 700 kPa	0.15-0.45 kPa	0.17 kPa
"	Lower chamber pressure	"	0 to 700 kPa	"	"
"	u_w (specimen top)	"	0 to 700 kPa	"	"
"	u_w (specimen bottom)	"	0 to 700 kPa	"	"
Miniature pressure transducer	u_w (specimen mid-height)	Druck	0 to 700 kPa	0.22 kPa	0.17 kPa
Volume change unit	Specimen volume change	Imperial College	100 cm^3	0.175 cm^3	0.024 cm^3
Load cell	Deviator stress, q	Imperial College	-2200 N to 2200 N		1.1 N
			-280kPa to 280kPa [1]		0.14 kPa
			0 to 280 kPa	0.36-1.03 kPa	"
			0 to -280 kPa	0.45-3.1 kPa	"
LVDT	External axial strain	Schlumberger / MPE	50-52 mm	28-60 µm	12.2 µm

				Cell 1		Cell 2	
				Standard error of calibration	Resolution	Standard error of calibration	Resolution
Submersible LVDT	Endcap axial strain	Schlumberger	10-11 mm	1-1.5 µm	2.44 µm	1.4-2.6 µm	0.64 µm
Proximity transducer	Local axial/radial strain	Sangamo	1-2 mm	0.3-0.9 µm	0.1-1.0 µm		
		RDP	2.5 mm			0.8-1.3 µm	0.05-0.4 µm

[1] Equivalent load cell stresses calculated for a 100mm diameter specimen

Table 5.3 - Summary of transducer calibration data

5.4.4 Pressure transducers

Conventional pressure transducers were used to independently record the cell pressure, the lower chamber pressure, the pore pressure at the top of the specimen, and the pore pressure at the bottom of the specimen. The transducers were manufactured by either Druck or Bell & Howell, although both had similar specifications.

The conventional pressure transducers were calibrated using a Budenburg dead weight tester (model 19041/380) with an oil interface. The cell pressure and back pressure transducers would have a water interface in the stress path apparatus, but it was assumed that the calibration characteristic would be the same. The calibrations were performed in three cycles from atmospheric pressure to 700kPa and back, in 50kPa increments.

The pore water pressure at the mid-height of the specimen was measured following Hight (1982), using a Druck, type PCDR81, miniature pressure transducer. It was essential that the porous element at the tip of the miniature pressure transducer was initially de-aired to ensure a suitably linear calibration. This was carried out by placing the transducer in de-aired water, under a vacuum, for several hours, followed by applying the maximum calibration pressure within the calibration apparatus and ensuring a steady response before proceeding.

The miniature pore pressure transducer was calibrated with the Budenburg dead weight tester but the porous element necessitated using a nitrogen supply instead of the oil interface used for the remaining pressure transducers. The calibration device provided slightly less control although produced calibrations of a similar standard to the other transducers.

A typical pressure transducer calibration is shown in Figure 5.9, which also shows how the

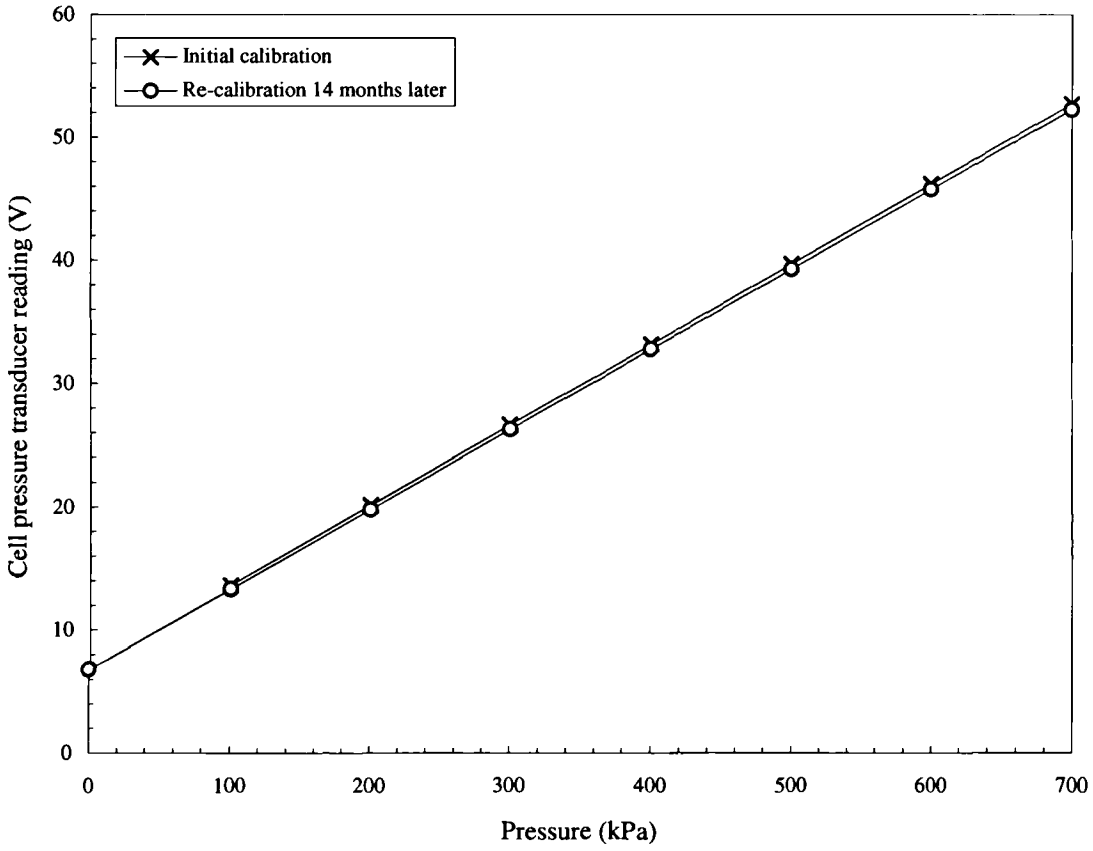

Figure 5.9 - Typical pressure transducer calibration showing change in transducer characteristic with time

response of this particular transducer changed from the initial calibration to a subsequent re-calibration carried out 14 months later (additional calibrations were carried out during this time). The change in the calibration shown here was the worst encountered during the experimental programme, although still slight. The gradient of the best fit straight line remained unchanged, while the position of the line was slightly offset.

5.4.5 Load cell

Both cells were fitted with internal Imperial College type load cells allowing the deviator load to be recorded directly above the specimen (El-Ruwayih, 1975; Hight, 1983). The design, consisting of three strain gauged arms within an oil filled container sealed with a thin membrane, allows for slightly eccentric loading and self-compensates for pressure changes within the cell.

The Imperial College type load cells have been criticised for both their high compliance under load and their non-linear characteristic when moving from compression to tension (Stallebrass, 1990a). The more robust Surrey University type load cells are less compliant and give a continuous linear response between tension and compression, but they are not as sensitive as the Imperial College type. The compliance effects were not a serious issue in the current work, since strains were measured locally on the specimen. Also, the discontinuous response between tension and compression was not an issue here, since all stress paths were intended to be carried out within the extension zone (see section 5.3.2).

As the testing was carried out with negative deviator stress on the specimen a tension connection between the specimen top cap and the load cell was required. This was provided by

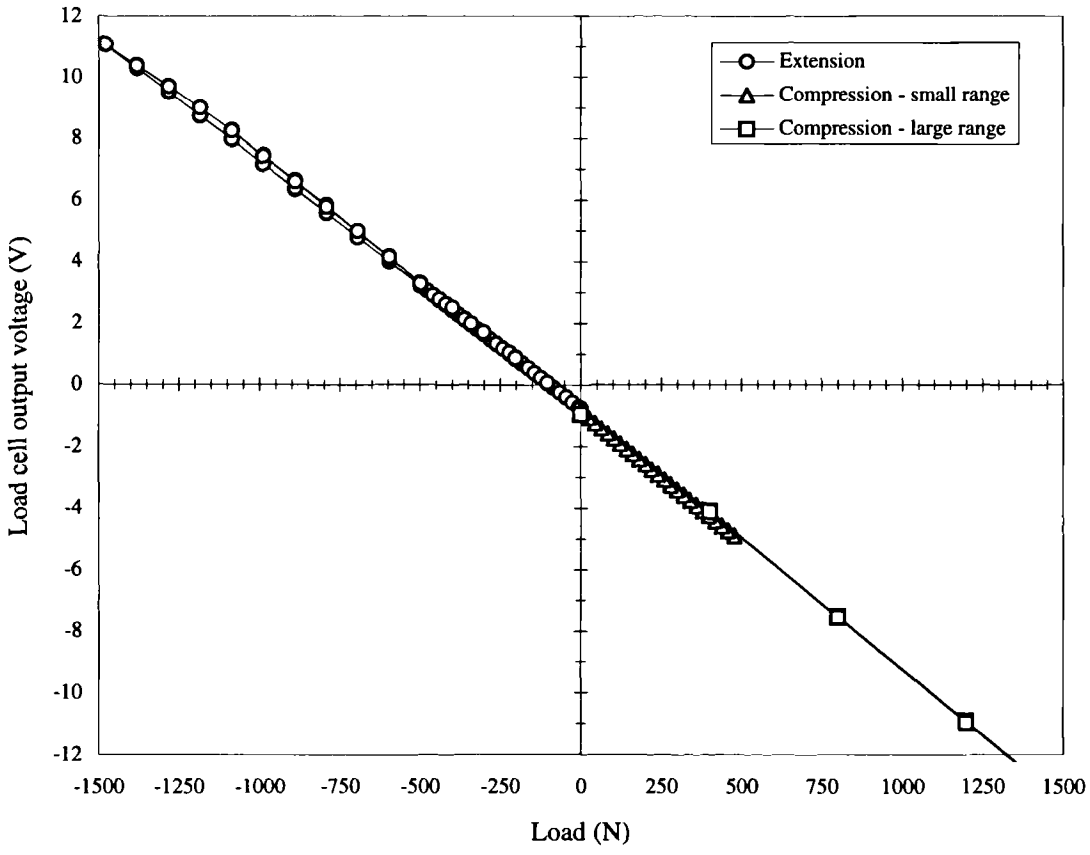

Figure 5.10 - Typical load cell calibration showing the characteristic response in tension and compression

a vacuum connection described by Hajj (1990). The type of vacuum connection used here has been reported to cause difficulties both during connection, and during testing, particularly through slippage of the endcap (Atkinson and Evans, 1985). An alternative, simpler design was proposed by Ng (1992) to alleviate these difficulties.

The Budenburg dead weight system was only capable of calibrating the load cell in compression, and in tension a less satisfactory method, in which dead weights were applied to a plate attached directly to the load cell by a steel bar, had to be adopted. The errors inherent in this procedure were minimised by individually weighing each of the dead weights using a digital balance, and by averaging many successive readings. The more accurate calibration in compression was also carried out as a check on the extension calibration, and as a backup in case of the failure of the tension connection at the top cap during testing.

It was found that there was generally more hysteresis in extension than in compression and that, in extension, the first half of the calibration cycle (with load increasing), was more linear than the second half (with load decreasing). Typical calibration curves for compression and extension are shown in Figure 5.10.

No attempt was made to correct the external axial strain measurements, made with an LVDT, for the effect of load cell compression, since the local measurement devices were relied on for such measurements and the degree of correction applied to external measurements is found to be relatively significant compared to the accuracy of the measurements (Jardine *et al.*, 1985).

5.4.6 Volume change units

A volume change unit of the Imperial College design was fitted to the back pressure lines of each triaxial cell. During stress path applications, the volumetric strain was calculated from the local strain transducers since both axial and radial measurements were available. The volume change units were not, therefore, essential but provided a back up set of measurements should the local measurements fail. The uniformity of specimen straining could be evaluated by comparing the externally measured volume change with that calculated from the local measurements. Since the local measurements were of relatively high resolution, it was necessary to calibrate the volume change unit as accurately as possible. Hajj (1990) adopted the method of Goodwin (1991) which employed the use of two GDS pressure/volume controllers for automatic calibration. The accuracy attained with this technique was not thought sufficient and a manual technique was used instead. The volume change units were calibrated separately for the cases of water either entering the top and leaving the bottom, or entering the bottom and leaving the top. Fixed volumes of approximately $10cm^3$ were prepared in a narrow tube burette, connected to the previously saturated back pressure system, and allowed to enter the volume change unit against a fixed back pressure of 400kPa. This was repeated for three cycles of volume change and then whole calibration was repeated to ensure the validity of the technique. Sivakumar (1993) found that the calibration of the volume change units depended on the back pressure applied but, since a fixed back pressure was to be maintained in the current work, calibration was only carried out for a single pressure. A typical calibration is shown in Figure 5.11. Since the device was required to measure changes in volume, rather than absolute volumes, it was only necessary to ensure that the gradient of the fitted linear calibration equation did not change with time. Changes in the offset did not affect the results. The calibration used was selected during a test, depending on whether water was entering the top or the bottom of the unit.

The volume change unit was dismantled and cleaned on a regular basis to check for the presence of algae which could affect its calibration. Prior to the initial test, after the system had been standing for several months, growth of algae was evident. However, during subsequent cleaning procedures, no further algae were visible

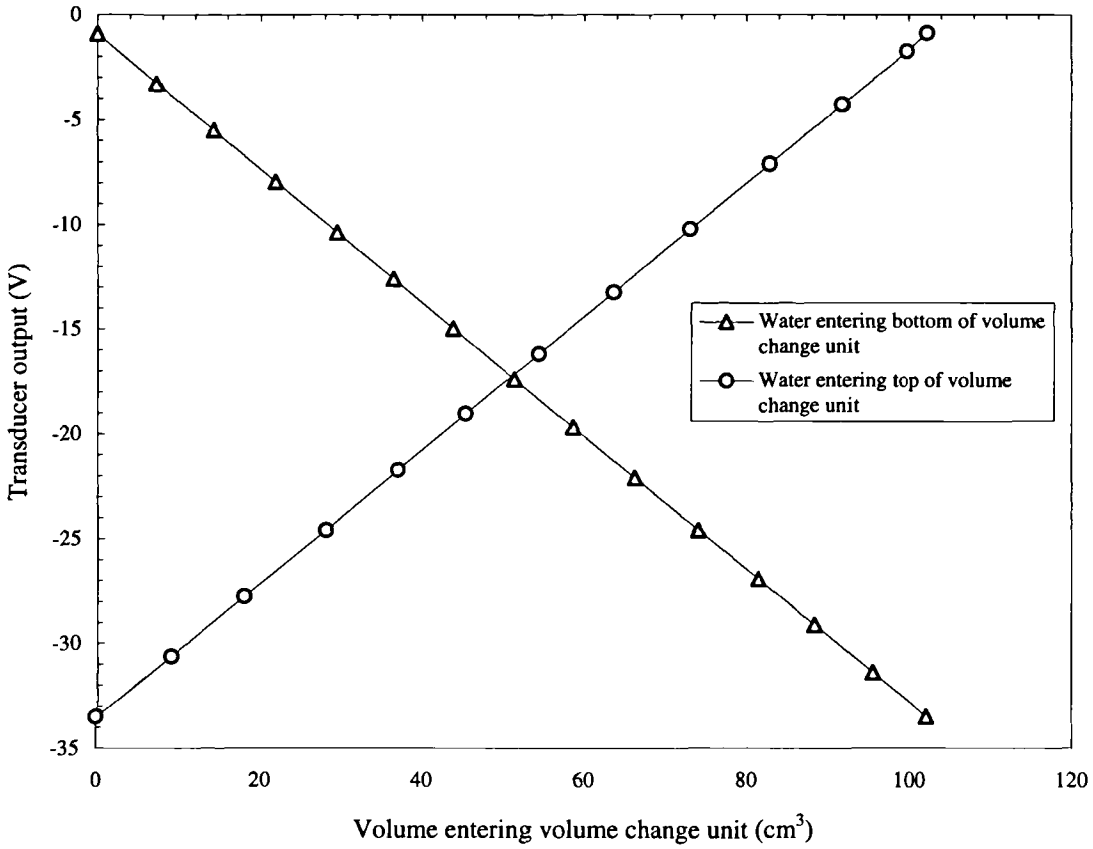

Figure 5.11 - Typical calibration response for a volume change unit for water entering either the top or the bottom of the unit

5.4.7 Displacement transducers

The strains incurred by the soil specimen during testing were recorded by three different types of displacement transducer, as described by Hajj (1990).

The movement of the loading piston of the stress path cell was recorded by two linear variable differential transducers (LVDTs) placed diametrically opposite each other on cross arms attached to the lower part of the piston. The axial strain calculated from these transducers was termed the 'external axial strain' and was affected by compliance errors and by bedding errors deriving from the specimen end caps as discussed in section 2.5.2.

The relative movement of the specimen end caps was recorded by two submersible LVDTs placed diametrically opposite each other on a mounting frame secured to the base pedestal as shown in Figure 5.8. The relative movement of the specimen top cap was recorded as the movement of the submersible LVDT's armature which acted on a stainless steel plate attached to the specimen end cap. Such strain measurements were termed 'end cap axial strain' and although effectively eliminating compliance and seating errors due to the lower piston, were still potentially affected by bedding, seating, and compliance errors caused by the specimen end caps.

The submersible LVDTs, being AC transducers, could not be interfaced using the AIU as with the other conventional instrumentation. On Cell 2, therefore, the submersible LVDTs were connected to the D100 device. However, on Cell 1, the gain settings on the System 16 were not flexible enough to accommodate both these transducers and the proximity transducers and consequently were connected to the AIU via a Sangamo, type OD3, signal conditioning unit. Consequently, the endcap strain measurements were at a greater resolution in Cell 2 than in Cell 1, although the transducers themselves were identical. The 10mm range of the transducer could be resolved to 2.44μm (although through averaging to 0.98μm) with the 2^{12} bit conversion of Cell 1, and to 0.61μm with the 2^{14} bit conversion of Cell 2.

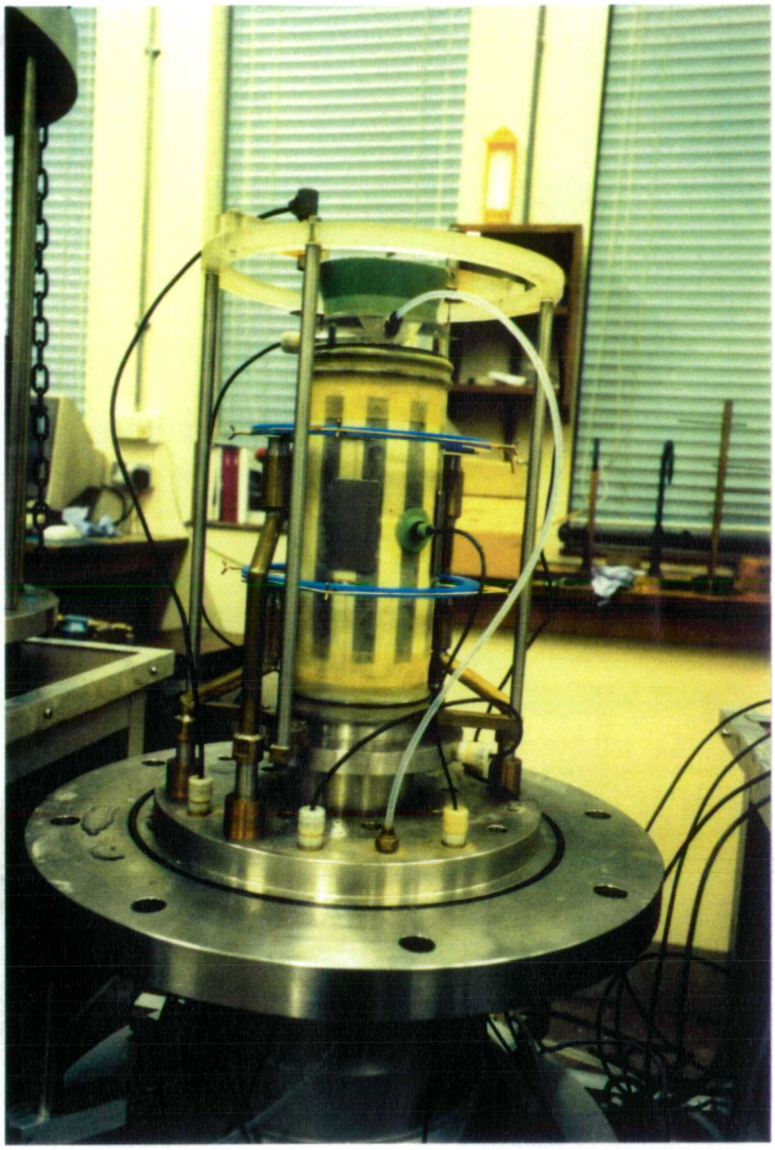

Figure 5.12 - Mounting the axial and radial proximity transducers in the stress path cells

To eliminate all errors due to compliance, bedding, and seating, the specimen strains were measured locally on the specimen. The apparatus, developed by Hajj (1990), consisted of eight proximity transducers (described in section 2.5.2), four for axial strain measurements and four for radial strain measurements, which were mounted as shown in Figure 5.12.

The proximity transducers used in cell 1 were cylindrical, manufactured by Sangamo, type SMP, and measured 10mm in length and 5mm diameter. They were individually mounted in a stainless steel housing which was subsequently threaded into a stainless steel tube which was in turn threaded and passed to the outside of the cell through an outer brass tube which was fixed to the cell wall or base. The threaded inner tube could be manoeuvred relative to the outer brass tube by a nut positioned outside the cell. This enabled the distance between the proximity transducer and its target to be adjusted from outside of the cell and effectively eliminated the drawback to using these proximity transducers for local strain measurements, which was their limited range (in this case) of only 2-5mm. The adjustable mounting mechanism for the proximity transducers can also be seen in Figure 5.12.

The original design of cell 1 incorporated this type of proximity transducer in preference to the more robust transducers used by Yung (1987) because of their smaller size and weight, greater

sensitivity, and much reduced cost (Hajj, 1990). However, they were not designed to be submerged in water and some form of protection was required. Hajj used two medical fingercots, each sealed with an o-ring and silicon sealant. Although this apparently proved effective, the current work revealed deficiencies in the seal which allowed ingress of moisture over an extended time period producing corrosion and permanent drifting of the transducer output. This necessitated the replacement of the original batch of transducers used by Hajj. The design was subsequently modified by replacing the medical fingercots with a more substantial 1mm thick membrane of a liquid rubber compound. The two-part compound was mixed thoroughly and allowed to partially cure for 1 hour under a vacuum to remove air bubbles from the mix. The mix was then placed in a specially designed mould and displaced by a plug having the same dimensions as the proximity transducer mounting. After 24 hours a flexible and waterproof cap was produced. This was sealed over the proximity transducer mounting with silicon sealant and two 0-rings. The thicker rubber cover did not affect the sensitivity of the instrument, since it did not alter the magnetic field generated around the metallic target. The cover did, however, reduce the working range of the proximity transducer to approximately 1mm.

The very limited range of the proximity transducers on cell 1 (1-2mm) necessitated regular adjustments to ensure they remained in their most sensitive working range. This, together with the wish for a more robust solution, led to the cell 2 design using larger RDP type transducers. These had a larger working range of 4-5mm and were suitable for submerged use. The mounting of the larger transducers was similar to that used in cell 1.

The externally mounted LVDTs had a range of 50mm and their linear calibrations were derived using a digital micrometer with a resolution of 1μm and a quoted accuracy over its 100mm range of 3μm. The internally mounted submersible LVDTs had a more limited range of 10mm and their linear calibrations were derived using a mechanical micrometer with a resolution of 0.5μm and a quoted accuracy over its 25mm range of 1μm.

It is standard practice to fit linear calibrations to the response of LVDTs. However, it was found that a degree of non-linearity occurred in their response. For example, Figure 5.13(a), shows a typical response of an externally mounted LVDT. Although the response is visually linear, Figure 5.13(b), showing the difference of each calibration data point from its associated best fit linear regression curve, reveals the degree of non-linearity. Since the non-linearity was found to be repeatable, it could be accounted for in the calibration by incorporating additional degrees of freedom into the regression, higher order polynomials being used. Although, the nature of polynomial regression (discussed below) is such that a numerically better fit will be calculated when a higher order polynomial is used, the polynomial must reflect the physical reality of the response. To find the most suitable curve, a least squares regression was carried out several times for each transducer calibration, each time increasing the degree of the polynomial by one. For each fitting curve the error residual was plotted as in Figure 5.13(c) and when the fit was adequate, the current polynomial was used as the fitting curve. The first order (linear) regression was always carried out, additionally, as this provided a direct comparison of the change in the transducer characteristics between subsequent re-calibrations.

It must be noted that this technique of higher order linear regression may only be used if the non-linearity of the transducer response is repeatable. If the residual error plot of the linear regression does not reveal definite trends then, although the standard error will reduce with increased order polynomials, the curve will simply be oscillating through the scattered calibration data and will bear no physical relation to the transducer characteristic.

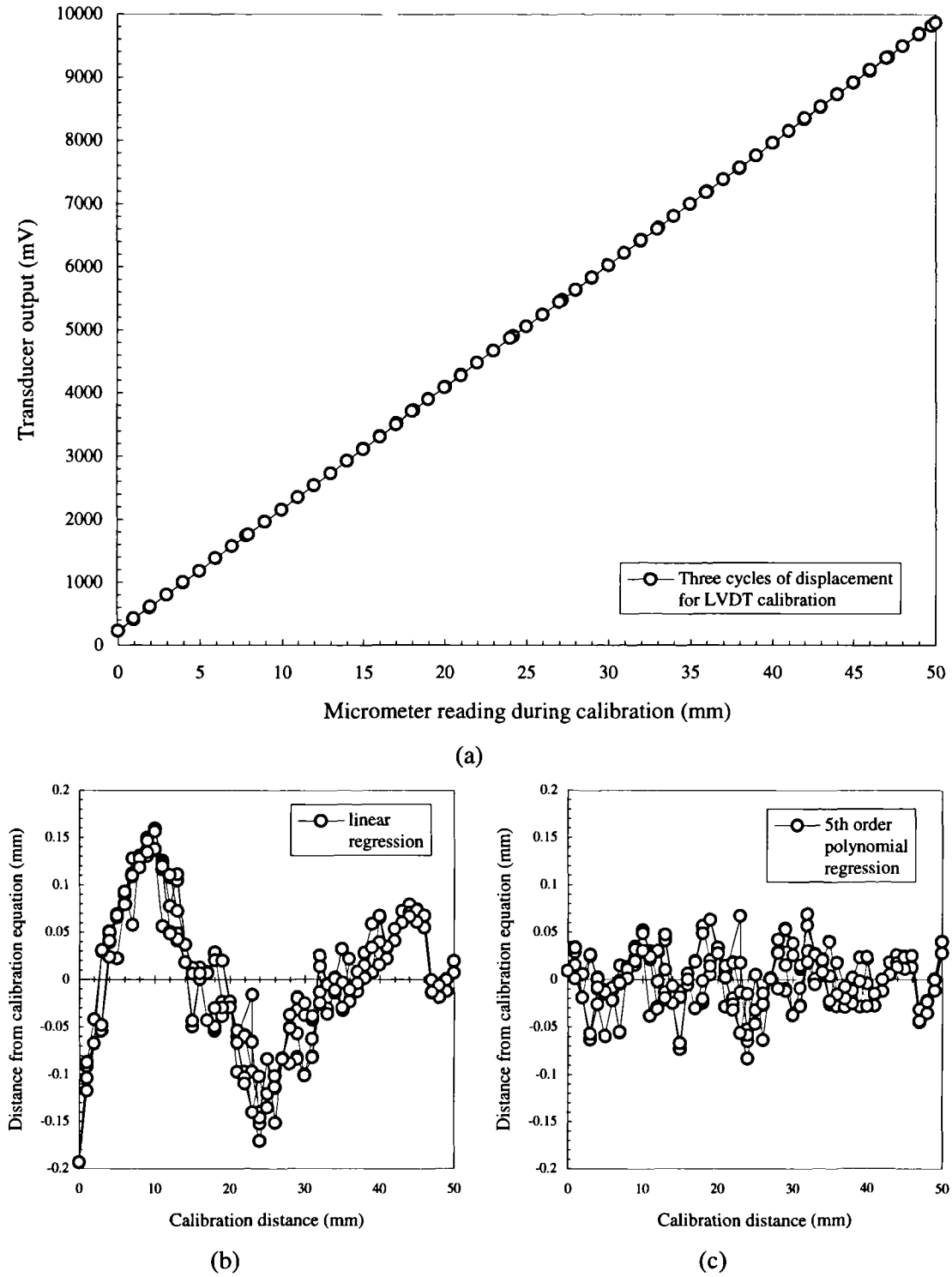

Figure 5.13 - The difference between regression curve fit and three cycles of (a) typical LVDT calibration data using (b) straight line and (c) polynomial fits.

In calibrating the submersible LVDTs, with the more accurate micrometer, the same general procedure was adopted as for the externally mounted LVDTs. However, at the end of each cycle of displacement, the armature was rotated through 60° within the transducer's barrel while keeping the transducer's output voltage constant. This ensured that the calibration was not affected by the orientation of the armature with respect to the barrel as this could not be readily controlled during setting up of the instrument in the triaxial cell. Additionally, Hajj (1990) showed that the co-linearity of the armature and the transducer barrel did not produce significant changes in the calibration characteristic. Following calibration, regression was

carried out as described above, steadily increasing the number of degrees of freedom until the non-linearity in the response was modelled sufficiently as well.

The calibration of the proximity transducers was more complex than for the LVDTs, since their output was markedly non-linear. Yung (1987) and Hajj (1990) both used slip gauges to provide known changes in distance for the calibration, but they found that the reputed accuracy of 0.2μm was difficult to achieve when multiple slip gauges were used. It was decided that the benefits gained from using the 0.5μm micrometer in terms of ease of use far outweighed any notional drop in accuracy. Additionally, it seemed reasonable to assume that the micrometer would have an enhanced accuracy when used over a relatively small section of its range. An alternative calibrating source would have been the Universal Horizontal Metroscope with which readings can be resolved to 0.1μm (Dasari *et al.*, 1995), although this device was unavailable at the time.

The micrometer was mounted in a specially designed rig to securely hold the proximity transducer in position. The magnetic stainless steel target was mounted on a pad of perspex 10mm thick to prevent the metal of the micrometer spindle affecting the changes in inductance monitored by the proximity transducer. The calibration device is shown in Figure 5.14.

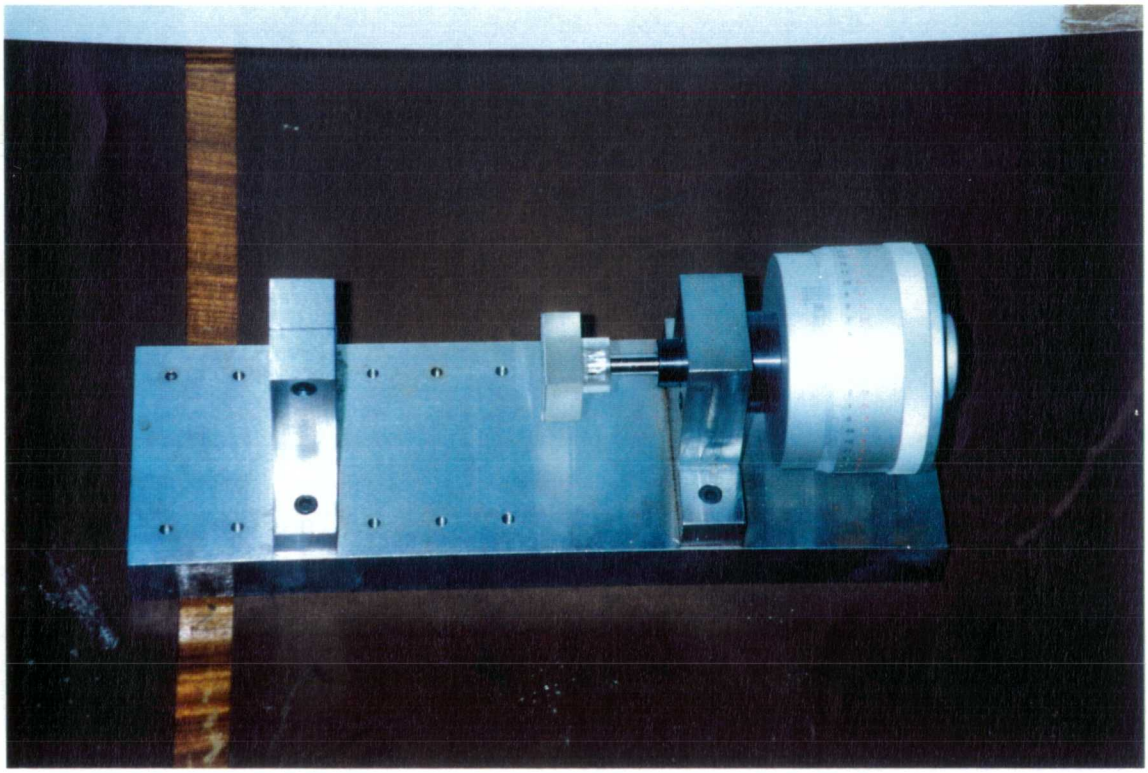

Figure 5.14 - Micrometer rig used for calibration of proximity transducers and submersible LVDTs

The non-linearity of the calibration was defined by varying the distance of the target over 3 cycles of the chosen working range of the transducer (1mm for Cell 1; 2.5mm for Cell 2) in increments of 20μm. To reduce electrical noise, each calibration point was derived from the average of readings taken over 1 second, generally consisting of more than 50 readings. A fixed time period is more satisfactory for averaging purposes than a fixed number of readings since electrical noise is generally related to the mains supply frequency; ideally data taken over a whole number of cycles should be averaged. Typical proximity transducer calibration curves are shown in Figure 5.15.

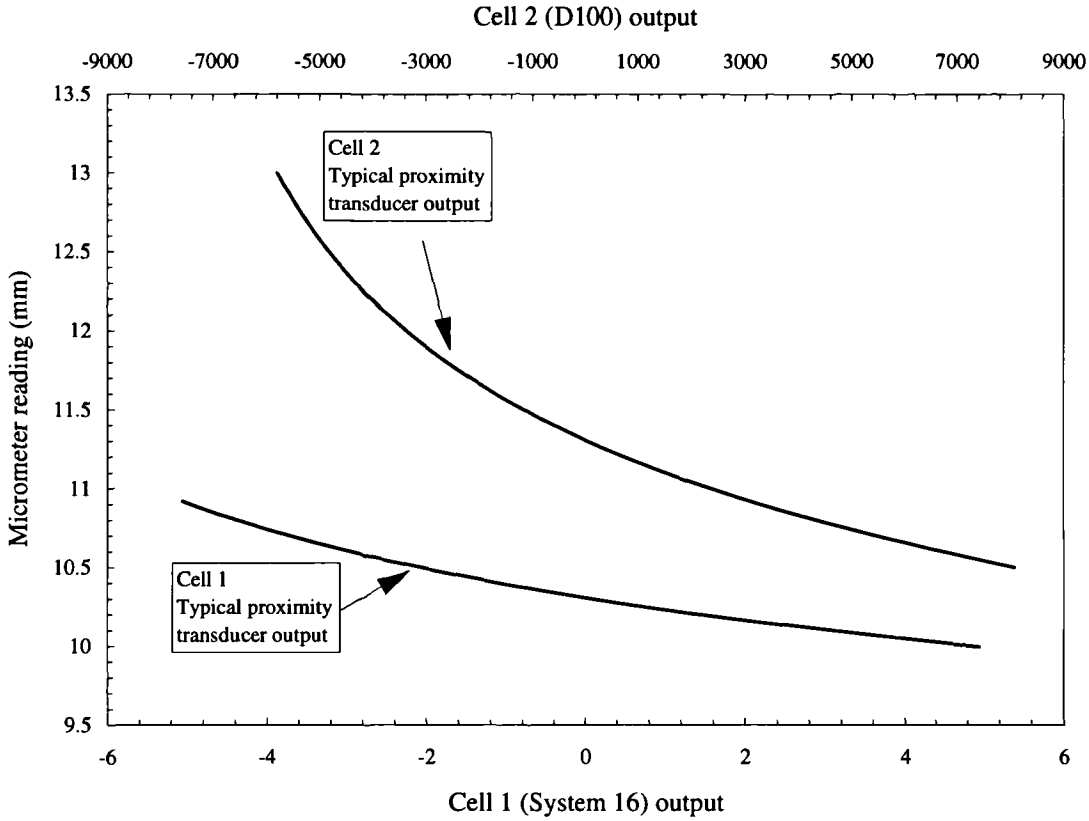

Figure 5.15 - Typical calibration curves for proximity transducers for both cells.

To fit an equation to this non-linear response, Yung (1987) split the response into a number of smaller regions and fitted polynomial variations to each of these plotted on a logarithmic scale. Hajj (1990) adopted Yung's (1987) technique of linearising the proximity transducer output but fitted a high order polynomial (up to order 11) over the entire range. The use of a high order polynomial regression requires justification, however, since it is being used to define the non-linearity rather than to follow slight deviations from a linear regression as was the case with the LVDTs. There is a distinct possibility that, when fitting a high order polynomial to scattered calibration data, such a function describing a smoothly non-linear function fitted would have many points of inflexion. The curve-fitting technique adopted for the present work was to fit an 8th order polynomial over the entire working range (the partial linearisation was not found to be beneficial) and to ensure the validity of the response by plotting the 1st and 2nd order differentials to reveal any points of inflexion. In every case it was shown that no points of inflexion existed and that the fitted calibration curve was continuously concave, reflecting the expected response of an inductance device. A typical analysis of a proximity transducer calibration is shown in Figure 5.16.

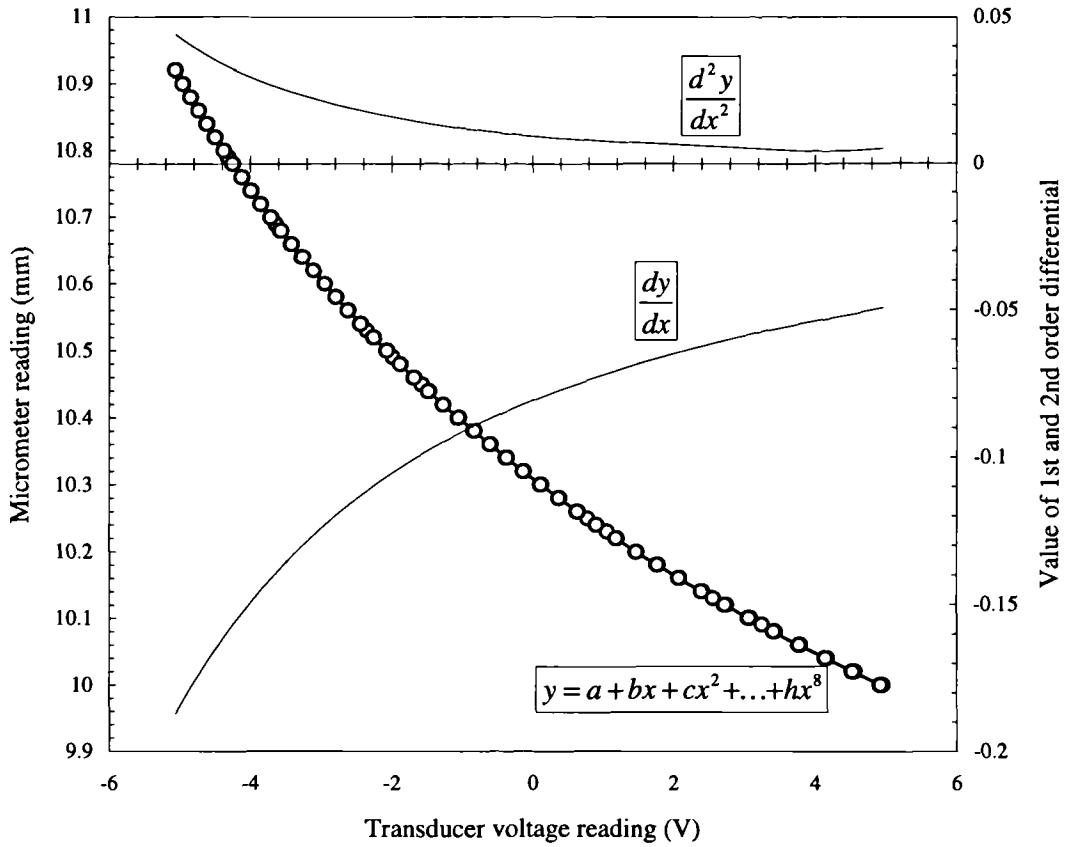

Figure 5.16 - Analysis of typical calibration curves for both stress path cells.

As noted earlier, the proximity transducer resolution is a function of the analogue to digital conversion and the 14-bit capacity of the D100 in Cell 2 provided greater resolution than the 12-bit capacity of the System 16 in Cell 1. In both cases, the resolution is greater the closer the target is to be transducer, and falls away rapidly as the distance increases. The resolution of each proximity transducer is shown in Figure 5.17(a) and Figure 5.17(b) for both Cell 1 and Cell 2 respectively. Figure 5.17(a) shows the improvement in the transducers over those used previously, since transducer 3 was from the original batch used by Hajj (1990).

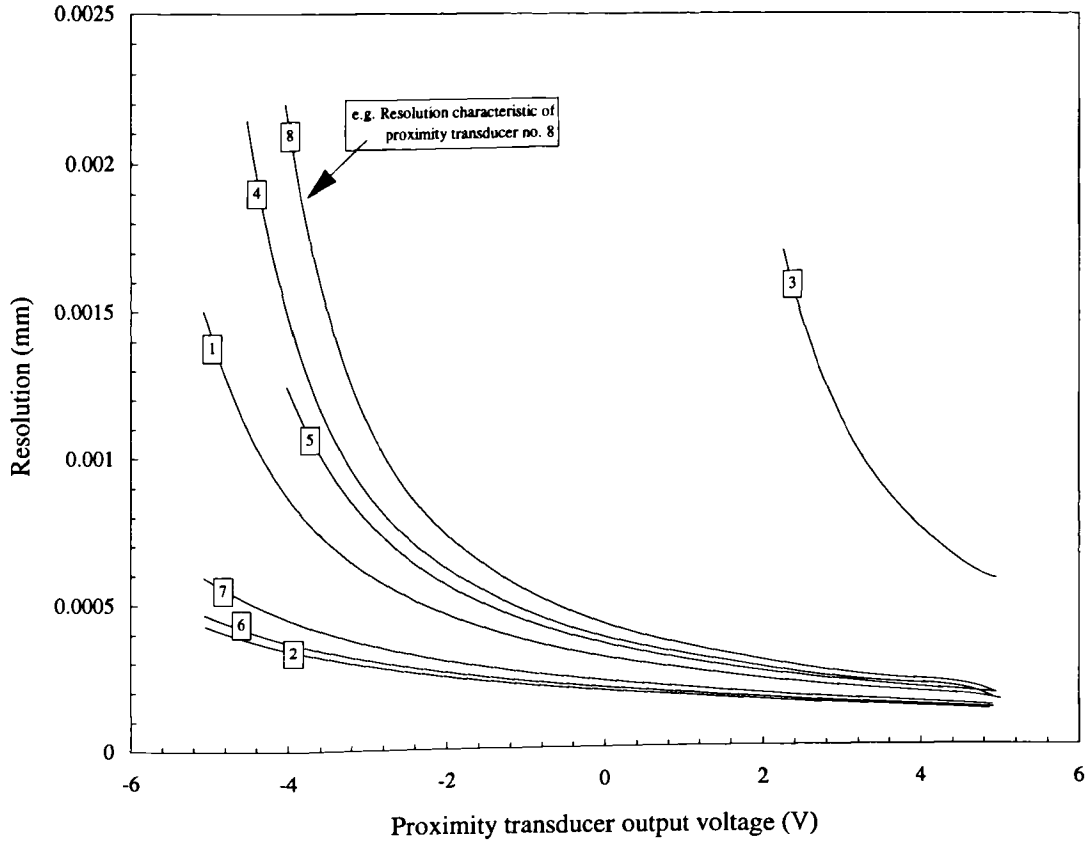

(a)

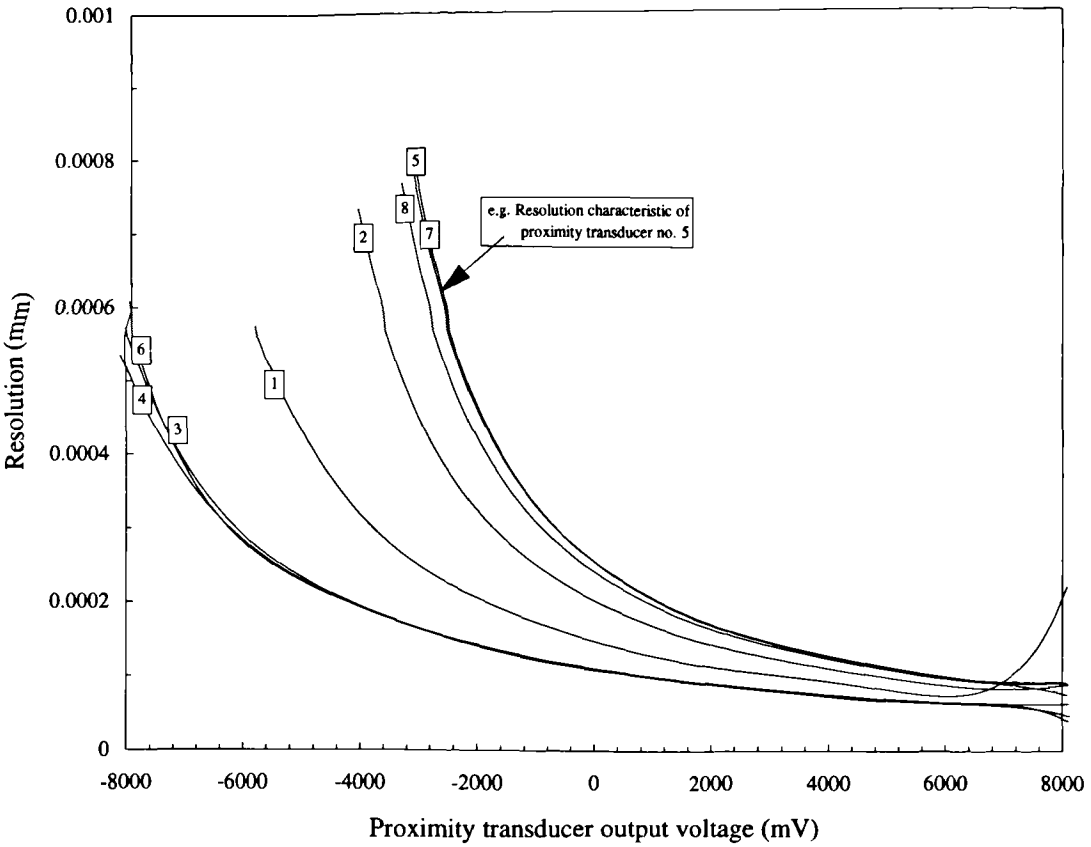

(b)

Figure 5.17 - Resolutions of proximity transducers for (a) cell 1 and (b) cell 2.

5.4.8 Stepper motor pressure control

The stepper motors, manufactured by Watson Smith, were identical on both Cells. Their full range consisted of 2000 steps and consequently the 800kPa supply pressure could be controlled in increments of 0.4kPa. This controlled pressure was passed directly, through an air-water interface to the cell pressure and the specimen back pressure lines. The lower chamber pressure, however, was controlled via an air-oil interface and transmitted to the specimen by the piston which had a bellofram area ratio of 2.25. Consequently, the minimum controllable axial stress increment was 0.9kPa. This suggests that the greatest accuracy to which a specified stress path may be followed using the current apparatus is approximately ±1kPa (see section 6.4.2).

5.4.9 Computer control program

Hajj (1990) developed a stress path control program specifically for the Cell 1 equipment and, with minor modifications, this was implemented for the Cell 2 apparatus. The program was further modified to include a greater range of error checking facilities and a graphical interface for the specification of stress paths.

It was discovered early on in the testing programme that the stress path followed tended to be either an upper bound or a lower bound of those allowed to the specified control limits. Therefore, the user-designated stress path was modified slightly by the program to compensate for the bias in the stress path which otherwise resulted in jumps in the stress path during the initial loading as shown in Figure 5.18. In this example, the control program would have modified the specified total mean normal stress (552.4kPa), reducing it by 0.5kPa, since the stress path followed is an upper bound of that prescribed. Although an apparently minor effect, it is the initial few kPa of the stress path over which the most sensitive control is required if the

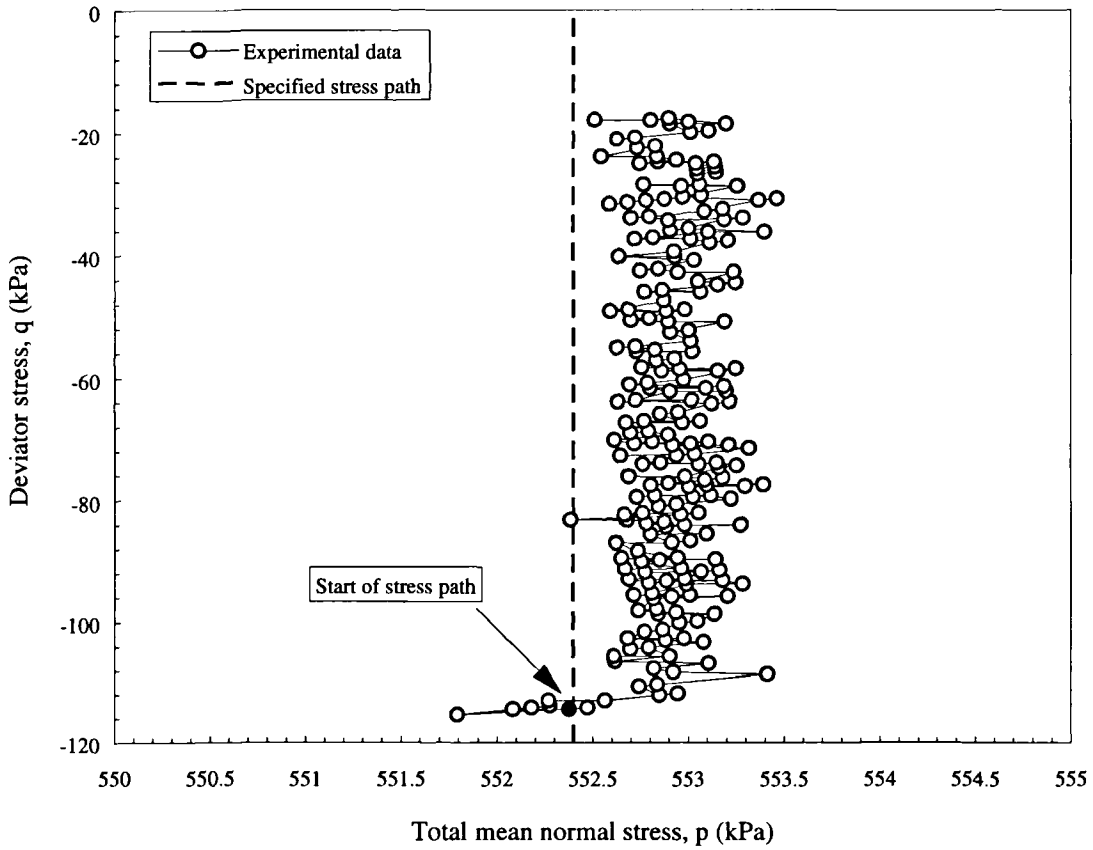

Figure 5.18 - An example of the biased stress path control produced by the unmodified control program

non-linearity of the soil stress-strain characteristic is to be recorded accurately. The modifications substantially eased the interpretation of the stress-strain response.

5.5 Testing procedure

This section describes the procedures for preparing a test specimen from a block sample of Oxford Clay, setting up the stress path apparatus, and carrying out the initial stages of saturation and consolidation to prepare the specimen for the stress paths described in section 5.2.

5.5.1 Specimen preparation

Triaxial specimens were prepared by trimming the block samples which had been obtained as described in sections 5.2.1 and 5.2.2. The trimming procedures varied as experienced was gained with handling and working with the Oxford Clay. The block samples obtained from the initial site investigation were trimmed by hand, but those obtained from Kempston Pit were prepared using the band saw technique described below.

The first three series of stress path tests were carried out on specimens trimmed from the two block samples of unweathered Oxford Clay from the Elstow excavation that had not dried out during storage. Initially, the block sample was carefully removed from its protective storage. This entailed removing the wooden storage case, the expandable foam, the layers of wax coated muslin, and finally the aluminium foil. The first block sample opened was viewed as a trial and a number of techniques were attempted to find a suitable approach to preparing a specimen in such a stiff, fissured material. The exposed block, a 300mm sided cube, was divided into quarters using a tensioned circular saw blade. An attempt was made at using a hand-held electrical saw but this was found to be unsuitable, having insufficient blade clearance. The original samples were retrieved using a chain saw and this would probably have been more effective at this stage if one had been available. A test specimen was trimmed from one quarter of the block while the remaining block was resealed and returned to storage. The samples were trimmed by hand using a trimming knife and scalpel, following the experience gained by Hird *et al.* (1987). The local environment around the sample was kept as humid as possible by keeping wet towels spread around its base. The specimen was trimmed to approximately the correct height and a smooth, level top surface obtained. For support, a temporary membrane was placed around the specimen and one of the 100mm specimen end caps of the lathe turntable placed on the top of the specimen. By sliding it from the edge of the table and onto a piece of wood at the same level, the specimen was turned upside down and installed onto the soil lathe. The temporary membrane was rolled back and the specimen base trimmed until the specimen was approximately 200mm length and a second smooth surface obtained. The second lathe turntable end cap was placed on the specimen base, the specimen righted, and then installed onto the soil lathe. The membrane was again removed and trimming proceeded once again with knife and scalpel, using the soil lathe guides to provide vertical sides to the specimen (Figure 5.19). The trimming process proved to be both slow and difficult and the length of time required to trim the specimen made the operation even more difficult, as the specimen dried and stress relief effects caused fissures to begin opening. The typical quality of a hand trimmed specimen of the Elstow site Oxford Clay can also be seen in Figure 5.19.

A hand trimming technique was initially adopted in the belief that it would cause less disturbance to the specimen than a mechanical technique. However, the extended time required to complete the trimming warranted an investigation of mechanical trimming aids. For the block samples obtained from Kempston Pit (see section 5.2.2), it was decided to use a band saw

to perform the initial trimming of the specimen. From the typical block sample size shown in Figure 5.20, the sample was to be brought to an approximately correct size before completing the trimming by hand, as before. The band saw was set to a relatively low speed, and the blade chosen had a relatively deep, but narrow, tooth size. It was found that the band saw was far more easy to use than envisaged and could very quickly be used to cut several specimen sized sections of the block sample (Figure 5.21) which were stored for future trimming. In view of this an attempt was made to form a triaxial specimen directly from one of these sections using the band saw, as shown in Figure 5.22. A circular piece of aluminium of 100mm diameter was used as a guide on the top surface of the specimen. The specimen was trimmed by rotating it within the band saw blade in slow, continuous actions, getting closer and closer to the guide. The final stage of the trimming process is shown in Figure 5.23, in which the precision to which the surface could be pared down can be seen. The final surface of the specimen was prepared using a trimming knife to remove any visual remnants of the blade action, although such trimming was minimal. Whilst the process of trimming a block sample by hand took several hours, it was found that, using a band saw, an accurately cylindrical triaxial specimen could be prepared in 10-15 minutes with apparently little to no extra disturbance to the specimen. Consequently, this technique was adopted for all future trimming operations.

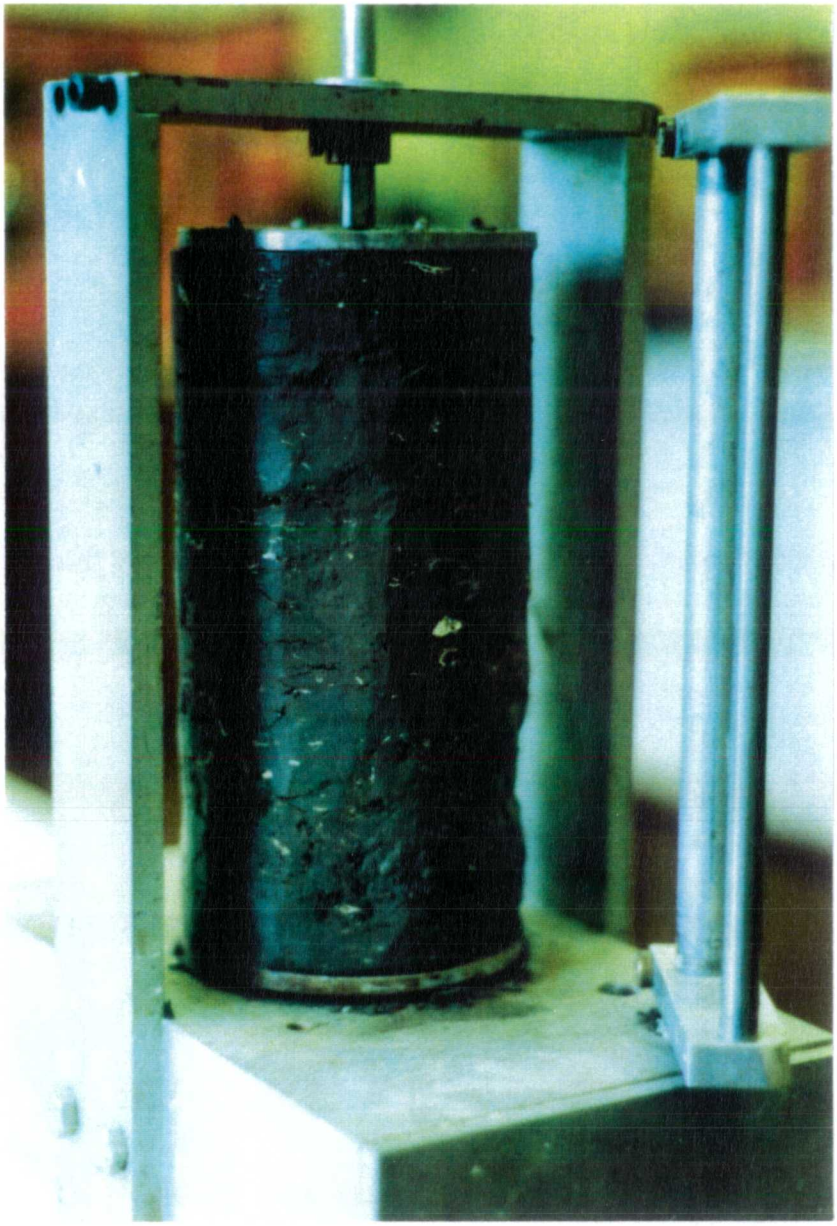

Figure 5.19 - Preparation of 100mm triaxial specimen from a block sample using a soil lathe

To facilitate the measurement of shear wave velocity using bender elements (see section 5.8), a piezoceramic element was required to be inserted 7-8mm into the ends of the specimen. Direct insertion into the stiff clay was not possible without damaging the elements. A 20mm diameter, 10mm deep circular recess was formed in the specimen ends. The removed clay was remoulded

by mixing it with a small amount of water and then placed back into the recess. The bender elements could then be inserted easily into the relatively soft clay. The amount of clay removed was thought small enough not to significantly affect the specimen response to static loading, or its shear wave velocity.

Figure 5.20 - One section of block sample retrieved from Kempston Pit showing fissure system

Figure 5.21 - Initial stage of band saw technique involved splitting the soil into manageable sections which could be sealed and stored easily

Figure 5.22 - Initial stages of trimming previously sealed block sample section

Figure 5.23 - Final stages of block sample trimming showing precision to which specimen may be formed

5.5.2 Setting up the stress path cell apparatus

The inclusion of the additional strain measurement devices, both upon the specimen and between its end caps, and the use of a miniature pore water pressure probe, required a carefully organised setting-up procedure.

Prior to preparing the soil specimen (see section 5.5.1), the stress path cell apparatus was prepared as fully as possible. After obtaining sufficient amounts of de-aired, de-ionised water, the miniature pore water pressure probe de-airing process was started. The probe was immersed in de-aired de-ionised water and sealed within a specially prepared 38mm triaxial cell. Additional connections were made to this cell through which the miniature pore water pressure probe could pass through and be sealed. A vacuum was applied to the cell such that air bubbles could be seen to escape from the porous stone of the transducer. The vacuum was applied for 4-5 hours and only removed when the transducer was required for installation.

A pair of 100mm diameter sintered bronze porous disks to be used as filter stones for the specimen were cleaned in an ultrasonic bath for 20 minutes, and then boiled in de-aired, de-ionised water for 30 minutes.

During this time, the de-airing of the stress path cell apparatus took place. The volume change unit was flushed with de-aired water ensuring that any trapped air was removed using both the top and base bleed valves. Six flushing cycles were used where one cycle involved flushing the top of the unit and then the base of the unit. The back pressure lines to the cell were then flushed around the volume change unit. The back pressure valves to the specimen were closed and a 400kPa back pressure applied to help maintain saturation within the back pressure system.

One of the prepared porous disks was then placed on the lower pedestal, and the lower back pressure valve opened slightly to flush water through the porous stone. This was required to ensure that the small gap between the filter stone and the circular intrusion of the bender element was filled with water.

The specimen was carefully transported by hand to the cell upon a small block of wood, while wrapped in a rubber membrane to both ensure specimen integrity and to prevent unnecessary drying out. The specimen was next lowered gently onto the lower porous plate such that the bender element was inserted in one clean action into the remoulded section of the specimen end. This was required to ensure a good coupling between the bender element and the soil specimen. The temporary membrane was then cut away and a dry filter paper drain attached to the specimen by slightly moistening its ends. The filter paper was held in position by the permanent membrane which was attached in the usual way. This membrane was secured to the lower pedestal by o-rings fitting into two grooves in the lower pedestal to which silicon grease had been applied. Any air bubbles seen to be trapped behind the membrane were eased out upwards.

Before attaching the top cap, the two blue perspex rings acting as mountings for the local axial strain targets were placed around the specimen. The second porous disk was placed onto the top cap and was flushed through by slightly opening the upper back pressure valve. Excess water was then removed and the assemblage was carefully lowered onto the specimen, again in a single smooth action, and ensuring that the orientation of the bender element was the same as that mounted in the lower pedestal. The specimen membrane was then secured to the top cap with two o-rings.

The local axial strain targets were next attached. This was achieved by balancing the blue perspex rings at the target positions upon their associated proximity transducers. The height of the proximity transducers was then manipulated so that the mounting rings were both horizontal, and such that a gauge length of 100mm was achieved. The mounting ring was held in position by an elastic band passing through the v-shaped notches in the ends of its four mounting arms and, additionally, the shaped bearing pads at the end of the arms were attached to the specimen with a small amount of silicon sealant (see Figure 5.12). This placing method was found to be easier to use than that devised by Hajj (1990), in which the bearing pads were secured at predefined positions on the specimen membrane. Additionally, having the targets initially resting upon the proximity transducers ensured that the target and the proximity transducer were initially perfectly parallel. Hajj also relied on marks on the specimen membrane to accurately attach the local radial targets. However, it was found that using the radial proximity transducers as guides was more satisfactory. To do this, the cell top was first slowly lowered into position (using a pulley system due to its size and weight) and, through the holes in the mid-height circumferential ring which were to receive the radial proximity transducers (see Figure 5.8), marks were placed upon the specimen membrane. The cell top was then raised and the radial targets were attached to the specimen membrane using silicon sealant. The cell top was again lowered, and the targets were held in position using the radial proximity transducers until the silicon sealant had set. This method ensured, again, that the target and transducer were initially parallel. The cell was left for 1 hour until the silicon sealant could support the targets, the cell top was again raised, and the final setting up of the cell completed.

The miniature pore pressure probe was attached at the mid-height of the specimen using a small rubber mould. This mould was positioned on the membrane in the position required and the outline to the mould drawn onto the specimen membrane as a positioning guide. A small hole, approximately 3mm diameter, was then cut in the centre of the outline, and the mould was attached to the membrane with a small amount of silicon sealant and held in position until it had set sufficiently. The miniature pore pressure transducer was then removed from the vacuum under which it had been stored and placed directly in position. A small amount of remoulded clay was first placed in the mould to ensure good contact between transducer and specimen. The probe was next pushed into position down the mould while pinching the mould sides allowing trapped air to escape behind the transducer rather than pass beneath the specimen membrane.

The mounting frame on which the end cap submersible LVDTs were supported was secured in position on the lower pedestal. The transducers were then attached to the ring and the positioning checked so that the plane of measurement was the same as for the local axial strain measurements. The vertical positioning of the transducers governed the positioning of the armatures within the recordable range and the armatures had to be positioned to remain in range during subsequent soil straining. This required them to be placed at the bottom of their range, as the specimen top would move down relative to the transducers during isotropic consolidation. This direction of the relative movement would also be the same during the initial extension stress path (see section 5.3.2) since the top cap would be held in position by the load cell connection.

The cell top was again lowered onto the cell body and this time it was secured in position using the retaining nuts. While lowering the cell body, the suction lead from the load cell top cap connector was passed through the cell middle plate where its connection was sealed. The radial proximity transducers were next mounted into the circumferential ring. The cell was filled with de-ionised water, which was found to prevent the growth of algae as occurred when tap water

was used. The apparatus was then left for approximately 1 hour allowing the cell water temperature to equilibrate with the surrounding air temperature, and so that the miniature pore pressure transducer voltage output could stabilise following connection.

5.5.3 Application of confining pressure

The application of a confining pressure to the soil specimen was carried out immediately after the setting-up procedure described in section 5.5.2.

A cell pressure was applied with the back pressure lines closed, to prevent drainage to the specimen. This allowed the specimen's pore water pressure to be raised to measurable, positive values, thereby giving an estimate of the initial effective mean normal stress within the specimen (Burland and Maswoswe, 1982). The degree to which this interpreted value represented the actual value depended on the initial saturation of the specimen. This was determined following a further rise in the specimen cell pressure from which a B value (Skempton, 1954) could be evaluated using equation 5.4.

$$B = \frac{\Delta u_w}{\Delta \sigma_3} \qquad (5.4)$$

where Δu_w and $\Delta \sigma_3$ are increments in pore water pressure and cell pressure respectively

A B value of 1 applies for a perfectly incompressible pore fluid. However, Black and Lee (1973) showed, for stiff clays, that if the degree of saturation was only slightly less than 100%, the observed B value could be significantly less than 1, as shown in Table 5.4. These values were derived assuming that no pore air would dissolve in the pore water due to the increase in confining pressure. For large increases in confining pressure, therefore, these values may be less applicable and a higher B value may be expected.

Soil stiffness	$S_r = 100\%$	$S_r = 99.5\%$	$S_r = 99\%$
Soft	0.9998	0.992	0.986
Medium stiff	0.9988	0.963	0.93
Stiff	0.9877	0.69	0.51
Very stiff	0.913	0.20	0.10

Table 5.4 - Relationship between degree of saturation, S_r, and the observed B value for a range of soil stiffnesses (Black and Lee, 1973)

Interpreting the *in situ* effective stress from the initial effective stress following application of confining pressure is further complicated for anisotropic soils. When sampling such soils, the removal of deviatoric load is coupled with volumetric effects and, in the undrained case, to changes in effective stress. (see later in section 6.2.2). The *in situ* effective mean normal stress can not, therefore, be recovered simply from application of confining pressure even for a perfectly sampled soil (a soil in which no changes in the mean effective normal stress are due to the sampling process). Skempton and Sowa (1963) related the *in situ* stress state for a perfectly sampled saturated soil to the measured soil suction by equation 5.5.

$$-u_s = \sigma'_v\left(\frac{1-2K_o}{3}\right)+\left(A-\frac{1}{3}\right)\sigma'_v(1-K_o) \quad \text{..... (5.5)}$$

where, u_s = soil suction following perfect sampling
σ'_v = *in situ* vertical effective stress
K_o = coefficient of earth pressure at rest (σ'_h/σ'_v)
A = pore pressure parameter during perfect sampling (Skempton, 1960)

The value of A may vary between one third and one half depending on the degree of anisotropy. The equation may, therefore, provide an estimate of a range of *in situ* horizontal stresses.

When a soil specimen was placed on the lower pedestal in the triaxial apparatus it came into contact with free water which would have reduced the soil suction and possibly caused swelling. Burland and Maswoswe (1982) used a small coil of fuse wire to maintain a gap between the soil and the lower pedestal and so reduce disturbance to the specimen. Upon application of cell pressure the specimen was forced downwards to rest on the lower pedestal while the fuse wire was forced into the soil. This technique was not used in the current work, however, because it was uncertain whether the fuse wire would adequately penetrate such a stiff soil. If the specimen descended unevenly upon application of confining pressure, the intimate connection required between the bender element and the specimen could not be assured.

5.5.4 Saturation and initial consolidation

Following initial application of confining pressure, the pore water pressure within the specimen was increased such that trapped air within the back pressure system, and throughout the specimen, would dissolve into solution. The target back pressure was 400kPa since initial testing had shown sufficient saturation was achieved at this value, and because this was the pressure at which the volume change unit had been calibrated. Initially, the back pressure was raised to be the same as that pore pressure registering following the application of confining pressure.

Saturation was carried out initially using the standard procedure (Head, 1985) of raising the cell pressure and the back pressure in consecutive increments, and in each stage measuring the B value. In most tests, however, the saturation procedure was varied in several ways to take advantage of the additional capabilities of the stress path apparatus. The first variation involved automatically raising the cell pressure at a slow, constant rate, and monitoring the pore water pressure response. In this way, an instantaneous B value could be monitored as the gradient of the graph of cell pressure against average pore water pressure. The rate of increase was chosen to prevent the development of non-uniform pore water pressure (at the middle of the specimen relative to its ends). A second technique involved raising both the cell pressure and the back pressure at a fixed, constant rate until the desired back pressure was achieved. In this way the applied effective stress was held constant as saturation was achieved. Alternatively, the rate of increase of cell pressure could be different from that of the back pressure if the final effective stress required was different from the initial one. A final variation of this technique, involved increasing the back pressure at a fixed rate while the cell pressure increased at a variable rate designed to keep the measured deviatoric strains zero. Each method resulted in adequate specimen saturation, but it was found that the process could be carried out far more rapidly with the back pressure and/or cell pressure controlled automatically.

5.5.5 Step consolidation stage

Using the additional capabilities of the stress path cell to vary the conventional saturation procedure, as described above, permits the traditionally separate stages of saturation and isotropic consolidation to be combined, i.e. the specimen was allowed to consolidated during the automatic saturation procedure.

In the current work, however, a step consolidation stage was additionally incorporated into the testing programme. This permitted the calculation of a suitable stress path loading rate as described later in section 6.4.7. Following saturation, the cell pressure supply was increased by 60-100kPa with the valve to the cell closed. The valve was then opened while the back pressure valves remained open. This caused a step change in the pore water pressure profile which then gradually reverted to the value set by the back pressure.

5.5.6 Preparation and carrying out of stress path probe stages

Following the step consolidation stage the specimen was in an isotropic state of stress usually with an effective mean normal stress of 60-100kPa higher than the value corresponding to the stress state at which suitable stiffness moduli were to be obtained by applying stress probes (see section 5.3.2). The top cap was then connected to the load cell using the vacuum connection, enabling the subsequent stress path probes to be carried out under negative deviator stress. The load cell was raised on its threaded mounting to its highest position to provide sufficient travel for the lower chamber to bring the specimen to eventual extension failure. With the valve to the lower chamber closed, the pressure in the lower chamber supply line was raised to the value required to balance the downward pressure exerted by the cell pressure, and then increased by a further 20kPa. The valve was then opened partially allowing oil under pressure to enter the lower chamber and raise the lower pedestal and the soil specimen. The specimen was raised until it was within 1cm of the load cell before the lower chamber pressure was reduced to exactly balance the cell pressure. The lower chamber pressure was then raised by 1-2kPa so that the specimen top cap very slowly came into contact with the load cell. The suction connection was then made by opening the valve on the load cell-top cap connector pressure line (which passed from the base of the load cell to the outside of the triaxial cell) to atmospheric pressure. For this stage it was ensured that the valve to the lower chamber was fully opened, since if the specimen top and load cell had not been initially in full contact before the suction connection was made, excessive strains could have developed in the specimen if the lower pedestal had not been free to move. Generally, less than 5kPa of deviator stress was applied to the specimen at this stage, although in one case 20kPa was required to ensure coupling between the top cap and the load cell.

It was originally planned to connect the load cell immediately after the application of the initial confining pressure. The automatic saturation techniques described in section 5.5.4 would have allowed the deviator stress to be kept at a constant slightly negative, or slightly positive value (the Imperial College type load cells having a discontinuous response between compression and tension). Early connection is advantageous, since if the load cell is connected following consolidation, any tilting of the specimen leads to difficulties in making the suction connection. However, the decision to include a stepped consolidation stage to evaluate testing rates required that the load cell connection was delayed until immediately before the stress path stages.

The stress path probes were carried out following the philosophy described in section 5.3.2. The individual test details are described and quantified in Chapter 6.

5.6 Interpretation of experimental data

5.6.1 Introduction to curve fitting techniques

The interpretation of discrete data recorded from transducers is required for both the calibration of instruments and the analysis of stress-strain data. This section discusses a number of aspects of the curve-fitting process.

Given a set of experimental data points, it is useful to be able to represent the data mathematically by fitting a model to the data in the form of a parametric equation. One important consideration in selecting an appropriate model is the pattern of underlying behaviour that the data represent. Ideally, the model parameters will reflect the underlying behaviour such that the curve fitting procedure produces values which have a physical justification and meaning.

Data modelling is commonly performed by regression or interpolation techniques. Interpolation guarantees that the fitted curve will pass through each and every data point, whereas regression simply ensures that an arbitrary function, that measures the agreement between the data and the model, is minimised.

For regression curve fits, error is assessed using the standard error and correlation coefficient. The standard error of the estimate is defined in equation 5.6 and quantifies the spread of the data points around the regression curve. The correlation coefficient is defined in equation 5.7 and as the quality of the fit increases, the standard error approaches zero and the correlation coefficient approaches unity.

$$S_r = \sqrt{\frac{\sum_{i=1}^{n_{points}} (y - y_i)^2}{n_{points} - n_{params}}} \quad \text{..... (5.6)}$$

$$R = \frac{S_t - S_r}{S_t} \quad \text{..... (5.7)}$$

where, y = value of regression model

y_i = value of data point

n_{points} = number of data points

n_{params} = number of parameters in regression model

S_t = standard deviation $= \sqrt{\frac{\sum_{i=1}^{n_{points}} (\bar{y} - y_i)^2}{n_{points} - 1}}$

$\bar{y}$ = mean of data points

The standard deviation (i.e. standard error of the mean) operates in exactly the same fashion as the standard error of the estimate defined above; however, it considers the spread around a constant value (the mean) as opposed to the spread around the regression model. This is the uncertainty of the dependent variable prior to regression. Thus, the improvement (or error reduction) due to describing the data in terms of a regression model can be quantified by subtracting the two quantities. Since the magnitude of the quantity is dependent on the scale of the data, this difference is normalised by the standard deviation (equation 5.7).

Regression models which consist of a linear combination of a particular set of functions are called linear models. The general form of this kind of model given in equation 5.8:

$$y(x)=\sum_{n=1}^{k} a_k X_k(x) \quad \text{..... (5.8)}$$

where $X_k(x)$ are fixed functions of x. The term *linear* refers only to dependence of the model on the parameters a_k; the functions $X_k(x)$ may be non-linear.

Typical models of this type are polynomials (equation 5.9) of which the straight line is the simplest. For each additional higher order term incorporated into the polynomial, a further point of inflexion, curve minimum, or curve maximum is produced on the fitted curve. A higher order polynomial will therefore fit a given set of data points numerically better than a lower order polynomial. However, it may oscillate wildly as the additional turning points are incorporated. Such curves, therefore, must be used with caution. High order polynomials were used during the transducer calibration process, although several measures were employed to ensure that the fitted curve truly reflected the underlying response (see section 5.4.7)

$$y = a + bx + cx^2 + ... + nx^n \quad \text{..... (5.9)}$$

where, $a, b, c, ..., n$ are constants

Non-linear regression models are more versatile for curve fitting than linear models. However, the determination of parameters is more involved. A number of non-linear models were tested in the current work, either for modelling the soils behaviour or non-linear transducer characteristics. The models thought most useful are presented in the following section.

When a suitable regression can not be formulated, interpolation is an option. One possibility interpolation technique is the use of *splines* which, instead of relying on a single equation, consist of many equations fitted successively to intervals of the data set. *Linear splines*, the simplest form of spline, approximate the range between data points by a straight line. *Quadratic* splines interpolate the range between data points by a 2nd order polynomial while ensuring that the first derivatives are equal at each spline connection. *Cubic* splines interpolate the range between data points by 3rd order polynomials. Cubic spline curve fitting ensures that both the first and second derivatives are continuous at a spline connection which gives a more aesthetically pleasing appearance than lower order splines. However, unless the data set is carefully chosen, the spline is likely to oscillate within the experimental scatter.

5.6.2 Chosen data analysis strategies

It was hoped that a single mathematical form of stress-strain relation could be formulated through curve fitting procedures and that through this the stiffness moduli could be calculated. However, as data became available during the experimental programme it was realised that the stress-strain response was not consistent enough to warrant a single curve-fitting procedure.

The most successful regression analysis was achieved using a curve from the family of power laws, a modified Ramberg-Osgood equation, as given in equation 5.10. This modified form of equation was proposed by El-Rumawi (1989) and was found to adequately describe a range of stress-strain curves for steel at elevated temperatures.

$$\varepsilon = \frac{\sigma}{A} + B\left(\frac{\sigma}{C}\right)^n \quad \text{..... (5.10)}$$

In the limit as stress and strain reduce to zero:

$$\sigma \to 0$$
$$\frac{\partial \varepsilon}{\partial \sigma} \to \frac{1}{A} \quad \text{..... (5.11)}$$

and so A can be fixed as the initial slope of the stress-strain curve.

To determine the constants A, B, C, and n the equation may be rearranged and expressed as follows:

$$y = mx + k \quad \text{..... (5.12)}$$

where, $y = \ln\left(\varepsilon - \frac{\sigma}{A}\right) - \ln B$

$$m = n$$
$$x = \ln \sigma$$
$$k = -n \ln C = n \ln\left(\frac{1}{C}\right)$$

This is the equation of a straight line. A is set at the initial slope of the stress-strain curve, and B is set at an appropriate value, the remaining constants, C and n, may be calculated from the slope and intercept of the line:

$$n = m$$
$$C = e^{n/k}$$

For any set of data the method of least squares may be used to determine the constants.

This modified Ramberg-Osgood equation may be differentiated to obtain tangent stiffness values:

$$\text{Tangent stiffness} = \frac{d\sigma}{d\varepsilon} = \frac{1}{\frac{1}{A} + \frac{nB}{C}\left(\frac{\sigma}{C}\right)^{n-1}} \quad \text{..... (5.13)}$$

Although this curve-fitting strategy fitted some of the stress-strain responses very well, where the stress-strain response was less regular, the fitting procedure smoothed over the apparent anomalies. It was felt that, at this stage of the analysis, it was desirable to retain the essence of the experimental response by plotting the raw data rather than a smoothed curve.

There were also difficulties in the production of stiffness curves from the stress-strain response. Where the Ramberg-Osgood type equation fitted well, a tangent stiffness equation could be easily derived. However, ill-fitting of the original equation is exaggerated in the tangent stiffness derivation and, consequently, in other cases the results for stiffness could not be relied on.

Alternatively, therefore, tangent stiffness data were derived from a linear spline interpolation for a reduced data set. This typically involved performing a linear regression on up to a 5kPa range of the stress-strain data (consisting of 10-20 discrete data points). The tangent stiffness calculated was assigned to the median of this range. A secant stiffness was calculated for the initial section of the stress-strain curve (up to a change of 5kPa) where the tangent stiffness calculation produced excessively scattered results.

The resulting stiffness variations were then plotted at discrete points and this more accurately reflected the response recorded in the stress path tests. Curve fitting was still required, however, to incorporate the response into a constitutive relation (see Chapter 7) and it was found that equation 5.14 invariably fitted better than the other non-linear models investigated (see section 5.6.1).

$$y = \frac{ab + cx^d}{b + x^d} \qquad (5.14)$$

This form of equation is ideally suited to modelling of the S-shaped stiffness curves and allows the modelling of the initial constant elastic stiffness, the rapid fall of stiffness through small and intermediate strains, and a constant, low, large strain stiffness.

An example of the form of the equation, and its suitability to fitting stiffness relations is shown in Figure 5.24. Also shown on this figure are a number of parametric variations showing the variety of curves which the equation is capable of modelling. For such non-linear regression analysis, numerical analysis is required to calculate to parameters of the regression curve. For the example shown here used a computer program based Marquardt-Levenberg method to solve the non-linear regressions.

Unfortunately, there is no closed form integration solution of this equation and, consequently, neither the stress-strain nor the secant stiffness relations can be derived using it. In the present work, however, this was not a requirement for the non-linearity as defined in Chapter 7 was based on tangent stiffness values appropriate for numerical analysis.

This equation was discovered late in the current work and, consequently, was not used in the numerical analyses described in Chapter 8. The non-linearity of the stiffness relations was instead approximated using fourth order polynomials fitted to a logarithmic scale of incremental strain energy (see later in section 7.5.4). These equations adequately described the response although extrapolation beyond the fitted range was not possible because of oscillations in the polynomial. The fitting procedure, therefore, additionally required the maximum and minimum stiffness to be specified similarly to Jardine *et al.* (1986). Equation 5.14 was, however, additionally incorporated at a later stage into the program coding of the chosen constitutive relation (see section 7.5) and it is suggested for use in any future work.

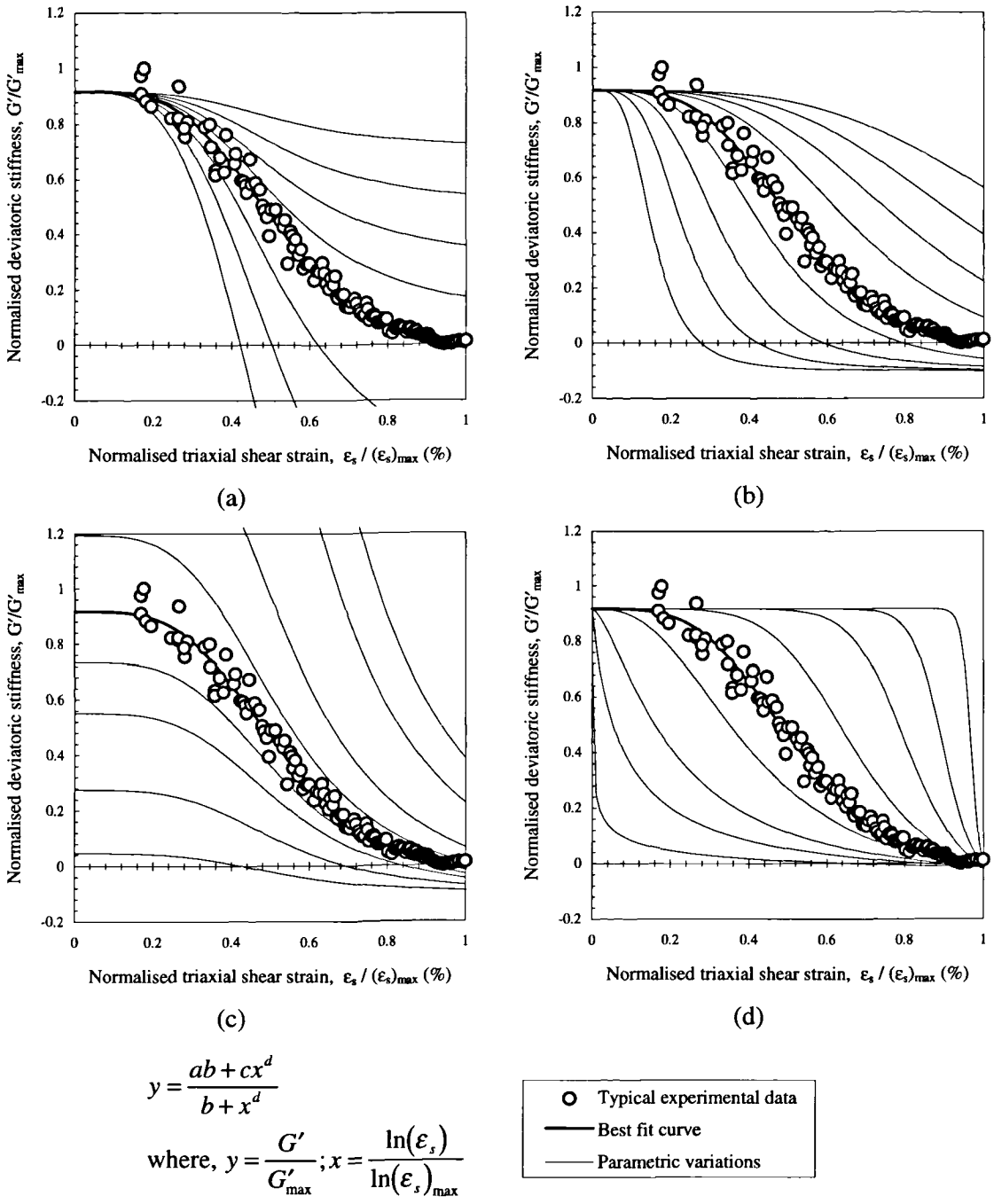

Figure 5.24 - Parametric variation of stiffness curve-fitting equation for (a) parameter 'a', (b) parameter 'b', (c) parameter 'c', (d) parameter 'd'

5.7 Dynamic testing using bender elements

5.7.1 Introduction

The general development and use of bender elements for wave velocity measurements through soil specimens is described in section 2.6.2. In this section, the apparatus and testing methods developed for the current work are described.

The addition of bender elements into the stress path cell is also useful since they provides a direct measurement of the very small strain shear modulus in the vertical plane and, therefore, a means of assessing the small strain anisotropic response (see later in section 6.5.4).

5.7.2 Equipment

The bender elements were manufactured at the School of Ocean Sciences, University of North Wales (Bennell, 1992). The biomorph plates from which the bender elements were constructed were obtained from Morgan Matroc Ltd. The piezoceramics, as supplied, were already bonded to a central brass plate in either series or parallel configurations, as required, in material type PZT-5B or PZT-5H. The individual elements were cut from a larger plate attached to a lathe using several shallow cuts with a small dentist's cutting wheel. The transducers were potted in Araldite (CIBA GEIGY) Resin MY 753 with hardener HY 951 supplied by Robnorganic Systems Ltd. The specimen end caps in both stress path cells were modified to each include a bender element, as shown in Figure 5.25.

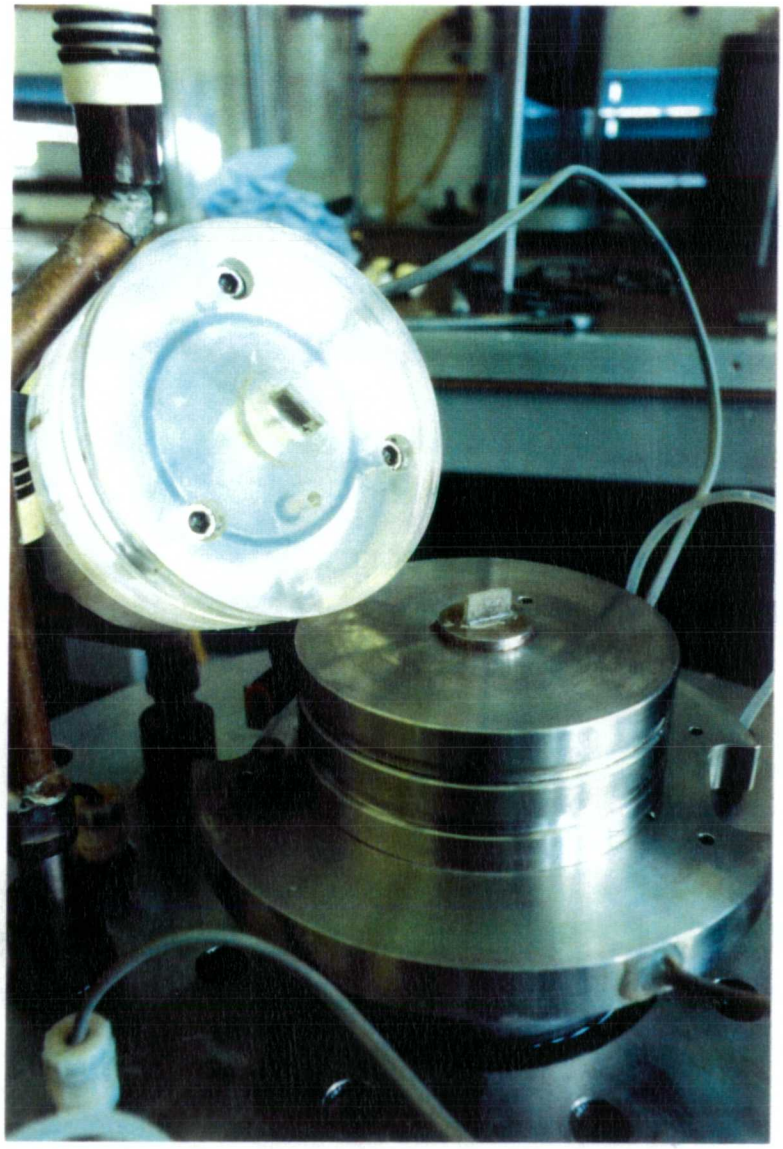

Figure 5.25 - Bender elements mounted into the specimen end caps

The transmitted and generated waveforms were recorded on a Gould digital storage type 20MHz 1425 oscilloscope. The generation of a wave at the bender element was controlled by a Phandor TG503 5MHz pulse or function generator which had a maximum voltage output amplitude of ±10V. In some cases, a

second function generator, a Continental Specialities Corporation type 4001, was used as a triggering mechanism for the first function generator.

The generated bender element output required amplification. It was found that a mains supplied amplifier generated too much interference and, consequently, a battery powered amplifier was manufactured, in which the two 9V batteries permitted much cleaner amplification.

A 'bender element test' consisted of the set of procedures described in section 5.7.3. For the current work, the procedure was performed manually, although it would have been possible to carry out each bender element test automatically using the RS232 and IEEE interfaces on the oscilloscope and function generators.

5.7.3 Testing procedure

The bender element mounted in the lower pedestal was used as the receiver element, since the cell base could be more easily earthed than the top cap. A continuous earth was ensured by soldering a wire connection between the lower pedestal and the cell base. The shielded bender element lead was connected via the battery powered amplifier to one channel of the oscilloscope. The bender element in the top cap was connected through a shielded lead to the function generator. The function generator was, in turn, connected to the triggering circuit of the oscilloscope. The second function generator was connected to the triggering circuit in the first function generator, allowing discrete wave pulses to be sent over an extended time period. A more advanced function generator would have not have needed a second function generator as a trigger, but the setup proved satisfactory.

A waveform, either a stepped square wave pulse or a sinusoidal pulse, was transmitted from the top cap bender element and, after travelling through the soil specimen, generated a response from the bender element in the lower pedestal. Using the captured response on the oscilloscope, it was possible to calculate the travel time of the wave form through the soil. The travel distance was required to subsequently calculate the wave velocity. Dyvik and Madshus (1985) and Atkinson and Viggiani (1995b) have both shown that the wave effectively travels between the tips of each bender element. The tip penetration of approximately 8mm was, therefore, subtracted from the current specimen length. The current specimen length was calculated after each bender element test using the current axial strain recorded between the endcaps. The bender element tests were performed at a number of stages along each path of a particular stress path test, and at each stage the current total and effective stress state of the specimen was recorded. It was only possible, however, to carry out bender element tests in 3 of the stress path tests (tests T04, T06 and T07 - see later in section 6.3.3).

The techniques for running the test differed slightly, depending on the type of transmitted waveform:

SQUARE WAVE BENDER ELEMENT TEST

The first type of test involved generating a continuous square wave of amplitude 20V at the upper bender element. The square wave was at a low enough frequency (typically less than 10Hz) to ensure that the energy of the generated wave had dissipated sufficiently not to interfere with a subsequent front. The pulse of the square wave triggered the oscilloscope channel recording, and a suitable time base was chosen to capture the wave trace generated at the lower bender element. It was found that the received wave form was generally swamped by system noise. Although all leads were shielded, and the system was suitably earthed, it was not possible to eliminate the background noise. The background noise was greatly reduced,

however, by using the stacking function on the oscilloscope which allowed an average trace of the wave form to be calculated from a number of previous traces. The degree of background noise is shown for a single trace, and subsequently, after stacking and averaging 256 consecutive traces, in Figure 5.26. A series of four stacked traces were generated, two due to a positive going and two due to negative going transmitted wave; the series of four results were overlaid and examined separately to check the consistency of the output.

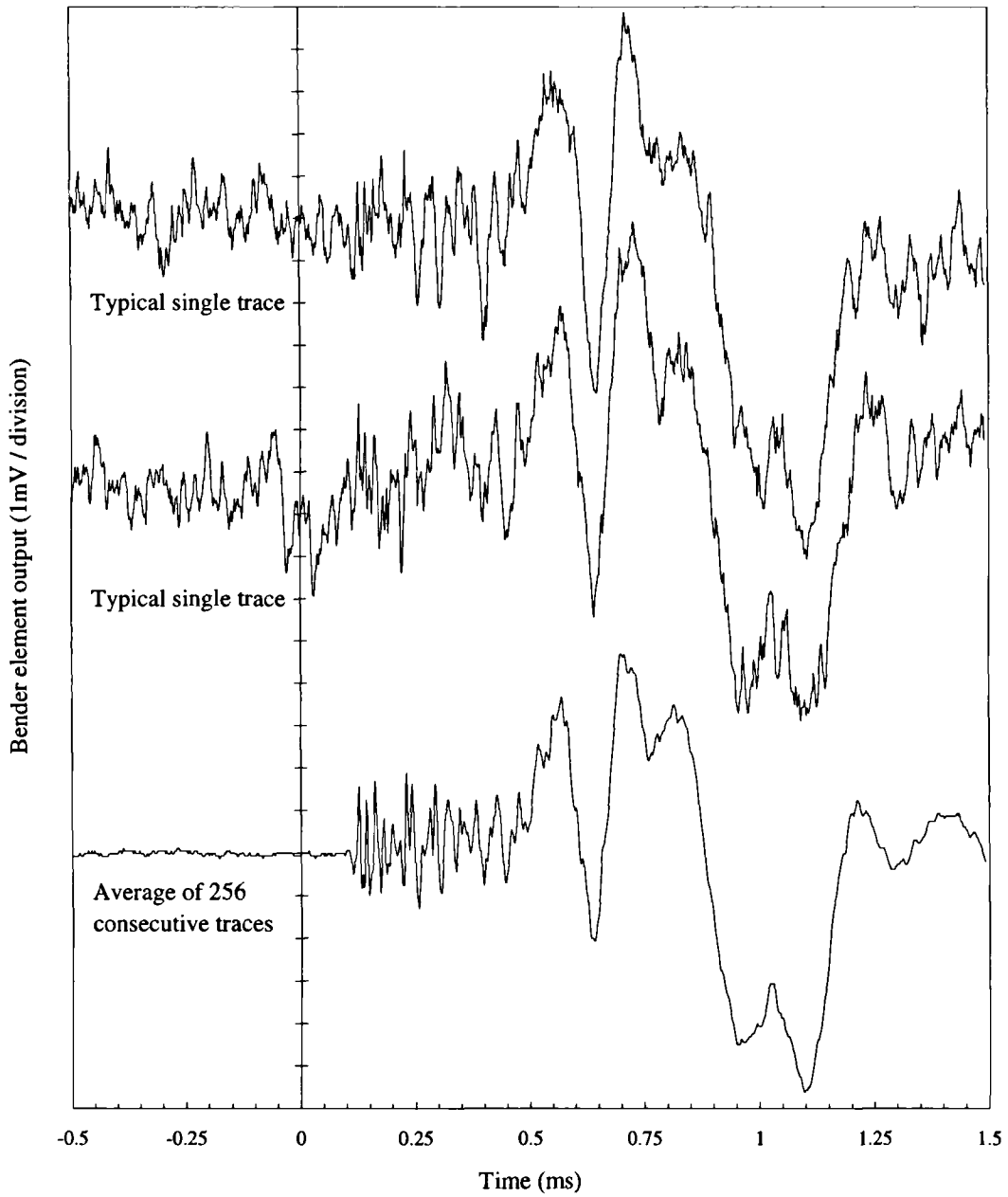

Figure 5.26 - Typical levels of noise in received bender element traces with and without the stacking and averaging procedure

SINUSOIDAL WAVE BENDER ELEMENT TEST

The majority of bender element tests were carried out using a square wave transmission, but a number of test series (a 'series' refers to bender element tests carried out on the same specimen within a short period of time of each other) were carried out using a sinusoidal input. The general procedure was the same as for the square wave input except in the generation of the pulse. The traces were generated by using the second function generator to simultaneously trigger a sine wave pulse from the first function generator and the oscilloscope channel recording. For each bender element test series, traces were obtained (using the same averaging process) for frequencies between 0.5kHz and 50kHz.

5.7.4 Analysing the bender element receiver trace

The bender element traces were analysed both manually, by visual inspection, and automatically, using spectral analysis techniques. These methods are described in section 2.6.5.

Following a bender element test, the stacked and averaged trace was transferred to a personal computer through an RS232 interface. The traces could be displayed and analysed using a module of the computer program StressPath (Pierpoint, 1996c), of which an example screen shot is shown in Figure 5.27. The program allowed many traces to be superimposed and, by magnifying sections of the trace, the travel times of discrete points of the waveform could be evaluated.

The spectral analysis of the waveform trace was carried out automatically using the macro language of the spreadsheet application, Microsoft Excel.

The bender element analysis is discussed later in Chapter 6, section 6.5.2.

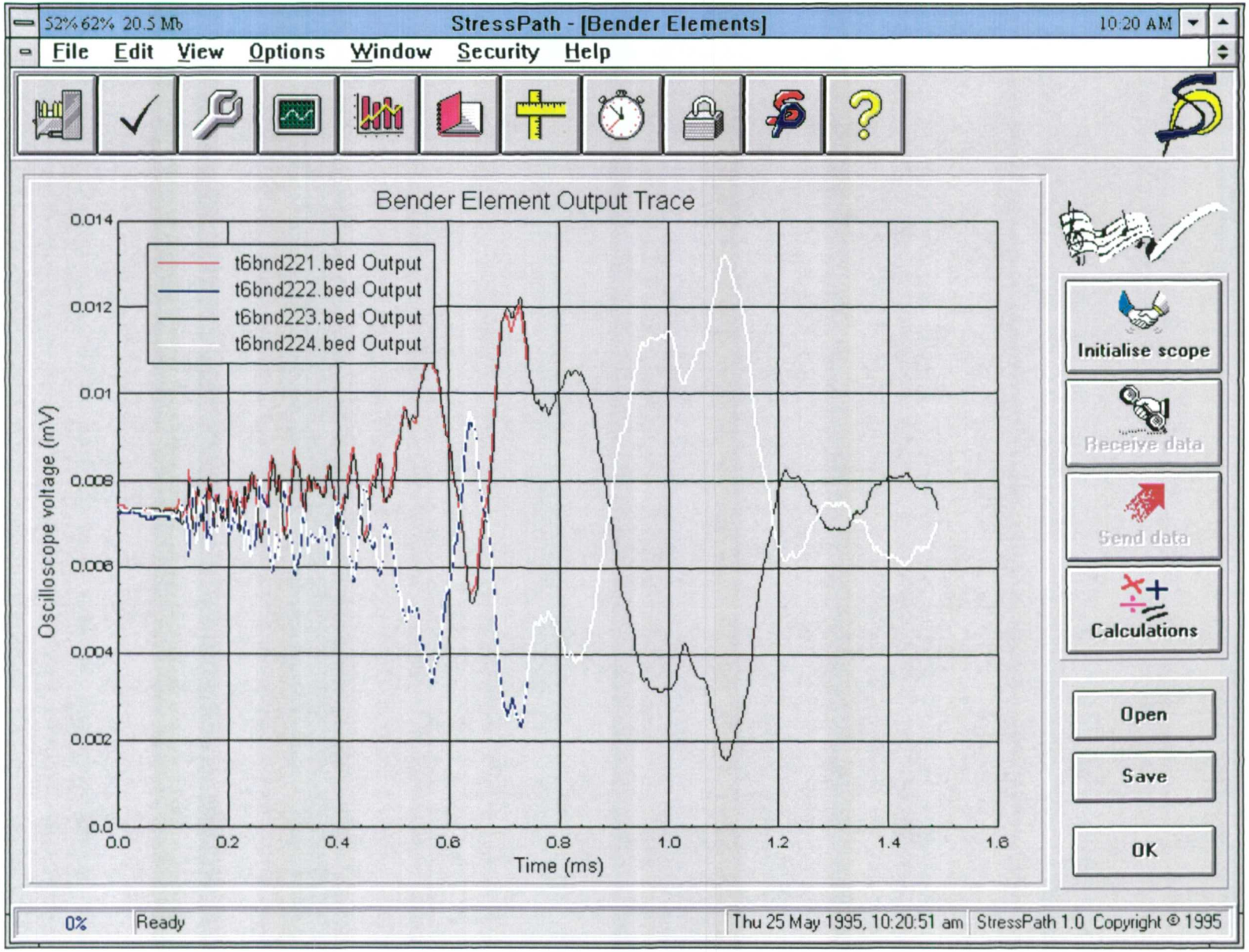

Figure 5.27 - Screen shot of bender element analysis module in StressPath for Windows program

5.8 High pressure oedometer tests

Although geological studies had provided an indication of the depth of previous overburden at the Elstow site (see section 3.3.2), it was decided that a quantitative measure was required to determine the approximate overconsolidation ratio of the block samples used in the stress path tests. The estimated previous maximum level of overburden was 500m above present ground level (Jackson and Fookes, 1974), corresponding to a vertical stress of approximately 5MPa. This figure was beyond the capabilities of conventional oedometer equipment but fortunately a high pressure oedometer apparatus was available which had been developed previously (Kadri, 1984). In principle, the equipment was the same as a conventional oedometer, but a maximum load of 440kg could be applied at a lever arm ratio of 15.5. Using a conventional oedometer sized specimen and loading ring, the maximum applied load corresponded to a vertical stress of approximately 15.5Mpa.

The oedometer test specimens were prepared from suitably sized pieces of the block samples in the conventional way. A sharpened trimming knife was used to first prepare a level lower surface to the specimen, and then to trim the sample to approximately 1cm from the sides of the oedometer ring. For the final stages of trimming a scalpel was used to remove thin layers of soil until the greased oedometer ring could be pushed into the sample with very little effort. The top and bottom surfaces were prepared with the trimming knife. The test specimen was then inspected within the ring and discarded if disturbance at the edges of the oedometer ring was apparent.

The oedometer rig was calibrated to remove compliance effects by loading up a steel specimen. After first loading to the maximum load then unloading to reduce initial seating errors, a series of three load-unload loops was carried out. The final calibration loop also included a smaller unload-reload cycle halfway through the loading cycle. A typical calibration is shown in Figure 5.28. Although the calibration loops were repeatable, they did exhibit a significant degree of hysteresis. Also, the magnitude of the compliance (up to 1mm) was significant compared with the vertical displacement of the specimen (up to 4mm) during a test. These factors affected the unload-reload cycles in an unpredictable way and it was not anticipated that such loops would produce acceptable results during a test.

The specimens were loaded in equal steps, equivalent to 1414kPa, up to the maximum load, with loading maintained for 48 hours before a subsequent load increment was applied. A single unload-reload loop was incorporated into the first test, although generally the specimen was both loaded and unloaded monotonically.

A total of three successful tests was carried on specimens obtained from either Elstow or the Kempston Pit. A summary of the successful tests is given in Table 5.5 and the test results are discussed later in section 6.3.2.

Test name	Block sample name	Source
HPO 01	E/EX17 24.910 / BL	Elstow site
HPO 02	E/EX17 24.910 / BL	Elstow site
HPO 04	KEMP / BL / 2	Kempston Pit

Table 5.5 - Summary of high pressure oedometer tests

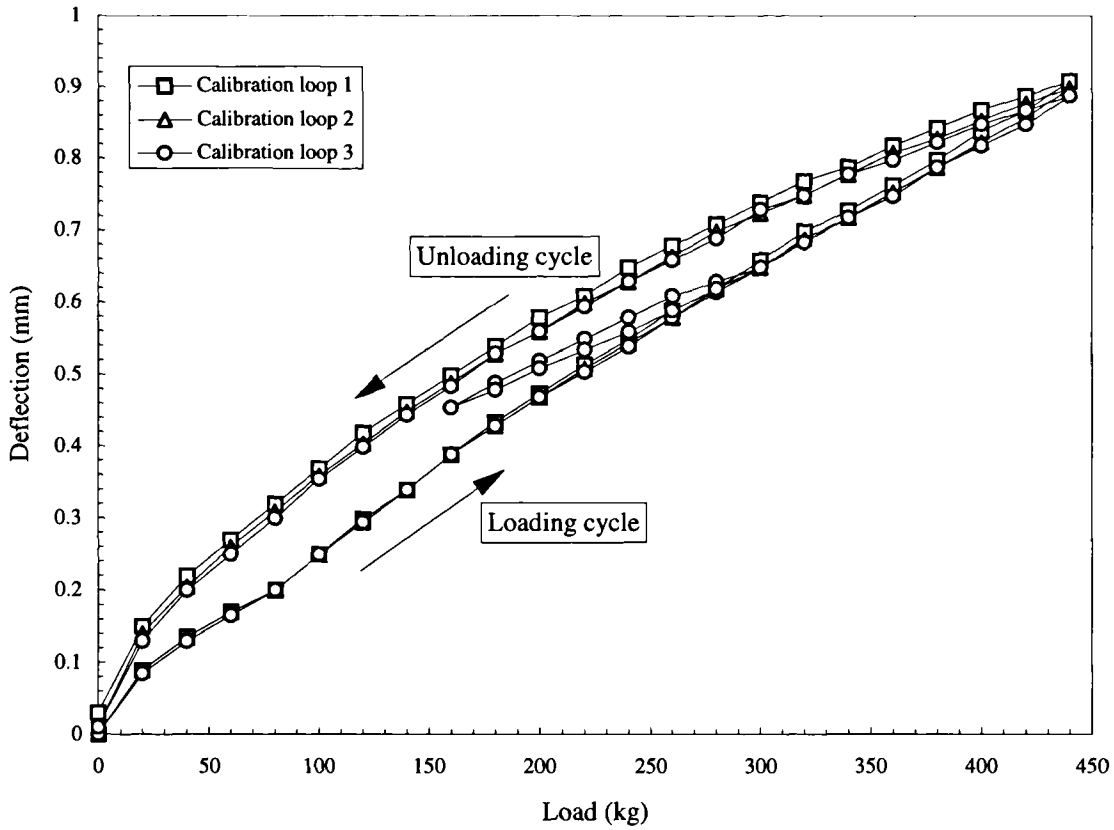

Figure 5.28 - Typical calibration of the high pressure oedometer cell

5.9 Suction measurement using filter paper tests

In order to quantify the combined effects of long term storage of the Elstow block samples, and of the sample disturbance of both the Elstow and Kempston Pit block samples, a series of filter paper tests (Gardner, 1937) was carried out to estimate the initial mean effective stress state within the samples. This could then be used to estimate the *in situ* stress state of the block sample and to compare this value with that calculated from the triaxial tests (see section 5.5.3).

A filter paper test is carried out by placing a filter paper between two flat surfaces of the soil specimen, sealing the unit to prevent moisture loss, and leaving it for approximately 1 week to allow the moisture content of the filter paper to equilibrate. Using a published calibration of filter paper water content against suction (Chandler and Gutierrez, 1986), the specimen matrix suction can be estimated.

Initially, an attempt was made to prepare a suitable test specimen by directly trimming the block samples but this proved to be both difficult and time consuming. An alternative method was developed using the preparation rig shown in Figure 5.29. The apparatus consisted of a perspex base onto which a slotted steel cover was placed. A section of the block sample was trimmed until it could fit within the steel cover, wrapped in cling film, and it was then placed on the perspex base. The steel cover was placed over this, fitting into grooves in the perspex base, and the cover was fixed by screws to the base. Masking tape was used to cover each of the grooves and expanding foam was then sprayed into the air gap between the specimen and the cage. Once the initial expansion of the foam had taken place, a wooden board was secured onto each end of the steel cover, and the apparatus was left for 3 hours to allow the foam to harden. A band saw was then used to cut into each of the grooves to separate the specimen into six sections. The support provided by the hardened foam minimised disturbance to the specimen during the splitting operation. The apparatus was then dismantled and the expanding foam and

cling film removed. The specimen was split apart, and a piece of Whatman's No. 42 filter paper was placed between each of the sections. It was found that the band saw provided a smooth surface in far less time, and with less disturbance, than if manual trimming was used. The soil specimen was then sealed in cling film and wax coated muslin gauze and left for 1 week while the moisture content of the filter papers equilibrated. The sealing was then removed and the weight of each filter paper determined to an accuracy of 1μg. The weighing process involved picking up each filter paper with a pair of tweezers and placing it on the high precision measurement scales and obtaining a reading within 20 seconds. The filter paper weight was then recorded at 10 second time intervals for 2 minutes. This allowed a plot of filter paper weight, and the inferred suction, against time, from which the suction at zero time could be extrapolated. The filter paper was then oven-dried for 24 hours and a time-weight relationship then evaluated. The calibrations relating filter paper water content to soil matrix suction are given in equations 5.15 and 5.16 for suctions less than and greater than 80kPa respectively.

$$s = 10^{(4.85-0.0622w)} \text{ , for } s > 80\text{kPa} \quad \text{(after Chandler and Gutierrez, 1986)} \quad \text{(5.15)}$$

$$s = 10^{(6.05-0.0622\log_{10} w)} \text{ , for } s < 80\text{kPa} \quad \text{(after Chandler } et\ al.\text{, 1992)} \quad \text{(5.16)}$$

where, s is the capillary pressure or inferred soil suction
w is the water content of the filter paper in %

The results of a typical filter paper test are shown in Figure 5.30 from which the inferred suctions at zero time for the five filter papers from a particular test specimen can be obtained. Also shown in this figure are the results of a test carried out on the same specimen by replacing the filter papers with unused ones and resealing the specimen for another week. The difference in the average inferred suction is approximately 50kPa and is probably attributable to a slight drying of the specimen during the week spent equilibrating.

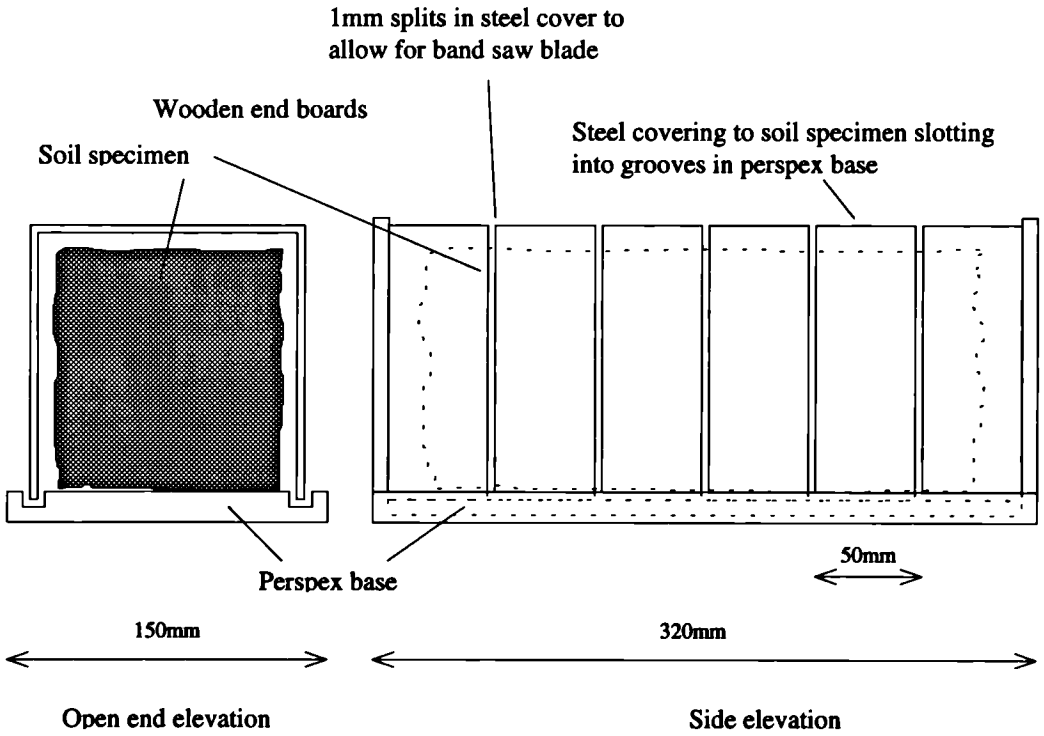

Figure 5.29 - Apparatus used to prepare specimen for filter paper tests

The variation in the inferred suctions from each filter paper was approximately 20kPa.

A total of 3 filter paper tests were carried out on block samples from both the Elstow site and Kempston pit and these are summarised in Table 5.6.

Test name	Block sample name	Associated stress path test	Sample origin
SUC 01	E/EX15 25.640 /BL	T01 / T02	Elstow
SUC 02	E/EX17 24.910 /BL	T03	Elstow
SUC 03	KEMP/BL2/21.5	T04 - T06 / T09	Kempston

Table 5.6 - Summary of filter paper suction tests

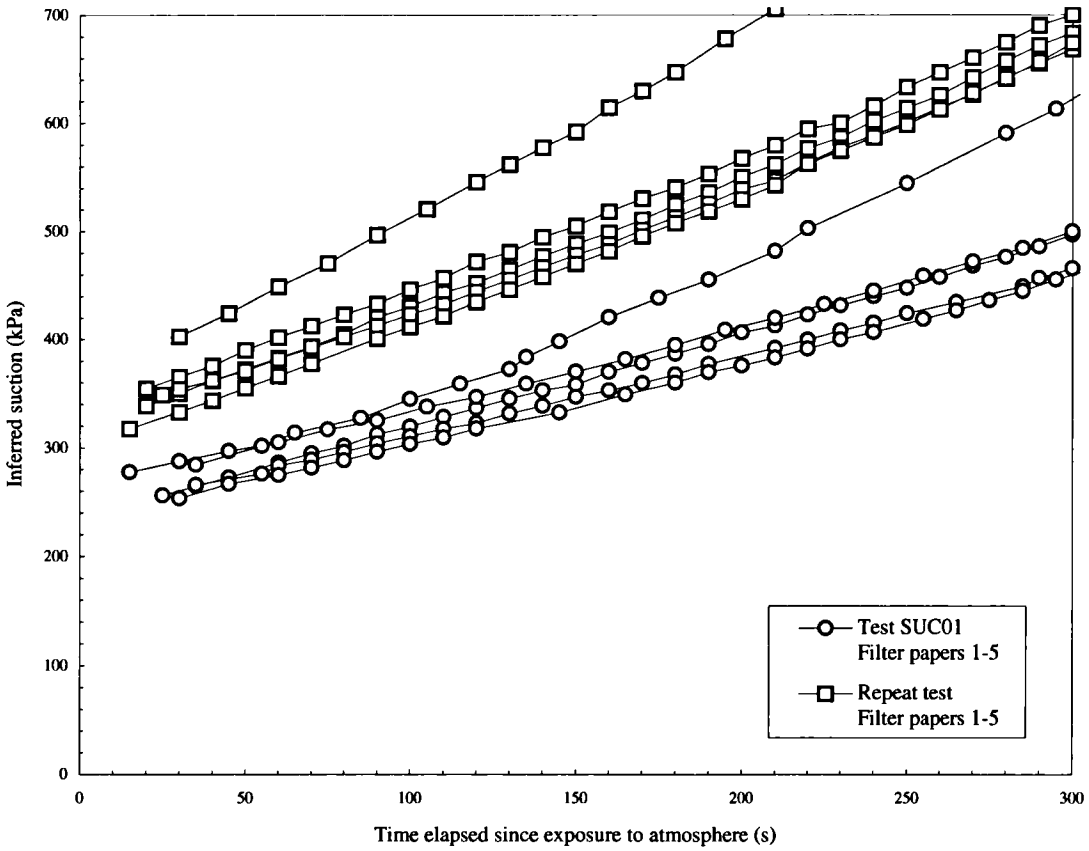

Figure 5.30 - Typical filter paper test results showing repeat test results using fresh filter papers on an identical specimen